THE JOURNAL OF

PHYSICAL

CHEMISTRY

Published biweekly by the American Chemical Society at 20th and Northampton Sts., Easton, Pennsylvania 18042. Second class postage paid at Washington, D.C. and at additional mailing offices.

Editorial Information

Instructions for authors are printed in the first issue of each volume. Please conform to these instructions when submitting manuscripts.

Manuscripts for publication should be submitted to *The Journal of Physical Chemistry*, Department of Chemistry, University of Minnesota, Minneapolis, Minn. 55455. Correspondence regarding **accepted papers and proofs** should be directed to the

Editorial Department at the ACS Easton address.

Page charges of $60.00 per page may be paid for papers published in this journal. Payment does not affect acceptance or scheduling of papers.

Bulk reprints or photocopies of individual articles are available. For information write to Business Operations, Books and Journals Division at the ACS Washington address.

Requests for **permission to reprint** should be directed to Permissions, Books and Journals Division at the ACS Washington address. The American Chemical Society and its Editors assume no responsibility for the statements and opinions advanced by contributors.

Subscription and Business Information

1977 Subscription rates—including surface postage

	U.S.	PUAS	Canada, Foreign
Member	$24.00	$33.00	$34.00
Nonmember	96.00	105.00	106.00
Supplementary material	15.00	19.00	20.00

Air mail and air freight rates are available from Membership & Subscription Services, at the ACS Columbus address.

New and renewal subscriptions should be sent with payment to the Office of the Controller at the ACS Washington address. **Changes of address** must include both old and new addresses with ZIP code and a recent mailing label. Send all address changes to the ACS Columbus address. Please allow six weeks for change to become effective. **Claims for missing numbers** will not be allowed if loss was due to failure of notice of change of address to be received in the time specified;

if claim is dated (a) North America—more than 90 days beyond issue date, (b) all other foreign more than 1 year beyond issue date; or if the reason given is "missing from files". Hard copy claims are handled at the ACS Columbus address.

Microfiche subscriptions are available at the same rates but are mailed first class to U.S. subscribers, air mail to the rest of the world. Direct all inquiries to Special Issues Sales, at the ACS Washington address or call (202) 872-4554. **Single issues** in hard copy and/or microfiche are available from Special Issues Sales at the ACS Washington address. Current year $4.75. Back issue rates available from Special Issues Sales. **Back volumes** are available in hard copy and/or microform. Write to Special Issues Sales at the ACS Washington address for further information. **Microfilm** editions of ACS periodical publications are available from volume 1 to the present. For further information, contact Special Issues Sales at the ACS Washington address. **Supplementary material** mentioned in the journal appears in the microfilm edition. Single copies may be ordered directly from Business Operations, Books and Journals Division, at the ACS Washington address.

	U.S.	PUAS, Canada	Other Foreign
Microfiche	$2.50	$3.00	$3.50
Photocopy			
1–7 pages	4.00	5.50	7.00
8–20 pages	5.00	6.50	8.00

Orders over 20 pages are available only on microfiche, 4 × 6 in., 24X, negative, silver halide. Orders must state photocopy or microfiche if both are available. Full bibliographic citation including names of all authors and prepayment are required. Prices are subject to change.

Notice to Authors last printed in the issue of January 13, 1977

THE JOURNAL OF

PHYSICAL CHEMISTRY

COMMUNICATIONS TO THE EDITOR

■ Supplementary and/or miniprint material for this paper is available separately (consult the masthead page for ordering information); it will also appear following the paper in the microfilm edition of this journal.

* In papers with more than one author, the asterisk indicates the name of the author to whom inquiries about the paper should be addressed.

AUTHOR INDEX

The Self-Exchange of Dinitrogen Behind Reflected Shock Waves[1a,b]

J. M. Bopp, R. D. Kern,* and T. Niki

Department of Chemistry, University of New Orleans, New Orleans, Louisiana 70122 (Received April 21, 1977)

Publication costs assisted by the National Science Foundation

The reaction of an equimolar mixture of $^{28}N_2$ and $^{30}N_2$ (4% each) diluted by a mixture of Ne (80%) and Kr (12%) was studied over the temperature and density range 4700–5400 K and 2.5–2.6 × 10^{-6} mol cm^{-3}, respectively. The reflected shock zone was sampled by a time-of-flight mass spectrometer at 20-μs intervals during typical observation periods of 0.5 ms. The product profiles were fit to the equation $(1 - 2f_{29}) = \exp(-k't^z)$, where f_{29} is the mole fraction of $^{29}N_2$. The time dependence z was determined to be 2.7 and the rate constants were best represented by the expression $k = 10^{-1.24\pm0.54} \exp(-138 \pm 10/RT) \mu s^{-2.7}$. The inert gas dependence was assumed to be first order as reported from a previous single-pulse shock tube investigation. The rate constants from the single-pulse study were recalculated using $z = 2.7$ and were combined with the results herein. The resulting Arrhenius parameters span the extended temperature range 3200–5400 K: log $A = 20.66 \pm 0.08$; $E = 140 \pm 1$ kcal mol^{-1}. The units of A are cm^3 mol^{-1} s$^{-2.7}$. The nonlinear time dependence for product formation confirms the earlier proposition of a mechanism which consists of a multistep sequence of reactions.

Introduction

Most of the shock tube work during the past 12 years concerned with exchange systems has dealt with D_2 reacting with a variety of relatively simple molecules: NH_3,[2] C_2H_2,[3] CH_4,[4] H_2S,[5] HCl,[6] HCN,[7] HBr,[8] and H_2.[9,10] The single-pulse shock tube technique has established the order for the reactants and inert gas and the activation energy for many of these reactions.[2,4a,5,9] Dynamic sampling of the reflected shock zone by time-of-flight mass spectrometry for the H_2–D_2 exchange measured the time dependence of product formation.[10] Recalculation of the single-pulse results[9a] taking account of nonlinear product growth produced a single Arrhenius line for both sets of data over the temperature range 1000–3000 K.[10]

Less work has been reported for heavy atom exchange. A recent study[11] confirmed the earlier single-pulse work[12] on the self-exchange of carbon monoxide. The temperature range was extended to an upper value of 4650 K and once again agreement was obtained between the single-pulse and the TOF dynamic sampling technique. Furthermore, the mechanism by which the exchange was proposed to take place was tested. The original proposal stated that the requirement for product formation is a critical amount of vibrational energy ($v = 7$–9) possessed by one of the reactant molecules.[12] However, population of these levels by mercury photosensitization at room temperature failed to produce the predicted amount of exchange.[11] This particular photolytic result has been confirmed by others.[13]

The self-exchange of dinitrogen, $^{28}N_2 + ^{30}N_2 \rightleftharpoons 2^{29}N_2$, has been studied with the single-pulse technique.[14] The reaction was found to be first order with respect to nitrogen and also to argon, the inert gas. The activation energy was determined to be 116 kcal mol^{-1} over the temperature range 3200–3800 K. The time dependence for product formation was assumed to be unity. The purpose of this investigation is to extend the temperature range, measure the time dependence and activation energy for the exchange, and to reconcile the two sets of data if possible.

Experimental Section

The apparatus employed herein has been described previously.[15] Isotopic nitrogen (99% enrichment) was purchased from Stohler Isotope Chemicals and was used without further purification. Linde dry grade nitrogen was twice purified by condensation onto a type 4A molecular
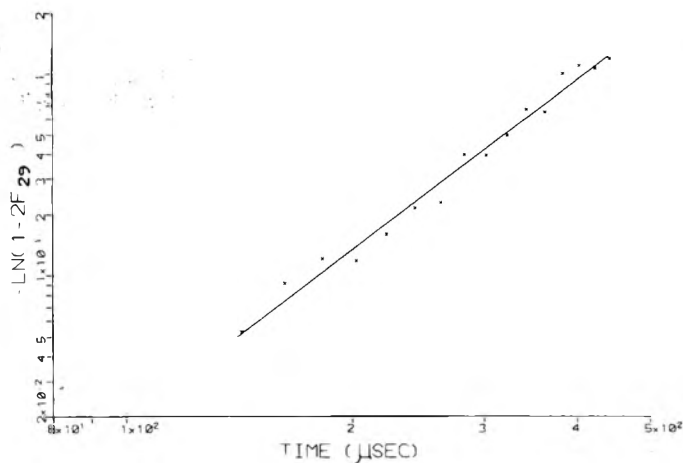
Figure 1. Time dependence plot for a run performed at 5280 K.

Figure 2. Fit of profile generated by eq 1 to experimental points for a run at 5280 K.

sieve trap at 77 K. In order to achieve the high temperatures required for exchange without saturating the TOF electron multiplier, a mixture of inert gases was used as the diluent. Matheson Research Grade Ne–1% Ar was used as received. Matheson Research Grade krypton was condensed and outgassed in a liquid nitrogen trap.

The isotopic exchange mixture, 4% ($^{28}N_2$), 4% ($^{30}N_2$), 12% Kr, and 80% Ne-Ar, was prepared by flowing each gas into a 2-L pyrex storage bulb at a predetermined pressure. After each component was added, the entire gas handling system was evacuated for at least 30 min. The reactant gas pressures were measured with a Wallace-Tiernan 0–10-in. H_2O differential pressure gauge while the diluent pressures were read from a Wallace-Tiernan 0–400-in. H_2O gauge. The mixture was allowed to stand for 24 h.

The mixture was permitted a maximum residence time of 30 s in the shock tube prior to diaphragm rupture. During this period an analog signal for O_2 was compared to that recorded from a standard mixture of 25 ppm of O_2 in neon. On this basis, it can be said that no experiment was performed at oxygen levels greater than 25 ppm. Spectra were recorded in the mass range m/e 15-50 at 20-μs intervals during total observation times equal to or less than 500 μs. The TOF ionizing voltage was set at 30 eV. All experiments were conducted at an initial test gas pressure of 5 Torr. Hydrogen was used as the driver gas and its initial pressure ranged from 2.0 to 2.3 atm. These driver pressures were necessary to achieve the desired temperature range for reaction but were also an "upper limit" with regard to the capacity of the shock tube–TOF pumping system. This limitation ruled out experiments at higher initial test pressures in order to determine the order dependence of the inert gas.

Results

The peak heights due to dinitrogen were measured as a function of reaction time and were fit to the following equation

$$1 - 2f_{29} = e^{-k't^z} \qquad (1)$$

where f_{29} is the mole fraction of $^{29}N_2$. The mole fraction was calculated by dividing the peak height for m/e 29 by the sum of the peak heights for all of the dinitrogen species. At equilibrium, f_{29} becomes equal to 0.5. The time dependence z was determined by making plots of the ln ln of the left-hand side of eq 1 vs. ln t. Within experimental error, the slope was constant and had a best value of 2.7 within the range $2.5 < z < 3$. A time dependence plot is depicted in Figure 1 for a run at 5280 K.
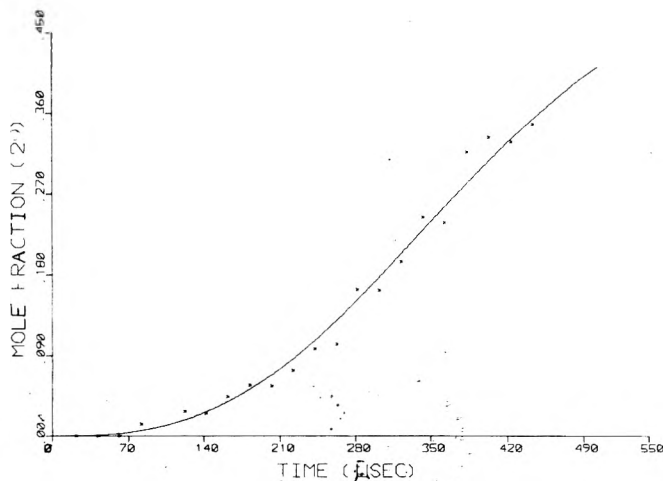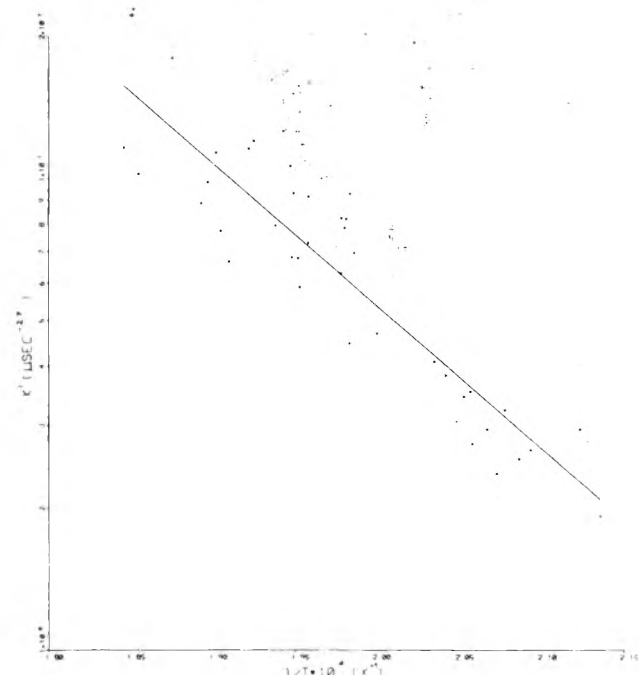
Figure 3. Arrhenius plot of k' rate constants.

All of the runs were then fit with eq 1 with $z = 2.7$ and the corresponding values for k' were calculated. The profile for the run at 5280 K is shown in Figure 2. An Arrhenius plot of the k' rate constants covering the temperature range 4700–5400 K is displayed in Figure 3.

The Arrhenius parameters were determined by least squares to have the following values:

$$k' = 10^{-1.24 \pm 0.45} \exp(-138 \pm 10/RT)\, \mu s^{-2.7} \qquad (2)$$

The units of the activation energy are expressed in kcal mol^{-1}. Assuming that unit order for inert gas dependence as determined by previous single pulse shock tube experiments[14] is applicable in the lower density range covered herein, the rate constants represented by eq 2 were divided by their respective reflected shock zone inert gas concentrations (0.92 ρ_5) and multiplied by the factor $10^{16.2}$ to convert from $\mu s^{-2.7}$ to $s^{-2.7}$. The rate constants along with their respective reflected zone temperatures and total concentrations ρ_5 are listed in Table I.

In order to compare the results reported herein with the previous single pulse work, the rate constants listed in series IA–IVB[14] were converted to the units $cm^3\, mol^{-1}\, s^{-2.7}$. A grand Arrhenius plot was constructed using both sets
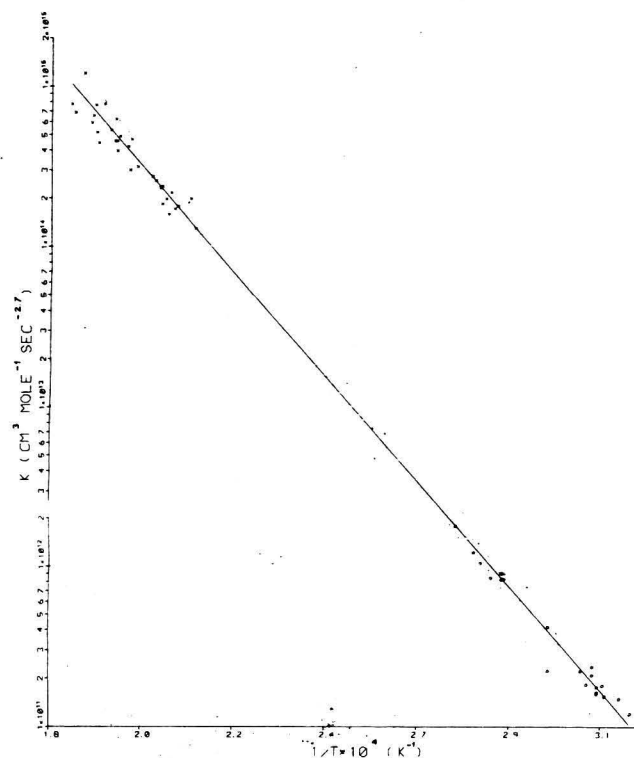
Figure 4. Arrhenius plot of single pulse rate constants (O) and those listed in the last column of Table I (X).

of rate constants and is displayed in Figure 4. The value of log A was determined to be 20.66 ± 0.08 and the value for the activation energy is 140 ± 1 kcal mol^{-1}. The units of A are cm^3 mol^{-1} s$^{-2.7}$. The temperature range extends from 3200 to 5400 K.

Discussion

The finding of a nonlinear time dependence for the formation of $^{29}N_2$ supports one of the conclusions reached by previous workers; namely, that the exchange does not proceed via a single bimolecular event.[14]

The magnitude of the activation energy argues against an atomic mechanism. The dissociation rate of dinitrogen has been measured behind reflected shock waves by vacuum UV absorption:[16]

$$N_2 + Ar \xrightarrow{k_{d_1}} 2N + Ar$$

$$N_2 + N_2 \xrightarrow{k_{d_2}} 2N + N_2$$
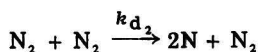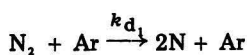
The Arrhenius equations for k_{d_1} and k_{d_2} gave identical values for the activation energy (192 kcal mol^{-1}) over the temperature range 8000–15000 K.

The three center exchange involving nitrogen atom has been investigated[17] and the activation energy was calculated to be at least 36 kcal mol^{-1}.

$$^{15}N + {}^{28}N_2 \rightarrow {}^{14}N + {}^{29}N_2$$

Following the argument previously presented for the H$_2$–D$_2$ system,[10] an atomic mechanism for the dinitrogen self-exchange predicts $z = 2$ and $E^* = 192 + 36 = 228$ kcal mol^{-1}. The ratio of O$_2$/N$_2$ stated herein is less than 3×10^{-4}. This ratio is less than the amount found to have very little effect upon the exchange rate, 0.01.[14] Hence, an atomic mechanism with or without an oxygen impurity less than 25 ppm may be ruled out. Also ruled out is a mechanism which involves an equilibrium amount of nitrogen atoms reacting in the three center exchange step. The predicted activation energy would be a minimum of

TABLE I: Rate Constants for the Self-Exchange of Dinitrogen^a

T_s, K	$10^6 \rho_s$, mol cm^{-3}	$10^8 k'$, μs$^{-2.7}$	10^{-14}cm^3 mol^{-1} s$^{-2.7}$
4681	2.51	1.92	1.32
4707	2.51	2.94	2.02
4776	2.52	2.65	1.81
4791	2.52	2.54	1.75
4812	2.52	3.22	2.20
4825	2.53	2.36	1.61
4839	2.53	2.94	2.00
4859	2.53	2.74	1.87
4862	2.53	3.53	2.40
4871	2.53	3.45	2.35
4898	2.53	3.83	2.60
4915	2.53	4.08	2.77
5000	2.54	4.69	3.18
5035	2.55	6.97	4.72
5043	2.55	4.49	3.04
5044	2.55	9.28	6.28
5049	2.55	8.24	5.57
5051	2.55	7.84	5.30
5055	2.55	8.25	5.58
5055	2.55	6.31	4.27
5106	2.55	7.30	4.93
5107	2.55	9.20	6.20
5120	2.55	5.92	3.99
5123	2.55	6.79	4.58
5132	2.56	9.31	6.28
5133	2.56	6.80	4.58
5137	2.56	10.6	7.17
5146	2.56	12.6	8.52
5159	2.56	7.98	5.38
5194	2.56	12.0	8.08
5203	2.56	11.5	7.76
5236	2.56	6.66	4.47
5249	2.57	7.73	5.19
5257	2.57	11.4	7.62
5271	2.57	9.79	6.57
5280	2.57	8.88	5.96
5333	2.57	18.0	12.1
5391	2.58	10.3	6.86
5418	2.58	11.6	7.74

^{a} The mixture consists of 4% $^{28}N_2$, 4% $^{30}N_2$, 12% Kr, and 80% Ne; $P_1 = 5$ Torr.

150 kcal mol^{-1}, the inert gas order would be zero, and the time dependence for $^{29}N_2$ formulation would be one.

The nonlinear time dependence definitely points to a mechanism which consists of a sequence of steps and, in that sense, supports a vibrational excitation mechanism. Furthermore, a value of $z > 1$ precludes the steady state approximation. This fact is consistent with the model that depicts molecules undergoing the exchange process as originating from a critical energy manifold at a rate greater than that required to replenish or maintain the population of the manifold at some equilibrium or quasiequilibrium condition. Unfortunately, the rate constants for the excitation and exchange steps are not known and the subsequent predictions for the reactant and inert gas order, the value for z, and the activation energy cannot be made.

However, the data and equations presented herein do reproduce the experimental profiles for product formation and the rate constants can be reconciled with those derived by the single-pulse technique after adjustment for the observed time dependence.

References and Notes

(1) (a) Paper presented at the 173rd National Meeting of the American Chemical Society, New Orleans, La., March, 1977. (b) Support of this work by the National Science Foundation, Grant CHE-7608529, is gratefully acknowledged.

(2) (a) A. Lifshitz, C. Lifshitz, and S. H. Bauer, *J. Am. Chem. Soc.*, **87**, 143 (1965); (b) A. Burcat and A. Lifshitz, *J. Chem. Phys.*, **52**, 337 (1970).

(3) S. H. Bauer and K. Kuritani, *J. Am. Chem. Soc.*, **87**, 150 (1965).
(4) (a) W. Watt, P. Borrell, D. Lewis, and S. H. Bauer, *J. Chem. Phys.*, **45**, 444 (1966); (b) W. C. Gardiner, J. M. Herrmann, W. G. Mallard, and J. H. Owen, *Int. J. Chem. Kinet.*, **8**, 111 (1976).
(5) A. Burcat, A. Lifshitz, D. Lewis, and S. H. Bauer, *J. Chem. Phys.*, **49**, 1449 (1968).
(6) R. D. Kern and G. G. Nika, *J. Phys. Chem.*, **75**, 171 (1971).
(7) J. M. Brupbacher and R. D. Kern, *J. Phys. Chem.*, **76**, 285 (1972).
(8) R. D. Kern and G. G. Nika, *J. Phys. Chem.*, **78**, 2549 (1974).
(9) (a) S. H. Bauer and E. Ossa, *J. Chem. Phys.*, **45**, 434 (1966); (b) A. Burcat and A. Lifshitz, *ibid.*, **47**, 3079 (1967).
(10) R. D. Kern and G. G. Nika, *J. Phys. Chem.*, **75**, 1615 (1971).

(11) A. F. Bopp, R. D. Kern, and B. V. O'Grady, *J. Phys. Chem.*, **79**, 1483 (1975).
(12) A. Bar-Nun and A. Lifshitz, *J. Chem. Phys.*, **51**, 1826 (1969).
(13) A. L. Rockwood and E. A. McCullough, presented at the 172nd National Meeting of the American Chemical Society, Physical Chemistry Division, Abstract 133, 1976.
(14) A. Bar-Nun and A. Lifshitz, *J. Chem. Phys.*, **47**, 2878 (1967).
(15) J. M. Brupbacher, R. D. Kern, and B. V. O'Grady, *J. Phys. Chem.*, **80**, 1031 (1976).
(16) J. P. Appleton, M. Steinberg, and D. J. Liquornik, *J. Chem. Phys.*, **48**, 599 (1968).
(17) R. K. Lyon, *Can. J. Chem.*, **50**, 1437 (1972).

Product Distributions and Rate Constants for the Reactions of CH_3^+, CH_4^+, $C_2H_2^+$, $C_2H_3^+$, $C_2H_4^+$, $C_2H_5^+$, and $C_2H_6^+$ Ions with CH_4, C_2H_2, C_2H_4, and C_2H_6[†]

J. K. Kim, V. G. Anicich, and W. T. Huntress, Jr.*

Jet Propulsion Laboratory, 4800 Oak Grove Drive, Pasadena, California 91103 (Received April 13, 1977)

Ion cyclotron resonance methods have been used to measure the product distributions and rate constants for the reactions of various CH_n^+ and $C_2H_n^+$ ions with CH_4, C_2H_2, C_2H_4, and C_2H_6. The product distributions for some of the reactions of $C_2H_2^+$, $C_2H_4^+$, and $C_2H_6^+$ ions are strongly affected by excess ion internal energy. Photoionization mass spectrometer experiments have been conducted in a few cases in order to obtain product distributions for reactions of these ions in the ground vibronic state.

I. Introduction

A number of hydrocarbon ion–molecule reactions are examined in this work by both ICR and photoionization mass spectrometer methods. The work was initiated in order to measure product distributions for these reactions. Accurate product distributions are not available for most of the reactions studied in this work, and many of the product distributions which are available from earlier ICR and from single-source, trapped-ion or tandem mass spectrometer experiments (see section III) are incomplete or are obtained for ions with excessive internal or kinetic energies. Parent ions obtained from C_2H_2, C_2H_4, and C_2H_6 by electron impact above threshold contain a large amount of excess internal energy, and this effect is readily observed in the product distributions for reactions of these ions. Careful attention is paid to the problem of excess ion energy in the present work, and photoionization experiments at threshold were conducted in some cases in order to verify the low energy, electron-impact results obtained from ICR experiments. Rate constants were also measured, and the results obtained for both product distributions and rate constants are compared to the more recent work on these reactions conducted at thermal or near-thermal ion kinetic energies.

II. Experimental Section

The JPL ion cyclotron resonance mass spectrometer was used to obtain product distributions and rate constants as previously described.[1,2] Product distributions were measured at constant magnetic field. The marginal os-

cillator frequency was changed in order to observe the various product ions during irradiation of the reactant ion at a single frequency. A Q-spoiler circuit was used to calibrate the sensitivity of the observing oscillator at the various frequencies used.[3] Rate constants were measured using the trapped ion method by observing the change in ion decay characteristics on addition of the reactant gas.[2] In a few cases, only the ratio of decay rates at long times could be used, such as for the $C_2H_4^+$–C_2H_2 reaction where the reactant ion actually increases at early times on addition of C_2H_2 because of the $C_2H_2^+$–C_2H_4 charge transfer reaction. For the reaction of $C_2H_6^+$ with C_2H_6, and for the reaction of $C_2H_4^+$ with C_2H_6 where $C_2H_4^+$ is prepared from C_2H_6 itself, the total sum method was used for obtaining the rate constant.[1]

Various gases were used for obtaining relatively clean sources of the reactant ions in ICR experiments. The CH_3^+ ions were obtained from CH_4 at 15 eV and from CH_3Cl at 18 eV. The CH_4^+, $C_2H_2^+$, and $C_2H_6^+$ ions were obtained from their parent gases at 16, 12.5–16, and 13–16 eV, respectively. The $C_2H_3^+$ ions were obtained from C_2H_3Cl at 16 eV, and $C_2H_5^+$ ions were obtained from both C_2H_5Cl at 16 eV and from C_2H_6 at 16 eV. Various sources were used for $C_2H_4^+$ including the parent gas at 13–16 eV, C_2H_5Cl at 13–16 eV, and C_2H_6 at 11–16 eV. No significant differences ($\pm15\%$) were noted in the rate constants for any of the reactions studied for reactant ions obtained from the various sources and under the various electron impact energy conditions given above. Significant changes were observed for the product distributions of some of the reactions of $C_2H_2^+$, $C_2H_4^+$, and $C_2H_6^+$ ions, but not for any of the reactions of CH_3^+, CH_4^+, $C_2H_3^+$, or $C_2H_5^+$ ions.

Photoionization experiments were conducted using the JPL-CIT photoionization mass spectrometer[4] where possible in order to obtain product distributions for those

TABLE I: Product Distribution and Rate Constants for Reactions of CH_3^+ Ions with C_2H_n Hydrocarbons

ΔH, kcal/ mol	Reaction	Product distribution	Rate constant, 10^{-9}/s
−59	$CH_3^+ + C_2H_2 \rightarrow C_3H_3^+ + H_2$	1.00	1.15, (1.54)[a]
−22	$CH_3^+ + C_2H_4 \rightarrow C_2H_3^+ + CH_4$	0.38	
−18	$\rightarrow C_3H_3^+ + 2H_2$	0.05	} 0.92
−57	$\rightarrow C_3H_5^+ + H_2$	0.57	
−39	$CH_3^+ + C_2H_6 \rightarrow C_2H_5^+ + CH_4$	0.85	
−24	$\rightarrow C_3H_5^+ + 2H_2$	0.09	} 1.74
−50	$\rightarrow C_3H_7^+ + H_2$	0.06	

[a] Reference 6.

reactions where the ICR experiments clearly showed that ion internal energy is a significant factor. For example, the lowest electron energy which could be usefully employed in the ICR experiments in order to accurately measure product distributions for reactions of $C_2H_2^+$ ions formed from acetylene was 12.5 eV. However, the ionization potential of acetylene is 11.40 eV (109.6 nm). In order to ensure that the distribution of vibrational energies in $C_2H_2^+$ ions formed by electron impact of C_2H_2 at 12.5 eV contains only a negligible fraction of vibrationally excited ions, photoionization experiments were conducted at 108.6 Å where $C_2H_2^+$ ions can only be formed in the ground vibronic state from C_2H_2.[5] Since CH_4 and C_2H_6 are not ionized at 108.6 Å, the product distributions were also measured for the $C_2H_2^+$–CH_4 and $C_2H_2^+$–C_2H_6 reactions in C_2H_2/CH_4 and C_2H_2/C_2H_6 gas mixtures. In these latter experiments, the C_2H_2 pressure in the ionization chamber was kept low so that reactions between $C_2H_2^+$ and C_2H_2 were not observed. The reagent gas was then added to sufficient pressure to result in about 1% conversion of $C_2H_2^+$ into product ions. Under these conditions, any new peaks appearing in the photoionization mass spectrum must then arise from the reaction of ground state $C_2H_2^+$ ions with the additive gas. The photoionization mass spectrometer was calibrated for mass discrimination effects by taking the primary photoionization mass spectra of butanes and comparing them to those measured with the ICR, where there is no mass discrimination. Only very small corrections, on the order of 10%, were required over the mass range from 25 to 55.

In addition to the $C_2H_2^+$–CH_4, $C_2H_2^+$–C_2H_2, and $C_2H_2^+$–C_2H_6 reactions, where ion internal energy was shown to have large effects, the product distributions for the $C_2H_4^+$–C_2H_2 and $C_2H_4^+$–C_2H_4 reactions were also measured using the photoionization mass spectrometer at 118.0 nm, where only the ground vibronic state of $C_2H_4^+$ is produced from ethylene[4] and where C_2H_2 is not ionized. The product distributions for the C_2H_2–C_2H_4 reaction, and for the reactions of $C_2H_6^+$ ions with C_2H_2 and C_2H_4, were not measured using the photoionization mass spectrometer since the ionization potential of the neutral reactant is lower than that of the parent species of the ionic reactant

in these cases. The $C_2H_4^+$–C_2H_6 and $C_2H_6^+$–C_2H_6 reactions were too slow for an accurate product distribution to be measured in photoionization mass spectrometer experiments near reactant ion threshold.

III. Results and Discussion

The results of this work are summarized in Tables I–VIII. The product distributions and rate constants for the reactions of CH_3^+ and CH_4^+ ions with C_2 hydrocarbons are given in Tables I and II. All of the rate constants for the reactions of $C_2H_n^+$ ions with methane and the C_2 hydrocarbons are listed together in Table III. The product distributions for these reactions are given in separate tables, one table each for the reactions of $C_2H_2^+$, $C_2H_3^+$, $C_2H_4^+$, $C_2H_5^+$, and $C_2H_6^+$ ions. Except for the reactions of CH_3^+ and CH_4^+ ions, where the reactions with C_2H_2, C_2H_4, and C_2H_6 are all discussed together, each reaction is covered in a separate section below where the results are discussed and a comparison is made with previous work. Of particular significance is the effect of ion internal energy on the reactions of the parent ions $C_2H_2^+$, $C_2H_4^+$, and $C_2H_6^+$, and the very large discrepancy between the present work and earlier work on the $C_2H_2^+$–CH_4, $C_2H_4^+$–C_2H_6, $C_2H_5^+$–C_2H_6, and $C_2H_6^+$–C_2H_6 reactions.

Reactions of CH_3^+ Ions. The reactions of CH_3^+ ions with C_2 hydrocarbons are quite fast. Hydride ion abstraction competes favorably with condensation via elimination of molecular hydrogen when both are exothermic. Condensation with loss of two molecules of hydrogen is also observed to a small extent when exothermic. The only previous work on these reactions is the CH_3^+–C_2H_2 data of Myher and Harrison.[6] These authors also give $C_3H_3^+$ as the product of this reaction, and report a rate constant in fair agreement with the present value. In the present work, no differences were noted in the measurements of product distributions or rate constants for CH_3^+ ions produced from methane at 15 eV or from CH_3Cl at 18 eV.

Reactions of CH_4^+ Ions. The reactions of CH_4^+ ions with C_2 hydrocarbons are also all quite fast. Charge transfer competes well with proton transfer in these reactions. Only a very small contribution is made to the CH_4^+–C_2H_2 and CH_4^+–C_2H_4 product distributions by condensation reactions. No condensation is observed in the CH_4^+–C_2H_6 reaction, and the mechanism of formation of $C_2H_4^+$ is most likely charge transfer followed by dissociation via loss of H_2. Although the proton affinity of C_2H_6 is larger than that of the CH_3 radical, proton transfer to give the $C_2H_7^+$ ion is not observed. The most likely mode of dissociation of any $C_2H_7^+$ ions which might be formed in the reaction is loss of H_2 to give $C_2H_5^+$. This process is nearly thermoneutral, and no $C_2H_5^+$ ions are observed. Dissociation of any $C_2H_7^+$ ions formed in the reaction to give $C_2H_4^+$ ions is endothermic by 84 kcal/mol.

As for the CH_3^+ reactions, the only previous quantitative work on these reactions is the CH_4^+–C_2H_2 data of Myher and Harrison.[6] These authors were not able to distinguish the charge transfer process in their experiments, but re-

TABLE II: Product Distribution and Rate Constants for Reactions of CH_4^+ Ions with C_2H_n Hydrocarbons

ΔH, kcal/mol	Reaction	Product distribution	Rate constant, 10^{-9} cm³/s
−29	$CH_4^+ + C_2H_2 \rightarrow C_2H_2^+ + CH_4$	0.45	
−28	$\rightarrow C_2H_3^+ + CH_3$	0.49	} 2.52, (1.84)[a]
−21	$\rightarrow C_3H_3^+ + H_2 + H$	0.06	
−52	$CH_4^+ + C_2H_4 \rightarrow C_2H_4^+ + CH_4$	0.75	
−35	$\rightarrow C_2H_5^+ + CH_3$	0.23	} 1.84
−9	$\rightarrow C_3H_5^+ + H_2 + H$	0.03	
−19	$CH_4^+ + C_2H_6 \rightarrow C_2H_4^+ + CH_4 + H_2$	1.00	1.91

[a] Reference 6. These authors also report a product ion ratio $C_2H_3^+/C_3H_3^+ = 10$.

TABLE III: Rate Constants for Reactions of $C_2H_n^+$ Hydrocarbon Ions with CH_4, C_2H_2, C_2H_4, and C_2H_6

	Rate constant, 10^{-9} cm^3/s	
Reaction	This work	Literature
$C_2H_2^+ + CH_4$	0.84	0.65,[9] 0.76,[6] 1.0[7]
$+ C_2H_2$		1.52,[17] 1.41,[9] 1.22,[13] 0.85[14]
$+ C_2H_4$	1.18	1.58[9]
$+ C_2H_6$	1.46	1.3,[23] 2.1[24]
$C_2H_3^+ + CH_4$	0.21	0.87,[24] 0.17[7]
$+ C_2H_2$	0.25	0.31,[23] 0.71[17]
$+ C_2H_4$	0.93	0.84[9]
$+ C_2H_6$	0.62	0.37,[23] 0.48[24]
$C_2H_4^+ + CH_4$	<0.001	<0.0001[7]
$+ C_2H_2$	0.79	0.83[23]
$+ C_2H_4$		0.80,[30] 0.85[9]
$+ C_2H_6$	0.0053	>0.005,[23] <0.01[24]
$C_2H_5^+ + CH_4$	<0.001	10^{-5}[32]
$+ C_2H_2$	0.19	0.10[23]
$+ C_2H_4$	0.39	0.32,[9] 0.61[27]
$+ C_2H_6$	0.04	0.10[28]
$C_2H_6^+ + CH_4$	<0.001	
$+ C_2H_2$	1.17	1.4[23]
$+ C_2H_4$	1.15	
$+ C_2H_6$	0.019	0.0185,[a] 0.032,[b] 0.07[20]

[a] Reference 23, "low ionizing energy". [b] Reference 23, 30 eV.

ported both $C_2H_3^+$ and $C_3H_3^+$ as product ions from the reaction with a product ion ratio $C_2H_3^+/C_3H_3^+$ of about 10, in close agreement with the present results. Myher and Harrison also measured a rate constant for the CH_4^+–C_2H_2 reaction which is somewhat larger than the present value.

$C_2H_2^+ + CH_4$. Both of the product distributions obtained in this work, at 12.5 eV in the ICR and at 108.6 Å in the photoionization instrument, are in excellent agreement with the recent product distribution obtained by the new SIFT (mass-selected flowing afterglow) method.[7] These results are in strong disagreement, however, with earlier work in which it appears that excess internal and/or kinetic energy in the reactant $C_2H_2^+$ ions are a contributing factor. Abramsom and Futrell[8] in early tandem mass spectrometer work at an unspecified center-of-mass kinetic energy give $C_2H_3^+$ as a major product ion, and also list an endothermic reaction product, $C_3H_3^+$, as 3% in the product distribution (not listed in Table IV). Herod and Harrison[9] also report $C_2H_3^+$ as the major product ion for this reaction in a study on reactions in methane where the $C_2H_2^+$ ion is produced in trapped ion experiments by the reactions

$$CH_2^+ + CH_4 \rightarrow C_2H_2^+ + 2H_2 \qquad (1)$$

$$CH^+ + CH_4 \rightarrow C_2H_2^+ + H_2 + H \qquad (2)$$
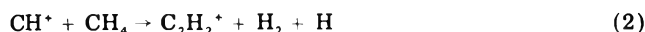
Myher and Harrison,[6] in earlier work on ion–molecule reactions in CH_4–C_2H_2 mixtures where $C_2H_2^+$ is produced by ionization of C_2H_2, give the product distribution reproduced in Table IV, which again gives $C_2H_3^+$ as a major product ion for this reaction. The ICR results at 16 eV show $C_2H_3^+$ to be a minor product ion in this reaction. The marked difference in the ICR product distributions measured at 16 and 12.5 eV in this work, and the photoionization results, show that $C_2H_3^+$ ions are only produced for reactions of vibrationally excited $C_2H_2^+$ ions with CH_4. Ground state $C_2H_2^+$ ions react with CH_4 to produce only $C_3H_4^+$ and $C_3H_5^+$ ions.

Excess internal energy in the reactant ions probably accounts for the difference between the present results and those of Myher and Harrison[6] and of Herod and Harrison.[9] In the former, excess ion kinetic energy may also be a contributing factor. Reaction 1 is slightly endothermic, by about +2 kcal/mol, so that excited $C_2H_2^+$ ions are not

TABLE IV: Product Distributions for Reactions of $C_2H_2^+$ Ions with Hydrocarbons

		This work			Product distribution	Literature[a]	
ΔH, kcal/mol	Reaction	16 eV	12.5 eV	PI			
+1	$C_2H_2^+ + CH_4 \rightarrow C_2H_3^+ + CH_3$	0.16	0.00	0.00	0.47 (18)	0.44 (6)	major (9)
−19	$\rightarrow C_3H_4^+ + H_2$	0.19	0.21	0.18	0.12	0.12	minor (9)
−31	$\rightarrow C_3H_5^+ + H$	0.64	0.79	0.82	0.41	0.44	
−34	$C_2H_2^+ + C_2H_2 \rightarrow C_4H_3^+ + H$	0.25	0.34	0.35	0.32	0.32 (12)	0.31 (13)
−12	$\rightarrow C_4H_2^+ + H_2$	0.75	0.66	0.65	0.68	0.68	0.69
+3	$C_2H_2^+ + C_2H_4 \rightarrow C_2H_3^+ + C_2H_3$		0.00		0.04		
−22	$\rightarrow C_3H_3^+ + CH_3$		0.34		0.70 (19)	0.45 (18)	
−41	$\rightarrow C_3H_5^+ + CH_3$		0.43		0.08	0.45	0.31 (14)
−35	$\rightarrow C_4H_5^+ + H$		0.00		0.01		0.69
−40	$\rightarrow C_4H_4^+ + H_2$		0.23		0.15	0.27	
−32	$C_2H_2^+ + C_2H_6 \rightarrow C_2H_4^+ + C_2H_4$		0.18	0.23			
−14	$\rightarrow C_2H_5^+ + C_2H_3$		0.09	0.16			0.27 (16)
−8	$\rightarrow C_3H_3^+ + (CH_4 + H_2)$		0.06	0.01			0.73
−35	$\rightarrow C_2H_4^+ + CH_4$		0.01	0.01			
−47	$\rightarrow C_3H_5^+ + CH_3$		0.54	0.52			0.29 (16)
−8	$\rightarrow C_4H_5^+ + H_2 + H$		0.05	0.00			0.71
−41	$\rightarrow C_4H_7^+ + H$		0.09	0.07			

[a] Reference number in parentheses. [b] Reference 9, "low ionizing energy". [c] Reference 11, 12.5 eV. [d] Reference 23. [e] Reference 5, threshold photoionization value. [e] Reference 6, 16 eV.

TABLE V: Product Distributions for Reactions of $C_2H_3^+$ Ions with Hydrocarbons

ΔH, kcal/mol	Reaction	This work	Literature
−33	$C_2H_3^+ + CH_4 \rightarrow C_3H_5^+ + H_2$	1.00	1.00 ⎱ (7), (8), (25), (26)
−16	$C_2H_3^+ + C_2H_2 \rightarrow C_4H_3^+ + H_2$	1.00	
−6	$C_2H_3^+ + C_2H_4 \rightarrow C_3H_5^+ + C_2H_2$	1.00	0.85 ⎱ (19) 1.00 ⎱ (18)
−41	$\rightarrow C_3H_3^+ + CH_4$	0.00	0.04
−42	$\rightarrow C_4H_5^+ + H_2$	0.00	0.08
−16	$C_2H_3^+ + C_2H_6 \rightarrow C_3H_5^+ + C_2H_4$	0.47	Major ⎱ (23)
−51	$\rightarrow C_3H_5^+ + CH_4$	0.40	Major
−46	$\rightarrow C_4H_7^+ + H_2$	0.13	Minor

TABLE VI: Product Distributions for Reactions of $C_2H_4^+$ Ions with Hydrocarbons

ΔH, kcal/mol	Reaction	EI	PI	Literature
	$C_2H_4^+ + CH_4 \rightarrow$ no reaction			
−19	$C_2H_4^+ + C_2H_2 \rightarrow C_3H_3^+ - CH_3$	0.80	0.84	0.81 ⎱ (29)
−18	$\rightarrow C_4H_5^+ - H$	0.20	0.16	0.19
−3	$C_2H_4^+ + C_2H_4 \rightarrow C_3H_3^+ - CH_4$	0.00	0.00	0.02 (9); 0.009 (19)
−17	$\rightarrow C_3H_5^+ + CH_3$	0.91	0.92	0.90 (9); 0.84 (19); 0.91 (29); 0.90 (18)
−29	$\rightarrow C_4H_6^+ + H_2$	0.00	0.00	0.003 (9); 0.004 (19)
−11	$\rightarrow C_4H_7^+ + H$	0.09	0.08	0.06 (9); 0.10 (19); 0.09 (29); 0.10 (18)
+12	$C_2H_4^+ + C_2H_6 \rightarrow C_2H_5^+ + C_2H_5$	0.00		0.23 ⎱ (31)
+55	$\rightarrow C_3H_3^+ + (CH_3 + 2H_2)$	0.00		0.23
+17	$\rightarrow C_3H_5^+ + (CH_3 + H_2)$	0.00		0.33
−22	$\rightarrow C_3H_6^+ + CH_4$	0.07		0.07 Minor ⎱ (23)
−9	$\rightarrow C_3H_7^+ + CH_3$	0.93		0.00 Major
+22	$\rightarrow C_4H_7^+ + H_2 + H$	0.00		0.05
−24	$\rightarrow C_4H_8^+ + H_2$	0.00		0.07
−5	$\rightarrow C_4H_9^+ + H$	0.00		0.02

TABLE VII: Product Distributions for Reactions of $C_2H_5^+$ Ions with Hydrocarbons

ΔH, kcal/mol	Reaction	This work	Literature
	$C_2H_5^+ + CH_4 \rightarrow$ no reaction		
−36	$C_2H_5^+ + C_2H_2 \rightarrow C_3H_3^+ + CH_4$	0.36	
−36	$\rightarrow C_4H_5^+ + H_2$	0.64	
+79	$C_2H_5^+ + C_2H_4 \rightarrow C_2H_6^+ + C_2H_3$	0.00	0.03 ⎱ (19)
−34	$\rightarrow C_3H_5^+ + CH_4$	1.00	0.85
+31	$\rightarrow C_3H_6^+ + CH_3$	0.00	0.07
−27	$\rightarrow C_4H_7^+ + H$	0.00	0.05
−27	$C_2H_5^+ + C_2H_6 \rightarrow C_3H_7^+ + CH_4$	0.00	0.00 ⎱ (31) 0.67 ⎱ a 0.13 ⎱ (27)
−23	$\rightarrow C_4H_9^+ + H_2$	1.00	1.00 0.33 0.87

^{a} Reference 23. For the reaction of $C_2D_5^+$ ions with C_2H_6 to give the appropriate mixed ions. These authors report that H^- abstraction from C_2H_6 to give $C_2H_5^+$ ions is the major product of the reaction, and give a distribution of 0.85, 0.10, and 0.05 for formation of $C_2H_5^+$, $C_3H_xD_{7-x}^+$, and $C_4H_xD_{9-x}^+$ ions in their experiment.

TABLE VIII: Product Distributions for Reactions of $C_2H_6^+$ Ions with Hydrocarbons

ΔH, kcal/mol	Reaction	This work	Literature
	$C_2H_6^+ + CH_4 \rightarrow$ no reaction		
−15	$C_2H_6^+ + C_2H_2 \rightarrow C_2H_5^+ + C_2H_3$	0.19	
−50	$\rightarrow C_3H_5^+ + CH_3$	0.70	
−44	$\rightarrow C_4H_7^+ + H$	0.11	
−25	$C_2H_6^+ + C_2H_4 \rightarrow C_2H_4^+ + C_2H_6$	1.00	
+19	$C_2H_6^+ + C_2H_6 \rightarrow C_2H_5^+ + C_2H_5 + H_2$	0.00	0.33 ⎱ (31)
−2	$\rightarrow C_3H_7^+ + (CH_3 + H_2)$	0.00	0.14
−12	$\rightarrow C_3H_8^+ + CH_4$	0.42	0.23
	$\rightarrow C_3H_9^+ + CH_3$	0.58	0.17
+3	$\rightarrow C_4H_9^+ + H_2 + H$	0.00	0.10
−13	$\rightarrow C_4H_{10}^+ + H_2$	0.00	0.04

likely to be formed by this reaction, but reaction 2 is very exothermic, by −30 kcal/mol,[10] and it is possible that this reaction may be responsible for production of excited $C_2H_2^+$ ions in Herod and Harrison's[9] experiment.

The rate constant determined for this reaction (Table III) is in fairly good agreement with the values reported by Myher and Harrison,[9] by Herod and Harrison,[9] and by Adams and Smith.[7] Measurements of the rate constant for $C_2H_2^+$ formed from C_2H_2 at 12.5 and at 16 eV yielded the same value within statistical error limits.

$C_2H_2^+ + C_2H_2$. The product distribution for this reaction has been studied extensively. The ICR result from

this work at 12.5 eV is in very good agreement with previous measurements done at low ionizing energy.[6,9,11 15] O'Malley and Jennings[11] have shown that the $C_4H_2^+$/ $C_4H_3^+$ product ion ratio decreases markedly between 12 and 16 eV, and then increases again due to formation of a new state of $C_2H_2^+$. Our product ion ratios at 12.5 and 16 eV agree well with the ratios at 12 and 16 eV measured by O'Malley and Jennings.[11] Our 16-eV result is also in good agreement with the results at 16 eV reported by Myher and Harrison.[6] The product distribution determined by tandem mass spectrometer[16] experiments is subject to two effects: the high ionization energy used (100 eV) and excess reactant ion kinetic energy. A number of other minor product ions were reported in the tandem results, most of which can only result from endothermic reactions involving kinetically excited $C_2H_2^+$ ions.

Measurements of the product distribution for this reaction using the JPL-CIT photoionization mass spectrometer have been previously reported by Buttrill.[15] These results showed a decrease in the $C_4H_2^+$/$C_4H_3^+$ product ion ratio from 0.48 for $v = 0$ $C_2H_2^+$ ions to 0.35 for $v = 1$ $C_2H_2^+$ ions. A redetermination of the ratio for $v = 0$ $C_2H_2^+$ ions at 108.6 nm in this work using improved detection equipment gives good agreement with the earlier photoionization value for $v = 0$ ions and with the present ICR measurement at 12.5 eV.

The rate constant for this reaction has previously been measured at 15 eV in this laboratory[17] and is in better agreement with the value reported by Herod and Harrison[9] than with the very early ICR[13] and single source mass spectrometer measurements.[14]

$C_2H_2^+ + C_2H_4$. The product distribution measured for this reaction is in good agreement with the earlier ICR work of Bowers, Elleman, and Beauchamp,[18] but is in considerable variance with both the tandem mass spectrometer results of Tiernan and Futrell[19] and with the single-source mass spectrometer results of Herod and Harrison.[9] The latter workers report $C_2H_3^+$ and $C_2H_4^+$ ions as products for this reaction, but do not assign any relative importance to the two channels. We do not observe any $C_2H_3^+$ ions from this reaction at 12.5 eV. In addition to the ions given in Table IV for the product distribution reported by Tiernan and Futrell,[19] these workers also report minor amounts of $C_2H_5^+$ (0.004) and $C_3H_5^+$ (0.007) ions. The reactions of $C_2H_2^+$ ions with C_2H_4 to give these latter product ions are endothermic by +2 and +39 kcal/mol respectively, and are probably the result of subsequent reactions of the $C_2H_3^+$ and $C_2H_4^+$ ions with C_2H_4 in the tandem collision chamber. This is verified by the decreasing importance of $C_2H_3^+$ and $C_2H_4^+$ ions in the tandem product distribution as the source pressure was raised from 5 to 50 μm.[19] In the present work, differences were noted in the product distribution at elevated ionization energies, but no attempt was made to construct a product distribution at these higher energies. Photoionization experiments on C_2H_2–C_2H_4 mixtures were not useful for determining a product distribution since C_2H_4 is also ionized at 108.6 nm. The rate constant determined for this reaction at 16 eV in acetylene/ethylene mixtures is somewhat lower than that determined by Herod and Harrison.[9]

$C_2H_2^+ + C_2H_6$. The ICR product distribution (electron impact at 12.5 eV) and photoionization product distribution (108.6 nm) measured in this work are in very good agreement. Some small changes in the product distribution were noted at 16 eV in ICR measurements, but an accurate product distribution was not determined at this energy. Bennett, Lias, and Field[20] report observation of

the adduct, $C_4H_8^+$, in high pressure mass spectrometer studies of this reaction at 3–5 Torr, and early ICR work by Wexler and Pobo[21] reported $C_2H_3^+$, $C_2H_4^+$, $C_2H_5^-$, $C_3H_3^+$, $C_3H_5^+$, $C_3H_6^+$, and $C_4H_7^+$ ions from this reaction. No actual product distribution was reported by Wexler and Pobo,[21] and these workers used 70-eV ionizing electrons, which results in formation of excited $C_2H_2^+$ ions. We observe no $C_2H_3^+$ or $C_3H_6^+$ ions from this reaction, and the reaction to give $C_3H_6^+$ ions is endothermic by +22 kcal/mol. McAllister[22] in later ICR work also reports $C_3H_3^+$ and $C_3H_5^+$ ions from this reaction. Blair, Heslin, and Harrison[23] report $C_2H_3^+$, $C_3H_4^+$, $C_2H_5^+$, $C_3H_3^+$, $C_3H_5^+$, $C_4H_5^+$, and $C_4H_7^+$ ions from this reaction in trapped-ion mass spectrometer work, but do not give a distribution for these product ions. The rate constant determined for the reaction in this work at 16 eV in C_2H_2/C_2H_6 mixtures is in better agreement with that measured by Blair, Heslin, and Harrison[23] than with the earlier single-source mass spectrometer result.[24]

$C_2H_3^+ + CH_4$. This reaction gives rise to only one product ion, $C_3H_5^+$, and has been previously reported by a number of workers.[7,8,25,26] Abramson and Futrell[8] also reported an endothermic reaction yielding the products $C_3H_6^+ + H$, but this observation is most likely the result of excess reactant ion kinetic energy in tandem mass spectrometer experiments. The rate constant obtained for the reaction is in good agreement with the recent SIFT measurement.[7]

$C_2H_3^+ + C_2H_2$. The reaction of $C_2H_3^+$ with C_2H_2 to produce $C_4H_3^+$ ions has been identified in earlier ICR work.[17] Here we confirm that this is the only product channel for the reaction. Burt et al.[27] have observed the stabilized intermediate ion, $C_4H_5^+$, at high pressures in flowing afterglow experiments. The rate constant measured in this work is in very good agreement with Blair, Heslin, and Harrison,[23] but is in poor agreement with the ICR value reported earlier.[17] The reason for this disagreement is not apparent.

$C_2H_3^+ + C_2H_4$. The product distribution for this reaction is in reasonable agreement with that reported by Tiernan and Futrell[19] in tandem mass spectrometer experiments except that we do not observe the small percentages of $C_3H_3^+$ and $C_4H_5^+$ ions. Bowers, Elleman, and Beauchamp[18] also report only the $C_2H_5^+$ product ion in earlier ICR work. Tiernan and Futrell[19] report very small percentages of $C_2H_4^+$, $C_3H_4^+$, $C_3H_5^+$, $C_4H_3^+$, and $C_4H_6^+$ ions in their product distribution, but these reactions are endothermic by +39, +34, +41, +80, and +9 kcal/mol, respectively. Burt et al.[27] also report production of $C_3H_5^+$ ions from this reaction in flowing afterglow experiments. The rate constant measured for this reaction is in good agreement with the value reported by Herod and Harrison.[9]

$C_2H_3^+ + C_2H_6$. The three reaction channels observed agree with those reported by Blair, Heslin, and Harrison.[23] These workers report $C_2H_5^+$ and $C_3H_5^+$ as the major reaction channels, in agreement with the present results. McAllister[22] has also observed the reaction producing $C_3H_5^+$ ions. Wexler and Pobo[21] in early ICR work reported two endothermic channels, producing $C_3H_6^+$ and $C_3H_7^+$ ions. These reactions were not observed in the present work. Ausloos, Rebbert, and Sieck[28] have observed that the intermediate ion, $C_4H_9^+$, can be collisionally stabilized before dissociation to $C_3H_5^+$ ions, and that it most likely has the *tert*-butyl structure. These latter workers, however, discounted the importance of $C_2H_5^+$ ion formation in their radiolysis experiments. The rate constant measured for this reaction is somewhat larger than that re-

ported in earlier mass spectrometer work.[23,24]

$C_2H_4^+ + CH_4$. The $C_2H_4^+$ ion is not reactive with CH_4. Adams and Smith[7] have measured an upper limit for the rate constant of 10^{-13} cm^3/s.

$C_2H_4^+ + C_2H_2$. The ICR product distributions measured for this reaction for $C_2H_4^+$ from C_2H_4 at 13 eV and for $C_2H_4^+$ from C_2H_6 at 16 eV are the same, and are in excellent agreement with the photoionization mass spectral product distribution obtained at 118.0 nm. The present results are also in very good agreement with the earlier ICR results of Buttrill.[29] The rate constant was measured under these same conditions and is in excellent agreement with the value reported by Blair, Heslin, and Harrison.[23]

$C_2H_4^+ + C_2H_4$. This reaction has been studied extensively. The ICR distributions measured in this work are the same for $C_2H_4^+$ from C_2H_4 at 16 eV, and for $C_2H_4^+$ from C_2H_5Cl at 13 eV ionization energy. They are both in good agreement with the earlier ICR work[18,29,30] and with the present photoionization mass spectrometer product distribution at 118.0 nm. We do not observe the $C_3H_4^+$ and $C_4H_6^+$ ions reported by Herod and Harrison[9] and by Tiernan and Futrell.[19] It is not likely that the small amount of $C_4H_6^+$ ions observed by these latter workers would be observed in the present experiments. The $C_3H_4^+$ ions should have been observable, and it seems possible that excess internal or kinetic energy may be the source of these product channels. Tiernan and Futrell[19] report very small amounts of $C_2H_5^+$, $C_2H_6^+$, $C_3H_2^+$, $C_3H_3^+$, and $C_3H_6^+$ in their product distribution, but these reactions are endothermic by +18, +34, +82, +22, and +58 kcal/mol respectively. The rate constant was not measured in this work, but has been reported in a previous ICR study from this laboratory.[30]

$C_2H_4^+ + C_2H_6$. The present work at 11 eV in pure ethane shows only two products from this reaction. This result is in agreement with the qualitative result of Blair, Heslin, and Harrison,[23] who also report $C_3H_7^+$ as the major channel and $C_3H_6^+$ as the minor channel. The present results are in major disagreement, however, with the ICR results of Dunbar, Shen, and Olah.[31] Dunbar, Shen, and Olah[31] worked at low ionizing energy (13 eV) but did not report the major ion, $C_3H_7^+$, which makes up 93% of the product distribution in the present work. A similar situation exists for the $C_2H_6^+ + C_2H_6$ reaction. In our own case, we have noted that C_3 hydrocarbon impurities in C_2H_6 samples can be a serious problem, and we have exercised extreme care in this regard. The electron energy must also be kept as low as possible in order to prevent formation of a significant fraction of excited $C_2H_4^+$ ions. Even for $C_2H_4^+$ ions formed from either C_2H_4 or C_2H_6 at 16 eV electron energy we do not observe any reaction to give $C_2H_5^+$, $C_3H_3^+$, $C_3H_5^+$, $C_4H_8^+$, $C_4H_7^+$, or $C_4H_9^+$ ions. Effects from reaction of excited $C_2H_4^+$ ions is also obvious in the work of Wexler and Pobo,[21] who report $C_2H_5^+$, $C_3H_5^+$, and $C_2H_3^+$ ions from this reaction in addition to $C_3H_6^+$ and $C_3H_7^+$ ions. The reaction to produce $C_2H_3^+$ is endothermic by +62 kcal/mol. Unfortunately, the rate constant for this reaction (measured for $C_2H_4^+$ from C_2H_6 at 11 eV) is too slow for an accurate photoionization experiment to be conducted on this reaction using the present apparatus.

Support for the present results is found in the earlier work of Bennett, Lias, and Field[20] who also present evidence that $C_3H_6^+$ and $C_3H_7^+$ ions are the only likely products of this reaction. Ausloos, Rebbert, and Sieck[28] have shown that H_2 transfer to give the same products as reactants occurs very rapidly (0.90 × 10^{-9} cm^3/s), which accounts for the small total rate constants for the other

reactive channels given in Table VI. Bennett, Lias, and Field[20] have also observed the stabilized intermediate ion, $C_4H_{10}^+$, in high pressure mass spectrometer experiments.

$C_2H_5^+ + CH_4$. $C_2H_5^+$ ions react with CH_4 at too slow a rate to be observable in the ICR apparatus. Hiraoka and Kebarle[32] have measured a rate constant at room temperature of about 10^{-14} cm^3/s for the reaction

$$C_2H_5^+ + CH_4 \rightarrow C_3H_7^+ + H_2 \qquad (3)$$

$C_2H_5^+ + C_2H_2$. Blair, Heslin, and Harrison[23] have measured a rate constant for this reaction, and Burt et al.[27] have reported both $C_3H_3^+$ product ions and collisionally stabilized $C_4H_7^+$ at high pressures in flowing afterglow experiments. The present work shows two reaction channels, yielding both $C_3H_3^+$ and $C_4H_5^+$ ions. The product distribution and rate constant measured for $C_2H_5^+$ ions produced from either C_2H_5Cl at 16 eV or from C_2H_6 at 16 eV give the same result. The rate constant measured in this work is somewhat larger than the value reported by Blair, Heslin, and Harrison.[23]

$C_2H_5^+ + C_2H_4$. The only product ion observed in the present work for this reaction is $C_3H_5^+$. Herod and Harrison[9] also report $C_3H_5^+$ as the major product ion, and Burt et al.[27] report both $C_3H_5^+$ and the collisionally stabilized $C_4H_9^+$ ion from this reaction. Tiernan and Futrell,[19] in addition to $C_3H_5^+$, also report smaller percentages of $C_2H_6^+$, $C_3H_6^+$, and $C_4H_7^+$ in tandem mass spectrometer work. The reactions to give $C_2H_6^+$ and $C_3H_6^+$ are endothermic by a large amount.

$C_2H_5^+ + C_2H_6$. The only product ion observed for this reaction is the $C_4H_9^+$ ion. The ICR work of Dunbar, Shen, and Olah[31] at low ionizing energy also shows only $C_4H_9^+$ ions, but the earlier ICR work of Wexler and Pobo[21] at 70 eV identifies $C_3H_7^+$ as a product ion. The $C_3H_7^+$ ion has also been identified as a product of this reaction by Blair, Heslin, and Harrison,[23] by Burt et al.,[27] and by Bennett, Lias, and Field.[20] Ausloos, Rebbert, and Sieck[28] identify the structure of the $C_4H_9^+$ product as sec-butyl ion and also report "resonant" H$^-$ transfer to regenerate the reactants. This latter reaction is not observable in the present case and may account for the rather small rate constant we measure for production of $C_4H_9^+$ ions. Blair, Heslin, and Harrison[23] also report H abstraction in reactions of $C_2D_5^+$ with C_2H_6 and report that the rate constant for this reaction is some 5.5 times the total for production of $C_4H_9^+$ and $C_3H_7^+$ ions. We have observed an apparent reaction to give $C_3H_7^+$ in impure samples of C_2H_6 and attribute the observation to a fast reaction with C_3H_8 impurity.[33] No ejection signals for this reaction were evident for very pure ethane samples.

$C_2H_6^+ + CH_4$. $C_2H_6^+$ ions are not reactive with methane. The upper limit measured for this reaction in the present work is 10^{-12} cm^3/s.

$C_2H_6^+ + C_2H_2$. The rate constant measured in this work for $C_2H_6^+$ ions from C_2H_6 at 16 eV is somewhat smaller than the value reported by Blair, Heslin, and Harrison.[23] These latter workers did not study the products for the reaction. The product distribution listed in Table VIII is the first measured for this reaction.

$C_2H_6^+ + C_2H_4$. This reaction has not been previously studied. Charge transfer is the only reaction channel observed, and the rate constant is large. For these experiments $C_2H_6^+$ ions were prepared from C_2H_6 at 16 eV.

$C_2H_6^+ + C_2H_6$. In contrast to the ICR product distribution previously reported by Dunbar, Shen, and Olah[31] for this reaction at 13 eV, we observe only two product ions at 13 eV: $C_3H_8^+$ and $C_3H_9^+$. At 30 eV ionizing energy we do observe $C_2H_4^+$, $C_3H_6^+$, and $C_3H_7^+$ as products of the

TABLE IX: Thermochemical Data Used for Calculating Heats of Reaction

Species	ΔH_f, kcal/mol	Source
Ions		
$CH_3{}^+$	260	a
$CH_4{}^+$	276	a
$C_2H_2{}^+$	317	a
$C_2H_3{}^+$	267	b
$C_2H_4{}^+$	253	a
$C_2H_5{}^+$	219	a
$C_2H_6{}^+$	245	a
$C_2H_7{}^+$	202	c
$C_3H_2{}^+$	365	a
$C_3H_3{}^+$	256 (cyclo)	d
$C_3H_4{}^+$	280 (allene)	a
$C_3H_5{}^+$	226 (allyl)	d
$C_3H_6{}^+$	229	a
$C_3H_7{}^+$	190 (iso)	a
$C_3H_8{}^+$	231	a
$C_3H_9{}^+$	195	e
$C_4H_2{}^+$	337	a
$C_4H_3{}^+$	307	a
$C_4H_4{}^+$	294	a
$C_4H_5{}^+$	237	a
$C_4H_6{}^+$	236	a
$C_4H_7{}^+$	204 (n-)	d
$C_4H_8{}^+$	209 (iso)	a
$C_4H_9{}^+$	176 (tertiary)	a
$C_4H_{10}{}^+$	212 (iso)	a
Neutrals		
H	52	a
H_2	0	a
CH_3	33	a
CH_4	−18	a
C_2H_2	54	a
C_2H_3	65	a
C_2H_4	12	a
C_2H_5	25	a
C_2H_6	−20	a

a National Standard Reference Data Series, National Bureau of Standards (U.S.), No. 26 (1969). b Reference 17. c From the proton affinity of ethane $PA(C_2H_6) = 144$ kcal/mol reported by D. K. Bohme, private communication. d F. P. Lossing, *Can. J. Chem.*, 50, 3973 (1972). e K. Hiraoka and P. Kebarle, *ibid.*, 53, 970 (1975).

reaction for excited $C_2H_6{}^+$ ions, but even at 30 eV we do not observe the $C_2H_5{}^-$, $C_4H_9{}^+$, or $C_4H_{10}{}^+$ ion products previously reported by Dunbar, Shen, and Olah.[31] At 70-eV ionizing energy, Wexler and Pobo[21] report $C_2H_4{}^+$, $C_2H_7{}^+$, and $C_3H_9{}^+$ ions from this reaction in earlier ICR work. We did not observe the reaction to give $C_2H_7{}^+$ ions at 13 or 30 eV, but did observe that it is possible to force the reaction to produce $C_2H_5{}^+$ ions by kinetic excitation of the $C_2H_6{}^+$ ions in low amplitude double resonance experiments (by observing an increase in the intensity at mass 29 when irradiating mass 30 at low radio-frequency amplitudes). The reactions to produce $C_2H_4{}^+$ and $C_2H_7{}^+$ are endothermic by +8 and +2 kcal/mol respectively. Blair, Heslin, and Harrison[23] also report $C_2H_4{}^+$ and $C_2H_5{}^+$ ions from this reaction in trapped-ion mass spectrometer experiments at 10.8 eV electron ionizing energy in ethane. Bennett, Lias, and Field[20] in high pressure mass spectrometer work also identify $C_3H_8{}^+$ and $C_3H_9{}^+$ as definite products of the reaction, but were unable to confirm whether or not $C_4H_9{}^+$ and $C_4H_{11}{}^+$ ions were also products. These workers used high electron energies, and their observation of $C_2H_7{}^+$ ions as a product of the reaction clearly shows that a certain fraction of their reactant ions were excited. Bennett, Lias and Field[20] also observed the collisionally stabilized intermediate, $C_4H_{12}{}^+$ at high pressures.

The photoionization cross section at threshold (107.6 nm) for formation of ground state $C_2H_6{}^+$ ions from C_2H_6 is too small, and the rate constant for the reaction is too small, for a good product distribution to be obtained using the present photoionization instrument. Photoionization experiments have been previously conducted on this reaction at high pressures using argon resonance radiation (106.7, 104.8 nm).[28,34] Even at these wavelengths it is clear that the ethane ions are excited since in at least one of these studies the reaction to give $C_2H_4{}^+$ was reported.[28] Searles, Sieck, and Ausloos[34] report in argon resonance line photoionization experiments that the reaction of $C_2D_6{}^+$ ions with C_2D_6 proceeds to give the deuterated equivalents of $C_3H_8{}^+$, $C_3H_9{}^+$, and $C_4H_9{}^+$ at low pressures (5 mTorr), with an increase in the yield of the deuterated equivalents of $C_4H_{11}{}^+$ and the dimer ion at 70 mTorr. These authors explain these results on the basis of stabilization of the intermediate ion. At very low pressures, 5×10^{-6} Torr in the ICR, we do not observe production of $C_4H_9{}^+$ or $C_4H_{11}{}^+$ ions and we apparently observe a much higher $C_3H_9{}^+/C_3H_8{}^+$ ratio than in the higher pressure work of Searles, Sieck, and Ausloos,[34] and of Bennett, Lias, and Field.[20] The rate constant measured in this work at 13 eV is in good agreement with the trapped-ion value of Blair, Heslin, and Harrison[23] at low ionizing energies. These latter workers show a large increase in the rate constant with increasing ionizing energy, which can explain the even higher value obtained by Bennett, Lias, and Field.[20]

Appendix

The heats of formation used for calculating the heats of reaction quoted in this work are listed in Table IX along with the source from which each number was taken. For hydrocarbon ions with several possible isomers, the heat of formation for the lowest energy structure was used in order to calculate a minimum heat of reaction. In most cases the heats of formation for several other higher energy structures are also given in the source listed for such ions.

References and Notes

(1) W. T. Huntress, Jr., and R. F. Pinizzotto, Jr., *J. Chem. Phys.*, **59**, 4742 (1973).
(2) J. K. Kim, L. P. Theard, and W. T. Huntress, Jr., *J. Chem. Phys.*, **62**, 45 (1975).
(3) V. G. Anicich and W. T. Huntress, Jr., *Rev. Sci. Instrum.*, **48**, 542 (1977).
(4) P. R. LeBreton, A. D. Williamson, and J. L. Beauchamp, *J. Chem. Phys.*, **62**, 1623 (1975).
(5) S. E. Buttrill, Jr., J. K. Kim, W. T. Huntress, Jr., P. R. LeBreton, and A. D. Williamson, *J. Chem. Phys.*, **61**, 2122 (1974).
(6) J. J. Myher and A. G. Harrison, *Can. J. Chem.*, **46**, 1755 (1968).
(7) N. G. Adams and D. Smith, *Chem. Phys. Lett.*, in press.
(8) F. P. Abramson and J. H. Futrell, *J. Chem. Phys.*, **45**, 1925 (1966).
(9) A. A. Herod and A. G. Harrison, *Int. J. Mass Spectrom. Ion Phys.*, **4**, 415 (1970).
(10) W. T. Huntress, Jr., J. B. Laudenslager, and R. F. Pinizzotto, Jr., *Int. J. Mass Spectrom. Ion Phys.*, **13**, 331 (1974).
(11) R. M. O'Malley and K. R. Jennings, *Int. J. Mass Spectrom. Ion Phys.*, **2**, 257 (1969).
(12) F. A. Baker and J. B. Hasted, *Phil. Trans. R. Soc. London*, **261**, 33 (1966).
(13) S. E. Buttrill, Jr., *J. Chem. Phys.*, **50**, 4125 (1969).
(14) M. S. B. Munson, *J. Phys. Chem.*, **69**, 572 (1965).
(15) S. E. Buttrill, Jr., *J. Chem. Phys.*, **62**, 1834 (1975).
(16) J. H. Futrell and T. O. Tiernan, *J. Phys. Chem.*, **72**, 158 (1968).
(17) S. E. Buttrill, Jr., J. K. Kim, W. T. Huntress, Jr., P. R. LeBreton, and A. D. Williamson, *J. Chem. Phys.*, **61**, 2122 (1974).
(18) M. T. Bowers, D. D. Elleman, and J. L. Beauchamp, *J. Phys. Chem.*, **72**, 3599 (1968).
(19) T. O. Tiernan and J. H. Futrell, *J. Phys. Chem.*, **72**, 3080 (1968).
(20) S. L. Bennett, S. G. Lias, and F. H. Field, *J. Phys. Chem.*, **76**, 3919 (1972).
(21) S. Wexler and L. G. Pobo, *J. Am. Chem. Soc.*, **93**, 1327 (1971).
(22) T. McAllister, *J. Chem. Phys.*, **56**, 5192 (1972).
(23) A. S. Blair, E. J. Heslin, and A. G. Harrison, *J. Am. Chem. Soc.*, **94**, 2935 (1972).
(24) M. S. B. Munson, J. L. Franklin, and F. H. Field, *J. Phys. Chem.*, **68**, 3098 (1964).

(25) F. H. Field and M. S. B. Munson, *J. Am. Chem. Soc.*, **87**, 3289 (1965).
(26) S. Wexler, A. Lifshitz, and A. Quattrochi, *Adv. Chem. Ser.*, **No. 58**, 193 (1966).
(27) J. A. Burt, J. L. Dunn, M. J. McEwan, M. M. Sutton, A. E. Roche, and H. I. Schiff, *J. Chem. Phys.*, **52**, 6062 (1970).
(28) P. Ausloos, R. E. Rebbert, and L. Wayne Sieck, *J. Chem. Phys.*, **54**, 2612 (1971).
(29) S. E. Buttrill, Jr., *J. Chem. Phys.*, **52**, 6174 (1970).

(30) W. T. Huntress, Jr., *J. Chem. Phys.*, **56**, 5111 (1972).
(31) R. C. Dunbar, J. Shen, and G. A. Olah, *J. Chem. Phys.*, **56**, 3794 (1972).
(32) K. Hiraoka and P. Kebarle, *J. Chem. Phys.*, **63**, 394 (1975).
(33) B. H. Solka, A. Y-K. Lau, and A. G. Harrison, *Can. J. Chem.*, **52**, 1798 (1974).
(34) S. K. Searles, L. Wayne Sieck, and P. Ausloos, *J. Chem. Phys.*, **53**, 849 (1970).

Polyelectrolyte Effects on Rates of Hydrated Electrons

C. D. Jonah, M. S. Matheson, and D. Meisel*

Chemistry Division, Argonne National Laboratory, Argonne, Illinois 60439 (Received April 25, 1977)

Publication costs assisted by Argonne National Laboratory

The effect of polyvinylsulfate (PVS) on the rate of the reaction of e_{aq}^- with several species highly reactive toward e_{aq}^- was investigated using the pulse-radiolysis technique. The rate of e_{aq}^- reactions with cations (Cu^{2+}, Cd^{2+}, Ni^{2+}, Zn^{2+}, $Ru(bpy)_3^{2+}$, $Fe(phen)_3^{2+}$, Cr^{3+}, Eu^{3+}) is greatly inhibited by the presence of the polyelectrolyte. On the other hand, the reaction with negatively or uncharged species (NO_3^- and O_2) is hardly affected. It is shown that using this kinetic method the effective number of available sites on the polymer can be titrated. Furthermore, the specificity constants of cations, inert toward e_{aq}^- (Mg^{2+}, Ca^{2+}, Ba^{2+}, Li^+, Na^+, K^+), could be determined by measuring their effect on the rate of the reaction of e_{aq}^- with a probe cation (Cu^{2+}) "condensed" on the polymer. As expected from measurements of thermodynamic properties of similar polyelectrolytes, and from theoretical models, it was found that divalent ions are bound to the polymer much stronger than are univalent ions. For ions of similar valence the specificity constant is larger, the smaller is the hydrated ionic radius.

Introduction

The interaction of polyelectrolytes with counterions has long been recognized to affect the thermodynamic properties (activity coefficients, osmotic coefficients, enthalpy of dilation, etc.) of the polyelectrolyte–counterions solutions.[2-5] This same interaction is expected, and often is found, to affect rates of charged species with the counterions. Such kinetic effects have been summarized in several review articles.[6-8] Most of these studies involve reactions in which at least one of the reactants is a bulky organic compound where the interaction between that reactant and the polyelectrolyte is not necessarily a pure electrostatic interaction. Large enhancement coefficients can be obtained for such reactions in which the interaction is primarily electrostatic, as was shown by the work of Morawetz and co-workers[9] and Ise and co-workers[10] on sensitized aquation of, and electron transfer to, Co(III) complexes.

In this study we explore the effect of small concentrations of polyvinylsulfate (PVS) on the rate of hydrated electrons, e_{aq}^-, with simple ions, using the pulse radiolysis technique. Due to the simplicity of the reactants the interaction is expected to be purely electrostatic. As expected, the rate of the reaction of e_{aq}^- with various cations is strongly retarded when the cations reside in the potential field of the polyelectrolyte. This results from exclusion of the cations from the bulk of the solution, exclusion of e_{aq}^- from the polymer field, and salt effect on the activity coefficient in the polymer domains.[7,8] It is expected that the kinetic effects would yield information relevant to the effective number of available sites in the polymer, the relative efficiency of fixation of the cations on the polyelectrolyte, and the occurrence of specific binding to macromolecules. The pulse radiolysis technique has been previously applied to studies of the interaction between several dyes and polyanions and rates of e_{aq}^- and

OH radicals with the same polyanions were reported.[11]

Experimental Section

The potassium salt of PVS was purified as described by Breslow and Kutner.[12] The specific viscosity of 1% PVS in water was measured and from the correlation between this and the intrinsic viscosity in 0.1 M Na_2SO_4[12] the average molecular weight was determined to be ~250 000. Concentrations for the polymer are given in equivalent units of charge (6.17×10^{-2} equiv/L for 1% PVS) and so are the concentrations for the metal ions ($n(M^{n+})$ equiv/L). Solutions for irradiations were prepared from 1% PVS stock solution a few hours before irradiation. All other chemicals were of reagent grade. Water used in this study was triply distilled. In order to avoid unnecessary effects of ions other than those studied no buffer was used in this study. However, the pH of the solutions was measured and found to be in the range of 6.5–5.5, except for those experiments where H^+ was deliberately added. Thus the effect of $[H^+]$ ions on the rate of e_{aq}^- decay is believed to occur only at the slowest decay rates of e_{aq}^-. Unless otherwise stated all solutions were deaerated by bubbling prepurified argon for 10 min using the syringe technique. The same technique was used to obtain the desired concentration of oxygen when needed.

The pulse radiolysis setup has already been described previously.[13] Electron pulses of ~4 ns width produced $(1–2) \times 10^{-6}$ M total concentration of radicals in 5-cm length cells. All solutions contained 10 mM of *tert*-butyl alcohol as OH scavenger. The *tert*-butyl alcohol radicals thus produced by hydrogen abstraction are known to be inert toward all scavengers used. The decay of e_{aq}^- ($(0.5–1) \times 10^{-6}$ M per pulse) was followed at 600 nm. The small yield (about 20% of the yield of e_{aq}^-) of hydrogen atoms cannot have any effect on the measured kinetics. The decay of e_{aq}^- was found to follow a pseudo-first-order rate
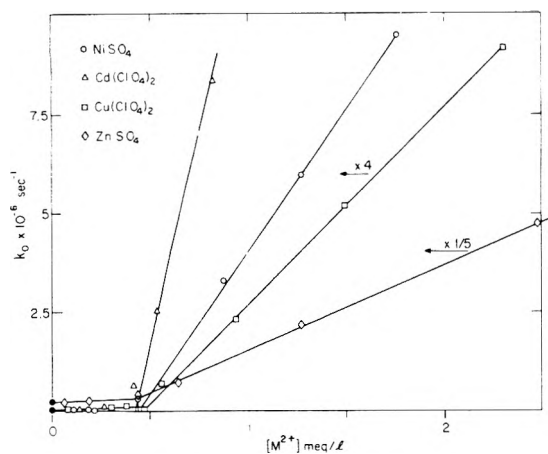
Figure 1. Dependence of the observed pseudo-first-order rate constant (corrected to $\mu = 0$) for the reaction of e_{aq}^- with divalent cations in the presence of 0.01% PVS. Numbers above arrows indicate multiplication factors for the ordinate scale.

Figure 2. Dependence of the observed pseudo-first-order rate constant for the reaction of e_{aq}^- with metal chelates. Experimental conditions as in Figure 1.

Figure 3. Dependence of the observed pseudo-first-order rate constant for the reaction of e_{aq}^- with trivalent cations. Experimental conditions as in Figure 1.

law in all experiments. The risetime of the electronic setup was less than 20 ns and cannot affect any of our results.

Results and Discussion

Effect of PVS on the Rate of e_{aq}^- with Cations. The effect of 0.01% PVS on the rate of the reaction of e_{aq}^- with several highly reactive divalent cations was measured at different concentrations of the cations. Results are summarized in Figure 1, where the pseudo-first-order rate constant for the reaction

$$M^{n+} + e_{aq}^- \rightarrow M^{(n-1)^+} \qquad (1)$$

is plotted against the concentration of M^{2+} (expressed in equiv/L). The range of k_1 for the free metal cations is from 6.4×10^{10} M^{-1} s^{-1} for Cd^{2+} to 1.5×10^9 M^{-1} s^{-1} for Zn^{2+}.[14] As can be seen in Figure 1, at low concentrations of M^{2+} the rate of reaction 1 is strongly inhibited. However, as soon as a certain value of $[M^{2+}]$ is reached the rate sharply increases, yielding from the slope nearly the same rate constant as in the absence of PVS. Obviously the interaction of the counter cations with the potential field of the negatively charged polyelectrolyte strongly inhibits its rate of the reaction with e_{aq}^-. In fact, with none of these metal ions could we measure k_1 for M^{n+}, which is in the potential field of the polyion. When no more M^{n+} can be added to the polymer the rate is restored. The extremely sharp increase in the observed rate constants (Figures 1–3) is a clear demonstration of the condensation phenomenon in polyelectrolytes often predicted[3,19] but rarely observed with such distinction.

In the absence of the metal cations the rate of the decay of e_{aq}^- hardly changes on addition of up to 0.1% PVS, which puts an upper limit for the rate constant of e_{aq}^- with polyvinylsulfate of $\leq 1.2 \times 10^6$ L/(equiv × s). On addition of small concentrations of M^{2+} some fluctuations, sometimes ranging up to an increase of ~50% in e_{aq}^- decay rate, were noticed. However, when the rate of decay of e_{aq}^- is that slow (tens of microseconds), even extremely low concentrations of impurities (most probably O_2 or H^+ at the level of ~10^{-6} M) would cause these random fluctuations.

The rate of the reaction of e_{aq}^- with M^{2+} in the presence of PVS can be analyzed in terms of the rate of bound and free cations:
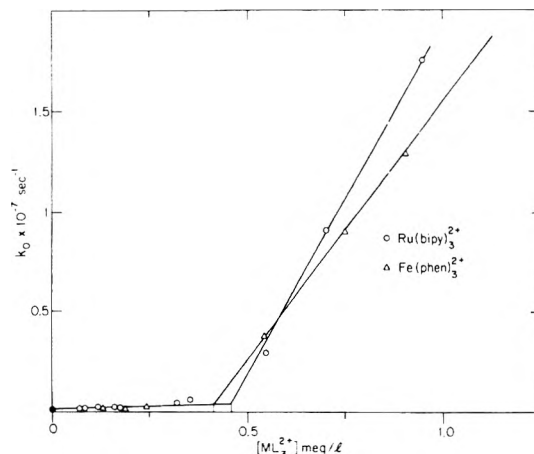
$$M^{n+}_f + e_{aq}^- \rightarrow M^{(n-1)^+}_f \qquad (1a)$$

$$M^{n+}_b + e_{aq}^- \rightarrow M^{(n-1)^+}_b \qquad (1b)$$
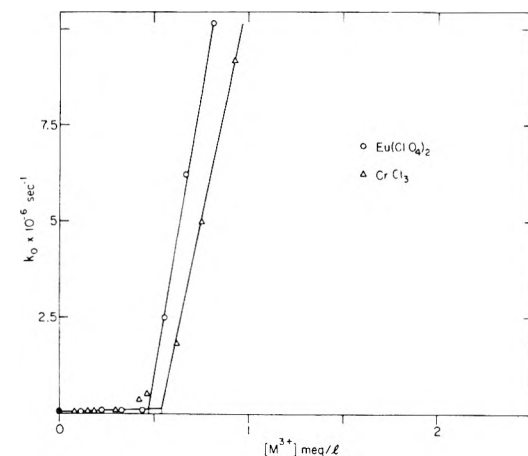
where the indices b and f denote bound and free cations, respectively. The observed pseudo-first-order rate constant k_{obsd} thus would be given by

$$k_{obsd} = k_{1a}[M^{n+}]_f + k_{1b}[M^{n+}]_b \qquad (I)$$

From Figure 1, it is clear that $k_{1b} \ll k_{1a}$ and the contribution of the second term on the right-hand side of eq I is very small even when $[M^{2+}]_b$ is high enough to cover nearly all of the effective number of available sites on the polymer. Since the ionic strength of the solution was not constant during most of the experiments described in this study, the rate constants to be reported were all corrected to zero ionic strength for the primary salt effect using

$$\log \frac{k}{k_0} = -\frac{Z_{M}^{n+} \mu^{1/2}}{1 + \mu^{1/2}} \qquad (II)$$

In calculating the ionic strength, μ, the amount of the free cations, including the original counterion, and the total amount of the added coion were all taken into account. These corrected rate constants were compared with rate constants measured or corrected to $\mu = 0$.[15] The strikingly sharp increase in k_{obsd} would not allow us to calculate the effective degree of dissociation of M^{2+}_b from the polymer. We, however, can use the dependence of the rate constant on $[M^{2+}]$ in the polyelectrolyte solution for titrating the effective number of available sites, $[P]_{eff}$, on the polymer. In Table I we summarize the results of such titrations with a variety of different metal cations along with the rate constants for the reaction of e_{aq}^- with M^{n+}. In Figure 2,

TABLE I: Effect of 0.01% PVS on the Rate of the Reaction of e_{aq}^- with Various Cations

Reactant	k_1,[a] $M^{-1} s^{-1}$	k_{1a},[b] $M^{-1} s^{-1}$	$[P]_{eff}$,[c] equiv/L
$ZnSO_4$	$(1.5 \pm 0.2) \times 10^9$	8.9×10^8	4.4×10^{-4}
$NiSO_4$	$(2.2 \pm 0.1) \times 10^{10}$	1.5×10^{10}	4.5×10^{-4}
$Cu(ClO_4)_2$	$(4.5 \pm 1.0) \times 10^{10}$	4.0×10^{10}	4.7×10^{-4}
$Cd(ClO_4)_2$	$(6.4 \pm 1.0) \times 10^{10}$	4.3×10^{10}	4.3×10^{-4}
$Ru(bpy)_3Cl_2$	$(6.0 \pm 1.0) \times 10^{10}$	7.0×10^{10}	4.6×10^{-4}
$Fe(Phen)_3(ClO_4)_2$	$(7.2 \pm 1.0) \times 10^{10}$ [d]	5.0×10^{10}	4.2×10^{-4}
$Eu(ClO_4)_3$	$(6.1 \pm 0.5) \times 10^{10}$	8.0×10^{10}	4.6×10^{-4}
$CrCl_3$	$(6.0 \pm 0.5) \times 10^{10}$	7.0×10^{10}	(5.3×10^{-4})
			$[P]^f_{eff} = (4.5 \pm 0.2) \times 10^{-4}$
O_2	$(1.9 \pm 0.2) \times 10^{10}$	1.95×10^{10}	
$NaNO_3$	$(1.0 \pm 0.1) \times 10^{10}$	8.75×10^9	

[a] When available taken from ref 15 at $\mu = 0$ with the range of most reliable values in ref 14. Otherwise taken from ref 14. [b] Taken from the slopes of the lines in Figures 1–3, above full coverage of available sites and corrected to $\mu = 0$. [c] Effective concentration of available sites in equivalents/liters. The stoichiometric concentration is 6.17×10^{-4} M. [d] Determined in this study. [f] Average of all the cations excluding Cr^{3+} (see text).

we display similar titration experiments of $[P]_{eff}$ in 0.01% PVS with the chelates tris(2,2'-bipyrine)ruthenium(II) and tris(1,10-phenanthroline)iron(II). In Figure 3, similar results for the trivalent cations of $Eu(ClO_4)_3$ and $CrCl_3$ are shown. It can be seen in Table I that all these cations, of different size and valency, yield the same $[P]_{eff}$ within the experimental error $[(4.5 \pm 0.2) \times 10^{-4}$ equiv/L]. This amounts to about 70% of the total stoichiometric concentration of sulfate groups on the polymer and is slightly larger than the fraction recently obtained from quenching and quenching reversal of excited $Ru(bpy)_3^{2+}$ emission.[16]

Obviously, $[P]_{eff}$ is very weakly, if at all, dependent on the radius or charge of the cation residing in the potential domains of the polyelectrolyte, as far as protection against reaction with e_{aq}^- is concerned. During the experiments with the trivalent cations some precipitation could be observed at concentrations lower than the breakpoint in Figure 3. This precipitation became heavier the closer $[M^{3+}]$ came to $[P]_{eff}$ and could be observed with trivalent cations, such as Nd^{3+} and In^{3+}, which were not investigated for their reactivity with e_{aq}^-. Nonetheless, k_{obsd} was measured for the reactants shown in Figure 3 without any difficulty. This is undoubtedly a fractionation precipitation phenomenon along the molecular weight distribution, which is often observed in polyelectrolytes.[17] Indeed, on increasing the concentration of PVS the precipitates could be redissolved.

The titration with Cr^{3+} yields a value of $[P]_{eff}$ which is $\sim$20% higher than the other cations. This is probably a result of some hydrolysis of the Cr^{3+} cation. The stability constant for $Cr(OH)^{2+}$ is approximately 10^{-4} M^{-1}. At the pH used in these experiments (6–5.8) most of the Cr^{3+} would be expected to complex with OH^- and Cr^{3+} would then behave like a divalent cation. However, the results in Table I indicate that most of the Cr^{3+} ions in the potential field of the polyelectrolyte are uncomplexed to OH^-.

Effect of Inert Cations on Binding of Cu^{2+} to PVS. In a recent communication, we have shown that Cu^{2+} cations bound to PVS can be replaced by practically any cation.[16] In such a situation the rate of e_{aq}^- decay in solutions containing Cu^{2+} bound to PVS should increase on addition of other cations which by themselves are inert toward a reaction with e_{aq}^-. In order to check this proposition and in order to obtain some quantitative measurement of the relative association constants of such inert cations we examined the rate of decay of e_{aq}^- in 0.01% PVS and 1.17 $\times 10^{-4}$ M $Cu(ClO_4)_2$ at different concentrations of alkaline and alkaline-earth cations. The experimental results are shown in Figure 4 for K^+, Na^+, and Li^+ and in Figure 5 for Ba^{2+}, Ca^{2+}, and Mg^{2+}. In all cases the rate constant for e_{aq}^- with Cu^{2+} is nearly completely restored to its value
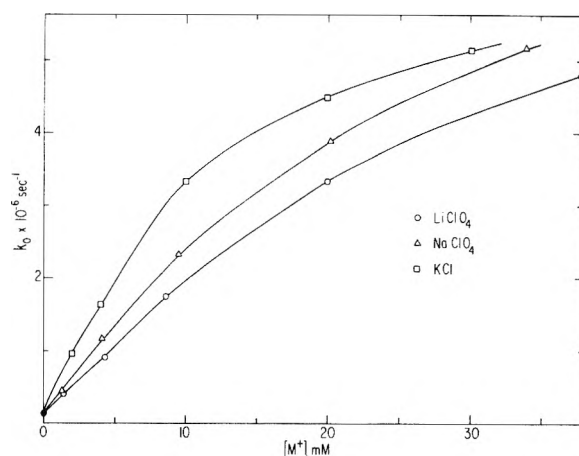
Figure 4. Effect of alkali metal cations on the rate constant of e_{aq}^- + Cu^{2+} in the presence of 0.01% PVS. $[Cu(ClO_4)_2] = 1.7 \times 10^{-4}$ M. The pseudo-first-order rate constant, k_0, is corrected for ionic strength effects to $\mu = 0$.
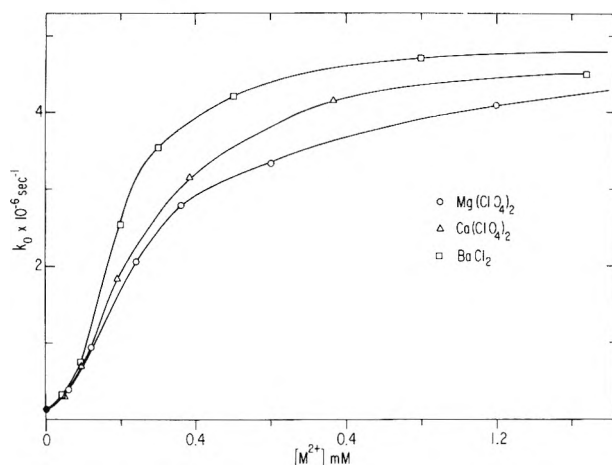
Figure 5. Effect of alkaline-earth cations on the rate constant of e_{aq}^- + Cu^{2+} in the presence of 0.01% PVS. Conditions for k_0 measurements are the same as in Figure 4.

in plain water on addition of the inert cations. This increase in the rate constant is clearly not a primary salt effect, which would be in the reverse direction, but should be attributed to the release of Cu^{2+} ions from the polymer to the solution. As expected, the divalent cations are much more effective in replacing Cu^{2+} than are the monovalent cations. However, the monovalent ions, at sufficiently higher concentration, are capable of replacing all Cu^{2+} on the polymer and releasing it to the bulk of the solution. The ability of the alkaline ions to replace divalent cations

TABLE II: Specificity Constants Obtained from the Effect of Inert Monovalent Cations on the Rate of Reaction of e_{aq}^- with Cu^{2+} [a]

Inert salt	$[M^+]$,[b] M	k_0,[c] s^{-1}	$[Cu^{2+}]_f/$ $[Cu^{2+}]_b$	$[M^+]_b/$ $[M^+]_f$	K_2[d]
KCl	2×10^{-3}	9.02×10^5	0.206	0.108	2.42×10^{-3}
	4×10^{-3}	1.57×10^6	0.425	0.066	1.85×10^{-3}
	1×10^{-2}	2.25×10^6	1.612	0.035	1.98×10^{-3}
	2×10^{-2}	4.22×10^6	4.043	0.020	1.62×10^{-3}
$NaClO_4$	1.36×10^{-3}	3.79×10^5	0.078	0.135	1.41×10^{-3}
	4.08×10^{-3}	1.11×10^6	0.268	0.060	9.57×10^{-4}
	9.52×10^{-3}	2.25×10^6	0.746	0.032	7.73×10^{-4}
	2.04×10^{-2}	3.82×10^6	2.656	0.019	9.33×10^{-4}
$LiClO_4$	1.43×10^{-3}	3.41×10^5	0.069	0.128	1.14×10^{-3}
	4.3×10^{-3}	8.48×10^5	0.191	0.054	5.69×10^{-4}
	8.6×10^{-3}	1.68×10^6	0.468	0.032	5.00×10^{-4}
	2.0×10^{-2}	3.26×10^6	1.623	0.018	5.18×10^{-4}

[a] 0.01% PVS and 1.17×10^{-4} M $Cu(ClO_4)_2$ in all solutions. $[P]_{eff} = 4.5 \times 10^{-4}$ equiv/L from Table I was assumed.
[b] The concentration of the added cation. [c] Observed pseudo-first-order rate constant corrected to $\mu = 0$ and corrected for the decay of e_{aq}^- in the absence of Cu^{2+}. [d] The specificity constant was calculated as $K_2 = ([Cu^{2+}]_f/[Cu^{2-}]_b)([M^+]_b/[M^+]_f)^2$.

TABLE III: Specificity Constants Obtained from the Effect of Inert Divalent Cations on the Rate of Reaction of e_{aq}^- with Cu^{2+} [a]

Inert salt	$[M^{2+}]$,[b] M	k_0, s^{-1}	$[Cu^{2+}]_f/$ $[Cu^{2+}]_b$	$[M^{2+}]_b/$ $[M^{2+}]_f$	K_2[d]
$BaCl_2$	3.0×10^{-4}	3.5×10^6	1.87	1.59	2.97
	5.0×10^{-4}	4.2×10^6	3.72	0.67	2.48
	1.0×10^{-3}	4.7×10^6	7.30	0.27	1.95
$CaCl_2$	1.92×10^{-4}	1.87×10^6	0.52	3.36	1.74
	3.84×10^{-4}	3.19×10^6	1.45	0.86	1.24
	7.68×10^{-4}	4.17×10^6	3.52	0.35	1.23
	1.44×10^{-3}	4.51×10^6	5.39	0.17	0.90
$Mg(ClO_4)_2$	2.4×10^{-4}	2.07×10^6	0.61	1.74	1.06
	3.6×10^{-4}	2.82×10^6	1.09	0.89	0.97
	6.0×10^{-4}	3.35×10^6	1.65	0.43	0.71
	1.2×10^{-3}	4.13×10^6	3.36	0.20	0.67

[a-c] See the corresponding footnote in Table II. [d] The specificity constant was calculated as $K_2 = ([Cu^{2+}]_f/[Cu^{2+}]_b) \cdot ([M^{2+}]_b/[M^{2+}]_f)$.

which are condensed on polyions seems to contradict the conclusions from the divergence of the phase integral in the Oosawa[3] and the Manning[19] models of the infinitely long charged rod. We do not believe that we are measuring an increased rate of reaction of e_{aq}^- with bound Cu^{2+}, because the screening of e_{aq}^- by such small concentrations of monovalent ions would not enable such a large increase in penetration of e_{aq}^- into the repulsive field of the polymer. The order of effectiveness in displacing Cu^{2+} for each of the groups is $K^+ > Na^+ > Li^+$ and $Ba^{2+} > Ca^{2+} > Mg^{2+}$. This same order of effectiveness of binding was also found for high charge density polyions in dilatometric measurements,[20] osmotic coefficient measurements,[21] enthalpy of dilution,[22] neutralization titrations,[23] etc. Obviously the order of increased degree of association parallels the order of decrease in the effective radius of the hydrated ions as is expected for an interaction which is principally Coulombic.[3]

The results in Figures 4 and 5 can be quantitatively analyzed in terms of the specificity constant of the following appropriate reaction

$$Cu^{2+}_b + \frac{2}{n}M^{n+}_f \rightleftarrows Cu^{2+}_f + \frac{2}{n}M^{n+}_b \qquad (2)$$
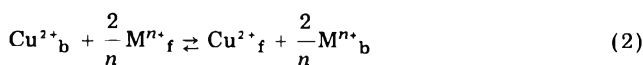
and

$$K_2 = \frac{[Cu^{2+}]_f}{[Cu^{2+}]_b} \left(\frac{[M^{n+}]_b}{[M^{n+}]_f}\right)^{2/n} \qquad (III)$$

From the observed pseudo-first-order rate constant for the

reaction of e_{aq}^- with Cu^{2+} (corrected to $\mu = 0$ and corrected for the slow decay in the absence of Cu^{2+}) and taking $k_{1a} = 4.5 \times 10^{10}$ M^{-1} s^{-1}, we calculate $[Cu^{2+}]_f$ and from this $[Cu^{2+}]_b$ as well. Taking the effective concentration of available sites as $[P]_{eff} = 4.5 \times 10^{-4}$ equiv/L (Table I) in 0.01% PVS we calculate $[M^{n+}]_b$ and $[M^{n+}]_f$. Results are summarized in Table II for the monovalent ions and Table III for the divalent ions. The concentration of e_{aq}^- is less than 1% of $[P]_{eff}$ so that the preexisting equilibrium cannot be perturbed by the reaction with e_{aq}^-. In Table II the background concentration of the counterion (6.17×10^{-4} M K^+) was taken into consideration. Although this is strictly correct for K^+, we added this concentration to Li^+ and Na^+ as well. Since the K_2 for K^+ is somewhat higher than the corresponding specificity constants for Li^+ and Na^+ this would tend to artificially increase the calculated K_2 for the corresponding metal cation at the lower concentration of M^+. In Table III the concentration of the background K^+ counterions was neglected since their effect is much smaller than that of the divalent ions. Inspection of Tables II and III reveals that K_2 is fairly constant over quite a large range of $[Cu^{2+}]_f/[Cu^{2+}]_b$, however, some drift in the direction of decreasing K_2 on increasing $[M^{n+}]$ can be observed. A similar drift is observed also in the case of the displacement of K^+ by H^+ on PVS as will be discussed below. Although the drift is quite small, we note that excluded volume considerations in the charged rod model[24] show that the specificity constant for replacing a larger ion by a smaller one should drop on increasing the mole fraction of the smaller ions. This is the case for K^+,

TABLE IV: Specificity Constants for the Exchange of K^+ by H^+ in 0.01% PVS

$[H^+]$, M	k_0,[a] s^{-1}	$[H^+]_b/[H^+]_f$[b]	$[K^+]_f/[K^+]_b$[c]	K_4
3.68×10^{-5d}	2.30×10^5	2.68	0.46	1.23
7.36×10^{-5d}	5.86×10^5	1.89	0.54	1.01
1.00×10^{-4d}	9.70×10^5	1.37	0.58	0.79
1.47×10^{-4d}	1.57×10^6	1.15	0.66	0.76
3.15×10^{-5e}	2.89×10^5	1.50	1.53	2.30
5.25×10^{-5e}	6.88×10^5	0.76	1.48	1.12
8.40×10^{-5e}	1.11×10^6	0.74	1.49	1.10
1.05×10^{-4e}	1.48×10^6	0.53	1.46	0.93
1.52×10^{-4e}	2.23×10^6	0.57	1.44	0.83
2.10×10^{-4e}	3.00×10^6	0.61	1.44	0.88
4.20×10^{-4e}	5.96×10^6	0.62	1.41	0.88

[a] Corrected for the decay of e_{aq}^- in the absence of added acid and to $\mu = 0$. [b] Assuming $k_3 = 2.3 \times 10^{10}$ M^{-1} s^{-1}.[14] [c] Assuming $[P]_{eff} = 4.5 \times 10^{-4}$ equiv/L from Table I. [d] Using sulfuric acid. [e] Using perchloric acid and keeping constant ionic strength at $([H^+] - [K^+]) = 5 \times 10^{-4}$ M above the background 6.17×10^{-4} M K^+.

Na^+, and Ba^{2+} (for which the effective hydrated radii are 1.5, 2, and 2.5 Å, respectively, compared with 3 Å for Cu^{2+})[25] given in Tables II and III. For Ca^{2+} the hydrated radius is comparable to that of Cu^{2+} while Mg^{2+} is somewhat bigger ($r = 4$ Å).

The Effect of PVS on the Rate of e_{aq}^- with H^+. Since the sulfate groups on the polyvinylsulfate polymer are usually assumed to behave as strong acids we considered it of some interest to measure the rate of the reaction of e_{aq}^- with H^+ ions in the presence of PVS. The decay of e_{aq}^- was then measured in 0.01% PVS at various concentrations of added H_2SO_4. The results of two sets of experiments are summarized in Table IV. In the first set the acid was added to 0.01% PVS solutions, letting the ionic strength change. In the other set the total ionic strength was kept constant by adding KCl and $HClO_4$ so that $([H^+] + [K^+]) = 5 \times 10^{-4}$ M. The results in Table IV clearly indicate that the rate of reaction 3 is slowed down

$$H^+ + e_{aq}^- \to H \qquad (3)$$

by the addition of the polymer. However, contrary to the case of the multivalent metal cations the inhibiting effect is much smaller and reaction 3 is relatively fast even when the added $[H^+]$ is much smaller than $[P]_{eff}$. At least two mechanisms can explain this relatively small inhibiting effect. Either the rate of $e_{aq}^- + H_b^+$ is relatively high (i.e., relatively high value for k_{1b} in eq I) or relatively small amounts of H^+ are bound while a large fraction is free in the bulk of the solution (both $[H^+]_b$ and k_{1b} are small). The results in the previous section indicate that e_{aq}^- is practically completely excluded from the potential domains of the polymer and we would not expect this behavior to change on addition of small amounts of H^+. We, therefore, assume that k_{1b} is vanishingly small and only free H^+ is liable to react with e_{aq}^-. This assumption is in line with the commonly accepted perception of the state of H^+ in strongly acidic polyelectrolytes. Under this assumption the observed rate constant can again be used as a probe to determine the concentration of H_f^+ and thus determine the relative association constant, namely, the specificity constant of H^+ to K^+:

$$H_f^+ + K_b^+ \rightleftharpoons H_b^+ + K_f^+ \qquad (4)$$

For these calculations we also assume that the effective concentration of available sites is always occupied either by K^+ or by H^+ and is equal to $[P]_{eff} = 4.5 \times 10^{-4}$ equiv/L obtained in Table I. This assumption is the expected result of the charged rod model[3,19] and is probably more strictly

fulfilled in those experiments where a small excess of K^+ was added at constant ionic strength. The results in Table IV indicate that the amount of specificity between K^+ and H^+ is rather small ($K_4 \sim 1$). A comparison of the effectiveness of binding of the alkaline cations (Table II) with that of H^+ indicates that the latter is more strongly bound than are Na^+ and Li^+. Since the charge of the H^+ ions can be channeled to the hydrogen atoms of the hydration water molecules which are closer to the backbone, this might provide the capability of closer approach for H^+. The decrease in K_4 observed in Table IV with increasing $[H^+]$ agrees with that interpretation of closer approach of H^+.

The Effect of PVS on the Rate of e_{aq}^- with NO_3^- and O_2. The existence of potential fields around the dissolved PVS molecules is expected to inhibit the rate of reaction between oppositely charged reactants, by binding one reactant and repelling the other. However, only small effects are expected for reactions of e_{aq}^- in PVS solutions if the added reactant is also negatively charged or if it is uncharged.[18] In order to check this expectation we measured the rate of the reaction of e_{aq}^- with NO_3^- ions and with oxygen in the presence of 0.01% PVS. As can be seen in Table I the rate constants of these reactions remain practically unchanged by the addition of PVS.

Conclusion

The pulse radiolysis technique is shown here to serve as a powerful tool in studying the counterion–polyion interactions. The reactants chosen here, as well as the polyelectrolyte, were those for which the interactions are believed to be mainly Coulombic. It is shown that the effect of size and charge of the counterion can be studied in great detail as well as the effective number of available sites. The extremely sharp increase in the rate constant for the reaction of e_{aq}^- with the metal cation was used as the end point in a kinetic titration of the effective available sites. Ions of smaller size and especially higher valence are shown to be bound more strongly than are those of lower valence and larger size.

References and Notes

(1) Work performed under the auspices of the Divison of Physical Research of the U.S. Energy Research and Development Administration.
(2) H. Morawetz, "Macromolecules in Solution", Interscience, New York, N.Y., 1965.
(3) F. Oosawa, "Polyelectrolytes", Marcel Dekker, New York, N.Y., 1971.
(4) E. Selegny, M. Mandel, and U. Strauss, Ed., "Polyelectrolytes", D. Reidel Publishing Co., Dordrecht, Holland, 1974.
(5) A. Rembaum and E. Selegny, Ed., "Polyelectrolytes and Their Applications", D. Reidel Publishing Co., Dordrecht, Holland, 1975.
(6) Reference 2, Chapter 9, p 409.
(7) N. Ise in ref 5, p 71.
(8) H. Morawetz, *Acc. Chem. Res.*, **3**, 354 (1970).
(9) (a) H. Morawetz and B. Vogel, *J. Am. Chem. Soc.*, **91**, 563 (1969); (b) H. Morawetz and G. Gordimer, *ibid.*, **92**, 7532 (1970).
(10) (a) N. Ise and Y. Matsuda, *J. Chem. Soc., Faraday Trans. 1*, **69**, 99 (1973); (b) S. Kunugi and N. Ise, *Z. Phys. Chem. (Frankfurt am Main)*, **91**, 174 (1974).
(11) E. A. Balazs, J. V. Davies, G. O. Phillips, and D. S. Scheufele, *J. Chem. Soc. C*, 1420, 1424, 1429 (1968).
(12) D. Breslow and A. Kutner, *J. Polym. Sci.*, **23**, 295 (1958).
(13) S. Gordon, K. H. Schmidt, and E. J. Hart, *J. Phys. Chem.*, **81**, 104 (1977).
(14) M. Anbar, M. Bambenek, and A. B. Ross, *Natl. Stand. Ref. Data Ser., Natl. Bar. Stand., No. 43* (1973).
(15) E. Peled and G. Czapski, *J. Phys. Chem.*, **74**, 2903 (1970).
(16) D. Meisel and M. S. Matheson, *J. Am. Chem. Soc.*, in press.
(17) J. E. Scott in "Methods of Biochemical Analysis", D. Glick, Ed., Interscience, London, 1960.
(18) (a) H. Morawetz, *J. Polym. Sci.*, **42**, 125 (1960); (b) H. Morawetz and J. A. Shafer, *J. Phys. Chem.*, **67**, 1293 (1963).
(19) G. Manning, ref 4, p 9.

(20) U. Strauss, ref 4, p 79.
(21) (a) D. Kozak, J. Kristen, and D. Dolar, *Z. Phys. Chem. (Frankfurt am Main)*, **76**, 85 (1971); (b) D. Kozak and D. Dolar, *ibid.*, **76**, 93 (1971).
(22) J. Skerjanc, *J. Phys. Chem.*, **77**, 2225 (1973).

(23) M. Rinaudo, M. Milas, J. LeMoigne, and P. Gramain, *Eur. Polym. J.*, **8**, 1073 (1972).
(24) H. P. Gregor and J. M. Gregor, *J. Chem. Phys.*, **66**, 1934 (1977).
(25) I. Klotz and R. Rosenberg, "Chemical Thermodynamics", W. A. Benjamin, Mellon Park, Calif., 1972, p 386.

A Comparative Analysis of the Interaction of Mannitol with Borate by Calorimetric and pH Techniques

W. J. Evans,* V. L. Frampton, and A. D. French

Southern Regional Research Center,[†] New Orleans, Louisiana 70179 (Received March 30, 1977)

Publications costs assisted by the Southern Regional Research Center

Thermodynamic aspects of the mannitol–borate interaction in aqueous solution were investigated by microcalorimetry and pH measurements. Both the calorimetric and pH analysis are consistent with the view that two successive equilibria are involved in this reaction. An iterative method was used to calculate K and ΔH values from the calorimetric data, whereas a program written in Fortran IV language was used to determine K values from the pH measurements. Values of the overall complexing constant derived from these two procedures are in reasonable accord, although the calorimetric ΔH values are not in agreement with those reported from temperature coefficient studies of pH on the mannitol–borate system. In general, K values derived from the calorimetric and pH measurements on the mannitol–borate system are not in agreement with previously reported values, which for the most part were determined from pH and potentiometric measurements on the mannitol–boric acid system. However, values of the overall complexing constant derived from pH measurements on the mannitol–boric acid system in the present work agree reasonably well with those derived from the calorimetric and pH measurements on the mannitol–borate system.

Introduction

The principal requirement for the reaction of polyols with borate, that the hydroxyl groups must be adjacent and cis, has made the reaction extremely useful in elucidating the structures of polyhydroxy compounds. It is now generally accepted that polyols of the proper configuration react with a $B(OH)_4^-$ ion in aqueous solution to form two types of complexes:
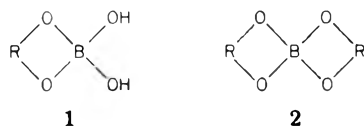
However, considerable controversy existed for many years concerning both the formation and stoichiometries of these compounds. Isbell et al. have given a lucid review of prior work.[1]

Aside from its usefulness in structural studies, the reaction of polyols with borates has far-reaching implications. It is well established that plants require small amounts of borate.[2,3] Many compounds of biological importance, such as, vitamins, coenzymes, enzyme substrates, and polysaccharides, contain hydroxyl groups in a position favorable to react with borate. We report in this paper the results of direct calorimetric measurements of the changes in enthalpy accompanying the interaction of borate with the simple polyhydroxy compound, mannitol. Values of the thermodynamic parameters, $\Delta G°$, $\Delta H°$, and $\Delta S°$, have been derived from the calorimetric data, and in addition, $\Delta G°$ values have been derived from pH measurements.

TABLE I: Heats of Interaction of Mannitol with Borate at 25 °C[a]

Mannitol concn, M	$-Q_{expt}$, mcal	$-Q_{calcd}$, mcal	$-(Q_{expt} - Q_{calcd})$, mcal	Final pH
0.09000	136.21	136.28	−0.07	6.722
0.08000	133.01	133.02	−0.01	6.918
0.07000	128.36	128.24	0.02	7.144
0.06000	121.12	121.00	0.12	7.425
0.05000	109.98	110.08	−0.10	7.724
0.04000	94.24	94.56	−0.32	8.055
0.03000	75.04	74.59	−0.45	8.378
0.02000	51.17	51.33	0.16	8.688
0.01000	26.09	26.13	0.04	8.945

[a] Borate concentration = 0.02708 M.

TABLE II: Thermodynamic Parameters for the Interaction of Borate (B⁻) with Mannitol (P) at 25 °C

	log K	$-\Delta G°$, kcal/mol	$-\Delta H°$, kcal/mol	$-\Delta S°$, eu
B⁻ + P = BP⁻	3.03 ± 0.05	4.18 ± 0.05	4.45 ± 0.06	1.1 ± 0.1
BP⁻ + P = BP₂⁻	2.05 ± 0.10	2.80 ± 0.10	4.75 ± 0.11	6.5 ± 0.2
B⁻ + 2P = BP₂⁻	5.08 ± 0.05	6.90 ± 0.05	9.20 ± 0.05	7.6 ± 0.1

The information presented should be useful in interpreting the action of borate on more complex materials.

Experimental Section

Materials. Mannitol, boric acid, and sodium tetraborate decahydrate (borax) were all analytical grade reagents. Concentrations of all mannitol and boric acid solutions were determined by weighing and appropriately diluting then with deionized, distilled water. The borax solutions were standardized with standard HCl, using methyl red

indicator. All solutions were prepared just prior to use.

Calorimetric Measurements. Heats of interaction of borate with mannitol were determined with a flow modification of a microcalorimeter previously described.[4] In a typical experiment, approximately 0.3 mL each of mannitol and borate solutions were flowed from two 10-mL Hamilton gas tight syringes into the calorimeter at equal flow rates of approximately 0.005 mL/s. Flow times were precisely controlled by a timing device connected to a Harvard Apparatus Co. infusion pump containing the two syringes. Appropriate corrections for viscous heating and heats of dilution were applied to the experimental heats. The concentrations listed in Tables I and II are the concentrations after mixing in the calorimeter, but before reaction.

pH Measurements. Measurements of pH were made with a Radiometer Model PHM64 research pH meter, using a GK 2401C electrode. All measurements were at 25.0 ± 0.01 °C. The meter was standardized with the standard buffers recommended by Bates.[5]

Calculations

A number of workers have determined the thermodynamic parameters, $\Delta G°$, $\Delta H°$, and $\Delta S°$, from calorimetric data alone. Christensen, Izatt, and their coworkers[6-8] have discussed the technique and methods of analysis in detail. In the present study we have chosen to use the Nelder-Mead Simplex[9] procedure for function minimization of the calorimetric data.

The procedure for the determination of stability constants from pH measurements on the mannitol–borate system has been previously described.[10,11]

Results

Some comments are in order regarding the correctional heats, aside from those of dilution, which have been taken into account for the experimental heats. Since there are changes in (H^+) ion concentrations, heats of ionization of the buffer acid need to be considered. However, correctional heats from this source were considered negligible because there are essentially no net changes in the unionized boric acid, which remains equal to the value it would have in the absence of mannitol.[10,11]

Other possible corrections to the experimental heats that we considered were thermal effects due to changes in optical rotatory properties. Although mannitol in aqueous solution is optically inactive or only slightly dextrorotatory, the addition of borates enhances the optical activity.[12] However, the changes which occur do so over a rather extended time interval.[13] Since the recorded calorimetric curves from the borate–mannitol experiments were indistinguishable from those of a typical rapid reaction, such as strong acid plus strong base, thermal effects from this source were also considered to be negligible.

The experimental thermal data from one series of experiments are listed, together with the Q_{calcd} values and the final pHs in Table I. Each individual result is the average of five experiments. The calculated error square sum was 3.77×10^{-7} cal². Two additional series of calorimetric experiments were carried out. The concentration ranges of mannitol in these two series were the same as those listed in Table I, whereas the borate concentrations were 0.02500 and 0.02146 M. The calculated error square sums were 3.86×10^{-7} and 5.28×10^{-7} cal², respectively. The thermodynamic parameters derived from the experimental heats are listed in Table II. The uncertainties are reported as standard deviations of the mean. The rather constant values of the enthalpies in the successive steps are in accord with the proposal of Poulsen and

TABLE III: pH Data for Calculating Complexing Constants[a]

(P_T)	pH	pH corrected	$(H^+) \times 10^6$ corrected	$K' \times 10^3$	(P)
0	9.176				
0.2000	5.668	5.651	2.234	2.053	0.154
0.3000	5.259	5.233	5.848	3.430	0.252
0.4000	4.988	4.954	11.12	4.678	0.352
0.5000	4.790	4.747	17.91	5.871	0.451
0.6000	4.628	4.576	26.55	7.127	0.551
0.7000	4.499	4.439	40.74	8.270	0.651
0.8000	4.391	4.322	47.64	9.386	0.751

[a] Borate concentration = 0.02505 M.

TABLE IV: Complexing Constants from pH Data on Mannitol–Borate at 25 °C

Mannitol concn range, M	Borate concn, M	$\log \beta_1$	$\log \beta_2$
0.20–0.8	0.05365	3.37 ± 0.09	5.11 ± 0.01
0.20–0.8	0.05010	3.46 ± 0.11	5.11 ± 0.01
0.20–0.8	0.02688	3.56 ± 0.08	5.09 ± 0.01
0.04–0.3	0.01075	3.13 ± 0.10	5.10 ± 0.01

Bjerrum[14] in that for most complex systems with uncharged ligands, the heats of the successive steps will be approximately constant, with the variation in free energy being mainly determined by the entropy change.

A typical set of data used for calculating the complexing constants from pH measurements on the mannitol–borate system is shown in Table III. Plots of K' vs. (P) resulted in straight lines with positive slopes and intercepts, which are best explained on the basis of two different borate complexes containing either one or two mannitol molecules.[10] Complexing constants derived from all the data are listed in Table IV, with the uncertainties reported as standard deviations.

Numerous quantitative investigations have been carried out on the interactions of boric acid and mannitol with rather widely varying results.[15-21] We therefore measured the pHs of mixtures of varying concentrations of mannitol and boric acid using a large excess of mannitol over that of boric acid. K values were derived from several such measurements using the expression reported by Ross and Catotti.[16] The average value of the Ks obtained from these measurements was $0.61 \pm 0.02 \times 10^{-4}$, which after division by the ionization constant of boric acid, corresponds to an average $\log \beta_2$ of 5.02.

We also carried out pH measurements on 0.1 M boric acid and varying concentrations of mannitol, from which the number of moles of mannitol, n, combining with 1 mol of boric acid, have been calculated using the relation derived by Boeseken et al.[22] The calculated n values from four such measurements were in precise agreement with the value, 2, reported by Boeseken et al.

Discussion

The study of complex equilibria by any means demands care and high precision of measurements. Cabani and Gianni[23] concluded from an error propagation analysis that the simultaneous determinations of K and ΔH by calorimetry could, under certain conditions, yield fictitious values of K and ΔH. However, Christensen et al.[24] pointed out the assumption of large systematic errors, as was used by Cabani and Gianni in their analysis, was unjustified. It is therefore pertinent to compare in some detail the results of the calorimetric and pH analyses.

For the calorimetric analysis an indication of how well the chosen β values and corresponding ΔH values describe

the data can be gained from an examination of the magnitudes of the error square sums and the correspondence of the experimental Q and calculated Q values, typical of which are those listed in Table I. The square root of the error square sums, after division by nine, i.e., the number of separate experiments, is about 2×10^{-4} cal. This value is comparable to the precision to be expected from the calorimeter over the ranges of experimental heats encountered. Although no attempt was made to conduct an error propagation analysis, we did find the calorimetric method to be quite sensitive to small changes in the experimental heats. For example, arbitrarily changing the values of three experimental points in one series by approximately 2×10^{-4} cal caused a change of over 30% in the calculated β values, yet the value of the error square sum from this analysis was smaller than that obtained from the original analysis. The three modified points were selected at random from the top, middle, and lower portions of the thermal titration curve. Therefore, it would appear, as suggested by Cabani and Gianni, that the calorimetric method can be quite susceptible to yielding misleading results.

As to the pH analysis, an examination of the data in Table IV shows that a few percent change in the slope can result in rather large changes in the intercepts. Thus, any constant or systematic error which might be present would not affect the values of the slopes but could result in significant changes in the intercepts. It is also a necessary requirement of the pH analysis that a high molar ratio of mannitol:borate be maintained. This results primarily in the formation of the BP_2^- complex, since the magnitude of the β_2 is appreciably larger than that of the β_1. With this bias toward the formation of the BP_2^- complex, it might be expected that better agreement would be obtained among the β_2 values than among the β_1 values. This is indicated by the data in Table IV. Another factor in the pH analysis is medium effect corrections to the observed pH values. As shown in Table III, these are appreciable, particularly at the higher concentrations of mannitol. Although the method of correction for medium effects seems reasonable,[11] to what extent it is valid is unknown. The calorimetric method is independent of any complications from medium effects.

From the above considerations it is apparent that either method can yield variable results despite much experi-

mental care. However, there seems to be no reason(s) for considering the calorimetric method the less reliable of the two procedures for this particular problem. The suggestion has been made that before it can be assumed the correct reactions and chosen β values have been used, it is necessary to conduct a large number of experiments with widely varying concentrations of the reactants, obtaining the same K and ΔH values at each of the different concentrations.[9,23] Although the condition of widely varying concentrations of reactants has only been partially fulfilled in the present calorimetric study, the calorimetric data in conjunction with that of the pH definitely indicate that the interaction between mannitol and borate ion involves successive equilibria. Moreover, the high affinity between these two materials is the result of favorable enthalpy changes.

References and Notes

(1) H. S. Isbell, J. F. Brewster, N. B. Holt, and H. L. Frush, *J. Res. Natl. Bur. Stand.*, **40**, 129 (1948).
(2) M. E. Winfield, *Aust. J. Exp. Biol. Med. Sci.*, **23**, 111 (1945).
(3) K. C. Berger, "Advances in Agronomy", Vol. I, Academic Press, New York, N.Y., 1949, pp 321–354.
(4) W. J. Evans, E. J. McCourtney, and W. B. Carney, *Chem. Instrum.*, **2**(2), 249 (1970).
(5) R. G. Bates, "Electrometric pH Determinations", Wiley, New York, N.Y., 1954.
(6) J. J. Christensen, R. M. Izatt, L. D. Hansen, and J. A. Partridge, *J. Phys. Chem.*, **70**, 2003 (1966).
(7) J. J. Christensen, D. P. Wrathall, and R. M. Izatt, *Anal. Chem.*, **40**, 175 (1968).
(8) D. J. Eatough, J. J. Christensen, and R. M. Izatt, *Thermochim. Acta*, **3**, 219 (1972).
(9) J. A. Nelder and R. Mead, *Comput. J.*, **7**, 308 (1965).
(10) G. L. Roy, A. L. Laferriere, and J. O. Edwards, *J. Inorg. Nucl. Chem.*, **4**, 106 (1957).
(11) J. M. Connor and V. C. Bulgrin, *J. Inorg. Nucl. Chem.*, **29**, 1953 (1967).
(12) L. Vignon, *Ann. Chim. Phys.*, (5) **2**, 440 (1874).
(13) Merck Index, Merck and Co., Rahway, N.J., 1960, p 637.
(14) I. Poulsen and J. Bjerrum, *Acta Chem. Scand.*, **9**, 1467 (1955).
(15) A. Deutsch and S. J. Osoling, *J. Am. Chem. Soc.*, **71**, 1673 (1949).
(16) S. K. Ross and A. J. Catotti, *J. Am. Chem. Scc.*, **71**, 3363 (1949).
(17) P. J. Antikainen, *Ann. Acad. Sci. Fennicae Ser.* A. II, 56 (1954).
(18) P. J. Antikainen, *Acta Chem. Scand.*, **9**, 1008 (1955).
(19) R. F. Nickerson, *J. Inorg. Nucl. Chem.*, **30**, 1447 (1968).
(20) R. F. Nickerson, *J. Inorg. Nucl. Chem.*, **32**, 1400 (1970).
(21) G. W. Campbell, *J. Inorg. Nucl. Chem.*, **31**, 2625 (1969).
(22) J. Boeseken, N. Vermas, and A. T. Kuchlin, *Recl. Trav. Chim. Pays-Bas*, **49**, 711 (1930).
(23) S. Cabani and P. Gianni, *J. Chem. Soc.* A, 547 (1968).
(24) J. J. Christensen, J. H. Rytting, and R. M. Izatt, *J. Chem. Soc.* A, 861 (1969).

Aqueous Solutions of Azoniaspiroalkane Halides. 4. Excess Apparent Molal Free Energies, Enthalpies, and Entropies

Antonio LoSurdo, Wen-Yang Wen,*

Jeppson Laboratory, Chemistry Department, Clark University, Worcester, Massachusetts 01610

Carmel Jolicoeur, and J.-L. Fortier

CACTUS, Centre d'Application en Calorimetrie et Thermodynamique, Universite de Sherbrooke, Department de Chimie, Sherbrooke, Quebec, Canada (Received April 18, 1977)

The osmotic coefficients and enthalpies of dilution of azoniaspiroalkane halides, $(CH_2)_nN^+(CH_2)_nX^-$ (where $n = 4, 5, 6$, and X = Br; for $n = 5$ and 6, X = Cl or I), in water have been determined at 25 °C by the isopiestic method and by the flow microcalorimetric method. From these data the activity coefficients, the relative apparent molal enthalpies, and the excess apparent molal entropies were calculated and compared with those of the corresponding tetraalkylammonium halides. The results show marked differences in thermodynamic properties of these two series of salts; these are discussed in terms of the ion–ion interactions and the hydration phenomena associated with the different cations. Compared to tetra-n-alkylammonium ions, the quaternary ions having bicyclo structure exhibit considerably weaker hydrophobic character and, thus, generally different excess thermodynamic functions.

Introduction

Previous investigations on the solution properties of hydrophobic ions containing either linear or cyclic alkyl groups have shown some important differences among the properties of these two types of solutes.[1-5] In view of the current wide interest toward the tetraalkylammonium ions as typical hydrophobic species,[6,7] it should be informative to pursue a comparative study on the solution behavior of the tetra-n-alkylammonium ions and their bicyclo analogues, the azoniaspiroalkane ions. Since the latter have no terminal methyl groups and their configuration is quite rigidly fixed, the study should supply information on the role of geometrical and dynamic configurational effects in the solution properties of these large quaternary ammonium salts.

In previous papers of this series, we reported the relative apparent molal enthalpies and the standard enthalpies of transfer from H_2O to D_2O (paper 1),[1] the apparent molal volumes and heat capacities (paper 2),[4] and the dielectric relaxation behavior (paper 3).[5] These studies led to the common conclusion that the hydrophobic character of the tetra-n-alkylammonium ions is considerably greater than that of the azoniaspiroalkane ions.

In this communication, we present experimental data on the osmotic and activity coefficients as well as heats of dilution of several azoniaspiroalkane halides in water at 25 °C. Though some enthalpies of dilution were reported in paper 1, they were based on heats of solution determined in a concentration range too low for making the corresponding isopiestic measurements. In view of this, we have measured the enthalpies of dilution with a flow microcalorimeter in the concentration range from 0.01 to around 1 m. The excess apparent molal free energies, enthalpies, and entropies were computed from the data and the results are compared below with those of the corresponding tetraalkylammonium halides.

Experimental Section

I. *Materials.* Azoniaspiroalkane halides were synthesized by a method adapted from Blicke and Hotelling,[8] and from Thomas and co-workers.[9,10] The detailed procedures used for the purification and analysis of some of the products have been described in paper 1.[1] The

chemical formulae and our abbreviated symbols for the seven azoniaspiroalkane halides are as follows: (a) $(CH_2)_4N^+(CH_2)_4Br^-$, "4.4 Br"; (b) $(CH_2)_5N^+(CH_2)_5X^-$ where X = Cl, Br, or I, "5.5 Cl", "5.5 Br", "5.5 I"; (c) $(CH_2)_6N^+(CH_2)_6X^-$, "6.6 Cl", "6.6 Br", "6.6 I".

Among these salts, the 6.6 Cl and 6.6 I have been prepared here for the first time. 6.6 Cl was obtained by allowing reagent grade 1,6-dichlorohexane (0.1 mol) to react with equimolar hexamethyleneimine in 50% aqueous 2-propanol containing 0.1 mol NaOH under vigorous stirring. The mixture was heated and refluxed with continuous stirring for 36 h or until everything dissolved and became one solution phase. After evaporation to dryness, the crude product was extracted with 1-butanol and purified by several recrystallizations from 2-propanol and absolute ethanol. Gravimetric analysis of the chloride ion and potentiometric titration of the cation[11] gave 99.85 and 99.9% respectively of the formula value of 6.6 Cl: mp 269–270 °C. 6.6 I was obtained similarly by allowing equimolar hexamethyleneimine to react with 1,6-diiodohexane in 2-propanol saturated with NaOH at 70 °C. Analysis of iodide ion and cation[11] gave 99.9% of the formula value.

II. *Apparatus and Procedure.* The isopiestic apparatus used in this work was similar to that employed by Owen and Cooke,[12] and by workers in our laboratory.[13] It consisted mainly of gold-plated silver and gold dishes with covers, copper blocks, glass desiccators, and rocking mechanisms. Gold dishes were used for the iodide solutions to avoid reactions with silver dishes forming silver iodide or its complexes.

During these experiments, the temperature was controlled at 25 ± 0.005 °C and the pressure in the desiccators was reduced in stages to 25 Torr. Equilibrium was judged to be established when the concentrations of a pair of solutions in duplicate dishes differed by less than 0.1% for the references and sample solutions. Weight loss due to water evaporation between the time of opening the desiccator and weighing the dish was corrected to the extent possible. All weights of salts and solutions were reduced to those in vacuo.

Enthalpies of dilution were measured using a Picker-type flow microcalorimeter,[14,15] with a sensitivity of 10^{-6}

°C and a precision of ±0.5%. The solution at an initial concentration m_i (molality) is introduced into the calorimeter at a flow rate of f (mL s^{-1}) and the solvent at a flow rate of f_0 (mL s^{-1}). The final concentration m_f is given by

$$m_f = m_i/(1 + f_0 d_0/D_i) \qquad (1)$$

where d_0 (g cm^{-3}) is the density of solvent, D_i (g s^{-1}), the weight flow rate of solvent from initial solution (m_i) given by

$$D_i = 1000 f_i d_i/(1000 + m_i M) \qquad (2)$$

where d_i (g cm^{-3}) is the density of initial solution and M, the solute molecular weight. The integral enthalpy of dilution ΔH_{dil} (cal mol^{-1}) is thus given by

$$\Delta H_{dil} = Q/n = W/4.184 D_i m_i \qquad (3)$$

Here Q is the measured heat, n the number of moles of solute, and W the power (watts) produced in the calorimetric flow cell. The experimental integral enthalpies of dilution are defined by

$$\Delta H_{dil} = \phi_L(m_f) - \phi_L(m_i) \qquad (4)$$

where $\phi_L(m_i)$ and $\phi_L(m_f)$ are the relative apparent molal enthalpies of the initial and final concentrations expressed in molality units. We tried to fit the experimental ΔH_{dil}[15] data to a power series in $m^{1/2}$ in order to represent ϕ_L as

$$\phi_L = A_L m^{1/2} + B_L m + C_L m^{3/2} + D_L m^2 + \cdots \qquad (5)$$

where A_L is the Debye–Hückel limiting slope of 472.0 cal mol$^{-3/2}$. It was found, however, that the fit at concentrations below 0.05 m was poor, because the experimental values in the dilute region changed too rapidly with concentration and showed sharp maximum. The data were, therefore, treated graphically.

Results

I. *Osmotic and Activity Coefficients.* The osmotic coefficients of azoniaspiroalkane halides in water were obtained by the isopiestic comparison method using NaCl solutions as the reference. The measured molalities of isopiestic solutions at 25 °C are given in Table I.[31] From these data and the osmotic coefficients of NaCl solutions listed by Robinson and Stokes,[16] the osmotic and activity coefficients of six of the azoniaspiroalkane salts were calculated. The osmotic coefficients of 6.6 I could not be determined by the isopiestic method due to the onset of saturation and crystallization at around 0.15 m in water at 25 °C. However, the low solubility did not preclude the measurements of the enthalpies of dilution of this salt.

The osmotic coefficients, ϕ, listed in Table II[31] were calculated from the following polynomial equations:

$$1 - \phi = 0.3908 m^{1/2} + Am + Bm^{3/2} + \cdots + Gm^4 \qquad (6)$$

where 0.3908 is the Debye–Hückel limiting value at 25 °C. Values of the coefficients $A, B, \ldots, G$ were evaluated from the experimental data by the method of least squares and given in Table Ia. The least-squares polynomials so obtained reproduced the experimental ϕ values with a standard deviation of ±0.001. The mean ionic activity coefficient $\gamma_\pm$ were calculated by the equation

$$\ln \gamma_\pm = \phi - 1 - 2 \int_0^{m^{1/2}} (1 - \phi)/m^{1/2} \, dm^{1/2} \qquad (7)$$

In addition to the least-squares method, the values of ϕ and $\gamma_\pm$ were also evaluated graphically. The two sets of data obtained were in good agreement with a standard deviation of ±0.001.

TABLE Ia: Coefficients for the Polynomial Equation, Eq 6, which Expresses the Osmotic Coefficients ϕ of Azoniaspiroalkane Halides in Water at 25 °C

Coefficient	4.4 Br	5.5 Br	6.6 Br
A	0.052011	0.14883	-0.055094
B	-0.34145	-0.52632	0.78398
C	0.23290	0.54056	-1.52338
D	-0.053501	-0.31539	0.99282
E	0	0.093378	-0.22125
F	0	-0.010798	0
G	0	0	0
$10^3 \sigma^a$	±0.96	±0.94	±1.7

Coefficient	5.5 Cl	5.5 I	6.6 Cl
A	-0.35452	0.72615	-0.041590
B	1.05836	-1.4454	-0.75951
C	-2.4627	1.3921	1.8054
D	2.7569	-0.68186	-2.0941
E	-1.6174	0.091702	1.2426
F	0.47943	0.039308	-0.36590
G	-0.056675	-0.010851	0.042597
$10^3 \sigma^a$	±1.4	±1.0	±0.69

^{a} Standard deviation for $\phi_{obsd} - \phi_{calcd}$, where ϕ_{obsd} is the experimental value of the osmotic coefficient and ϕ_{calcd} is the calculated value of the osmotic coefficient using eq 6.
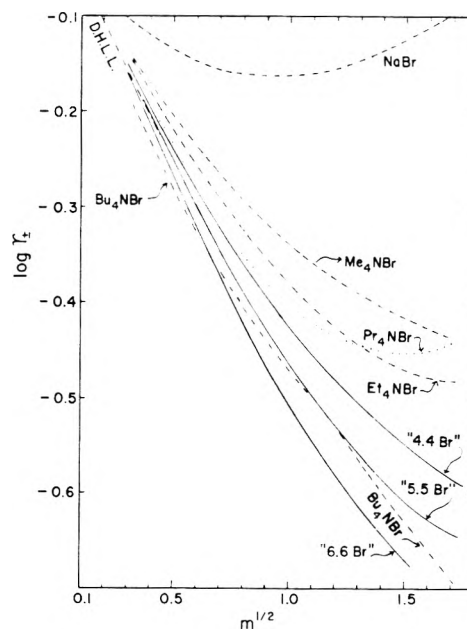
Figure 1. Plot of log $\gamma_\pm$ vs. $m^{1/2}$ for azoniaspiroalkane bromides and tetraalkylammonium bromides in water at 25 °C.

The values of log $\gamma_\pm$ are plotted in Figure 1 against $m^{1/2}$ for the three azoniaspiroalkane bromides and compared with those of the tetraalkylammonium bromides. In Figure 2 we report similar data and comparisons for the 5.5 Cl, 6.6 Cl, and 5.5 I. The log $\gamma_\pm$ data exhibit important deviations from the Debye–Hückel limiting law (DHLL), though generally not as large as those found with the R$_4$NX salts. The mean molal activity coefficients for the salts containing the spiro ions are strikingly lower than those for the tetraalkylammonium salts. Also, judging from the data at about 1.0 m, the dependence of log $\gamma_\pm$ on the size of the cation is the same within the bromide and the chloride series. This contrasts with the behavior in the R$_4$NX series, where the order of log $\gamma_\pm$ in the homologous series is inverted for the bromides and chlorides.[26,30]

II. *Enthalpies of Dilution.* The experimental values of initial molality (m_i), final molality (m_f), and the resulting integral enthalpies of dilution (ΔH_{dil}) for the seven azo-
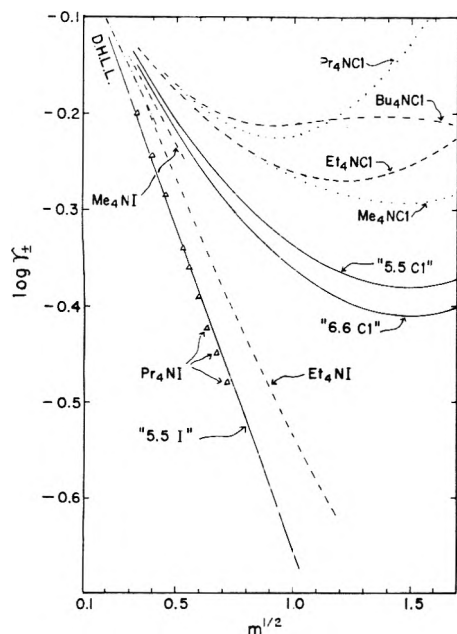
Figure 2. Plot of log $\gamma_{\pm}$ vs. $m^{1/2}$ for 5.5 Cl, 5.5 I, and 6.6 Cl as well as tetraalkylammonium chlorides and iodides in water at 25 °C.
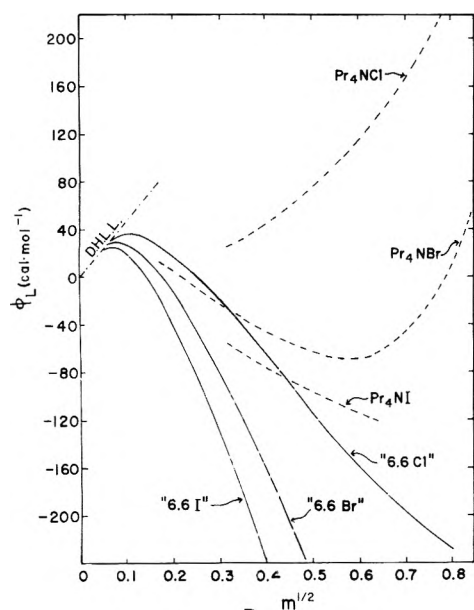
Figure 3. Plot of ϕ_L vs. $m^{1/2}$ for 6.6 Cl, 6.6 Br, and 6.6 I as well as tetrapropylammonium halides in water at 25 °C.

niaspiroalkane halides are shown in Table III.[31] The relative apparent molal enthalpies ϕ_L are given at various values of $m^{1/2}$ for these salts in Table IV[31] and plotted for the purpose of comparison in Figure 3. In a previous paper, Wilson and Wen[1] reported ϕ_L values for five of these halides obtained from heat of solution measurements in the range of $m^{1/2}$ below 0.60. The agreement of our ϕ_L data with those in ref 1 are good for 5.5 Br and 5.5 I, fair for 6.6 Br and 5.5 Cl, and poor for 4.4 Br, the values given in ref 1 being slightly greater (i.e., less negative) than those given in Table IV.[31] This discrepancy partly reflects the difficulties in obtaining precise values of ϕ_L at low concentrations and, hence, the whole ϕ_L vs. $m^{1/2}$ curve may be shifted somewhat up or down.

III. *Excess Entropies.* For the purpose of discussing the ion–ion interactions, we calculated the total excess free energy per kilogram of water defined as[21]

$$G^{ex} = \nu RTm(1 - \phi + \ln \gamma_{\pm}) \qquad (8)$$

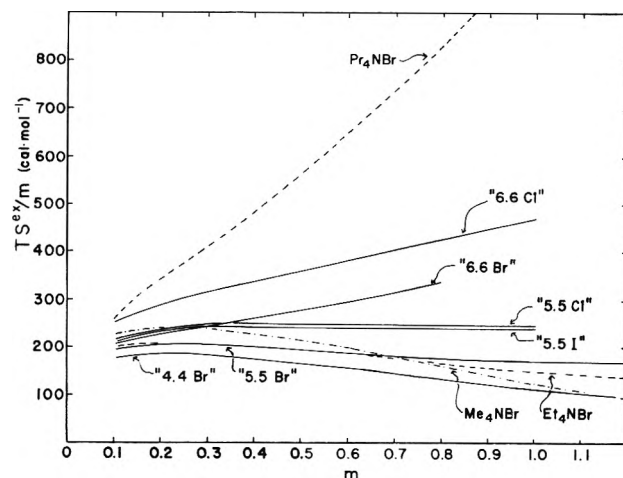where ν is the number of moles of ions produced by dis-

Figure 4. Plot of TS^{ex}/m vs. m for six azoniaspiroalkane halides and three tetraalkylammonium bromides in water at 25 °C.

sociation of 1 mol of electrolyte. One of the advantages of using this total excess function is that it is directly proportional to the corresponding excess molal quantity. Thus at 25 °C, for 1:1 electrolytes

$$G^{ex}/m = \phi_G - \phi_G{}^* = 1185.0(1 - \phi + \ln \gamma_{\pm}) \qquad (9)$$

where ϕ_G and $\phi_G{}^*$ represent the apparent molal free energies per mole of solute for the real and ideal solutions. Similarly, we have the excess apparent molal enthalpy which is

$$H^{ex}/m = \phi_L \qquad (10)$$

and the excess apparent molal entropy given by

$$TS^{ex}/m = (H^{ex} - G^{ex})/m = \phi_L -$$
$$1185.0(1 - \phi + \ln \gamma_{\pm}) \qquad (11)$$

The computed values of TS^{ex}/m are listed in Table V[31] for the six azoniaspiroalkane halides at concentrations of 0.1–1.2 m. These data are plotted against m and compared with similar data for the tetraalkylammonium bromides[22,23] in Figure 4.

Discussion

I. *Activity Coefficients.* As pointed out above, the activity coefficients of the azoniaspiroalkane halides are remarkably low compared with those of their tetra-n-alkylammonium analogues. The lowering of the excess free energy in solutions containing the bicyclic quaternary ions should reflect enhanced ion–ion attraction (or reduced ion–ion repulsion). This behavior may involve such effects as ion size, ion geometry, and ion solvation, and each of these require some further considerations.

(a) *Size-Effects and Distance of Closest Approach.* Judging from the apparent molal volumes of 5.5 Br and Et₄NBr (180.0 vs. 173.74 cm³ mol⁻¹, ref 4) the sizes of the quaternary ions 5.5⁺ and Et₄N⁺ are comparable, but the activity coefficient of the 5.5 Br salt is considerably lower than that of Et₄NBr. Therefore, size effects alone cannot account for the differences observed here.

On the other hand, the relatively fixed and compact geometry of the bicyclo ions may lead to a reduced ion–ion distance of closest approach. This aspect relates directly to a question raised earlier[27,28] on the possible penetration of the halide ions into the interchain space of the tetra-n-alkylammonium ions. The present results, together with the excess entropies described below, will help clarify this problem.

(b) *Geometrical Effects.* Consider, for example, the ions Et₄N⁺ or Pr₄N⁺ vs. 5.5⁺ or 6.6⁺; the latter may be assumed

to represent the R_4N^+ ions in a fixed configuration where the charged nitrogen center is more exposed to the solvent and thus capable of closer $N^+ \ldots Br^-$ interaction distances. More specifically, in tying the propyl groups of Pr_4N^+ to form 6.6^+, one must pull two of the C–N–C angles "shut" and thereby pull the other two angles "open". The wider opening of the two C–N–C angles is expected to predominate through making the ionic charge of the central nitrogen more accessible to the anion. The result is a reduction in the cation–anion distance of closest approach and a lowering in the mean ionic activity coefficient.

Following this reasoning, it would appear that penetration of the halide ion into the space between the chains of the R_4N^+ ion does not contribute a major reduction of the log $\gamma_\pm$ of the tetra-n-alkylammonium ions.

(c) *Solvent Structural Effects.* Alternately, the activity coefficients may be examined from the point of view of the solvent structural effects of the ions and the concept of mutual salting-out between the hydrophobic cations and the hydrophilic anions.[24-26] It was concluded from previous studies[1-5] that the hydrophobic character (and solvent structure promoting effects) of the bicyclo ions are significantly reduced when compared to their tetraalkyl analogues, due to the removal of terminal methyl groups and to further geometrical effects of the solute cations. Hence, the mutual salting-out arising from the antagonistic solvent structural perturbations of the cations and anions will be less important with the bicyclo ions and, consequently, G^{ex} would be lowered. The excess entropies allow us to further distinguish the relative importance of the contributions from mutual salting-out effects and changes in the distances of closest approach.

II. *Excess Molal Entropies.* The unusually large and positive excess molal entropies of the tetra-n-alkylammonium halides, e.g., Pr_4NBr, have been discussed in great details in earlier investigations.[22-30] The explanation rests mainly on the solvent structural effects associated with the hydration of the hydrophobic R_4N^+ ions (water structure stabilization by the alkyl chains which greatly reduces the partial molal entropy of these salts). As the concentration increases, these hydration cospheres are progressively destroyed due to overlap with hydration cospheres of other ions (anions and cations), thus releasing the solvent to the bulk state of higher entropy.

Returning to the comparison of the properties of the cyclic vs. tetraalkyl compounds, it is readily seen from Figure 4 that the excess entropies of 5.5 Br and Et_4NBr exhibit similar behavior. We may then conclude that, for the lower homologues, the solvent structural effect does not play the leading role in the ion–ion interactions. However, from the concentration dependence of TS^{ex}/m for 6.6 Br and Pr_4NBr, it seems obvious that the contribution from solvent structural effects is important in the case of Pr_4NBr and much less so for the 6.6 Br salt (we neglect here possible variations in entropy which could result from changes in the internal modes of the quaternary ions as the concentration is increased). This observation enables us to distinguish two types of behavior among the systems examined here.

For the lower members of the tetraalkyl and cyclic homologues (e.g., Me_4NBr, Et_4NBr, 4.4 Br, and 5.5 Br) entropy and solvent structural effects are similar, so differences in G^{ex} must arise from differences in the interaction energies and in the relative ion–ion distances of closest approach. With the larger ions, e.g., 6.6 Br and Pr_4NBr, contact-distance effects should still contribute to discriminate the G^{ex} behavior of these systems, but cosphere overlap entropy effects now appear important. The

increasing importance of entropy effects are evidenced from the relative magnitudes of the TS^{ex} and ϕ_L terms within a homologous series such as 4.4 Br, 5.5 Br, and 6.6 Br.

Conclusion

The excess thermodynamic functions reported here indicate further that, compared to the corresponding tetraalkylammonium ions, the azoniaspiroalkane ions having bicyclo structure exhibit considerably weaker hydrophobic character. This must be due to the fact that the spiro ions have no terminal methyl group and their methylene groups in the loop are relatively tightly connected together to yield geometric shapes which are not as conducive to hydrogen-bond formation by the surrounding water molecules as those of the tetraalkylammonium ions. The presence of the terminal methyl group at the end of a flexible chain seems to be an important factor in stabilizing the surrounding water structure. The remarkably low activity coefficients observed for the spiro salts are attributed to (a) the reduced ion–ion distance of closest approach in view of the exposed charged-nitrogen center of the cation and (b) the reduced mutual salting-out between the hydrophobic cation and the hydrophilic anion brought about by the weakened solvent structural effects.

Supplementary Material Available: Five tables containing isopiestic molalities (Table I), osmotic and activity coefficients (Table II), integral enthalpies of dilution (Table III), relative apparent molal enthalpies (Table IV), and excess molal entropies (Table V) of azoniaspiroalkane halides in water at 25 °C (9 pages). Ordering information is available on any current masthead page.

References and Notes

(1) D. P. Wilson and W.-Y. Wen, *J. Phys. Chem.*, **79**, 1527 (1975).
(2) C. Jolicoeur, J. Boileau, S. Bazinet, and P. Picker, *Can. J. Chem.*, **53**, 716 (1975).
(3) S. Cabani, G. Conti, and L. Lepori, *J. Phys. Chem.*, **76**, 1338, 1343 (1972); **78**, 1030 (1974).
(4) W.-Y. Wen, A. LoSurdo, C. Jolicoeur, and J. Boileau, *J. Phys. Chem.*, **80**, 466 (1976).
(5) W.-Y. Wen and U. Kaatze, *J. Phys. Chem.*, **81**, 177 (1977).
(6) W.-Y. Wen, "Aqueous Solutions of Symmetrical Tetraalkylammonium Salts", in "Water and Aqueous Solutions", R. A. Horne, Ed., Wiley, New York, N.Y., 1972, pp 613-661.
(7) F. Franks, "The Hydrophobic Interaction", in "Water, A Comprehensive Treatise", F. Franks, Ed., Plenum Press, New York, N. Y., 1974, pp 1-94.
(8) F. F. Blicke and E. B. Hotelling, *J. Am. Chem. Soc.*, **76**, 5099 (1954).
(9) J. Thomas, *J. Med. Pharm. Chem.*, **3**, 45 (1961).
(10) B. D. Roufogalis and J. Thomas, *J. Pharm. Pharmacol.*, **20**, 153 (1968).
(11) (a) D. P. Wilson, Ph.D. Thesis, Clark University, 1974. (b) The cation analysis was carried out by a potentiometric titration method adopted from J. S. Fritz, "Acid-Base Titration in Non-aqueous Solvents", Allyn and Bacon, Boston, Mass., 1973.
(12) B. B. Owen and T. F. Cooke, *J. Am. Chem. Soc.*, **59**, 2273 (1937).
(13) W.-Y. Wen, K. Miyajima, and A. Otsuka, *J. Phys. Chem.*, **75**, 2148 (1971); W.-Y. Wen and C. L. Chen, *ibid.*, **73**, 2895 (1969); W.-Y. Wen, S. Saito, and C. M. Lee, *ibid.*, **70**, 1244 (1966); W.-Y. Wen, and S. Saito, *ibid.*, **69**, 3569 (1965).
(14) P. Picker, C. Jolicoeur, and J. E. Desnoyers, *J. Chem. Thermodyn.*, **1**, 469 (1969).
(15) J.-L. Fortier, P.-A. Leduc, and J. E. Desnoyers, *J. Solution Chem.*, **3**, 323 (1974).
(16) R. A. Robinson and R. H. Stokes, "Electrolyte Solutions", 2nd ed, Butterworths, London, 1959.
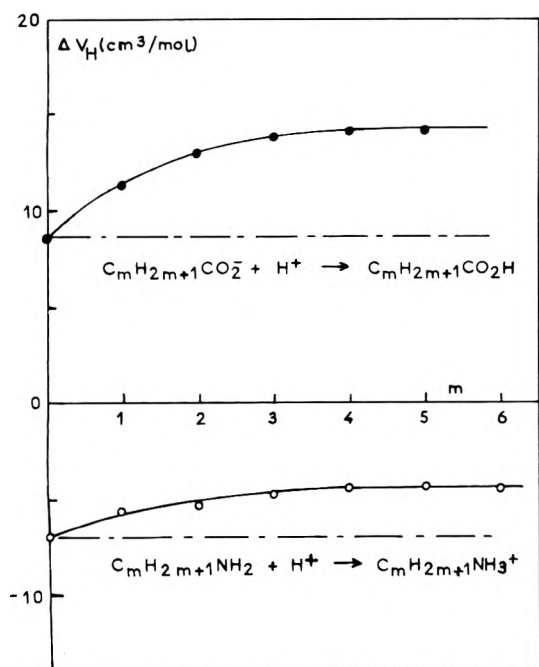(17) S. Lindenbaum and G. E. Boyd, *J. Phys. Chem.*, **68**, 911 (1964).

(18) B. J. Levien, *Austr. J. Chem.*, **18**, 1161 (1965), for Me₄NBr.
(19) J. P. Rupert, Ph.D. Thesis, University of Pittsburgh, 1969, for Et₄NCl and Bu₄NCl.
(20) J. C. Ku, Ph.D. Thesis, University of Pittsburgh, 1971, for Et₄NBr and Bu₄NBr.
(21) H. L. Friedman "Ionic Solution Theory", Interscience, New York, N.Y., 1962.
(22) S. Lindenbaum, *J. Phys. Chem.*, **70**, 814 (1966).
(23) A. S. Levine and R. H. Wood, *J. Phys. Chem.*, **77**, 2390 (1973).
(24) H. S. Frank, *J. Phys. Chem.*, **67**, 1554 (1963); *Z. Phys. Chem.*, **228**, 364 (1965).

(25) W.-Y. Wen, S. Saito, and C.-M. Lee, *J. Phys. Chem.*, **70**, 1244 (1966).
(26) J. E. Desnoyers and C. Jolicoeur in "Modern Aspects of Electrochemistry, No. 5", J. O'M. Bockris and B. E. Conway, Ed., Plenum Press, New York, N.Y., 1969, Chapter 1.
(27) P. S. Ramanathan, C. V. Krishnan, and H. L. Friedman, *J. Solution Chem.*, **1**, 237 (1972).
(28) R. W. Kreis and R. H. Wood, *J. Phys. Chem.*, **75**, 2319 (1971).
(29) R. B. Cassel and W.-Y. Wen, *J. Phys. Chem.*, **76**, 1369 (1972).
(30) W.-Y. Wen, *J. Solution Chem.*, **2**, 253 (1973).
(31) Available as supplementary material. See the paragraph at the end of the paper.

On the Volume Changes upon Protonation of *n*-Alkylcarboxylate Ions and *n*-Alkylamines in Aqueous Solutions. Extension to the Interpretation of Volumic Effects Observed in Solutions of Molecular Ions, Polyelectrolytes, Micellar Detergents, and Proteins

R. Zana

CNRS, Centre de Recherches sur les Macromolécules, 6, rue Boussingault, 67083, Strasbourg, Cedex, France (Received April 4, 1977)

It is shown that the increase of the volume change upon protonation of *n*-alkylcarboxylate ions and *n*-alkylamines with the alkyl chain length can be explained in terms of two antagonistic effects: (i) a reduction of the electrostriction of the water molecules by the charged group caused by the increasing steric hindrance of the alkyl chain and (ii) a structure rearrangement of the water molecules about the alkyl chain under the effect of the charged group. These two effects also provide an explanation for the dependence of the volume change upon protonation of *n*-alkylcarboxylates and *n*-alkylamines on the degree of branching of the alkyl chain and the substitution degree of the charged nitrogen center. The dependence of the partial molal volumes of *n*-alkylcarboxylate and *n*-alkylammonium ions on different parameters is also explained. Finally the relevance of the structural effect to the interpretation of volumic effects observed with more complex systems is examined.

I. Introduction

The standard volume change $\Delta V°(RCO_2^-)$, associated with the protonation reaction (eq 1) of *n*-alkylcarboxylate

$$RCO_2^- + H^+ \rightarrow RCO_2H \qquad (1)$$

ions are positive.[1-3] They increase with the number *m* of carbon atoms of the alkyl group $R = C_mH_{2m+1}$, up to $m = 3$, and then level off as is shown in Figure 1.

On the other hand, the volume change, $\Delta V°(RNH_2)$, upon protonation of *n*-alkylamines following reaction 2

$$RNH_2 + H^+ \rightarrow RNH_3^+ \qquad (2)$$

becomes less and less negative as *m* increases[4] (see Figure 2). This last result is rather unexpected. Indeed, whichever interpretation is given to the increase of $\Delta V°(RCO_2^-)$ with *m*, one would have expected an opposite variation of $\Delta V°(RNH_2)$ had the factors determining the value of this quantity been the same as those in *n*-alkylcarboxylate solutions (see below).

The increase of $\Delta V°(RCO_2^-)$ with *m* has been attributed by King[2] to the electrically charged carboxylate group which would induce some kind of "melting of structured water" around the alkyl chain. Although it is probably better to talk about a rearrangement of water molecules around the alkyl chain under the influence of the carboxylate group rather than of "melting", this effect alone would lead to predict a decrease of $\Delta V°(RNH_2)$ upon increasing *m*.

Since King's report a large number of accurate $\Delta V°$ values have been reported for both RNH₂ and RCO₂⁻. These results raise additional problems concerning in particular the changes of $\Delta V°$ with the branching of the alkyl chain in the vicinity of the charged group[5] and the

effect of an increased substitution of the nitrogen atom in the case of alkylamines.[4] The purpose of this paper is to propose an explanation for the increases of the $\Delta V°$'s for *n*-alkylcarboxylate ions and *n*-alkylamines and for some of the above observations concerning the values of $\Delta V°$. The relevance of this explanation to the interpretation of volumic effects observed with more complex systems is examined.

II. Volume Changes upon Protonation of *n*-Alkylcarboxylate Ions and *n*-Alkylamines

In this section we attempt to give a description of the effects which may determine a change of $\Delta V°$ with *m* for RCO₂⁻ and RNH₂. For this purpose, reactions 1 and 2 will be written in the form of thermodynamic cycles, where virtual uncharged species such as RCO₂ and RNH₃ are introduced.

1. *n-Alkylcarboxylate Ions.* Reaction 1 can be written as

$$RCO_2^- + H^+ \rightarrow RCO_2H$$
$$\searrow \qquad \nearrow$$
$$RCO_2 + H \qquad (3)$$

The standard volume change $\Delta V°(RCO_2^-)$ can be expressed in terms of the partial molal volumes at infinite dilution according to

$$\Delta V°(RCO_2^-) = [\overline{V}°(RCO_2H) - \overline{V}°(RCO_2)] + \delta_V(RCO_2^-) - \overline{V}°(H^+) \qquad (4)$$

with

$$\delta_V(RCO_2^-) = \overline{V}°(RCO_2) - \overline{V}°(RCO_2^-) \qquad (4a)$$

Figure 1. Standard volume change ΔV° upon protonation of n-alkylcarboxylate ions[3] and n-alkylamines[4] at 25 °C.
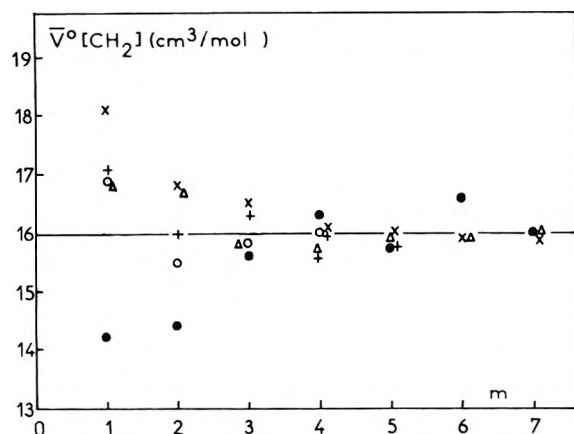

Figure 2. Variation of the methylene group contribution $\bar{V}^\circ(CH_2)$ at infinite dilution and 25 °C, with the number of carbon atoms between the methylene group and the functional group for (O) n-alkyl alcohols;[7,18] (Δ) n-alkylamines;[4a] (+) n-alkylcarboxylic acids;[2a,19,20] (●) n-alkylcarboxylate ions;[2a,19] and (X) n-alkylammonium ions.[21]

The term in brackets on the right-hand side of eq 4 represents the volume increment associated with the addition of a hydrogen atom onto an oxygen atom. This increment must therefore be practically independent of the size or structure of the alkyl R group. From data reported in the literature (comparison between the partial molal volume of acetone[6] and 2-propanol,[7] cyclohexanol[4] and cyclohexanone[8]) as well as from calculations of volume increments based on Bondi's data[9] and interatomic angles and distances, we found this increment to be 1.5 ± 0.5 cm³/mol, independent of the nature of R. On the other hand, $\bar{V}^\circ(H^+) = -5.4$ cm³/mol.[10,11] From eq 4 and 4a it is therefore clear that the increase of $\Delta V^\circ(RCO_2^-)$ with m can arise only from the change of $\delta_v(RCO_2^-)$ with m. We now have to consider the physical meaning of this quantity.

$\delta_v(RCO_2^-)$ is the difference between the partial molal volumes of two species, one neutral and the other electrically charged, but otherwise geometrically identical. The difference between these two quantities will therefore essentially involve differences of interaction with the surrounding solvent molecules. For the sake of simplicity we shall first consider the case of the formate ion, that is

$R = H$. $\Delta V^\circ(HCO_2^-)$ has been determined by several authors[1-3] and its average value is 8.4 ± 0.2 cm³/mol. Inserting the various numerical values into eq 4 yields

$$\delta_V(HCO_2^-) = \bar{V}^\circ(HCO_2) - \bar{V}^\circ(HCO_2^-)$$
$$= 1.5 \pm 0.7 \text{ cm}^3/\text{mol} \qquad (5)$$

Since the ion HCO_2^- and the virtual species HCO_2 are geometrically identical, two effects will contribute to δ_v-(HCO_2^-): (i) the electrostriction of the surrounding water molecules under the effect of the electrostatic field of the carboxylate ion and (ii) a change of H bonding with solvent molecules upon charging of the $-CO_2$ group. This change will affect the strength of the H bonding but not so much the number of H bonds. At the present time, the contribution of H bonding between water and solute molecules, to the partial molal volume of the solute, is not known with any accuracy.[2] One cannot discard the possibility that a compensation between the contributions of effects (i) and (ii) is the reason for the small value of $\delta_v(HCO_2^-)$. It is more likely, however, that the change in the H-bond contribution to the value of $\delta_v(HCO_2^-)$ is small and does not affect very much the essential conclusion which can be drawn from the value of $\delta_v(HCO_2^-)$, namely, that the electrostriction of the carboxylate group is small. Various explanations have been proposed for this finding.[2a] Note that King[2a] has obtained for the electrostriction of the formate ion a value very close to that of $\delta_v(HCO_2^-)$.

Let us now turn to n-alkylcarboxylate ions. We can write

$$\Delta V^\circ(RCO_2^-) - \Delta V^\circ(HCO_2^-) = \delta_V(RCO_2^-)$$
$$- \delta_V(HCO_2^-) \qquad (6)$$

Upon substitution of the H atom of the formate ion by the n-alkyl R group, two effects may result in changes of ΔV°. The first one is a reduction of the electrostriction of the CO_2^- group, owing to the steric hindrance due to the alkyl group which renders part of the carboxylate group inaccessible to water molecules. This effect should increase with the size of the alkyl group, but remains small owing to the small value of $\delta_v(HCO_2^-)$. The contribution of this effect to the change of $\Delta V^\circ(RCO_2^-)$ with the size of R can be approximated as the product of $\delta_v(HCO_2^-)$ by the fraction f of surface area of the carboxylate group which is "covered" by the alkyl group. For $R = CH_3$, van der Waals radii[9] and bond length and angles yield $f = 0.3$. Therefore the reduction of electrostriction for a substituting methyl group amounts to about -0.5 cm³/mol. This value is much smaller than the change of ΔV° in going from HCO_2^- to $CH_3CO_2^-$ and in addition has a sign opposite to that of the actually observed change.

The second effect arises from a rearrangement of the water molecules about the alkyl group under the action of the charged carboxylate group. This effect may be understood in terms of an overlap of Gurney's cospheres[12] of the alkyl group and electrically charged group. In his recent review, Friedman[13] states that "in cases in which the data are available, when only two cospheres overlap the effect is mutually destructive". The cosphere breakdown will affect both the cosphere of the alkyl group (rearrangement of water molecules) and that of the charged group (reduction of electrostriction, but not for steric reason). Note that we are now in a situation where the two overlapping cospheres are on the same molecular ion, while Friedman was dealing with cases where the two cospheres referred to two separate species.[13] Since the carboxylate group can contribute only little to volume changes, the increase of ΔV° observed in substituting the H atom of HCO_2^- by the alkyl R group must essentially

TABLE I: Effect of the Alkyl Chain Length on the $\Delta V°$ for n-Alkylcarboxylate Ions

m	0		1		2		3		4		5
$\Delta V°_m,^a$ cm^3/mol	8.4		11.4		13		13.9		14.2		14.2
d, nm		0.22		0.31		0.45		0.56$_5$		0.71	
$(\Delta V°_{m+1} - \Delta V°_m)d^{2\,b}$		0.17 ± 0.01^c		0.15 ± 0.02		0.18 ± 0.04		0.1 ± 0.06		0 ± 0.1	

^{a} Values selected from ref 1-3. ^{b} The error limits have been calculated assuming an uncertainty of 0.2 cm^3/mol on the difference $\Delta V°_{m+1} - \Delta V°_m$. In fact Hoiland[3] quotes an uncertainty of 0.2 cm^3/mol on $\Delta V°_m$. ^{c} The difference $\Delta V°(CH_3CO_2^-) - \Delta V°(HCO_2^-)$ has been corrected for the reduction of electrostriction (see text).

arise from a disruption of the cosphere of the alkyl group. For R = CH$_3$ the corresponding volume change amounts to $\Delta V°(CH_2CO_2^-) - \Delta V°(HCO_2^-)$ minus the reduction of electrostriction = 3.5 cm^3/mol. This numerical value is an important one. It represents the volume increase resulting from the rearrangement of the water molecules surrounding the methyl group upon neutralization of the electrical charge of the carboxylate group. The results of Figure 1 show that $\Delta V°$ increases sizeably in going from acetate to propionate and butyrate, although not as much as from formate to acetate. It may therefore be assumed that the cosphere of the α-CH$_2$, with respect to the CO$_2^-$ group, is completely disrupted (this point is further discussed in paragraph III.4). On this assumption the volume increase which arises from the rearrangement of the water molecules brought about by the introduction of a methylene group into water, owing to the so-called hydrophobic hydration, is also equal to 3.5 cm^3/mol. The fact that this rearrangement occurs with an increase of volume is in agreement with the original proposal of Frank and Evans[14] about the structure of water around hydrophobic groups.

The above can be summarized by stating that the increase of $\Delta V°(RCO_2^-)$ with m is essentially due to the rearrangement of the water molecules about the alkyl group, when the electrical charge of the carboxylate is neutralized upon protonation. These water molecules then adopt whichever structure they normally have around hydrophobic solutes.

The volume increase induced by the effect of the carboxylate group on water molecules about a given CH$_2$ group separated by m carbon atoms from the CO$_2^-$ can be taken as

$$\delta(\Delta V°_{m+1}) = \Delta V°(C_{m+1}H_{2m+3}CO_2^-) - \Delta V°(C_mH_{2m+1}CO_2^-) \qquad (7)$$

The distance d between the mth CH$_2$ and the carboxylate can be determined graphically assuming an extended configuration of the alkyl chain. For the four first C atoms Table I indicates that the product $d^2\delta(\Delta V°_{m+1})$ is constant, within the experimental uncertainty, as if the rearrangement of the water molecules about the alkyl group was induced by the electrical field of the CO$_2^-$ group.

2. *n-Alkylamines.* Reaction 2 can be written as

$$RNH_2 + H^+ \rightarrow RNH_3^+$$
$$\downarrow \qquad \uparrow$$
$$RNH_2 + H \rightarrow RNH_3 \qquad (8)$$

The volume change $\Delta V°(RNH_2)$ is given by

$$\Delta V°(RNH_2) = [\overline{V}°(RNH_3) - \overline{V}°(RNH_2)] - \overline{V}°(H^+) - \delta_V(RNH_3^+) \qquad (9)$$

with

$$\delta_V(RNH_3^+) = \overline{V}°(RNH_3) - \overline{V}°(RNH_3^+) \qquad (9a)$$

In eq 9 the δ_V term appears with a negative sign. This is the reason why, in the Introduction, we stated that $\Delta V°(RNH_2)$ should have shown, upon increasing m, a

variation opposite to that of $\Delta V°(RCO_2^-)$, had the effects determining these volume changes been comparable in both series.

As in the case of RCO$_2^-$, the term in brackets in eq 9 represents the volume increment for the addition of one H atom on to a nitrogen which has been found to be 1.5 $\pm$ 0.5 cm^3/mol.

We first consider the case of ammonia, i.e., R = H. $\Delta V°(NH_3)$ has been found to be -7.0 cm^3/mol.[4,15] Inserting the numerical values into eq 9 yields $\delta_V(NH_4^+) = 13.9 \pm$ 1.2 cm^3/mol. Thus, $\delta_V(NH_4^+)$ is almost 10 times larger than $\delta_V(HCO_2^-)$. It must be pointed out that the N–H bond lengths in NH$_3$ and NH$_4^+$ are very close.[16] Thus the large value of $\delta_V(NH_4^+)$ does not arise from a difference in the intrinsic volumes of NH$_4$ and NH$_4^+$. If, as for the formate ion, we assume that the volume contribution due to the change of H bonding in the course of the charging process may be neglected, we come to the conclusion that the electrostriction of NH$_4^+$ is large.

Accordingly, the substitution of one H atom of NH$_4^+$ by an alkyl group will result in a large reduction of electrostriction and thus to a sizeable increase of volume, while this effect was quite small for alkylcarboxylates. On the other hand, the charged nitrogen center will tend to disrupt the arrangement of the water molecules around the alkyl chain, and thus give rise to a volume decrease. To illustrate the result of these two antagonistic effects let us consider the substitution of one H atom of NH$_4^+$ by a methyl group. The reduction of electrostriction owing to steric reasons can be approximated as $\delta_V(NH_4^+)$ times the fraction f of surface area of NH$_4^+$ blocked by the methyl group. Calculations based on van der Waals radii yield $f = 0.35$. The reduction of electrostriction therefore amounts to 4.9 cm^3/mol. On the other hand, we may assume that the volume effect induced by the ammonium group on the α-CH$_2$ group is the same as that induced by a carboxylate, that is 3.5 cm^3/mol (this is equivalent to assuming that the volume change associated with the disruption of the water structure about an alkyl group is independent of the sign of the electrical charge inducing this disruption[17]). We thus have $\Delta V°(CH_3NH_2) = \Delta V°(NH_3) + 4.9 - 3.5 = -5.6$ cm^3/mol. This value coincides with the experimental value of the volume change upon protonation of methylamine.[4] We realize that this agreement may be fortuitous. The limitations of the above approximated calculations clearly appear when one attempts to extend them to higher n-alkylamines. The values calculated for ethylamine and n-propylamine were found to be more negative than the experimental ones. Nevertheless, it may be said that the reverse variation observed for $\Delta V°(RNH_2)$ with respect to $\Delta V°(RCO_2^-)$, with the alkyl chain length, is indeed the result of two antagonistic effects upon increasing size of R: (i) a positive contribution resulting from the reduction of electrostriction of the charged nitrogen center by the alkyl group and (ii) a negative contribution due to the disruption of the water structure around the alkyl chain. Note that a third effect, namely, the cosphere overlap effect,[13] may be at play in the case of the protonation of alkylamines. This effect has

TABLE II: Effect of Branching on the $\Delta V°$ for Alkylcarboxylate Ions

Ion	$\Delta V°$, cm^3/mol
Butyrate	13.9[a]
Isobutyrate	14.9[a]
Valerate	14.2[a]
Isovalerate	14.9[a]
Trimethylacetate	17.5[b]

[a] From ref 3. [b] Average value from ref 1 and 22.

been neglected with the RCO_2^- series because the electrostriction of the carboxylate group is small. With RNH_3^+ ions the disruption of the water structure around the ammonium group owing to the overlap of its cosphere and that of the alkyl chain may also contribute to the volume change upon protonation (positive contribution). This contribution cannot be properly evaluated at the present time.

III. Interpretation of Various Volumic Effects Involving Alkylcarboxylate and Alkylammonium Ions

The expressions of $\Delta V°(RCO_2^-)$ and of $\Delta V°(RNH_2)$ given by eq 4 and 9 involve $\bar{V}°(RCO_2^-)$ and $\bar{V}°(RNH_3^+)$. In fact, the variations of the $\Delta V°$'s with the characteristics of the alkyl R group come about from changes of $\bar{V}°$-(RCO_2^-) and $\bar{V}°(RNH_3^+)$ owing to the effects discussed above. It is therefore in principle identical to look at changes of $\Delta V°$'s or of $\bar{V}°(RCO_2^-)$ and $\bar{V}°(RNH_3^+)$. This remark makes our task much easier because there exist in the literature a large body of $\bar{V}°$ results which can be explained in terms of "steric" reduction of electrostriction and water structure rearrangement.

1. *Methylene Group Contribution to the Partial Molal Volumes of n-Alkyl Alcohols, Amines, Carboxylic Acids, Ammonium Ions, and Carboxylate Ions.* The methylene group contribution, $\bar{V}°(CH_2)$, for the mth methylene group in the alkyl chain defined as

$$\bar{V}°_m(CH_2) = \bar{V}°(C_mH_{2m+1}X)$$
$$- \bar{V}°(C_{m-1}H_{2m-1}X) \quad (10)$$

where $X = OH$,[7,18] NH_2,[4a] CO_2H,[2a,19,20] CO_2^-,[2a,19] and NH_3^+[21] is plotted as a function of m on Figure 2. It can be seen that for $m < 5$, $\bar{V}°_m(CH_2)$ increases for RCO_2^-, decreases for RNH_3^+, but remains practically constant for the three series of uncharged compounds (in going from $m = 1$ to 2, $\bar{V}°_m(CH_2)$ decreases by about 1 cm^3/mol. This variation may be due to a small change of the contribution of the packing of water molecules to $\bar{V}°_m(CH_2)$, for the first substitution). The increase of $\bar{V}°_m(CH_2)$ with m for RCO_2^- simply reflects the fact that the structure of water molecules around a given methylene group is less perturbed, as the distance between this group and the carboxylate is increased. On the other hand, $\bar{V}°_m(CH_2)$ decreases for RNH_3^+ because the reduction of electrostriction due to the substituting alkyl group overcomes the contribution of the water structure perturbation (see above).

2. *Influence of the Degree of Branching of the Alkyl Chain on $\bar{V}°(RCO_2^-)$ and $\bar{V}°(RNH_3^+)$, and on $\Delta V°(RCO_2^-)$.* When the branching of the alkyl chain is increased at a point in the chain sufficiently close to the charged group, $\Delta V°(RCO_2^-)$ should increase and $\bar{V}°(RCO_2^-)$ decrease, because the amount of water molecules surrounding the alkyl group under the influence of the charged group increases. Opposite variations should be found for $\Delta V°(RNH_3^+)$ and $\bar{V}°(RNH_3^+)$, upon branching, because the reduction of electrostriction is now the predominating effect.

TABLE III: Partial Molal Volumes of Isomeric Butanols, Butylcarboxylic Acids, Butylcarboxylate Ions, and Butylammonium Ions (cm^3/mol) in Water at 25 °C

| Alkyl group | Head group | | | |
	OH[a]	CO_2H[b]	CO_2^- [c]	NH_3^+ [c]
n-Butyl	86 6$_5$	100.5	92.3$_0$	80.1$_3$
Isobutyl	86 7$_5$	100.5	92.0$_9$	80.1$_5$
sec-Butyl	86 5$_5$	100.5	90.0$_4$	80.8$_5$
tert-Butyl	87 6$_0$	100.5	88.9$_6$	82.2$_9$

[a] From ref 23. [b] From ref 24. [c] From ref 5 with $\bar{V}°(Na^+) = 6.61$ cm^3/mol and $\bar{V}°(Cl^-) = 23.23$ cm^3/mol.[10,11]

The results listed in Tables II and III confirm these predictions. As expected, the increase of $\Delta V°$ is larger in going from butyrate to isobutyrate than from valerate to isovalerate. Indeed the branching occurs farther from the carboxylate in the second case than in the first. The very large increase of $\Delta V°$ observed in going from isovalerate to trimethylacetate[1,22] (see Table II) is due to the fact that three methyl groups are now in α position with respect to the carboxylate.

On the other hand, the partial molal volumes of the butylcarboxylate ions increase and those of the butylammonium ions decrease upon increasing branching.[5] The $\bar{V}°$'s of the uncharged compounds (alcohols,[23] carboxylic acids[24]) are hardly affected by the branching of the alkyl chain (see Table III).

3. *Effect of the Degree of Substitution of the Nitrogen Center upon the Volume Change of Protonation of Amines.* The method used to evaluate $\Delta V°(CH_3NH_2)$ from $\Delta V°(NH_3)$ has been extended to calculate the $\Delta V°$'s for di- and trimethylamine. The fractions f of surface area of the charged nitrogen center blocked by the second and third substituting methyl groups have been found to be 0.28$_5$ and 0.22. The corresponding decreases of electrostriction are therefore 13.9 × 0.28$_5$ = 3.9 cm^3/mol and 13.9 × 0.22 = 3.1 cm^3/mol. On the other hand, the contributions of the water structure rearrangement have been calculated to be -3.2 and -3.0 cm^3/mol (the overlap of the spheres equivalent to the methyl groups has been taken into account in the calculation of these quantities). Using these numerical values we can write $\Delta V°[(CH_3)_2NH] = \Delta V°[(CH_3NH_2)] + 3.9 - 3.2 = -4.9$ cm^3/mol (experimental value -5.1 cm^3/mol[4a]) and $\Delta V°[(CH_3)_3N] = \Delta V°[(CH_3)_2NH]_3 + 3.1 - 3.0 = -4.8$ cm^3/mol (experimental value -6.0 cm^3/mol[4a]). Note that the calculated $\Delta V°$'s would be -5.2 and -5.6 cm^3/mol for $(CH_3)_2NH$ and $(CH_3)_3N$ if we assumed a constant increment of 3.5 cm^3/mol for the contribution of the structure rearrangement about each substituting methyl group.

Thus, these approximate calculations permit us to account semiquantitatively for the so far unexplained[4a] very small changes in $\Delta V°$ in going from methylamine to dimethylamine and trimethylamine. Note that it is only for the substitution of the charged nitrogen atom by methyl groups that the reduction of electrostriction is closely compensated by the structural rearrangement of water molecules. For larger substituting alkyl groups, such as ethyl or propyl, the effect of the decrease of electrostriction would overcompensate that of the structural rearrangement and result in a decrease of $|\Delta V°|$ upon increasing substitution. This is indeed what has been found.[4a]

4. *Remarks about the Tetramethylammonium (TMA) Ion.* From the study of the excess ultrasonic absorption in systems where TMA ions are in the presence of strong chelating agents[25] or polyions[26] as well as from a consideration of the various contributions to the partial molal volume of the TMA ion,[27] it has been concluded that water

molecules around TMA ions have about the same volume as in bulk water. The volume of these water molecules could have been modified by two main effects: the electrostriction by the charged nitrogen center and the hydrophobic hydration of the methyl groups. The first effect is likely to be negligible because water molecules cannot approach the charged nitrogen, owing to the steric hindrance of the methyl groups. The contribution of the second effect must therefore also be negligible. This conclusion has two implications. The first one is that indeed a charged group brings about a disruption of the water structure around a hydrophobic group close to or bound to the charged group. Thus the behavior of the TMA ion supports the assumption made throughout this paper. The second implication is that the disruption must be complete. This supports the assumption made above when discussing the value of the difference $\Delta V°(CH_3CO_2^-)$ $- \Delta V°(HCO_2^-)$.

5. *Variation of the Volume Change upon Tetra-alkylammonium (TAA) Ion Pairing with Ionic Strength.* Thus far we have dealt with solutions where the charged group and the alkyl group belong to the same molecular ion. However, the rearrangement of water molecules was found to give rise to a significant volume change up to a distance equivalent to three carbon–carbon bond lengths, i.e., about 0.4 nm (see Table I). Therefore when an ion comes sufficiently close to a hydrophobic solute, either because the solution is concentrated or due to fluctuations, the same kind of rearrangement is expected to occur and to give rise to a volume decrease. Part of the change of the volume decrease upon pairing of TAA ions at increasing ionic strength μ may be due to such an effect. Indeed when μ is increased the distance between the added ions and the alkyl chains of the TAA ions decreases, thereby resulting in a greater disruption of the arrangement of the water molecules about the chains. The volume of these water molecules becomes closer to that in bulk water. As a result the volume decrease upon TAA ion pairing should become smaller and smaller, as experimentally observed.[28]

IV. Relevance of the Postulated Structural Rearrangement for the Interpretation of Volumic Effects Arising in Aqueous Solutions of Polyelectrolytes, Micellar Ionic Detergents, Proteins, and Heterocyclic Aromatic Compounds

1. *Polyelectrolyte and Ionic Micellar Solutions.* In these systems a fairly large fraction of counterions is specifically bound or close to the charged sites, in the Stern Layer.[26,29,30] With TAA counterions, the effect of the charged sites on the water molecules about the alkyl chains of the TAA counterions, when these ions are bound to or close enough to the sites, should result in a volume contraction.

It has indeed been observed that the interaction between large TAA ions and polyions gives rise to a negative volume change if TMA is used as a reference ion.[22,31,32] On the other hand, the volume change upon micellization of ionic detergents is smaller in the presence of large TAA ions than with TMA or alkali metal ions, thus revealing the existence of a negative contribution with the former.[33,34]

2. *Protein Solutions.* The denaturation of globular proteins involves the transfer of hydrophobic side chains from a hydrophobic environment to water. On the basis of results obtained for the dissolution of model hydrophobic compounds in water, the denaturation of proteins was expected to give rise to a large volume contraction. In fact the measurements yielded small and sometimes positive volume changes.[35] A partial explanation for these

findings may lie in the fact that in the denatured state, the transferred hydrophobic side chains are often close to protein charged groups. To a large extent these groups will prevent the rearrangement of water molecules that should have occurred about the hydrophobic side chains, upon transfer to water. This process will therefore result in a small volume change.

3. *Stacking of Heterocyclic Aromatic Compounds.* The stacking of neutral derivatives of purine gives rise to negative volume changes[36] ("normal" hydrophobic effect[14]). On the contrary, charged derivatives such as nucleotides yield positive volume changes.[37] These apparently contradictory findings can be easily reconciled by assuming that the electrical charge brings about a large disruption of the arrangement of the water molecules about the aromatic heterocycles. As a result the volume change upon stacking may be less negative and eventually positive for charged derivatives, while it is negative for the uncharged compounds.

Conclusion

The assumption that an electrically charged group can bring about a rearrangement of the water molecules around neighboring alkyl groups, in conjunction with the reduction of electrostriction of the charged group owing to the steric hindrance of the alkyl group, has permitted us to account for (1) the variation of the volume change upon protonation of n-alkylamines and n-alkylcarboxylate ions with the alkyl chain length and branching, and with the substitution degree of the nitrogen center and (2) the changes of the partial molal volumes of alkylammonium and alkylcarboxylate ions with the alkyl chain length and branching.

Moreover the assumed rearrangement of water molecules may be relevant to the interpretation of several volumic effects which have been observed in aqueous solutions of large tetraalkylammonium ions, polyelectrolytes, micellar detergents, proteins, and heterocyclic aromatic compounds.

Finally, it should be pointed out that the calculations which lead to the δ_V's can be extended to any physicochemical property X (entropy, enthalpy, specific heat, adiabatic compressibility, viscosity coefficient B, etc.) provided that the partial molal quantities $\bar{X}°$ obey the additivity law and that the change of $\bar{X}°$ upon protonation and $\bar{X}°(H^+)$ are known. The δ_X's should be very helpful to assess the effect of a molecular ion on the water molecules close to it. Work along these lines is in progress.

References and Notes

(1) W. Kauzmann, A. Bodanzski, and J. Rasper, *J. Am. Chem. Soc.*, **84**, 1777 (1962).
(2) (a) E. King, *J. Phys. Chem.*, **73**, 1220 (1969); (b) Recently there has been some attempts (S. Terasawa, H. Itsuki, and S. Arakawa, *J. Phys. Chem.*, **79**, 2345 (1975); J. T. Edward, P. G. Farrell, and F. Shahidi, *J. Chem. Soc., Faraday Trans. 1*, **73**, 705 (1977); F. Shahidi, P. G. Farrell, and J. T. Edward, *ibid.*, **73**, 715 (1977)) to evaluate the contribution of H bonding to the partial molal volume (pmv) of various classes of compounds, mostly nonelectrolytes, by comparing their pmv to that of hypothetical hydrocarbons with the same van der Waals volume. This approach rests on the assumption that hydrocarbons do not interact with water. In fact we know that hydrocarbons bring about changes in the time average structure of water and therefore cannot be used as reference compounds. Nevertheless, this approach looks promising.
(3) H. Hoiland, *J. Chem. Soc., Faraday Trans. 1*, **70**, 1180 (1974).
(4) (a) S. Cabani, G. Conti, and L. Lepori, *J. Phys. Chem.*, **78**, 1030 (1974); (b) S. Cabani, G. Conti, L. Lepori, and G. Leva, *ibid.*, **76**, 1343 (1972).

(5) M. Sakurai, T. Komatsu, and T. Nakagawa, *J. Solution Chem.*, **4**, 511 (1975).

(6) O. Kiyohara, G. Perron, and J. Desnoyers, *Can. J. Chem.*, **53**, 3263 (1975).

(7) M. Friedman and A. Scheraga, *J. Phys. Chem.*, **69**, 3795 (1965).

(8) $\bar{V}°$(cyclohexanone) = 99.5 cm³/mol. (K. Kale and R. Zana, unpublished measurements.)

(9) A. Bondi, *J. Phys. Chem.*, **68**, 41 (1964).

(10) R. Zana and E. Yeager, *J. Phys. Chem.*, **71**, 521 (1967).

(11) F. Millero, *Chem. Rev.*, **71**, 147 (1971).

(12) R. W. Gurney, "Ionic Processes in Solution", McGraw-Hill, New York, N.Y., 1953.

(13) H. L. Friedman and C. V. Krishnan, *Water, Compr. Treat.*, **3**, 16–18, 115–16 (1973).

(14) H. Frank and M. Evans, *J. Chem. Phys.*, **13**, 507 (1945); G. Nemethy and H. A. Scheraga, *J. Chem. Phys.*, **36**, 3401 (1962); *J. Phys. Chem.*, **66**, 1773 (1962); *ibid.*, **67**, 2888 (1963); G. Nemethy, *Angew. Chem., Int. Ed. Engl.*, **6**, 195 (1967).

(15) R. H. Stockes, *Aust. J. Chem.*, **28**, 2109 (1975); N. A. North, *J. Phys. Chem.*, **77**, 93 (1973).

(16) R. Seymour and A. Pryor, *Acta Crystallogr., Sect. B*, **26**, 1487 (1970), and references therein.

(17) The volume changes for the protonation of the phenate ion PhO⁻ and of aniline PhNH₂ have been measured (see S. D. Hamann and M. Linton, *J. Chem. Soc., Faraday Trans. 1*, **70**, 2239 (1974); **71**, 485 (1975)). Calculations similar to those reported in paragraph II lead to

$$\delta_V(\text{PhO}^-) = \bar{V}°(\text{PhO}) - \bar{V}°(\text{PhO}^-) = 11.5 \text{ cm}^3/\text{mol}$$

$$\delta_V(\text{PhNH}_2) = \bar{V}°(\text{PhNH}_3) - \bar{V}°(\text{PhNH}_3^+) = 11.4 \text{ cm}^3/\text{mol}$$

These δ_V's contain contributions of the structure rearrangement of water molecules and of the reduction of electrostriction upon substitution of the H atoms of HO⁻ and of NH₄⁺ by a phenyl group for PhO⁻ and PhNH₃⁺, respectively. The reduction of electrostriction has been calculated on geometric ground, as described in section II.2 for CH₃NH₂ and referring to the values $\delta_V(\text{NH}_4^+)$ = 13.9 cm³/mol and $\delta_V(\text{HO}^-)$ = 15.1 cm³/mol (calculated from the volume change of the reaction H⁺ + HO⁻ → H₂O). The contributions of the structure rearrangement of the water molecules around the phenyl group of PhO⁻ and PhNH₃⁺ under the effect of the charged groups were found

to −1.8 and −1.7 cm³/mol, respectively. This result supports our assumption that the contribution of the structure rearrangement may, to a first approximation, be assumed to be independent of the sign of the perturbing electrical charge.

(18) S. Terasawa, H. Itsuki, and S. Arakawa, *J. Phys. Chem.*, **79**, 2345 (1975); M. Manabe and M. Koda, *Bull. Chem. Soc. Jpn.*, **48**, 2367 (1975); T. Nakajima, T. Komatsu, and T. Nakagawa, *ibid.*, **48**, 783 (1975); C. Jolicoeur and G. Lacroix, *Can. J. Chem.*, **54**, 624 (1976).

(19) M. Sakurai, T. Komatsu, and T. Nakagawa, *Bull. Chem. Soc. Jpn.*, **48**, 3491 (1975).

(20) H. Hoiland, *Acta Chem. Scand., Ser. A*, **28**, 699 (1974).

(21) J. Desnoyers and M. Arel, *Can. J. Chem.*, **45**, 359 (1967).

(22) J. Komiyama, Y. Takeda, M. Ando, and T. Iijima, *Polymer*, **15**, 568 (1974); *Eur. Polym. J.*, **12**, 201 (1975).

(23) F. Franks and T. Smith, *Trans. Faraday Soc.*, **64**, 2962 (1968).

(24) M. Palma and J. P. Morel, *J. Chim. Phys. Physicochim. Biol.*, **73**, 645 (1976).

(25) M. Eigen, *Pure Appl. Chem.*, **6**, 97 (1963).

(26) C. Tondre and R. Zana, *J. Phys. Chem.*, **10**, 2635 (1971); *Biophys. Chem.*, **1**, 367 (1974); and references therein.

(27) L. Labiberté and B. Conway, *J. Phys. Chem.*, **74**, 4116 (1970).

(28) W. Y. Wen and K. Nara, *J. Phys. Chem.*, **71**, 3907 (1967); **72**, 1137 (1968); W. Y. Wen, K. Nara, and R. Wood, *ibid.*, **72**, 3048 (1968).

(29) K. Shirahama, *Bull. Chem. Soc. Jpn.*, **47**, 3165 (1974); T. Sasaki, M. Mattori, J. Sasaki, and K. Nukina, *ibid.*, **48**, 1397 (1975).

(30) D. Stigter, *J. Phys. Chem.*, **68**, 3603 (1964).

(31) G. Boyd and K. Bunzl, *J. Am. Chem. Soc.*, **96**, 2054 (1974).

(32) C. Tondre, K. Kale, and R. Zana, *Eur. Polym. J.*, in press.

(33) G. Musbally, G. Perron, and J. Desnoyers, *J. Colloid Interface Sci.*, **54**, 80 (1976); P. Leduc and J. Desnoyers, *Can. J. Chem.*, **51**, 2993 (1973).

(34) K. Kale and R. Zana, *J. Colloid Interface. Sci.*, in press.

(35) J. F. Brandts, R. Oliveira, and C. Westwort, *Biochemistry*, **10**, 1038 (1970); S. A. Hawley, *ibid.*, **10**, 2436 (1970); S. J. Gill and R. L. Glogovsky, *J. Phys. Chem.*, **69**, 1515 (1965).

(36) D. Kasarda, *Biochem. Biophys. Acta*, **217**, 535 (1970); D. Porschke and F. Eggers, *Eur. J. Biochem.*, **26**, 490 (1972); A. Cesaro, E. Russo, and V. Crescenzi, *J. Phys. Chem.*, **80**, 335 (1976); U. Gaarz and H. D. Ludemann, *Ber. Bunsenges. Phys. Chem.*, **80**, 607 (1976).

(37) A. Colter and F. Grunwald, *J. Phys. Chem.*, **74**, 3637 (1970); J. Lang, J. Sturm, and R. Zana, *ibid.*, **78**, 80 (1974), and unpublished results on cytidine 5'-monophosphate.

Thermodynamics of Electrolytes. 8. High-Temperature Properties, Including Enthalpy and Heat Capacity, with Application to Sodium Chloride

Leonard F. Silvester and Kenneth S. Pitzer*

Department of Chemistry and Lawrence Berkeley Laboratory, University of California, Berkeley, California 94720 (Received April 18, 1977)

The ion-interaction type of equation which has proven so successful for activity and osmotic coefficients of both pure and mixed electrolytes near room temperature is extended for wide temperature ranges and for the enthalpy and heat capacity. An improved equation is obtained for the dielectric constant of water over a wide range of temperature and density; it is used to calculate the Debye–Hückel parameters to 350 °C for enthalpy and heat capacity as well as for osmotic and activity coefficients. These equations are applied to the extensive array of thermodynamic data for aqueous sodium chloride from 0 to 300 °C. Good agreement is obtained and the equations thus provide a convenient analytical representation of the thermodynamic properties of NaCl(aq). Also the results indicate that at 300 °C sodium chloride is still a strong electrolyte with little tendency toward the formation of ion pairs.

While aqueous electrolytes have been very extensively studied at room temperature, much less attention has been given to these systems at high temperatures. By far the most thoroughly studied example is sodium chloride. In this paper we first extend to enthalpy and heat capacity the equations developed in earlier papers in this series.[1-4] The dielectric properties of water over a wide temperature range are reviewed and an improved equation derived; this combined with an equation for the density of water yields the various Debye–Hückel parameters as a function of

temperature. The various data for aqueous sodium chloride under saturation pressure, including osmotic coefficients, enthalpies, and heat capacities, are then fitted simultaneously to the equations with good accuracy through 300 °C and 6 M.

Since the dielectric constant of water is only about 20 at 300 °C, it was not evident that a strong-electrolyte treatment would be satisfactory at that temperature. It is significant that there is no need to assume any specific ion pairing under these conditions. This and other

questions are discussed in terms of the results obtained.

General Equations

The basic equations for enthalpy and heat capacity will be derived in general form for an electrolyte with ionic charges z_M and z_X for the positive and negative ions in electronic units. Likewise ν_M and ν_X are the numbers of ions of each type in the formula and $\nu = \nu_M + \nu_X$. Thus the results of this section will be applicable to various valence types of electrolytes.

The total excess Gibbs energy is

$$G^{ex} = n_w \nu m R T (1 - \phi + \ln \gamma_\pm) \qquad (1)$$

where n_W is the number of kilograms of solvent, m is the molality, R is the gas constant, T designates the temperature in K, ϕ is the osmotic coefficient, and $\gamma_\pm$ is the activity coefficient.

Equation 1 may be rewritten as

$$G^{ex} = n_1 \overline{G}_1^{ex} + n_2 \overline{G}_2^{ex} \qquad (2)$$

where n_1 and n_2 are the number of moles of solvent and solute, respectively, and $\overline{G}_1^{ex}$ is the partial molal excess Gibbs energy of the solvent, and $\overline{G}_2^{ex}$ is the partial molal excess Gibbs energy of the solute.

The quantities $\overline{G}_1^{ex}$ and $\overline{G}_2^{ex}$ are related to ϕ and $\ln \gamma_\pm$ by

$$\overline{G}_1^{ex} = (\nu n_2/n_1)RT(1 - \phi) \qquad (3)$$

$$\overline{G}_2^{ex} = \nu R T \ln \gamma_\pm \qquad (4)$$

We now adopt the general form given in paper I[1] and II[2] of this series for G_{ex} which leads to the following equations for ϕ and $\ln \gamma_\pm$ of a pure electrolyte:

$$\phi - 1 = -|z_M z_X| A_\phi \frac{I^{1/2}}{1 + bI^{1/2}} + m \frac{2\nu_M \nu_X}{\nu}(\beta_{MX}^{(0)} + \beta_{MX}^{(1)} e^{-\alpha I^{1/2}}) + m^2 \frac{2(\nu_M \nu_X)^{3/2}}{\nu} C_{MX}^\phi \qquad (5)$$

$$\ln \gamma_\pm = -|z_M z_X| A_\phi \left(\frac{I^{1/2}}{1 + bI^{1/2}} + \frac{2}{b}\ln(1 + bI^{1/2}) \right) + m\frac{2\nu_M \nu_X}{\nu}\left(2\beta_{MX}^{(0)} + \frac{2\beta_{MX}^{(1)}}{\alpha^2 I}\left(1 - \left(1 + \alpha I^{1/2} - \frac{\alpha^2 I}{2}\right)e^{-\alpha I^{1/2}}\right)\right) + \frac{3m^2}{2}\left(\frac{2(\nu_M \nu_X)^{3/2}}{\nu}\right)C_{MX}^\phi \qquad (6)$$

I is the ionic strength

$$I = {}^1/_2 \sum_i m_i z_i^2$$

and A_ϕ is the Debye–Hückel coefficient for the osmotic function given as

$$A_\phi = \frac{1}{3}\left(\frac{2\pi N_0 \rho_w}{1000}\right)^{1/2}\left(\frac{e^2}{DkT}\right)^{3/2} = \frac{A_\gamma}{3} \qquad (7)$$

where N_0 is Avagadro's number, ρ_w is the density of the solvent, and D the static dielectric constant of pure water, k is Boltzmann's constant, and e is the absolute electronic charge. Since the values of ν_M, ν_X, and ν for any 1–1 salt (e.g., NaCl) are 1, 1, and 2 the factor $(2\nu_M \nu_X/2)$ is unity.

The leading term in eq 5 and 6 arises from the long-range electrostatic interactions; the coefficients $\beta_{MX}^{(0)}$ and $\beta_{MX}^{(1)}$ account for various types of short-range interactions between M and X, and for indirect forces arising from the solvent; the third coefficient C_{MX}^ϕ is for triple ion interactions and is important only at high concentrations. The

parameter b was given the value 1.2 for all electrolytes and α is 2.0 for all 1–1 and most other solutes; b and α are taken as temperature independent. The quantities $\beta_{MX}^{(0)}$, $\beta_{MX}^{(1)}$, and C_{MX}^ϕ are adjusted for a given salt at fixed temperature by a least-squares fit of osmotic and/or activity coefficient data.

Equations 5 and 6 are consistent with the standard states adopted for this study which are the pure solvent at the same temperature and pressure of the solution and for the solute the limiting state in which $\gamma_\pm$ approaches unity as the concentration becomes infinitely dilute, this to apply at every temperature and pressure.

The relative enthalpy, L, of an electrolyte solution is defined to be

$$L = H - H° \qquad (8)$$

where H is the total enthalpy of the solution and $H°$ that of the components of the solution in their standard states.

The quantity L is related to G^{ex} by the equation

$$L = -T^2(\partial(G^{ex}/T)/\partial T)_{P,m} \qquad (9)$$

Equations 1 and 9 yield for L

$$L = \nu m R T^2[(\partial \phi/\partial T)_{P,m} - (\partial \ln \gamma_\pm/\partial T)_{P,m}] \qquad (10)$$

The apparent relative molal enthalpy, $^\phi L$, is defined as

$$^\phi L = \frac{L - n_1 \overline{L}_1°}{n_2} = \frac{L}{n_2} \qquad (11)$$

Taking the appropriate derivatives of eq 5 and 6 as prescribed by eq 10 and 11, one obtains for $^\phi L$ the result

$$^\phi L = \nu |z_M z_X|(A_H/3.6)\ln(1 + 1.2 I^{1/2}) - 2\nu_M \nu_X R T^2(m B'_{MX} + m^2 C'_{MX}) \qquad (12)$$

where

$$B'_{MX} = (\partial B_{MX}/\partial T)_{I,P} \qquad (13)$$

$$B_{MX} = \beta_{MX}^{(0)} + (2\beta_{MX}^{(1)}/\alpha^2 I)[1 - (1 + \alpha I^{1/2}) \times \exp(-\alpha I^{1/2})] \qquad (14)$$

$$C'_{MX} = {}^1/_2(\nu_M \nu_X)^{1/2}(\partial C_{MX}^\phi/\partial T)_{I,P} \qquad (15)$$

The quantity A_H is the Debye–Hückel coefficient for enthalpy

$$A_H = -9 A_\phi R T^2[T^{-1} + (\partial \ln D/\partial T)_P + \alpha_w/3] \qquad (16)$$

where $\alpha_w = (\partial \ln V/\partial T)_P$ is the coefficient of thermal expansion of water.

A common type of enthalpy measurement is the heat of dilution. If this is reported for the dilution of solution containing 1 mol of solute from m_1 to m_2, it is related as follows to the apparent molal enthalpy:

$$\Delta \overline{H}_D(m_1 \rightarrow m_2) = {}^\phi L_2 - {}^\phi L_1 \qquad (17)$$

The integral heat of solution of a salt MX is taken as the heat effect for the reaction

$$n_2 MX(s) + n_1 H_2O(l) = n_2 MX(aq, m)$$
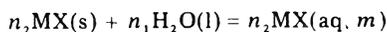
The enthalpy change for this reaction is given as

$$\Delta H_s = n_1 \overline{H}_1 + n_2 \overline{H}_2 - n_1 H_1°- n_2 H_2°(s) \qquad (18)$$

which may be rewritten as

$$\Delta H_s = L + n_2(\overline{H}_2° - H_2°(s))$$

As the concentration m approaches zero, we have

$$\lim_{m \rightarrow 0}(\Delta H_s/n_2) = \Delta \overline{H}_s° = (\overline{H}_2° - H_2°(s)) \qquad (19)$$

TABLE I: Array of Coefficients for Eq 29

		e_{ij}				
i	j	0	1	2	3	4
0		88.287	−78.1110993	77.6526372	0	0
1		−0.67033927	0.443465512	−0.135474228	−0.334969862	
2		$1.99954913 \times 10^{-3}$	$-8.71140434 \times 10^{-4}$	$-1.10849697 \times 10^{-4}$		
3		$-2.71567936 \times 10^{-6}$	$5.91444341 \times 10^{-7}$			
4		$1.40598463 \times 10^{-9}$				

where $\Delta \bar{H}_s{}^\circ$ is the heat of solution per mole of salt at infinite dilution. At finite concentrations we therefore have

$$\Delta \bar{H}_s = \Delta \bar{H}_s{}^\circ + {}^\phi L \qquad (20)$$

The value of $\Delta \bar{H}_s{}^\circ$ at a given temperature may be found by fitting the experimental values of $\Delta \bar{H}_s$ to eq 12 and 20 treating $\Delta \bar{H}_s{}^\circ$ as an adjustable parameter.

The total relative heat capacity, J, is defined as

$$J = C_P - C_P{}^\circ = C_P - (n_1 C_{P_1}{}^\circ + n_2 \bar{C}_{P_2}{}^\circ) \qquad (21a)$$

where $\bar{C}_{P_2}{}^\circ$ is the partial molal heat capacity of the solute at infinite dilution and $C_{P_1}{}^\circ$ is the molal heat capacity of pure water. Also

$$J = (\partial L / \partial T)_{P,m} \qquad (21b)$$

The apparent molal heat capacity, ${}^\phi C_P$, is defined to be

$${}^\phi C_P = (C_P - n_1 C_{P_1}{}^\circ)/n_2 \qquad (22)$$

From eq 11 and 21b, we find that

$${}^\phi C_P - \bar{C}_{P_2}{}^\circ = (\partial {}^\phi L / \partial T)_{P,m} \qquad (23)$$

The temperature derivative of eq 12 yields

$${}^\phi C_P = \bar{C}_{P_2}{}^\circ + \nu |z_M z_X| (A_J/3.6) \ln (1 + 1.2 I^{1/2}) - 2\nu_M \nu_X R T^2 (m B_{MX}'' + m^2 C_{MX}'') \qquad (24)$$

where

$$B_{MX}'' = \left(\frac{\partial^2 B_{MX}}{\partial T^2} \right)_{P,m} + \frac{2}{T} \left(\frac{\partial B_{MX}}{\partial T} \right)_{P,m} \qquad (25)$$

and

$$C_{MX}'' = {}^1/_2 (\nu_M \nu_X)^{1/2} \left[\left(\frac{\partial^2 C_{MX}^\phi}{\partial T^2} \right)_{P,m} + \frac{2}{T} \left(\frac{\partial C_{MX}^\phi}{\partial T} \right)_{P,m} \right] \qquad (26)$$

$$A_J = (\partial A_H / \partial T)_P \qquad (27)$$

Heat capacity data on electrolytes are obtained by direct measurements on the solution using a calorimeter. The resulting total heat capacities, converted to ${}^\phi C_P$, may then be fitted to eq 24 treating $\bar{C}_{P_2}{}^\circ$ as an adjustable parameter. Values of $\bar{C}_{P_2}{}^\circ$ may also be obtained from heat of solution data according to

$$(\partial \Delta \bar{H}_s{}^\circ / \partial T)_P = \bar{C}_{P_2}{}^\circ - C_{P_2}{}^\circ (s) \qquad (28)$$

provided $C_{P_2}{}^\circ (s)$, the heat capacity of the pure salt in the solid phase, is known.

Debye–Hückel Parameters

The parameters A_φ, A_H, and A_J as given in eq 7, 16, and 27 depend only on the thermodynamic and electrostatic properties of water.

The density of pure water, ρ_w, and its temperature derivatives were computed from the equation of state for liquid water given by Keenan and Keyes.[5] A detailed description of the equation may be found in the appendix of Keenan and Keyes[5] steam tables or from Helgeson and Kirkham.[6]
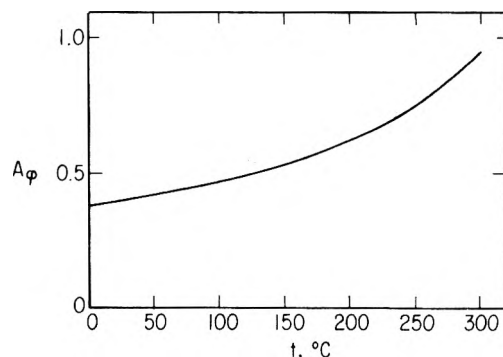

Figure 1. Debye–Hückel osmotic coefficient parameter vs. temperature.

The electrostatic properties of pure water were obtained by fitting the data on the static dielectric constant of water given by Oshry,[7] Owen et al.,[8] and Heger[9] to a slightly modified version of an equation originally proposed by Helgeson and Kirkham:[6]

$$D = \sum_{i=0}^{4} \sum_{j=0}^{4-i} e_{ij} t^i \rho_w{}^j \qquad (29)$$

where t is the temperature in degrees Celsius and e_{ij} is an array of temperature and pressure independent coefficients determined from a least-squares analysis of the data and given in Table I.

The data on the dielectric constant of water covers a much wider pressure interval than the Keenan–Keyes[30] equation of state which is limited to pressures up to 1 kbar. Consequently, instead of using data on D only up to 1 kbar we have used the entire array of data and weighted each data point up to 1 kbar as unity and those above as $(1.0/\text{pressure (kbar)})^2$. We have found that a much better overall fit resulted by assigning the value of 88.726 (D at 0 °C as given by Owens et al.[34]) to e_{00}, and setting e_{03} and e_{04} to zero.

Values of A^ϕ, A_H, and A_J along the liquid–vapor saturation curve of water are tabulated in Table II and plotted in Figures 1–3.

The values in Table II for A_ϕ from 0 to 100 °C agree well with those recently chosen for that range[10] but A_H and especially A_J are sensitive to the derivatives of the dielectric constant. While A_H at 25 °C in Table II is not significantly different from the value[10] in recent use, the values of A_J and those of A_H at other temperatures differ by as much as 20%. It is not clear whether the present results are better or not for the range 0–100 °C at 1 atm. However our interest in a much wider range of temperature and pressure forced us to depend primarily on data extending over these conditions, and these data do not agree as well as is desired with investigations limited to 1 atm and 0–100 °C. Further measurements of the dielectric constant of water with maximum attainable accuracy are to be desired.

Application to NaCl(aq)

Before discussing the details of our calculations we note that above 100 °C the data relate to the saturation pressure while below 100 °C the pressure is a constant 1 atm. This

TABLE II: Debye–Hückel Parameters for the Osmotic Coefficient, Enthalpy, and Heat Capacity[a]

t, °C	A_ϕ	A_H/cal mol^{-1}	A_J/cal K^{-1} mol^{-1}
0	0.3770	411	9.6
10	0.3820	516	11.3
20	0.3878	635	12.3
25	0.3910	698	12.8
30	0.3944	762	13.2
40	0.4017	899	14.2
50	0.4098	1046	15.2
60	0.4185	1203	16.3
70	0.4279	1372	17.6
80	0.4380	1555	19.0
90	0.4488	1753	20.7
100	0.4603	1969	22.5
110	0.4725	2204	24.6
120	0.4855	2461	26.9
130	0.4992	2743	29.6
140	0.5137	3053	32.6
150	0.5291	3394	36.1
160	0.5454	3773	40.1
170	0.5627	4193	44.8
180	0.5810	4664	50.4
190	0.6005	5194	57.1
200	0.6212	5796	65.4
220	0.6670	7285	88.8
240	0.7200	9336	127
260	0.7829	12315	194
280	0.8596	16935	323
300	0.9576	24789	604
325	1.1323	45943	1779
350	1.4436	125150	11948

[a] 1 cal = 4.184 J.
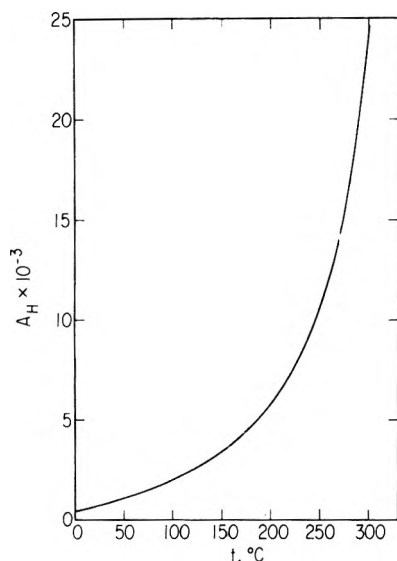
Figure 2. Debye–Hückel enthalpy parameter vs. temperature.

shift of reference pressure is unfortunate but unavoidable. It leads, in principle, to some small correction terms in certain temperature derivative relationships. These appear, as can best be judged at this time, to be within experimental uncertainties, but more accurate tests may be feasible when volumetric data are more fully examined.

The extensive array of experimental results for aqueous sodium chloride is listed in Table III. The first column gives the reference number, the second column the type of data, osmotic coefficient, enthalpy, etc., the third column lists the experimental method, the fourth column lists the temperature range, and the fifth column the concentration range. The freezing point depression data of Scatchard and Prentiss[12] were recalculated using a cryoscopic constant of 1.860 and the method outlined by Pitzer and
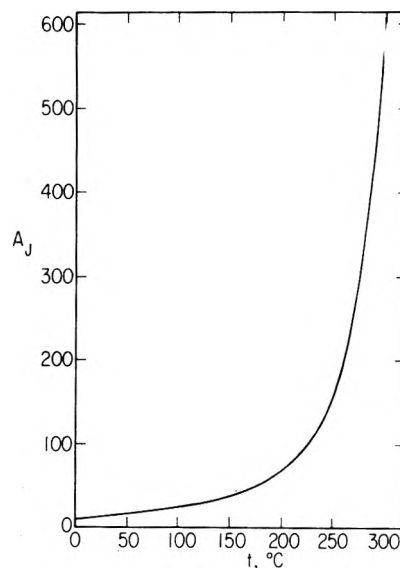
Figure 3. Debye–Hückel heat capacity parameter vs. temperature.

TABLE III: Data on Aqueous NaCl Solutions

Ref	Data type	Method[a]	T range, °C	m
12	ϕ	fdp	0	0.002–1.0
13	ϕ	isop	0	0.1–4.0
14	ϕ	isop	15	0.1–4.0
15	$\gamma_\pm$	emf	15–45	0.002–0.1
16	$\gamma_\pm$	emf	15–50	0.01–1.0
17	ϕ	vp	20–30	2.0–4.0
18	ϕ	vp	25–100	1.0–6.1
19	ϕ	bp	60–100	0.05–1.0
20	ϕ	bp	60–100	1.0–4.0
21	ϕ	vp	125–250	0.5–3.0
22	ϕ	vp	75–300	4.8–(6.4–10.4)
23	ϕ	vp	125–300	0.1–3.5
24	ΔH_s	cal	0–100	0.001–0.03
25	ΔH_s	cal	100–200	0.007–0.04
26	ΔH_D	cal	25–100	0.04–5.0
27	ΔH_D	cal	40–80	0.005–6.0
28	C_P	cal	24.15	0.001–2.0
29	C_P	cal	25.0	0.01–3.0
30	ϕC_P	cal	25.0	0.04–2.3
31	C_P	cal	1.5–45	0.01–3.0
32	C_P	cal	80–200	0.35–2.1

[a] fpd, freezing point depression; isop, isopiestic; vp, vapor pressure lowering; bp, boiling point elevation; emf, electrochemical cell; cal, calorimeter.

Brewer;[10] the remaining osmotic and activity coefficient data were used as reported in the original literature. The experimental enthalpy data were used as reported. The thermochemical calorie equal to 4.184 J is used throughout.

The concentration dependence of the data in Table III at any single experimental temperature may be reproduced by appropriate application of eq 5, 6, 12, and 24. The problem then reduces to finding suitable analytical forms to describe the temperature dependence of $\beta^{(0)}$, $\beta^{(1)}$, and C^ϕ. The following general forms were found to reproduce the entire array of data in Table III.

$$\beta^{(0)} = q_1 + q_2\left(\frac{1}{T} - \frac{1}{T_r}\right) + q_3 \ln(T/T_r) +$$
$$q_4(T - T_r) + q_5(T^2 - T_r^2) \tag{30}$$

$$\beta^{(1)} = q_6 + q_9(T - T_r) + q_{10}(T^2 - T_r^2) \tag{31}$$

$$C^\phi = q_{11} + q_{12}\left(\frac{1}{T} - \frac{1}{T_r}\right) + q_{13} \ln(T/T_r) +$$
$$q_{14}(T - T_r) \tag{32}$$

TABLE IV: Coefficients for Eq 30, 31, 32, and 34

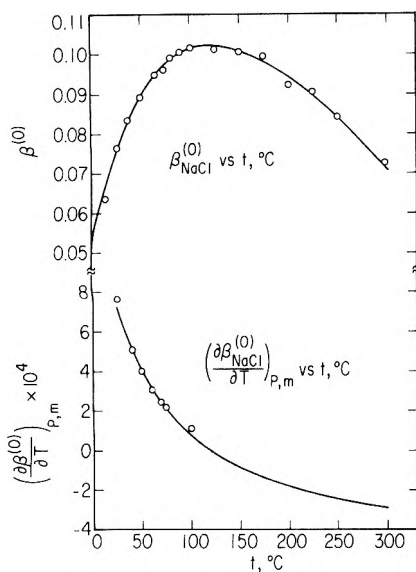|	
$q_1 = 0.0765$	$q_{11} = 0.00127$
$q_2 = -777.03$	$q_{12} = 33.317$
$q_3 = -4.4706$	$q_{13} = 0.09421$
$q_4 = 0.008946$	$q_{14} = -4.655 \times 10^{-5}$
$q_5 = -3.3158 \times 10^{-6}$	$q_{16} = 41587.11$
$q_6 = 0.2664$	$q_{17} = -315.90$
$q_9 = 6.1608 \times 10^{-5}$	$q_{18} = 0.8514$
$q_{10} = 1.0715 \times 10^{-6}$	$q_{19} = -8.3637 \times 10^{-4}$

Figure 4.

T_r is 298.15 K. The values of q_1, q_6, and q_{11} for NaCl at 25 °C are given by Pitzer and Mayorga.[2] Various other analytical forms were tried, ranging from a simple power series in T, to a rather complicated form given by Gibbard et al.,[18] and all proved less satisfactory.

The heat capacity data at each single experimental temperature were fitted to eq 24 and the resulting $\bar{C}_{P_2}{}^\circ$ values were found to be reproduced by the equation

$$\overline{C}_{P_2}{}^\circ = C_{P_s}{}^\circ(T) + q_{17} + 2q_{18}T + 3q_{19}T^2 \qquad (33)$$

where $C_{P_s}{}^\circ(T)$ is the heat capacity of the solid reported by Kelley[33]

$$C_{P_2}(s) = 10.98 + 0.0039T \qquad T \geqslant 298.15 \text{ K}$$

From eq 28 and 33 the temperature variation of $\Delta \bar{H}_s{}^\circ$ is

$$\Delta \overline{H}_s{}^\circ(T) = q_{16} + q_{17}T + q_{18}T^2 + q_{19}T^3 \qquad (34)$$

An important difference in functional form between eq 12 and 24 compared to eq 5 and 6 is the factor $(2\nu_M\nu_X RT^2)$ which reduces for NaCl to $2RT^2$. Consequently to ensure proper weighting of the enthalpy and heat capacity data in relation to the osmotic-activity coefficient data, the former were weighted as $(1.0/2RT^2)$. In addition, each data point, regardless of the temperature or type of data, was weighted as unity for concentrations up to 4 M, and as $(16/m^2)$ for concentrations greater than 4 M.

The final assignment of the q_i's was done by a simultaneous fitting of the data array in Table III using a computer least-squares analysis. The results are listed in Table IV.

The values of $\beta^{(0)}$, $\beta^{(1)}$, and C^ϕ as computed from eq 30–32 are plotted against temperature in Figures 4, 5, and 6, respectively. Shown as points for comparison are the values of $\beta^{(0)}$, $\beta^{(1)}$, and C^ϕ obtained at each experimental temperature from the separate analysis of the osmotic-activity coefficient at that temperature. In the lower half of Figures 4, 5, and 6 the curves for $\partial\beta^{(0)}/\partial T$, $\partial\beta^{(1)}/\partial T$, and
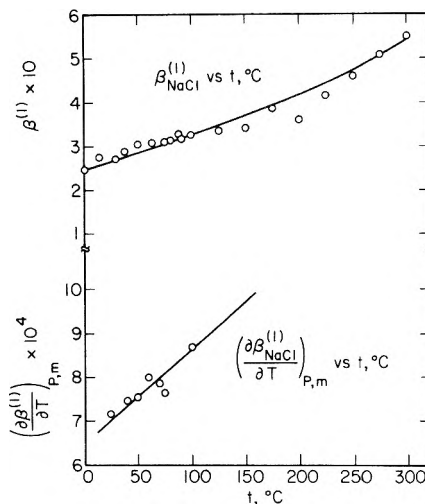
Figure 5.
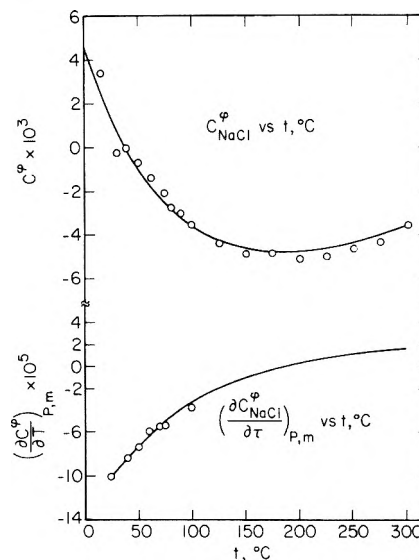
Figure 6.
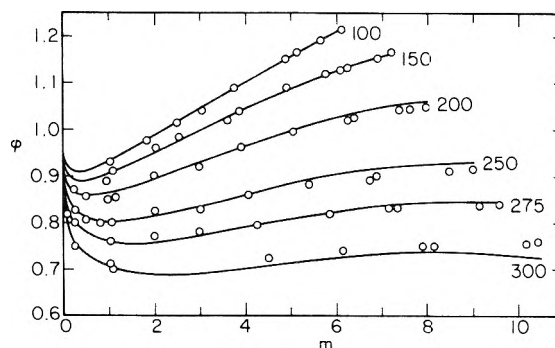
Figure 7. Osmotic coefficient for NaCl solutions from 100 to 300 °C.

$\partial C^\phi/\partial T$ obtained by taking the temperature derivative of eq 30–32 are plotted vs. the temperature along with the corresponding values from enthalpy data at a given temperature.

The number of parameters in eq 30–34 were chosen as the minimum needed to reproduce the data approximately within experimental uncertainty but with care to avoid over-fitting the data.

The standard deviation of fit for each type of data at a given temperature was compared for the overall calculation with that for the particular set of data. The agreement for the overall fit is almost as good as for the individual fits. The details of these comparisons of
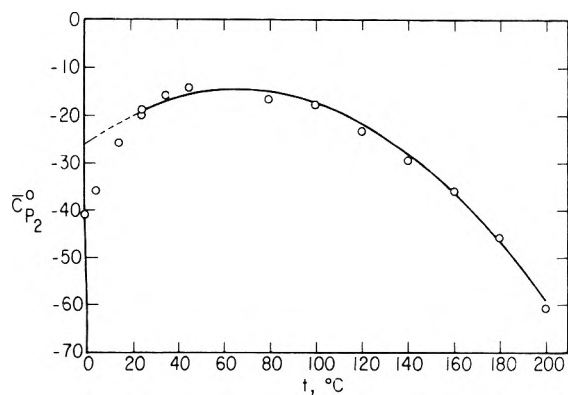
Figure 8. Heat capacity at infinite dilution for NaCl solutions.

TABLE V: Comparison of Activity Coefficients for Saturated NaCl(aq) from Different Sources

		γ_{satd} from	
t, °C	m_{satd}	Solubility[a]	Soln data[b]
0	6.096	0.922	0.927
25	6.146	(1.008)	1.008
50	6.274	1.024	1.022
75	6.460	0.987	0.986
100	6.680	0.922	0.915
125	6.935	0.831	0.825
150	7.198	0.730	0.724
175	7.573	0.615	0.620
200	7.973	0.504	0.515
225	8.435	0.397	0.412
250	8.989	0.299	0.313
275	9.649	0.215	0.220
300	10.413	0.146	0.137

[a] From eq 35 and 36. [b] From eq 6 and 30-32.

standard deviations are given elsewhere.[34]

In Figure 7, the experimental values of the osmotic coefficient and the smoothed curve generated from the composite fit are plotted against the molality for several isotherms. The smoothed curves generally pass within the experimental error for most of the data points. The overall standard deviation of fit is ±0.005 for the osmotic-activity coefficient data over the temperature range 0–300 °C.

The enthalpy data of Ensor and Anderson[27] at 50 and 80 °C were not incorporated into the final array of data as analysis of these data gave results somewhat inconsistent with the other data. The overall fit for the heat of dilution data is ±4.9 cal mol^{-1} over the temperature range 25–100 °C.

The values of $\bar{C}_{P_2}°$ and those generated by eq 33 are plotted vs. the temperature in Figure 8. Values of $\bar{C}_{P_2}°$ below 25 °C as determined by Perron et al.[31] are also plotted in Figure 8. The dashed curve represents the extrapolation of eq 33 to 0 °C from 25 °C.

There is a dramatic change in $\bar{C}_{P_2}°$ as the solution approaches 0 °C which may be related to structural changes in the solvent. The results presented in Figure 8 clearly indicate that the description of $\bar{C}_{P_2}°$ over the entire temperature range will require a much more complicated temperature function, or an alternate functional form than that given by eq 33. Consequently we have not incorporated into the final data array any heat capacity data or heat of solution data below 25 °C.

The overall standard deviation of fit for the heat of solution data is ±40 cal/mol and the over fit to the apparent molal heat capacity is ±1.8 cal K^{-1} mol^{-1}.

Liu and Lindsay[22] made extensive thermodynamic calculations based on the osmotic measurements and compared the results with some other thermodynamic data. Their equations, however, were fitted only to osmotic coefficients and hence represent a different approach than ours.

Gibbard et al.[18] followed an approach more like ours in fitting enthalpies and heat capacities as well as osmotic coefficients. They used 20 arbitrary parameters compared to our 12 for eq 30–32. Our tabulated values of the osmotic coefficient generally agree within ±0.001 to ±0.002 with those tabulated by Gibbard for temperatures 0–100 °C and from ±0.003 to ±0.005 for temperatures between 100 and 200 °C. In their analysis, Gibbard et al.[18] selected from the results of Liu and Lindsay[22] only data between 1.0 and 6.0 m, whereas we have use of the entire composition range ($\simeq$0.1–10 M). Consequently the differences between the two sets of equations is not surprising.

We believe our equations have advantages in both convenience and general accuracy, all functions considered. The results, however, do not differ very much from those tabulated in detail by Gibbard et al. Hence no tables of

values are presented here, although extensive tables have been prepared and are given elsewhere.[34] Particularly if the Debye–Hückel parameter is taken (or interpolated) from Table II, the remaining equations are very easily solved for the function and exact conditions of interest; hence the need for extensive tables is reduced.

Thermodynamics of Saturated Solutions

The solubility equilibrium was not considered in developing the equations for the solution properties; hence it can provide a check on their accuracy. At the lower temperatures the solubility of NaCl is well known[35] and Liu and Lindsay[22] determined solubilities above 75 °C. The standard Gibbs energy of solution is

$$\Delta G_s° = -2RT \ln (m\gamma)_{satd} \tag{35}$$

At 25 °C substitution of m_{satd} = 6.146 M and the value of γ_{satd} = 1.008 from our equations yields $\Delta G_s°$ = -2161 cal mol^{-1}. This value agrees well with those from most recent sources.[36] As noted by Liu and Lindsay,[22] however, the value $\Delta G_s°$ = -2250 cal mol^{-1} reported by Gardener et al.[25] is seriously in error. It appears that this discrepancy arose from the use of entropies of Na$^+$ and Cl$^-$ from inconsistent sources; in any case the -2250 value should be discarded.

An equation for $\Delta G_s°$ as a function of temperature can be obtained by integration of eq 34

$$\Delta G_s°/T = -\int(\Delta H_s°/T^2)\,dT = q_{16}/T - q_{17} \ln T - q_{18}T - 1/2 q_{19}T^2 + q_{20} \tag{36}$$

The constant of integration q_{20} can be evaluated from $\Delta G_s°$ at 25 °C and is found to be -1729.93$_2$ cal deg^{-1} mol^{-1}.

We may now apply eq 35 and 36 at other temperatures to obtain values of the activity coefficient in the saturated solution γ_{satd} and these may be compared with those calculated from eq 6, 30, 31, and 32. This comparison, which is given in Table V, shows very good agreement when it is considered that our evaluation of parameters gave rapidly decreased weight to data above 4 M.

Discussion

The most striking aspect of these results is that the properties at 300 °C are so similar, qualitatively, to those at 25 °C. The greatest change is in the Debye–Hückel parameter itself. A_ϕ doubles from 25 to 300 °C while A_H and A_J increase by much larger factors. While changes in absolute temperature and density are substantial, it is the decrease in dielectric constant which dominates this situation. Thus all of the "limiting law" effects are intensified at higher temperature.

If there were strong ion pairing, the second virial coefficient parameters $\beta^{(0)}$ and $\beta^{(1)}$ would become large

negative quantities. Indeed, if this ion pairing became very strong, the virial coefficient form of equations would fail completely. Only the slightest tendency in this direction is observed in the negative slope for $\beta^{(0)}$ above about 150 °C (Figure 4). However even at 300 °C, $\beta^{(0)}$ is still positive with a value close to that for 25 °C; also $\beta^{(1)}$ increases steadily with temperature. This conclusion is in agreement with that from conductance data.[37]

We know that anhydrous NaCl vapor consists primarily of ion-pair molecules and that a mixed vapor of NaCl with H_2O must also approach that character under certain conditions. However at 300 °C there is little indication of this trend and the general nature of aqueous NaCl is the same as at lower temperature.

The parameter b in eq 5 is related, theoretically, to the interionic distance at which strong repulsive forces arise. For convenience in treating mixed electrolytes, b is kept the same for all solutes and this leads to an interlocking effect with $\beta^{(1)}$ (and to some degree also $\beta^{(0)}$).

Here for mathematical convenience we also hold b constant with respect to temperature and find no difficulty. However it is to be noted that simple Debye–Hückel theory would have a parameter such as b increase with temperature as $(\rho_w/DT)^{1/2}$. In our case, with b constant, it is of interest to note that $\beta^{(1)}$ increases approximately as $(\rho_w/DT)^{1/2}$.

The term for triple ion interaction C^ϕ is very small throughout the range and shows no indication of extreme behavior up to 300 °C.

Finally, it is to be noted that the equations here presented give an essentially complete description of the thermodynamic properties of aqueous NaCl at saturation pressure. Thus quantities of engineering interest such as the total enthalpy and entropy of the liquid can be calculated. This is described and tables are presented elsewhere.[34]

References and Notes

(1) K. S. Pitzer, *J. Phys. Chem.*, **77**, 268 (1973).
(2) K. S. Pitzer and G. Mayorga, *J. Phys. Chem.*, **77**, 2300 (1973).
(3) K. S. Pitzer and G. Mayorga, *J. Solution Chem.*, **3**, 539 (1974).
(4) K. S. Pitzer and J. J. Kim, *J. Am. Chem. Soc.*, **96**, 5701 (1974).
(5) J. H. Keenan and F. G. Keyes, P. G. Hill, and J. G. Moore, "Steam Tables", Wiley, New York, N.Y., 1969.
(6) H. C. Helgeson and D. H. Kirkham, *Am. J. Sci.*, **274**, 1089 (1974).
(7) H. I. Oshry, Ph.D. Dissertation, University of Pittsburgh, Pittsburgh, Pa., 1949.
(8) B. B. Owen, R. C. Miller, and H. L. Cogan, *J. Phys. Chem.*, **65**, 2065 (1961).
(9) K. Heger, Ph.D. Dissertation, University of Karlsruhe, Karlsruhe, West Germany, 1969.
(10) K. S. Pitzer and L. Brewer, revised edition of "Thermodynamics", G. N. Lewis and M. Randall, Ed., McGraw-Hill, New York, N.Y., 1961.
(11) W. T. Lindsay and C. T. Liu, "Vapor Pressure Lowering of Aqueous Solutions at Elevated Temperatures", Report No. 347, Office of Saline Water, U.S. Government Printing Office, Washington, D.C., Catalog No. I 1.88:347.
(12) G. Scatchard and S. S. Prentiss, *J. Am. Chem. Soc.*, **55**, 4355 (1933).
(13) R. F. Platford, *J. Chem. Eng. Data*, **18**, 215 (1973).
(14) C. W. Childs and R. F. Platford, *Aust. J. Chem.*, **24**, 2487 (1971).
(15) G. J. Janz and A. R. Gordon, *J. Am. Chem. Soc.*, **65**, 218 (1943).
(16) A. H. Truesdell, *Science*, **161**, 884 (1968).
(17) P. Olynyk and A. R. Gordon, *J. Am. Chem. Soc.*, **65**, 224 (1943).
(18) H. F. Gibbard, Jr., G. Scatchard, R. A. Rocesseau, and J. L. Creek, *J. Chem. Eng. Data*, **19**, 281 (1974).
(19) R. P. Smith, *J. Am. Chem. Soc.*, **61**, 500 (1939).
(20) R. P. Smith and D. S. Hirtle, *J. Am. Chem. Soc.*, **61**, 1123 (1939).
(21) E. R. Gardner, *Trans. Faraday Soc.*, **65**, 91 (1969).
(22) C. Liu and W. T. Lindsay, *J. Solution Chem.*, **1**, 45 (1972); see also "Thermodynamic Properties of Aqueous Solutions at High Temperatures", final report to Office of Saline Water under Contract 14-01-0001-2126, 1971.
(23) C. Liu and W. T. Lindsay, *J. Phys. Chem.*, **74**, 341 (1970); see also ref 11.
(24) C. M. Criss and J. W. Cobble, *J. Am. Chem. Soc.*, **83**, 3223 (1961).
(25) W. L. Gardner, R. E. Mitchell, and J. W. Cobble, *J. Phys. Chem.*, **73**, 2025 (1969).
(26) E. E. Messikomer and R. H. Wood, *J. Chem. Thermodyn.*, **7**, 119 (1975).
(27) D. D. Ensor and H. L. Anderson, *J. Chem. Eng. Data*, **18**, 205 (1973).
(28) P. Picker, P. A. Leduc, P. R. Philip, and J. E. Desnoyers, *J. Chem. Thermodyn.*, **3**, 631 (1971).
(29) J. L. Fortier, P. A. Leduc, and J. E. Desnoyers, *J. Solution Chem.*, **3**, 377 (1974).
(30) M. Randall and F. D. Rossini, *J. Am. Chem. Soc.*, **51**, 323 (1929).
(31) G. Perron, J. L. Fortier, and J. E. Desnoyers, *J. Chem. Thermodyn.*, **7**, 1177 (1975).
(32) S. Likke and L. A. Bromley, *J. Chem. Eng. Data*, **18**, 189 (1973).
(33) K. K. Kelly, *U. S. Bur. Mines, Bull.* **No. 477** (1950).
(34) L. F. Silvester and K. S. Pitzer, "The Thermodynamics of Geothermal Brines. I. Thermodynamic Properties of Vapor-Saturated NaCl Solutions", Lawrence Berkeley Laboratory Report LBL-4456, 1976.
(35) A. Seidell, "Solubilities of Inorganic and Metal-Organic Compounds", 4th ed, W. F. Linke, Ed., American Chemical Society, Washington, D.C., 1965.
(36) *CODATA Bull.* **No. 5** and 6 (1971); *Natl. Bur. Stand. (U.S.), Circ.*, **No. 500** (1952).
(37) J. M. Wright, W. T. Lindsay, and T. R. Druga, *USAEC Rep.* WAPD-TM-204 (1961).

An Examination of the Limiting Laws of Polyelectrolytes and Counterion Condensation

K. Iwasa

Department of Chemistry, Indiana University, Bloomington, Indiana 47401 (Received February 25, 1977)

Counterion condensation, which has been formulated in terms of the critical charge density of polymers, is reformulated by means of the free energy minimum with respect to the number of condensed counterions in the Debye–Hückel approximation. Though the former is shown to be consistent with the latter in the salt free limit, there is a difference if salt is present. While the difference is unnoticeable for polyelectrolyte systems with single counterion species, it is important for the activity coefficient of divalent counterions in mixed counterion systems, e.g., an aqueous solution of Na^+, Ca^{2+}, Cl^-, and polystyrenesulfonate. The present formalism based on the free energy minimum gives better agreement with the activity measurement of the mixed counterion system, without causing any new inconsistencies with other experimental results reported so far.

I. Introduction

The existence of the critical charge density of polyelectrolytes has been discussed in order to explain thermodynamical and other properties. Above the critical polymer charge density, some kind of singularity in the ionic distribution, especially of counterions, has been proposed. This has been called counterion condensation. Theoretical justifications[1-5] of the counterion condensation are mainly based on the application of Poisson–Boltzmann type considerations to the cylindrical geometry of polymers whose radii are infinitesimal.[6]

Recently the cluster theory[7,8] applied to this system has been examined.[9-11] It was suggested that the cluster theory gives better agreement with the activity measurements below, or in the neighborhood of, the critical charge density. It gives, however, appreciably higher values for coion activity coefficients at higher charge density region where the formalism based on the counterion condensation provides rather reasonable values, though the predicted values are somewhat lower than experiments[11,12] if the salt is not in excess.

Another problem is the difficulty in predicting the behavior of a polyelectrolyte system with a mixture of mono- and divalent counterions, which we will call hereafter the "mixed counterion system" for brevity. While the mean activity coefficient for the mono-monovalent salt is well predicted over the whole range of the composition ratio of the two counterions, the mean activity coefficient of the mono-divalent salt is predicted only partly, in the region of high divalent counterion equivalent fractions.[13]

The reason for this disagreement is that with the decrease of the ratio of the divalent counterions we reach a point where all the divalent counterions must be condensed according to the counterion condensation as it has been formulated. This situation is phenomenologically explained by an ϵ parameter introduced by Kwak et al.[13] In order to explain the experimental result a finite portion of the divalent counterions must remain uncondensed. In addition to an examination in the excess of the monovalent counterions,[14] we should establish how the uncondensed ratio of the divalent counterions is evaluated throughout the composition ratio.

In the present paper we will examine the free energy of the system and give an alternative principle of the counterion condensation as the free energy minimum with respect to the number of condensed counterions. We will begin with the single counterion system and then examine the mixed counterion system, which has been shown to be

very sensitive to the uncondensed amount of divalent counterions.

II. Counterion Condensation

We consider a system of volume V, which consists of polyions, counterions, and coions. Let the equivalent concentration of polyions be n_p, and let all the small mobile ions be monovalent, for simplicity. We denote the concentration of counterions and that of coions by n_+ and n_-, respectively, assuming the charged groups of the polyions are monovalent and negative.

First, we consider no condensation. In the Debye–Hückel approximation, we have for the excess free energy F of the system

$$\mathfrak{F} \equiv F/(VkT) = \mathfrak{F}_0 + \mathfrak{F}_{DH} \qquad (1)$$

where k is the Boltzmann constant, T the temperature, $\mathfrak{F}_0$ the contribution from small ion–small ion interaction,[10,15] and $\mathfrak{F}_{DH}$ that from polyion–small ion interaction given by[4,8]

$$\mathfrak{F}_{DH} = -{}^1\!/_2 \xi n_p \log \lambda a^2(n_+ + n_-) \qquad (2)$$

Here we assumed the conformation of polyions is rodlike with radius a, ξ is the reduced linear charge density, defined by $\xi = \lambda/(4\pi b)$ with the Bjerrum length $\lambda/4\pi = e^2/(\epsilon kT)$. We denote by ϵ, b, and e the dielectric constant of the solvent, the mean spacing of charged groups of the polymer, and the elementary charge, respectively. The assumption of the polyion conformation in evaluating the free energy has been well discussed.[16]

Next we assume that the counterion condensation is taking place. The excess free energy $F^{(1)}$ is then given by $\mathfrak{F}^{(1)} = F^{(1)}/VkT$ with

$$\mathfrak{F}^{(1)} = \mathfrak{F}_0^{(1)} + \mathfrak{F}_{DH}^{(1)} + \mathfrak{F}_S^{(1)} + \mathfrak{F}_B^{(1)} \qquad (3)$$

where $\mathfrak{F}_0^{(1)}$ has the same meaning as $\mathfrak{F}_0$ in (1), and $\mathfrak{F}_{DH}^{(1)}$ is the effective Debye–Hückel term contribution of polyion–small ion interaction. Let the condensed amount of the counterions be N_{1c}, then we have

$$\mathfrak{F}_{DH}^{(1)} = -{}^1\!/_2 \xi n_p^{-1}(n_p - n_{1c})^2 \times$$
$$\log [\lambda a^2(n_+ + n_- - n_{1c})] \qquad (4)$$

with $n_{1c} = N_{1c}/V$, assuming the condensed region is very small compared with V, the volume of the whole system. We have two terms which did not appear in eq 1. One is the entropy change due to the condensation

$$\mathfrak{F}_S^{(1)} = (n_+ - n_{1c}) \log (n_+ - n_{1c})n_w^{-1} -$$
$$n_+ \log n_+ n_w^{-1} \qquad (5)$$

TABLE I: Activity Coefficients of a Polyelectrolyte System with Monovalent Counterions[a]

| | Present theory | | | Manning's result | | Exptl |
x	f_l	$\ln \gamma_+ - \ln \gamma_+^0$	$\ln \gamma_\pm - \ln \gamma_\pm^0$	$\ln \gamma_+$	$\ln \gamma_\pm$	$\ln \gamma_\pm - \ln \gamma_\pm^0$
0.1	0.536	-0.647	-0.0397	-0.0690	-0.0389	
0.6	0.620	-0.319	-0.187	-0.324	-0.186	-0.161 ± 0.02
1.1	0.627	-0.487	-0.288	-0.493	-0.287	-0.264 ± 0.02
2.1	0.633	-0.703	-0.423	-0.708	-0.422	(-0.403 ± 0.07)[b]
5.1	0.639	-1.006	-0.624	-1.009	-0.624	
10.0	0.641	-1.197	-0.760	-1.199	-0.760	-0.633 ± 0.007

[a] $a = 10$ Å, $\xi = 2.8$, $n_p = 0.01$. Experimental data are adopted from ref 11 (NaPSS plus NaCl).   [b] An interpolated value.

where n_w is the concentration of the solvent. This term arises because our $\mathcal{F}^{(1)}$ is the excess free energy. Although eq 4 includes the entropy contribution and is the excess free energy of a system with the polymer charge density $\xi n_p^{-1}(n_p - n_{1c})$, $(n_+ - n_{1c})$ counterions, and n_- coions, our $\mathcal{F}^{(1)}$ is the excess free energy of the system with n_+ counterions and n_- coions. The other is the last term $\mathcal{F}_B^{(1)}$, which is the binding free energy of counterions in the condensed phase. It includes the entropy term. NMR measurements carried out by Leyte group[17,18] show that the counterions are freely moving in the condensation layer surrounding the polymer. This should imply that the site binding model is inadequate. Though it is difficult to give an explicit form for the last term, it should be independent of n_+ and n_-.

The differentiation of eq 3 with respect to n_+ and n_- gives the activity coefficient of counterions and coions, respectively

$$\log \gamma_+ = (\partial/\partial n_+)\mathcal{F}^{(1)} \qquad \log \gamma_- = (\partial/\partial n_-)\mathcal{F}^{(1)}$$

Thus we have

$$\log \gamma_- - \log \gamma_-^0 = -\tfrac{1}{2}\xi n_p^{-1}(n_p - n_{1c})^2(n_+ + n_- - n_{1c})^{-1} \tag{6a}$$

$$\log \gamma_+ - \log \gamma_+^0 = (\log \gamma_- - \log \gamma^0) + \log[(n_+ - n_{1c})/n_+] \tag{6b}$$

where $\log \gamma^0$'s are derivatives of $\mathcal{F}_0^{(1)}$, the salt correction term.[10,15] Considering the practical concentrations of salt and polymer, this term is evaluated with sufficient accuracy by the Debye–Hückel term of the salts. The excess osmotic pressure π^{ex} is given by

$$-\pi^{ex} = \frac{\partial}{\partial V}(F^{(1)}/kT)_{T,\xi,\text{ no. of ions}} = \tfrac{1}{2}\xi n_p^{-1}(n_p - n_{1c})^2 + n_{1c} \tag{7}$$

If we assume the condensed ratio of the counterion $f_{1c} = n_{1c}/n_p$ is given by

$$f_{1c} = 1 - \xi^{-1} \tag{8}$$

as has been proposed by the previous counterion condensation theories, eq 6 and 7 are exactly the same as Manning's limiting law.[4,5]

The functional form of eq 7 shows that condition 8 gives the maximum value of osmotic pressure with respect to n_{1c}. Condition 8 also gives the maximum value of the mean activity coefficient $\gamma_\pm$ in the salt free limit. Since the limiting law based on (8) gives even lower values for $\gamma_\pm$ compared with experiments,[11,12] condition 8 yields the optimal agreement with experimental data in our framework.

In the salt free limit, we are able to give a functional form of $\mathcal{F}_B^{(1)}$ so that the free energy minimum condition with respect to n_{1c} is equivalent to (8). That is

$$\mathcal{F}_B^{(1)} = n_{1c}[\tfrac{1}{2} - \log(\lambda a^2 n_w)] \tag{9}$$

provided that the polymer concentration is low. This condition is usually satisfied experimentally. The details are discussed later. If there is a finite amount of salt in our system, the free energy minimum using eq 9 is inconsistent with (8). Though we can modify the binding free energy to be consistent with (8), the resulting $\mathcal{F}_B^{(1)}$ is then not only a function of n_{1c} but also is dependent on n_+ and n_-. This is inconsistent with our assumption that $\mathcal{F}_B^{(1)}$ is independent of salt concentration and therefore inconsistent with eq 6 and 7. Thus the limiting laws based on the counterion condensation are invalid if a finite amount of salt is present. We will proceed tentatively assuming the binding free energy is given by (9). We should also notice that the $\mathcal{F}_B^{(1)}$ term is important. In fact, if we drop this term, the result is quite poor. Since our binding free energy $\mathcal{F}_B^{(1)}$ is now proportional to n_{1c}, the mixing entropy contribution to this term should not be important.

Next, we will explicitly examine the minimization of (3) with respect to n_{1c}. Under the salt free condition, the derivative of $\mathcal{F}^{(1)}$ with respect to n_{1c} gives

$$\partial\mathcal{F}^{(1)}/\partial n_{1c} = -A\xi(1 - f_{1c} - \xi^{-1})$$

with

$$A = -\tfrac{1}{2} - \log \lambda a^2 n_p - \log(1 - f_{1c})$$

Considering the usual experimental condition, the polymer concentration n_p is low enough to allow A to be positive. Thus we obtain the minimum of $\mathcal{F}^{(1)}$ with respect to n_{1c} at $f_{1c} = n_{1c}/n_p = 1 - \xi^{-1}$, if $\xi > 1$. For $\xi < 1$, we have $\partial\mathcal{F}^{(1)}/\partial n_{1c} > 0$ and $n_{1c} = 0$ gives the minimum. In this case, (3) is equivalent to (1). If a finite amount of salt is present in our system, the critical behavior becomes less sharp, apparently approaching the cluster expansion result.[10]

In Table I, we compare the activity coefficients evaluated by the two methods, i.e., one is based on (8), and the other based on the free energy minimum. Even though there is a difference, especially in the excess salt region, it does not exceed experimental uncertainties.

The extension to divalent counterion systems is straightforward. We have the excess free energy $F^{(2)}$

$$\mathcal{F}^{(2)} \equiv F^{(2)}/(VkT) = \mathcal{F}_0^{(2)} + \mathcal{F}_{DH}^{(2)} + \mathcal{F}_s^{(2)} + \mathcal{F}_B^{(2)} \tag{10}$$

Each term on the right-hand side of (10) bears a similar meaning as in eq 3. The first term $\mathcal{F}_0^{(2)}$ is the contribution of small ion–small ion interaction, and the second term is given by

$$\mathcal{F}_{DH}^{(2)} = -\tfrac{1}{2}\xi n_p(1 - f_{2c}) \log[\lambda a^2(4n_{2+} + n_- - 4n_{2c})] \tag{11}$$

where we denote the concentration of the divalent counterion by n_{2+}, n_{2c} is the corresponding concentration of the condensed counterion, and $f_{2c} = 2n_{2c}/n_p$. The entropy contribution due to the condensation is

$$\mathcal{F}_s^{(2)} = (n_{2+} - n_{2c}) \log [(n_{2+} - n_{2c})n_w^{-1}] - n_{2+} \log [n_{2+}n_w^{-1}] \quad (12)$$

After an argument similar to that mentioned in the monovalent case, we have for the binding free energy

$$\mathcal{F}_B^{(2)} = n_{2c}[{}^1/{}_2 - \log 4\lambda a^2 n_w] \quad (13)$$

corresponding to the critical charge density condition for the divalent counterion system

$$1 - f_{2c} = (2\xi)^{-1} \quad (14)$$

In the salt free limit, eq 13 together with eq 10–12 and the minimization with respect to n_{2c} are equivalent to (14) if $\xi > {}^1/{}_2$. This is quite similar to the monovalent counterion system. An interesting observation in this system is, while the maximization of the osmotic pressure is equivalent to the critical charge density condition (14), that of the mean activity coefficient $\gamma_\pm$ is different even in the salt free condition. On the other hand, condition 14 gives surprisingly good agreement with the activity measurements.[11]

III. Mixed Counterion System

In the preceding chapter we have formulated counterion condensation based on the free energy minimum in the systems with a single counterion species. This formalism is now readily extended to mixed counterion systems, e.g., a system with Ca^{2+}, Na^+, Cl^-, and polyion$^-$.

We consider a similar system as in the previous chapter, but now we have monovalent and divalent counterions, the concentrations of which are n_+ and n_{2+}, respectively. In a similar approximation as (3) and (10), we have

$$\mathcal{F} = \mathcal{F}_0 + \mathcal{F}_{DH}{}^M + \mathcal{F}_s^{(1)} + \mathcal{F}_s^{(2)} + \mathcal{F}_B^{(1)} + \mathcal{F}_B^{(2)} \quad (15)$$

The second term on the right-hand side, the free energy contribution from the polyion–small ion interaction, is given by

$$\mathcal{F}_{DH}{}^M = -{}^1/{}_2\xi n_p^{-1}(n_p - n_{1c} - 2n_{2c})^2 \times \log [\lambda a^2(4n_2 + n_+ + n_- - 4n_{2c} - n_{1c})] \quad (16)$$

where n_{1c} and n_{2c} represent the corresponding concentration of the condensed monovalent and divalent counterions, respectively. Other terms have been defined by (5), (9), (12), and (13). We now have to choose n_{1c} and n_{2c} so as to minimize (15).

The activity coefficients are given by differentiation with respect to the concentration of each ion species. We obtain

$$\log \gamma_- - \log \gamma_-^0 = -{}^1/{}_2\xi n_p^{-1}(n_p - n_{1c} - 2n_{2c})^2(4n_{2+} + n_+ + n_- - 4n_{2c} - n_{1c})^{-1} \quad (17a)$$

$$\log \gamma_+ - \log \gamma_+^0 = (\log \gamma_- - \log \gamma_-^0) + \log [(n_+ - n_{1c})/n_+] \quad (17b)$$

$$\log \gamma_{2+} - \log \gamma_{2+}^0 = 4(\log \gamma_- - \log \gamma_-^0) + \log [(n_{2+} - n_{2c})/n_{2+}] \quad (17c)$$

where γ_-, γ_+, and γ_{2+} are the single ion activity coefficient of coions, and of monovalent and of divalent counterions, respectively. The mean activity coefficient of monovalent salt and that of divalent salt are given by

$$\log \gamma_\pm (\text{monovalent}) = {}^1/{}_2(\log \gamma_+ + \log \gamma_-)$$
$$\log \gamma_\pm (\text{divalent}) = {}^1/{}_3(\log \gamma_{2-} + 2 \log \gamma_-)$$

The excess osmotic pressure π^{ex} is given by

$$-(\pi^{ex} - \pi_0{}^{ex}) = {}^1/{}_2\xi n_p^{-1}(n_p - n_{1c} - n_{2c})^2 + n_{1c} + n_{2c} \quad (18)$$
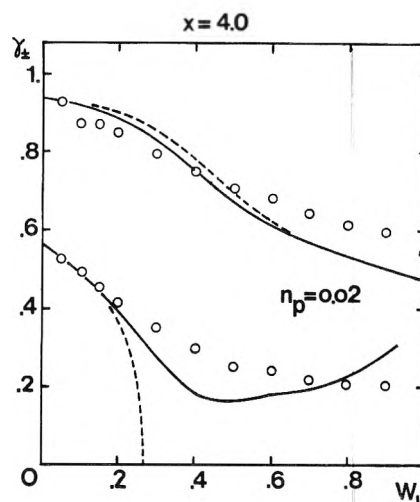
Figure 1. Corrected $\gamma_\pm$ values for monovalent salt (upper lines) and divalent salt (lower lines) at $x = 9$: (full lines) present theory; (broken lines) Manning's theory (extended version). Experimental values are adopted from ref 13. Values for NaCl (upper points) and $CaCl_2$ (lower points) at $n_p = 0.02$.
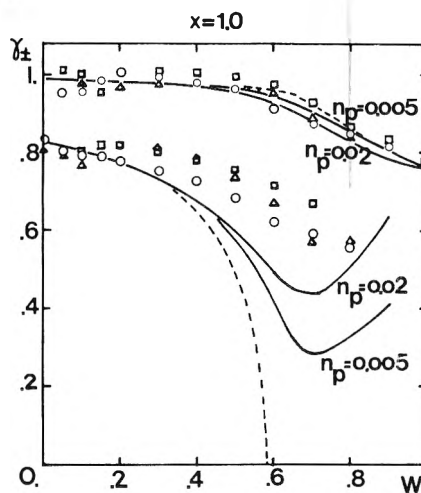

Figure 2. Corrected $\gamma_\pm$ values for monovalent salt (upper lines) and divalent salt (lower lines) at $x = 1$: (full lines) present theory; (broken lines) Manning's theory (extended version). Experimental values are adopted from ref 13. Values for NaCl (upper points) and $CaCl_2$ (lower points) at $n_p = 0.02$ (O), $n_p = 0.01$ (□), and $n_p = 0.005$ (Δ).

where $-\pi_0{}^{ex}$ arises from the differentiation of $\mathcal{F}_0 V$.

Numerical calculations were carried out in order to compare with the experimental data of the activity coefficients.[13] We used the STEPT package of the QCPE program[19] to minimize $\mathcal{F}$ with respect to n_{1c} and n_{2c}. The reduced charge density ξ is set to be 2.8 and the polymer radius a is assumed to be 10 Å, from the geometrical consideration of the polymer, polystyrenesulfonate (PSS). The results are shown in Figures 1–3. The experimental data are corrected to exclude the salt term (i.e., the subtraction of the left-hand side of eq 17 is performed).

First, our values for the mean activity coefficient of $CaCl_2$ are not falling to zero as the increase of the monovalent counterion's ratio w_1 to the total counterions, though the effective charge density is roughly approximated by the extended version[13] of Manning's formalism. This situation is illustrated by Figure 4, which shows the effective charge density of the polymer against the ratio w_1. The regions I, II, and III, defined as follows, proposed originally by Oosawa[3] and Manning,[5] based on the consideration of the critical charge density, are approximately retained. There are enough divalent counterions, in region I, to achieve the effective charge density of $1/2$, the critical
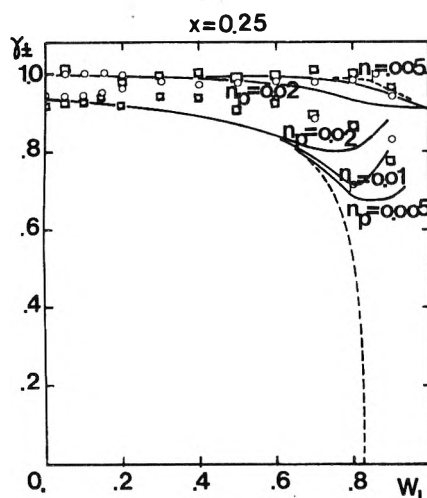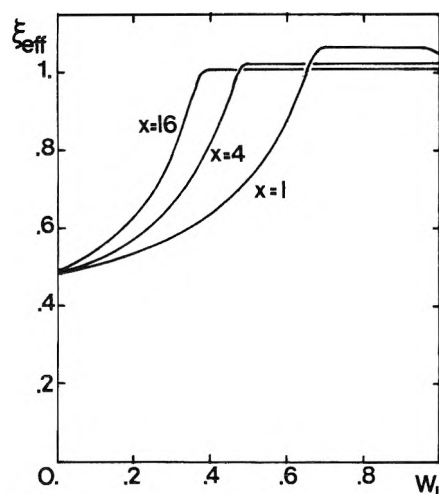
Figure 3. Corrected $\gamma_\pm$ values for monovalent salt (upper lines) and divalent salt (lower lines) at $x = 0.25$: (full lines) present theory; (broken lines) Manning's theory (extended version). Experimental values are adopted from ref 13. Values for NaCl (upper points) and CaCl$_2$ (lower points) at $n_p = 0.02$ (O) and $n_p = 0.01$ (□).

Figure 4. The effective charge density ξ_{eff} vs. composition ratio w_1. $\xi_{eff} = \xi n_p^{-1}(n_p - n_{1c} - 2n_{2c})$.

charge density for divalent counterions. In region III, the effective charge density is unity, the critical charge density for monovalent counterions. In region II, the effective charge density has intermediate values. Our result shows, however, a certain deviation from the simple scheme, and a finite amount of divalent counterions remain uncondensed. This, in turn, keeps log γ_{2+} finite, and gives better agreement with the experiment.

Second, we can explain the ϵ parameter introduced by Kwak et al.[13] They assumed the ratio $(1 - f_2)$ of the uncondensed divalent counterion to the total divalent counterion should be greater than, or equal to, a value ϵ throughout regions I, II, and III, i.e.

$$1 - f_2 \geq \epsilon \quad \text{with } \epsilon > 0$$

where we defined $f_2 = n_{2c}/n_{2+}$. That is, in effect, an empirical modification of Oosawa–Manning's formalism. If the critical charge density condition requires smaller values of $(1 - f_2)$ than ϵ, they put $(1 - f_2) = \epsilon$, and got a reasonable agreement with the experimental data. There has been no theoretical reason why there is such a nonzero parameter. If the ratio x ($= n_p/n_-$) of the equivalent concentration of the polymer to the equivalent salt concentration is greater than 4, the ϵ value was found to be around 0.1, and larger values of ϵ were needed for smaller values of x in order to explain the experiment. Our for-

TABLE II: Minimum Value of $(1 - f_2)$ Compared with ϵ Parameter Introduced by Ref 13 ($n_p = 0.01$)

x	min $(1 - f_2)$	ϵ
16	0.013	0.1
9	0.014	0.1
4	0.021	0.1
1	0.082	0.3
0.25	0.411	0.5

malism demonstrates that the minimum values of $(1 - f_2)$ show similar behavior, as shown in Table II. This does indicate that the counterion condensation formulated by Oosawa and Manning holds good only if x is large (i.e., in the salt free limit). This confirms our argument about the consistency of the limiting laws, described in the previous chapter.

Although our agreement with the experiment is good in general, there is a discrepancy: We find a minimum of $\gamma_\pm(CaCl_2)$ against the counterion composition ratio w_1, while the experiment shows a monotonic decrease with increasing w_1. This minimum is attributed to the existence of a maximum of f_2, the condensed ratio of the divalent counterions, between $w_1 = 0$ and 1. In order to clarify the situation, let us consider the behavior of f_2 where w_1 is close to unity. In this region the total excess free energy is quite sensitive to a change of f_1, the condensed monovalent counterion's ratio to the total monovalent counterions, and rather insensitive to f_2, because the weight of $\mathfrak{F}_s^{(1)}$ is greater than that of $\mathfrak{F}_s^{(2)}$. Therefore we obtain an increase of f_2 with a decrease of w_1 in the neighborhood of $w_1 = 1$. A similar tendency is also expected by a different treatment.[14] On the other hand, in the neighborhood of $w_1 = 0$ we have $f_1 \simeq 0$, and we obtain an increase of f_2 with an increase of w_1. Thus we should have a maximum of f_2 between $w_1 = 0$ and 1. This corresponds to the minimum of $\gamma_\pm(CaCl_2)$.

In addition to the existence of the minimum, we obtain a polymer concentration dependence of the mean activity coefficient for the divalent salt. The mean activity coefficient for the monovalent salt is approximately independent of n_p, the equivalent polymer concentration, and is in a good agreement with the experiment. The mean activity coefficient for the divalent salt should, however, decrease around its minimum, with decreasing n_p. The experimental data do not show such a clear tendency.

Finally, we should stress that we do not get any new inconsistencies with other experiments reported so far. In the case of the salt free system, the calculated single ion activity coefficient for the divalent ions drops sharply to a small value (still nonzero). This is consistent with the experiment of Rinaudo and Milas.[20] Though the osmotic coefficient calculated by Manning[5] shows a shifted maximum to a smaller w_1 value compared with Dolar's data[21] under the salt free condition, our calculation does not show a meaningful difference from Manning's result. Other observations[17,23-25] are also not sensitive enough to distinguish the two theories.

References and Notes

(1) N. Imai and T. Onishi, *J. Chem. Phys.*, **30**, 1115 (1959).
(2) A. D. MacGillivray, *J. Chem. Phys.*, **45**, 2184 (1966).
(3) F. Oosawa, "Polyelectrolytes", Marcel Dekker, New York, N.Y., 1971.
(4) G. S. Manning, *J. Chem. Phys.*, **51**, 924 (1969).
(5) G. S. Manning in "Polyelectrolytes", E. Selegny, Ed., Reidel Publishing Co., Dordrecht, Holland, 1974, p 9.

(6) G. S. Manning, preprint. While the manuscript was in preparation another kind of derivation was given by him.
(7) G. S. Manning and B. H. Zimm, *J. Chem. Phys.*, **43**, 4250 (1965).
(8) G. S. Manning, *J. Chem. Phys.*, **51**, 3249 (1969).
(9) K. Iwasa, *J. Chem. Phys.*, **62**, 2976 (1975).
(10) K. Iwasa and J. C. T. Kwak, *J. Phys. Chem.*, **81**, 408 (1977).
(11) J. C. T. Kwak, M. C. O'Brien, and D. A. MacLean, *J. Phys. Chem.*, **80**, 808 (1976).
(12) (a) M. Rinaudo and M. Milas, *Chem. Phys. Lett.*, **41**, 456 (1976); (b) T. Ueda and Y. Kobatake, *J. Phys. Chem.*, **77**, 2995 (1973).
(13) J. C. T. Kwak, N. J. Morrison, E. J. Spiro, and K. Iwasa, *J. Phys. Chem.*, **80**, 2753 (1976).
(14) G. S. Manning, *Biophys. Chem.*, to be published.
(15) K. Iwasa and J. C. T. Kwak, *J. Phys. Chem.*, **80**, 215 (1976).
(16) In addition to ref 3–8 and 11–15, see also S. A. Rice and M. Nagasawa, "Polyelectrolytes", Academic Press, New York, N.Y., 1961;

(17) K. Iwasa, *J. Chem. Phys.*, **64**, 3679 (1976).
(17) J. J. van der Klink, L. H. Zuiderweg, and J. C. Leyte, *J. Chem. Phys.*, **60**, 2391 (1974).
(18) J. C. Leyte and J. J. van der Klink, *J. Chem. Phys.*, **62**, 749 (1975).
(19) J. P. Chandler, Quantum Chemistry Program Exchange, No. 307, Department of Chemistry, Indiana University, Bloomington, Ind., 1975.
(20) M. Rinaudo and M. Milas, *Eur. Polym. J.*, **8**, 737 (1972).
(21) D. Dolar in "Polyelectrolytes", E. Selegny, Ed., Reidel Publishing Co., Dordrecht, Holland, 1974, p 97.
(22) D. Dolar and D. Kozak in Abstracts of IUPAC Symposium on Macromolecules, Leiden, Vol. 1, 1970.
(23) A. Ikegami, *J. Polym. Sci., Part A2*, 907 (1964).
(24) R. Zana, C. Tondre, M. Rinaudo, and M. Milas, *J. Chim. Physicochim. Biol.*, **68**, 1258 (1971).
(25) G. E. Boyd, D. P. Wilson, and G. S. Manning, *J. Phys. Chem.*, **80**, 808 (1976).

Phase Transition and Dye Aggregation in Phospholipid–Amphiphilic Dye Liposome Bilayers

Kazue Kurihara, Yoshinori Toyoshima,[†] and Mitsunori Sukigara*

Institute of Industrial Science, University of Tokyo, Roppongi, Minato-ku, Tokyo 106, Japan (Received March 8, 1977)

The visible absorption spectra of N,N'-distearylquinocarbocyanine iodide (SQCC) incorporated into egg yolk phosphatidylcholine liposome bilayers were examined, varying the SQCC/phosphatidylcholine molar ratio from 1:5900 to 1:62, in the temperature range from −15 to 30 °C. Reversible thermal changes in the spectra were observed, particularly between two characteristic temperatures depending on the molar ratio of SQCC/phosphatidylcholine and interpreted in terms of the dimer formation of SQCC in the liposome bilayers. The stability of the SQCC dimer in the lipid bilayers was found to depend on the physical state of the acyl chains in the lipids which form the bilayers; the dimer form is preferable in the solid phase in which the acyl chains of the lipids are in the all-trans configuration, on the other hand, the monomer is more stable than the dimer when the acyl chains are in the fluid state. The dimerization constant of SQCC in the liposome bilayer was determined as 3.2 (L/mol) in the fluid phase (at 25 °C), and 1.30×10^3 in the solid phase (at −10 °C). In the intermediate temperature range, coexistance of the solid phase and fluid phase in each liposome bilayer is suggested by the fact that an apparent dimerization constant depends on the molar ratio of SQCC/phosphatidylcholine as well as on temperature.

Introduction

Some amphiphilic dyes composed of a hydrophilic chromophore and one or two lipophilic long acyl chains are incorporated into phospholipid bilayers, forming a two-dimensional lattice.[1] The two-dimensional arrangement of dyes of this type is useful as a model for studying energy transfer and trapping processes such as those of the photosynthetic unit of green plants, partly because the distance between the photosensitive groups on the membrane surfaces is controlled over a wide range by varying the ratio of dyes to the structure lipids.[2] In addition to this, studies on the organization of the amphiphilic dyes in the lipid bilayers seem to be important in connection with investigation of the arrangement of chlorophyll molecules localized within the thylakoid membranes of chloroplasts. In the thylakoid membrane supposedly composed of a two-dimensional array of lipids and proteins, chlorophyll, which is a typical natural amphiphilic dye, exists in some aggregated forms.[3,4] The aggregated chlorophyll molecules within the membrane play important roles in the photosynthetic units, where existence of specific interactions of chlorophyll–lipids,

chlorophyll–proteins, or chlorophyll–chlorophyll are expected. From this point of view, Lee[5] studied the aggregation of chlorophyll a incorporated into phosphatidylcholine bilayers by measurements of the absorption spectra and fluorescence intensities of chlorophyll a and found that proportion of aggregated chlorophyll a was increased at the expense of monomer, when the lipids were in the solid state. However the structure of the aggregates has not yet been determined.

Despite its obvious importance as stated above, there has been very little effort to study quantitatively the organization of the amphiphilic dyes incorporated into lipid bilayers.

We have carried out investigations on the aggregate formation of an amphiphilic dye, N,N'-distearylquinocarbocyanine iodide (SQCC), incorporated into egg yolk phosphatidylcholine liposome bilayers. Reversible thermal changes in the absorption spectra of SQCC in the liposome bilayers demonstrated the dimer formation of SQCC. A difference of three orders of magnitude in the dimerization constant between the solid state and the fluid state with respect to the acyl chains of the lipids was observed. The width of the transition temperature region where the solid phase and fluid phase coexist in each liposome bilayer depends on the amount of SQCC contained in each li-

---

[†] Present address: Faculty of Integrated Arts and Sciences, Hiroshima University, Higashisenda-machi, Hiroshima 730, Japan.
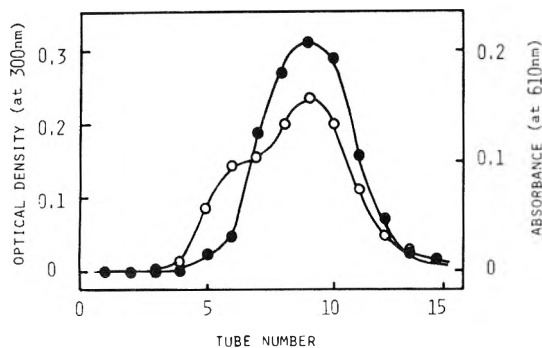
Figure 1. Sepharose 4B elution profiles of liposomes consist of phosphatidylcholine and SQCC: (O) optical density attributed to scattering by liposomes at 300 nm; (●) absorbance of SQCC at 610 nm.

posome. This coincides with the results of recent studies on the phase separation observed in the bilayers composed of different lipid mixtures.[6,7] Aggregation of the amphiphilic dyes in the lipid bilayers was found to depend on the temperature and molecular structure of the dye as well as the structure lipids through the physical state of their acyl chains.

Experimental Section

Materials. Phosphatidylcholine was extracted from hen egg yolk and purified by the method of Pangborn,[8] forming a phosphatidylcholine–cadmium complex. N,N'-distearylquinocarbocyanine iodide (SQCC) was purchased from the Japanese Research Institute for Photosensitizing Dyes Co. Ltd. and used without further purification. The purities of phosphatidylcholine and SQCC were checked by thin layer chromatography. KCl and tris(hydroxymethyl)aminomethane of analytical grade were used as received.

Preparation of Phosphatidylcholine–Dye Liposome. Phosphatidylcholine colyophilized with SQCC of a desired composition from benzene solution under vacuum was suspended in 10 mL of buffered 1.0 M KCl solution (1.0 M KCl in 0.01 M tris Cl at pH 7.5). The electrolyte concentrations in the dispersion media were carefully kept constant throughout the experiments. The suspension was ultrasonically irradiated (Otake Seisakusho OT-5202) for 1 h at 20 kHz and at 28 °C under an argon atmosphere. After centrifugation at 13 000 rpm for 10 min, the resulting supernatant was subjected to gel phase chromatography (GPC) at 4 °C on a Sepharose 4B column (1.6 × 40 cm) to obtain single-lamella liposomes of a homogeneous size. The GPC elution profile of the dispersion monitored by the optical density at 300 nm is shown in Figure 1 together with that of SQCC absorption at 610 nm. The fractions eluting after the peak, exhibiting a linear relation between the optical density at 300 nm and lipid phosphorus content, were used in the experiments, because they have been found to contain liposomes of homogeneous size.[9] A linear relationship between the optical density at 300 nm and the absorption at 610 nm was also observed for fractions around the peak of the elution profile. This fact indicates that SQCC in the preparations are captured throughout in the liposome bilayers. Phosphatidylcholine concentrations in the liposome dispersions are expressed in terms of lipid phosphorous in mole/liter, as determined by the Fiske–Subbarow method,[10] and they may be converted into volume fraction, N, if desired, using an average molecular weight of 770 and a partial specific volume of 0.985 determined for egg phosphatidylcholine.[9] SQCC concentrations in the liposome dispersions were estimated from the absorption intensities at 610 nm attributed to the SQCC monomer band at 25 °C, using the
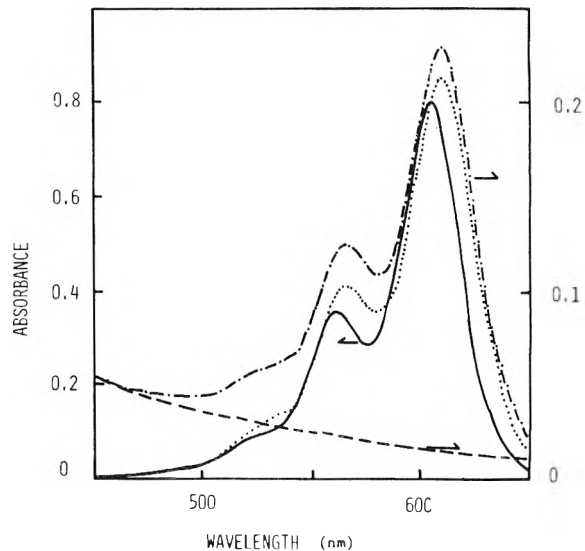
Figure 2. Absorption spectra of SQCC and light scattering by liposomes: (—) absorption of SQCC in methanol (4.7×10^{-6} M) at 25 °C; (–·–·) apparent absorption of liposome dispersion at a SQCC/phosphatidylcholine molar ratio of 1:5900; (– – –) light scattering by liposomes; (·····) absorption of SQCC in the liposome.

molecular extinction coefficient determined in methanol, $\epsilon_{610} = 1.67 \times 10^5$ L/mol. At this temperature the portion of aggregated SQCC molecules is negligibly small.

Measurements. Spectral measurements were performed on a Beckman 25 spectrophotometer with a temperature controlled cell holder. The temperature of a sample was regulated within ±0.1 °C during measurement and monitored with a thermister immersed in the sample cuvet. The concentration of SQCC in each sample solution was kept at ca. 4.7×10^{-6} mol/L, and the SQCC to phosphatidylcholine molar ratio was adjusted by varying the amount of phosphatidylcholine. Dry nitrogen gas was injected into the cell compartment to prevent the surface of the cell from fogging over at lower temperatures.

Results and Discussion

The absorption spectrum of SQCC in methanol is shown in Figure 2, compared with the spectrum in the liposome bilayers at a SQCC/phosphatidylcholine molar ratio of 1:5900. The spectrum in methanol has two distinct peaks at 562 and 605 nm and a shoulder around 520 nm and it is virtually independent of temperature throughout the range from –15 to 30 °C. The absorbance at the main peak (605 nm) in methanol, A_{605}, was found to be proportional to the concentration of SQCC and absorbances at 518 and 562 nm, A_{518} and A_{562}, relative to A_{605} were invariant over the concentration range from 10^{-6} to 10^{-4} M. These results suggest that the three absorption bands appearing in the visible wavelength in methanol are attributed to the SQCC monomer. The spectrum in the liposome system at lower SQCC/phosphatidylcholine molar ratios such as 1:5900 was essentially similar to that in methanol over the whole temperature range studied, except for the contribution to light scattering by the liposomes and trivial differences in the two peak positions (564 and 610 nm). On the other hand, in liposome systems at higher SQCC/phosphatidylcholine molar ratios, a remarkable increase in the absorbance at 518 nm was observed with the loss of the extinction at 610 nm with decreasing temperature below a critical point which depends on the molar ratio. Figure 3 demonstrates a typical example of reversible thermal change in the spectrum observed at a molar ratio of 1:62. An isosbestic point at 545 nm was also observed at other molar ratios. In Figure 4, plots of A_{518}/A_{610} as a function
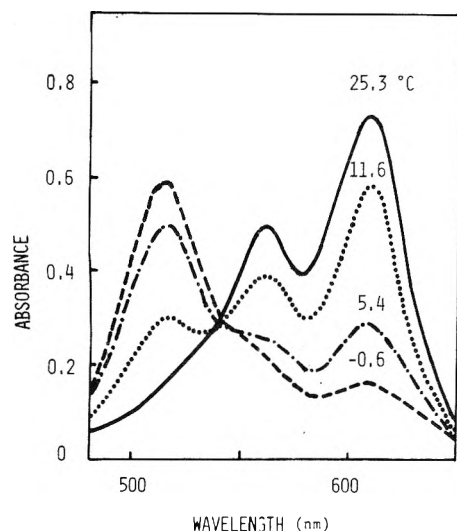
Figure 3. Thermal change of the absorption spectrum of SQCC in the liposomes at a SQCC/phosphatidylcholine molar ratio of 1:62.
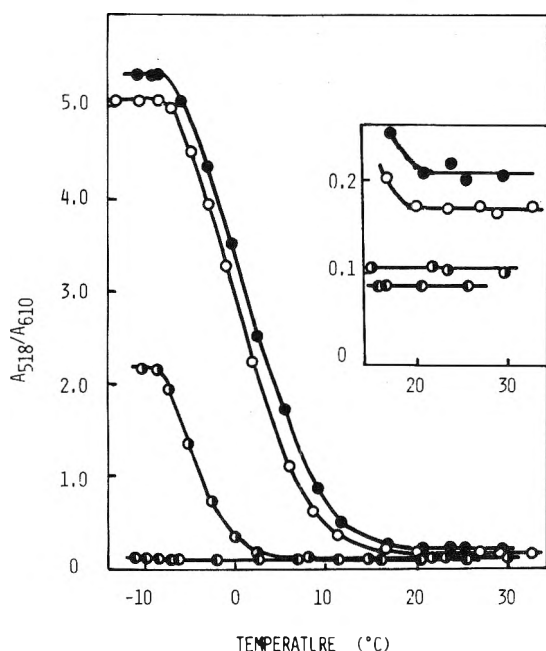

Figure 4. Plots of A_{518}/A_{610} against temperature at various SQCC/phosphatidylcholine molar ratios: (●) 1:62; (○) 1:76; (◐) 1:357; (◑) 1:5900.

of temperature show an abrupt variation in magnitude between the two critical temperatures for each composition except for the case of a molar ratio of 1:5900. In other temperature ranges, A_{518}/A_{610} is almost independent of temperature, but increases with the molar ratio. This behavior of the spectra suggests the formation of a certain aggregate of SQCC molecules in the liposome bilayers with an absorption maximum at 518 nm. In the liposomes at a molar ratio of 1:5900, the average number of SQCC molecules in each liposome is estimated to be 0.45, using the liposome molecular weight of 2.06×10^6 daltons determined by Huang.[9] Consequently no variation in A_{518}/A_{610} was observed at a molar ratio of 1:5900 throughout the temperature range studied except for an insignificant increase below -6 °C which is due to the fluctuation of SQCC distribution in the liposomes (see Appendix). These considerations lead to the conclusion that the shoulder observed around 520 nm in the system with a molar ratio of 1:5900 is attributed to the monomer. Thus the contribution of the monomers to the absorbance at 518 nm should be taken into account in the discussion

on the characteristics of SQCC aggregate as follows

$$A_{518}' = A_{518} - 0.086 A_{610} \tag{1}$$

where A_{518} and A_{518}' are the apparent absorbance at 518 nm and the part attributed to the SQCC aggregate, respectively, and 0.086 is the magnitude of A_{518}/A_{610} obtained at a molar ratio of 1:5900.

Hereafter we are concerned with the characteristics of the SQCC aggregates in the liposome bilayers. Taking into consideration that the thermal variation of the spectrum is reversible with one isosbestic point, we confine ourselves to examining two-component systems with regard to SQCC molecules, monomer, and n-mer under equilibrium condition in each liposome with an equilibrium constant K_n

$$K_n = C_n/C_M{}^n \tag{2}$$

where C_M and C_n represent the concentrations of monomer and n-mer of SQCC in each liposome (mole/liter of lipids). Using the concentrations of the monomer and n-mer in the liposome dispersions, C_M' and C_n' (mole/liter of the dispersion), or the absorbances corresponding to the monomer and n-mer bands, A_{610} and A_{518}', eq 2 is written in the form

$$K_n = (C_n'/C_M'{}^n) N^{n-1}$$
$$= (A_{518}'/A_{610}{}^n)(\epsilon_{610}{}^n/\epsilon_{518}') N^{n-1} \tag{3}$$

where N is the volume fraction of lipid in the dispersion and ϵ_{610} and ϵ_{518}' are the molecular extinction coefficients of the monomer and n-mer at 610 and 518 nm, respectively. Equation 3 is rearranged as

$$\log (A_{518}'/N) = n \log (A_{610}/N) + \log (\epsilon_{518}'/\epsilon_{610}{}^n) + \log K_n \tag{4}$$

Equation 4 indicates that plots of A_{518}'/N against A_{610}/N both on a logarithmic scale for the liposome dispersions with different phosphatidylcholine contents at a constant temperature yield a straight line with slope n, if each ϵ_{518}', ϵ_{610}, and K_n are independent of the SQCC concentration and SQCC/phosphatidylcholine molar ratio. When the lipids of the liposomes are in a macroscopically homogeneous phase, K_n is independent of the molar ratio at a given temperature and pressure. However if there exist two lipid phases with different compositions, K_n defined by eq 2 is not regarded as constant independent of the molar ratio in general. Therefore the linear relation between $\log (A_{518}'/N)$ and $\log (A_{610}/N)$ based on eq 4 should be examined at the temperature range where the lipids are in a homogeneous phase at any molar ratio. The prediction from eq 4 is demonstrated in Figure 5 with the data obtained at 25 and -10 °C at the molar ratio ranging from 1:360 to 1:62. It will be shown later that under the above conditions the lipids are in a homogeneous fluid state and solid state at 25 and -10 °C, respectively. The values of n determined from the slopes of the two straight lines in Figure 5 are 2 for both phases, consequently it may be concluded that the excess absorbance at 518 nm, A_{518}', is attributed to the formation of the SQCC dimer in the liposome bilayers. In a different way, let us confirm again that the remarkable thermal changes in the spectra are due to the shift of the equilibrium between the monomer and dimer of SQCC. If SQCC molecules exist in either monomer or dimer form in the lipid bilayers, the following equation must hold over the temperature range studied:

$$(1/2)\Delta C_M' - \Delta C_D' =$$
$$(1/2)\Delta A_{610}/\epsilon_{610} - \Delta A_{518}'/\epsilon_{518}' = 0 \tag{5}$$

where $\Delta C_M'$ and ΔA_{610} are the differences in the concentration and absorbance of the monomer between
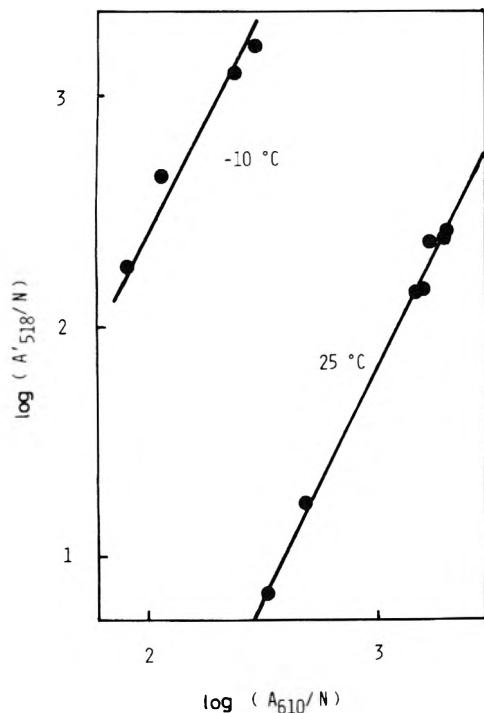
Figure 5. The linear relation between log (A_{518}'/N) and log (A_{610}/N) based on eq 4, including the data at SQCC/phosphatidylcholine molar ratios ranging from 1:360 to 1:62. The solid lines are drawn with slope of 2.
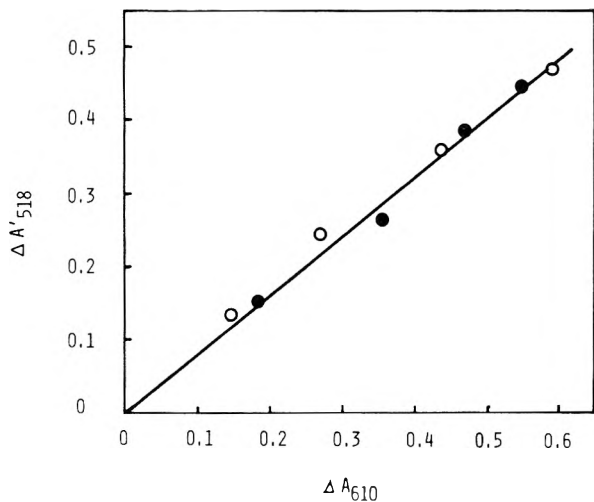

Figure 6. Plots of $\Delta A_{518}'$ against ΔA_{610}: (●) SQCC/phosphatidylcholine molar ratio of 1:62; (O) 1:76. The reference temperature, T_0, was chosen to be 25 °C.

temperature T and an arbitrarily given temperature T_0 and ΔC_D and $\Delta A_{518}'$ are the corresponding values for the dimer. In the approximation that the molecular extinction coefficients ϵ_{610} and ϵ_{518}' are independent of the temperature and the concentrations of the monomer and dimer, eq 5 requires a linear relationship between ΔA_{610} and $\Delta A_{518}'$. As illustrated in Figure 6, the plots based on eq 5 with the data obtained in the liposome systems at the molar ratios of 1:76 and 1:62 fall on a straight line. Similar results were obtained for other systems. The slope of the straight line in Figure 6 gives $\epsilon_{518}'/\epsilon_{610} = 1.60$. A combination of this value and an ϵ_{610} of 1.67×10^5 obtained in methanol solution yields $\epsilon_{518}' = 2.67 \times 10^5$ L/mol. Using these values for the extinction coefficients of the monomer and dimer in the liposome dispersions, the dimerization constant, K_2, of SQCC defined by

$$K_2 = C_D/C_M{}^2 = N(A_{518}'/A_{610}{}^2)(\epsilon_{610}{}^2/\epsilon_{518}') \qquad (6)$$
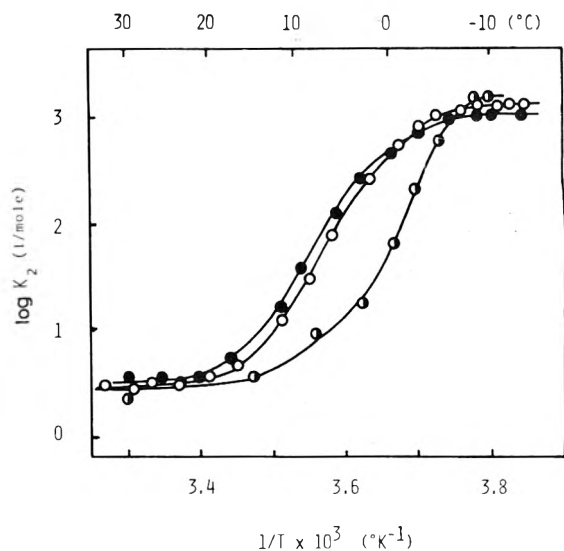
Figure 7. Arrehenius plots of K_2 at various SQCC/phosphatidylcholine molar ratios: (●) 1:62; (O) 1:72; (◑) 1:357.

is calculated from the data for A_{610}, A_{518}', and N. In Figure 7, K_2's obtained at three different molar ratios are shown as a function of temperature in the form of Arrhenius plots. With decreasing temperature, each curve exhibits an abrupt increase in the magnitude of K_2 at a critical point, T_1, which increases with the molar ratio. Above T_1, the plots converge to a single line, which demonstrates that the lipids in the liposomes are in one homogeneous phase. The value of K_2 is 3.2 L/mol at 25 °C, for instance, and the standard free energy increment for the dimerization is estimated to be less than 1 kcal/mol from the tangent of the curve at the corresponding temperature. When the temperature decreases to ca. −6 °C, each curve shows saturation and the magnitude are close to each other. The saturation temperature of ca. −6 °C (indicated by T_2) corresponds to the calorimetrically measured solid to fluid phase transition temperature of pure egg yolk phosphatidylcholine.[11] Therefore the lipids in the liposome bilayers below −6 °C are considered to be in a homogeneous solid state in which the acyl chains of the lipids are in the all-trans configuration, while it is easily supposed that the homogeneous phase which appears above T_1 is a fluid phase in which the acyl chains are in free-rotational motion around carbon−carbon bonds.[12] A thermodynamic requirement that K_2 is independent of the molar ratio in one phase seems unsatisfactory in the solid state. Figure 7 displays a small but systematic variation in K_2 with the molar ratio below T_2. However, this discrepancy between the thermodynamic requirement and the experimental data is explainable by the fluctuation in the SQCC distribution in the liposomes. If the effect of the fluctuation in the SQCC distribution on the dimerization constant is taken into consideration, eq 6 should be rewritten as follows:

$$\log K_2 + \log (1 + 2/\overline{M}') = \log (A_{518}'/A_{610}{}^2) + \log N + \log (\epsilon_{610}{}^2/\epsilon_{518}') \qquad (7)$$

where $\overline{M}'$ is the average number of monomers in each liposome (see eq A7). It should be noted that the factor 2 in log $(1 + 2/\overline{M}')$ of eq 7 is caused by considering the independence of each layer in a liposome bilayer with respect to dimer formation. The contribution of the fluctuation to the dimerization constant is estimated for two typical cases of the molar ratios, 1:62 and 1:357. Using a dimerization constant of 1.30×10^3 in the solid phase, $\overline{M}'$ are calculated as 5 and 2, and the resultant contri-

butions to log $(1 + 2/\overline{M}')$ are 0.146 and 0.301 at molar ratios of 1:62 and 1:357, respectively. The difference between the above values, 0.155, agrees reasonably with the difference in log K_2 at the corresponding molar ratios shown in Figure 7. Above T_1, $\overline{M}'$ is large enough to neglect the effect of the fluctuation, because of the stabilization of the monomer in the fluid phase.

On the contrary, in the transition temperature range between T_1 and T_2, K_2 depends on the SQCC/phosphatidylcholine molar ratio as well as on temperature. This fact cannot be expected in one homogeneous phase on the basis of thermodynamics. Moreover, the fluid to solid phase transition does not occur sharply but over a wide temperature range as shown in Figure 7. These results suggest that in the present systems two different phases may exist in each liposome between T_1 and T_2. Similar behaviors were recently observed by Shimshick and McConnel[6] in the liposome bilayers composed of a mixture of two different lipids, e.g., dipalmitoylphosphatidylcholine (DPPC) and dimyristoylphosphatidylcholine (DMPC). Unfortunately the structure lipid used in the present work is egg phosphatidylcholine containing various types of the acyl chains; as a result its phase transition temperature, T_c, is not clear cut. However it was observed calorimetrically to be around −7 °C.[11] This value is in reasonable agreement with the saturation temperature in K_2, T_2, in the present observations. The other critical temperature, T_1, in the present systems increased with the SQCC/phosphatidylcholine molar ratio. Judging from these results in comparison with the results obtained in DPPC–DMPC,[6] the T_c of SQCC, if it exists, is supposed to be at a fairly high temperature. This agrees with the well-known concept that the T_c of the lipid with long saturated normal hydrocarbon chains is at a relatively high temperature.[12-15] Thus aggregation of the amphiphilic dyes in the lipid bilayers strongly depends on the temperature and the molecular structures of the dye as well as the structure lipids through the physical states of their acyl chains.

Finally average numbers of the monomer and dimer are estimated by using the dimerization constant, K_2, of 3.22 in the fluid phase and 1.30×10^3 in the solid phase. For example, for a SQCC/phosphatidylcholine ratio of 1:62, where 43 SQCC molecules are expected to exist in a liposome, the average number of the monomer and dimer in each liposome are 38 and 2.5 in the fluid phase and 5 and 19 in the solid phase, respectively.

Appendix

The effect of the fluctuation of the SQCC concentration in each liposome on the apparent equilibrium constant is discussed. We introduce a distribution function f(x) defined by

$$f(x) = n(x)/N' \tag{A1}$$

where $n(x)$ is the molar concentration of the liposomes (mole of liposome/liter) containing x moles of SQCC per liter of lipids, and N' is the total molar concentration of liposomes in the dispersion. The observable absorbances due to the monomer and dimer in the dispersion are expressed in terms of

$$A_M = N\epsilon_M \int_0^\infty M(x)\, f(x)\, dx \tag{A2}$$

$$A_D = (N\epsilon_D/2)\int_0^\infty D(x)\, f(x)\, dx \tag{A3}$$

respectively. Here $M(x)$ and $D(x)$ are the concentrations of SQCC monomer and dimer (mole/liter of lipids) in the liposomes containing x moles of SQCC per liter of lipids. A combination of eq A2 and A3 leads to

$$A_D/A_M{}^2 = (1/zN)(\epsilon_D/\epsilon_M{}^2)\int_0^\infty D(x)\, f(x)\, dx / \\ (\int_0^\infty M(x)\, f(x)\, dx)^2 = \\ (K/N)(\epsilon_D/\epsilon_M{}^2)[\overline{M^2}/\overline{M}^2] \tag{A4}$$

where the bar represents an averaged value. In the derivation of the second expression, K was assumed to be constant and independent of x as follows:

$$K = D(x)/M(x)^2 \tag{A5}$$

This assumption is valid at the temperature range where phase separation does not occur. Assuming a Poisson distribution for f(x), the fluctuation of the monomer concentration expressed in number per liposome, $\Delta M'$, is given by

$$\Delta M' = \overline{M'^2} - \overline{M}'^2 = \overline{M}' \tag{A6}$$

Rearrangement of eq A4 with eq A6 gives

$$\log (A_D/A_M{}^2) + \log N + \log (\epsilon_M{}^2/\epsilon_D) = \\ \log K + \log (1 + 1/\overline{M}') \tag{A7}$$

as a final expression.

References and Notes

(1) H. G. Weller, Jr., and H. T. Tien, *Biochim. Biophys. Acta*, **325**, 433 (1973).
(2) G. S. Beddart, G. Porter, F. R. S. Weese, and G. M. Weese, *Proc. R. Soc. London, Ser. A*, **342**, 317 (1975).
(3) D. Branton, *Ann. Rev. Plant Physiol.*, **20**, 209 (1969).
(4) L. Csorba, J. Szabad, L. Erdei, and Cs. Fajszi, *Photochem. Photobiol.*, **21**, 377 (1975).
(5) A. G. Lee, *Biochemistry*, **14**, 4397 (1975).
(6) E. J. Shimshick and H. M. McConnel, *Biochemistry*, **12**, 2351 (1973).
(7) A. G. Lee, *Biochim. Biophys. Acta*, **413**, 11 (1975).
(8) M. C. Pangborn, *J. Biol. Chem.*, **188**, 471 (1951).
(9) C. Huang, *Biochemistry*, **8**, 344 (1969).
(10) C. H. Fiske and Y. Subbarow, *J. Biol. Chem.*, **66**, 375 (1925).
(11) D. Chapman, "Form and Function of Phospholipids", G. B. Ansell, R. M. C. Dawson, and J. N. Hawthorne Ed., Elsevier, Amsterdam, 1973.
(12) J. L. Lippert and W. L. Peticolas, *Biochim. Biophys. Acta*, **282**, 8 (1972).
(13) D. Lichtenberg, N. O. Petersen, J.-L. Girardet, M. Kainosho, P. A. Knoon, C. H. A. Seiter, G. W. Feigenson, and S. I. Chan, *Biochim. Biophys. Acta*, **382**, 10 (1975).
(14) H. J. Hinz and J. M. Sturtvant, *J. Biol. Chem.*, **241**, 6071 (1972).
(15) E. Sackmann and T. Träuble, *J. Am. Chem. Soc.*, **94**, 4482 (1972).

The Role of Hydrogen Bonding in the Formation of Bile Salt Micelles

D. G. Oakenfull* and L. R. Fisher

CSIRO Division of Food Research, P.O. Box 52, North Ryde, New South Wales 2113, Australia (Received November 22, 1976)

Publication costs assisted by the Commonwealth Scientific and Industrial Research Organization

Bile salts are biological detergents. They form micelles which help to solubilize and disperse dietary lipids. Bile salts are nearly flat molecules with a hydrophobic surface and a hydrophilic surface. The currently accepted model for the structure of bile salt micelles in water is that the monomers associate by interaction between the hydrophobic faces. Further growth may occur at high bile salt concentrations by hydrogen bonding between these hydrophobically stabilized subunits. We present here evidence which suggests that the first stage in the formation of bile salt micelles is the formation of hydrogen bonded dimers. Evidence from the conductance of bile salt solutions and the volume change on micelle formations suggests that hydrogen bonding is the major force associated with the formation of dimers. On the basis of this evidence we propose a new model for the structure of bile salt micelles, in which the basic building blocks are hydrogen bonded dimers.

Introduction

Bile salts (Figure 1) are detergents which are synthesized in the liver. They form small aggregates (micelles) which help to solubilize and disperse dietary lipids in the small intestine.[1] Information about the formation and structure of these micelles is needed to develop a fuller understanding of the physiological role of bile salts.

The structure of bile salt micelles must be different from that of more commonly studied detergent micelles. The commonly accepted picture of micelle structure comes from studies on compounds having a hydrocarbon "tail" (an *n*-alkyl hydrocarbon chain containing 8 to 18 carbon atoms) joined to a polar head group.[2] The micelles formed by these compounds above a certain concentration (the critical micelle concentration, or cmc) are nearly spherical aggregates with the polar groups on the surface and the hydrocarbon chains forming a core. Such aggregates are stabilized by hydrophobic interaction between the hydrocarbon chains.[3]

Bile salts have a completely different structure to these more commonly studied detergents. They are steroids with a C-24 carboxylate group and up to three hydroxyl groups attached to the steroid nucleus (see Figure 1). The steroid nucleus is shaped like an elongated saucer because the A ring is cis with respect to the B ring. The hydroxyl groups are all directed toward the concave surface of the molecule. Bile salt molecules thus have a hydrophobic surface and a hydrophilic surface, rather than the hydrophobic tail and hydrophilic head group of conventional detergent molecules. Thus the packing of bile salt micelles must be quite different from the packing of conventional detergent micelles.

The currently accepted model[4] for the structure of bile salt micelles is that the aggregates ("primary" micelles) of up to nine or ten molecules are built up by "back-to-back" hydrophobic interaction between the nonpolar surfaces of the bile salt molecules, with the hydrophilic surfaces pointing outward (see Figure 2). Where conditions favor the formation of larger "secondary" micelles, two or more primary micelles are linked by hydrogen bonding between the hydroxyl groups.

The only direct evidence for this model is a high resolution proton NMR study of aqueous sodium cholate and sodium deoxycholate solutions.[5] This study suggested that the environment of the C-18 methyl group changes on micelle formation, whereas that of the C-12 proton does not change. However these results can equally well be explained by other models.

We have studied the conductance of sodium cholate and sodium deoxycholate solutions in water at 25 °C. The results show that association (probably dimerization) occurs at concentrations below the critical micelle concentration. This ("premicellar") association persists in the presence of a large concentration of ethanol (mole fraction = 0.3). It is known that this concentration of ethanol is high enough to destroy hydrophobic interactions.[6] We therefore suggest that premicellar aggregation between bile salt molecules is due to polyfunctional hydrogen bonding rather than hydrophobic interaction.

These results suggest that hydrogen bonding is important in the building up of the primary micelles (at concentrations near the cmc). We have also studied the volume change on micelle formation for aqueous solutions of sodium cholate and sodium deoxycholate. The results for both compounds support the view that hydrogen bonding plays an important role in the formation of bile salt micelles.

Experimental Section

(1) *Materials.* For the conductance experiments, cholic and deoxycholic acids were recrystallized from ethanol. Their melting points were 197 and 176 °C, respectively. Purity was confirmed by thin layer chromatography.[7] Solutions of the sodium salts were prepared by adding the calculated quantity of the bile acid to standardized sodium hydroxide solutions. The pH of the resulting solution was always between 7 and 8. The water used was from an all-glass still and was passed through a mixed-bed ion-exchange column (Bio-Rad AG 501-X8(D)) before use. The conductivity of the water was always below 1×10^{-6} ohm^{-1} cm^{-1}.

(2) *Conductance Measurements.* Conductance measurements were made with a Wayne-Kerr universal bridge (B224). The cell was fitted with platinized platinum electrodes and was of a type for use with solutions which have a tendency to froth (see Figure 13 of ref 8). The cell constant (15.72) was checked before and after each set of experiments by using a standard potassium chloride solution. All solutions were thermostated at 25.00 °C (±0.05 °C). We could detect no change in conductance with time after the test solution had reached thermostat temperature.

(3) *Density Measurements.* Solutions of the bile salts were prepared in 0.02 M TRIS (2-amino-2-(hydroxymethyl)propane-1,3-diol) buffer (pH 8.93). The buffer was added because of the marked pH dependence of cmc and aggregation number for some bile salts.[4] An Anton Paar
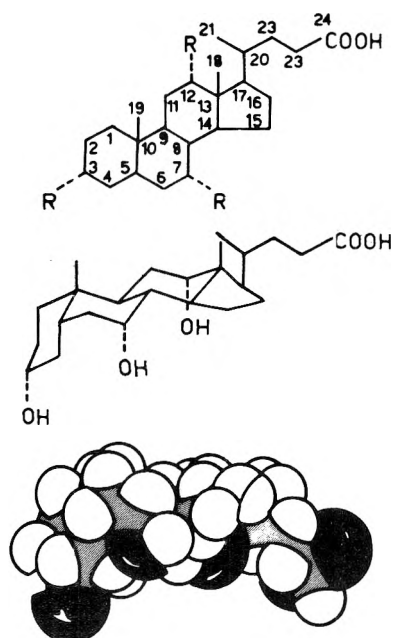
Figure 1. The structure of the bile salts: (top) structural formula (cholate, R-3 = R-7 = R-12 = OH; deoxycholate, R-3 = R-12 = OH, R-7 = H; lithocholate, R-3 = OH, R-7 = R-12 = H; (center) conformation; (bottom) Courtauld space-filling model.
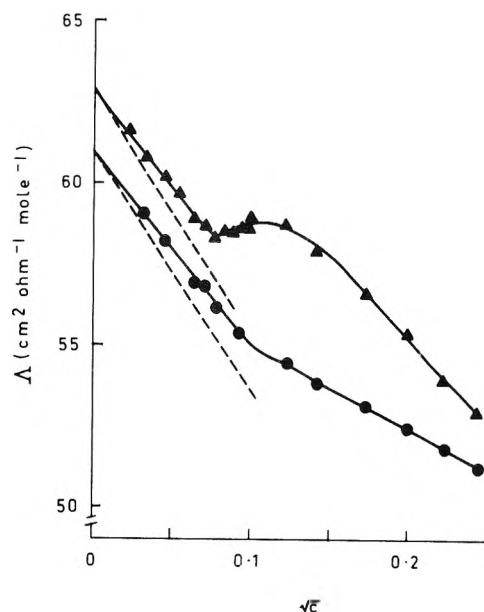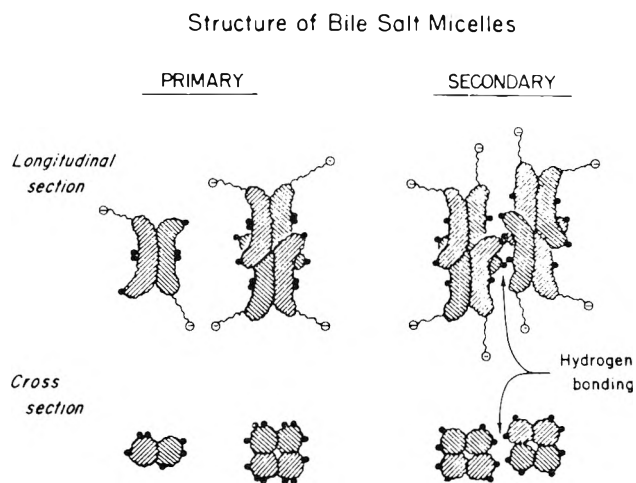
Structure of Bile Salt Micelles

Figure 2. Small, Penkett, and Chapman's model for the structure of bile salt micelles. (Reproduced, with permission, from D. M. Small, *Adv. Chem. Ser.*, **No. 84**, 31 (1968).)

precision density meter (DMA 02C), fitted with an ultrathermostat, was used to measure density to a precision of $\pm 10^{-6}$ g cm^{-3}. To avoid errors from small variations in the buffer concentration, a single large batch of buffer solution was prepared for use throughout each series of experiments.

Results and Discussion

(1) *Conductance of Bile Salt Solutions.* The equivalent conductance of sodium cholate and sodium deoxycholate solutions in water at 25 °C is plotted against the square root of the molar concentration in Figure 3. In both cases there is a sharp break in the curve, the break corresponding to the critical micelle concentration as determined by other methods.[4] The break is much sharper than that found at 40 °C by Norman.[9]

The most informative feature of our conductance curves is the section below the cmc. For both bile salts the equivalent conductance decreases less with concentration than is predicted by the Onsager equation[10] for a 1:1 electrolyte.[11] (The theoretical behavior is shown by the

Figure 3. The equivalent conductance of sodium cholate (●) and sodium deoxycholate (▲) solutions in water at 25 °C: (solid lines) curves fitted to experimental data; (dotted lines) theoretical curves from Onsager equation, assuming no aggregation.
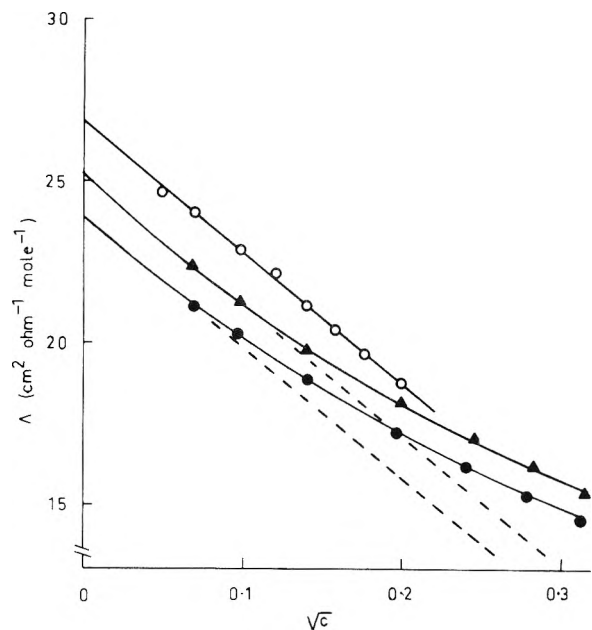
Figure 4. The equivalent conductance of sodium cholate (●), sodium deoxycholate (▲) and sodium lithocholate (O) solutions in 0.3 mole fraction ethanol–water at 25 °C: (solid lines) calculated curves allowing for dimerization; (dotted lines) calculated curves assuming no dimerization.

dotted lines in Figure 3.) The difference is substantially greater than experimental error, and is unlikely to be due to hydrolysis since the difference in pH between the weakest and most concentrated solutions was less than 0.5 pH units. Furthermore, the electrolyte concentration is low enough (<0.01 mmol L^{-1}) for the Onsager equation to be reasonably exact.[10]

Sodium cholate and sodium deoxycholate solutions in 0.1 mole fraction ethanol–water[12] and 0.3 mole fraction ethanol–water (Figure 4) show similar deviations from ideal behavior. However, sodium lithocholate in these ethanol–water mixtures obeys the Onsager equation up to a bile salt concentration of 0.04 mol L^{-1} (Figure 4). Thus it is unlikely that the observed deviations from the Onsager equation are a consequence of the size and asymmetry of

TABLE I: Values of Λ_0, $\Lambda_0{}^D$, and K_D for Bile Salts at 25 °C in Water and in 0.3 Mole Fraction Ethanol–Water

Solvent	Bile salt	Λ_0, Ω^{-1} mol^{-1} cm^{-1}	$\Lambda_0{}^D$, Ω^{-1} mol^{-1} cm^{-1}	K_D,[a] L mol^{-1}
Water	Sodium cholate	61.0	110	18 ± 1
	Sodium deoxycholate	64.8	140	13 ± 1
0.3 mole fraction	Sodium cholate	23.9	115	1.0 ± 0.1
ethanol–water	Sodium deoxycholate	25.3	130	0.5 ± 0.1
	Sodium lithocholate	26.9		

[a] Errors are calculated from the scatter of experimental points.

the bile salt anions. Unfortunately, sodium lithocholate is too insoluble in pure water for a direct comparison with the results shown in Figure 3.

The most likely explanation for the deviation from the Onsager equation is that premicellar aggregation of the bile acid anions is occurring. An adequate representation of the experimental data can be obtained by assuming that the aggregates are dimers. The solid curve in Figure 3 (for concentrations below the cmc) was calculated on this basis, using the treatment of Mukerjee, Mysels, and Dulin.[13] Using the appropriate form of the Onsager equation, they derived an expression for the equivalent conductance of a partially dimerized species as the sum of the contributions from the monomeric and dimeric forms. There are two unknown quantities: the limiting equivalent conductance of the dimer ($\Lambda_0{}^D$) and the dimerization constant (K_D). We used a programmable calculator to find the values of $\Lambda_0{}^D$ and K_D which gave the best fit to the experimental data. These values are given in Table I.

Conductance results for bile salts in the mixed solvent 0.3 mole fraction ethanol–water (52% ethanol by weight) at 25 °C are given in Figure 4. (The theoretical behavior is shown by dotted lines.) Addition of ethanol raises the cmc, so that all data points in Figure 4 are below the cmc. The significant feature is that in the mixed solvent the conductance of sodium cholate and sodium deoxycholate solutions again decreases less with bile salt concentration than is predicted by the Onsager equation. The addition of ethanol has thus not prevented premicellar aggregation.

It has been shown from conductance measurements,[6] calculations based on the solubility of hydrocarbons,[14] and from the stability of detergent micelles in ethanol–water mixtures[15,16] that 0.3 mole fraction of ethanol in water is more than sufficient to completely disrupt hydrophobic interaction between solute molecules. Hydrophobic interaction depends on the rearrangement of the water molecules surrounding the hydrophobic molecule. The details of the structure of the molecule, whether it is linear, branched, or cyclic hydrocarbon, seem not to be important.[17,18] Thus we assume that hydrophobic interaction between the steroid nuclei is destroyed in 0.3 mole fraction ethanol–water. Hence the bile salt dimers appear to be held together by hydrogen bonds. Although monofunctional hydrogen bonds have no significant stability in aqueous solutions, simultaneous formation of two or more hydrogen bonds does lead to intermolecular association (examples are the dimerization of carboxylic acids[19,20] and the association of urea and acetyltetraglycine ethyl ester[21]). It is also known[22] that di- and trihydroxy bile acids in carbon tetrachloride solution display abnormally persistent self-association through multiple hydrogen bonding.

Our interpretation is further supported by the fact that sodium lithocholate, with only one hydroxyl group, does not form premicellar aggregates, while sodium dehydrocholate, the triketo analogue of sodium cholate, does not form micelles at all.[23]

(2) *The Apparent Molar Volume of Bile Salts in Aqueous Solution.* The density of solutions of sodium
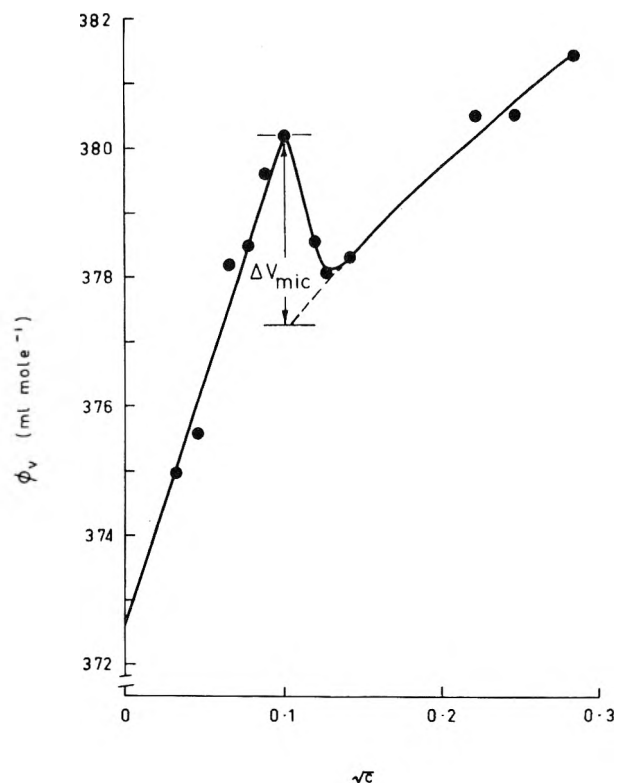

Figure 5. Apparent molar volume of sodium cholate in 0.02 M TRIS buffer plotted against $c^{1/2}$ (temperature 25 °C). (Dotted line is extrapolation of experimental curve above cmc to cmc.)

TABLE II: Partial Molar Volumes ($\bar{V}$) and ΔV_{mic} for Bile Salts in 0.02 M TRIS Buffer at 25 °C

Bile salt	$\bar{V}$, cm^3 mol^{-1}	ΔV_{mic}, cm^3 mol^{-1}
Sodium cholate	372.6	−2.8 ± 0.5
Sodium deoxycholate	320.8	−3 ± 1

cholate and sodium deoxycholate in TRIS buffer (0.02 M) was measured at 25 °C over a range of concentrations spanning the cmc in each case. Apparent molar volumes (ϕ_v) were calculated for each concentration from the expression[24]

$$\phi_V = (M/d_0) - 1000(d - d_0)/cd_0$$

where M is the molecular weight of the bile salt, c is the molar concentration, d is the density of the solution, and d_0 is the density of the pure solvent.

Figure 5 shows values of ϕ_v plotted against $c^{1/2}$. Below the cmc the plots are linear and typical of unassociated 1:1 electrolytes (the data are not accurate enough for deviations due to premicellar aggregation to be detectable). At the cmc there is a sharp decrease in ϕ_v. Thus micelle formation is accompanied by a volume reduction. The value of the volume change at the cmc (ΔV_{mic}) was estimated for each bile salt as shown in Figure 5. Values of
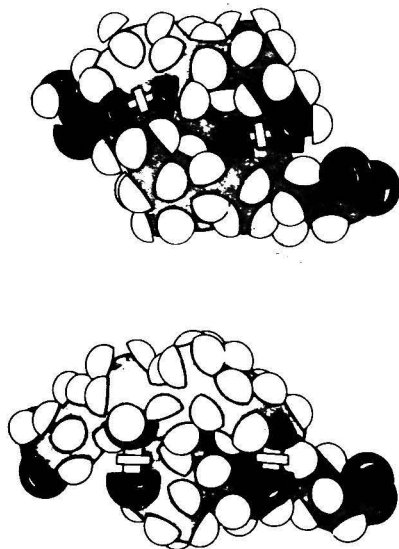
Figure 6. Edge-on view of Courtauld space-filling model of hydrogen-bonded dimers. Dark hemispheres represent oxygen atoms, light hemispheres hydrogen atoms. The shaded background represents the carbon skeleton: (top) cholate dimer (the third hydrogen bond is central and below the plane of the paper); (bottom) deoxycholate dimer.

ΔV_{mic} and the partial molar volume (ϕ_v extrapolated to zero concentration) for each bile salt are given in Table II.

The fact that bile salt micelles are formed with a reduction in volume is further evidence for the importance of hydrogen bonding in these structures. The volume of formation of a hydrogen bond has been calculated[25] as ~ -3.4 mL mol^{-1}. An experimental estimate[20] from the dimerization of carboxylic acids is ~ -7 mL mol^{-1}. In contrast, hydrophobic interaction is accompanied by a substantial volume increase.[26] If "back-to-back" hydrophobic interaction can be considered as equivalent to hydrophobic interaction between two C_{12} alkyl chains, then the corresponding volume of interaction would be about $+100$ mL/mol.[25] Thus ΔV_{mic} would be positive unless hydrogen bond formation were the major contributor to bile salt aggregation at the cmc.

(3) *The Structure of Bile Salt Micelles.* The models which we propose for the structure of sodium cholate and sodium deoxycholate micelles are shown in Figure 6. The structure of the bile salts is such that in the dimers the maximum number of hydrogen bonds (three for the cholate, two for the deoxycholate) can be formed, with the charged carboxyl groups widely separated to minimize electrostatic repulsion. The proposed dimer structures permit the formation of linear hydrogen bonds of maximum strength. The distance between carboxylate groups is about 1.8 nm.

There appears also to be a hydrophobic contribution to the stabilization of the dimers. This is indicated by the fact that in 0.3 mole fraction ethanol–water, in which any hydrophobic contribution should be eliminated,[6] K_D is lower than that in pure water. This combination of hydrophobic interaction and hydrogen bonding as stabilizing influences is not unique; it occurs, for example, in the formation of nucleoside base pairs.[27]

There are two reasonable ways in which dimers could aggregate further to form micelles. Aggregation could occur by "back-to-back" hydrophobic interaction between the dimers in a manner similar to that suggested by Small, Penkett, and Chapman[5] as the first step in bile salt monomer association. This "back-to-back" configuration is consistent with Small, Penkett, and Chapman's NMR

results.[5] They showed that the high resolution signal from the C-18 proton of sodium cholate (situated in the center of the hydrophobic surface) is broadened upon micelle formation, while the corresponding signal from the C-12 proton (situated near the edge) is unaffected.

However, the negative volume of micelle formation makes it unlikely that hydrophobic interaction contributes significantly to aggregation at the cmc. Thus we propose that, since the dimers have residual hydrogen bond donor and acceptor groups, polyfunctional hydrogen bonding contributes to the formation of larger aggregates such as tetramers. Examination of Courtauld space-filling models (see Figure 6) shows that this is possible. The C-12 proton is situated in a slight hollow, and thus further aggregation could involve polyfunctional hydrogen bonding without any effect on the NMR signal from this proton.

In conclusion, it is interesting to speculate that the 3,7,12 positioning of the hydroxyl groups is an optimum configuration developed in the course of evolution. The bile acids and related bile alcohols of almost all vertebrates have this configuration of hydroxyl groups, with a few exceptions[28] which are thought to represent evolutionary blind alleys. This evolutionary conservatism seems unlikely if the hydroxyl groups were only required for nonspecific hydrogen bonding. It supports the micelle structure proposed here, which requires the hydroxyl groups to be positioned so as to optimize hydrogen bonded dimerization with the charged carboxylate groups separated as widely as possible.

References and Notes

(1) E. J. Masoro, "Physiological Chemistry of Lipids in Mammals", W. B. Saunders, Philadelphia, Pa., 1968, pp 188–194.
(2) L. R. Fisher and D. G. Oakenfull, *Chem. Soc. Rev.*, **6**, 25 (1977).
(3) Hydrocarbons dissolved in water tend to associate, with a consequent decrease in the entropy of the solution. Such association is termed "hydrophobic interaction". The major contribution to the entropy change probably comes from rearrangement of the water molecules.
(4) D. M. Small, *Adv. Chem. Ser.*, **No. 84**, 31 (1968).
(5) D. M. Small, S. A. Penkett, and D. Chapman, *Biochim. Biophys. Acta*, **176**, 178 (1969).
(6) D. G. Oakenfull and D. E. Fenwick, *J. Phys. Chem.*, **78**, 1759 (1974).
(7) J. G. Kirchner, "Technique of Organic Chemistry", Vol. III, A. M. Weissberger, Ed., Interscience, New York, N.Y., 1967, p 607.
(8) T. Shedlovsky, "Physical Methods of Organic Chemistry", Vol. 1, A. Weissberger, Ed., 2nd ed, Interscience, New York, N.Y., 1949, Part II, p 1651.
(9) A. Norman, *Acta Chem. Scand.*, **14**, 1300 (1960).
(10) R. A. Robinson and R. H. Stokes, "Electrolyte Solutions", Butterworths, London, 1955.
(11) The Onsager equation is of the form $\Lambda = \Lambda_0 - Ac^{1/2}$, where Λ is the equivalent conductance of the solution, Λ_0 is the limiting equivalent conductance, c is the molar concentration, and A is a constant which can be calculated from the physical properties of the solvent.
(12) D. Oakenfull and D. E. Fenwick, *Aust. J. Chem.*, **30**, 335 (1977).
(13) P. Mukerjee, K. J. Mysels, and C. J. Dulin, *J. Phys. Chem.*, **62**, 1390 (1958).
(14) M. Yaacobi and A. Ben-Naim, *J. Solution Chem.*, **2**, 425 (1973).
(15) P. Becher, *J. Colloid Interface Sci.*, **20**, 728 (1965).
(16) B. D. Flockhart, *J. Colloid Interface Sci.*, **12**, 557 (1957).
(17) R. B. Hermann, *J. Phys. Chem.*, **76**, 2754 (1972).
(18) J. A. Reynolds, D. B. Gilbert, and C. Tanford, *Proc. Natl. Acad. Sci., U.S.A.*, **71**, 2925 (1974).
(19) E. E. Schrier, M. Pottle, and H. A. Scheraga, *J. Am. Chem. Soc.*, **86**, 3444 (1964).
(20) K. Suzuki, Y. Taniguchi, and T. Watanabe, *J. Phys. Chem.*, **77**, 1918 (1973).
(21) D. R. Robinson and W. P. Jencks, *J. Am. Chem. Soc.*, **87**, 2462 (1965).
(22) W. S. Bennet, G. Eglinton, and S. Kovac, *Nature (London)*, **214**, 776 (1967).
(23) K. W. Heaton, "Bile Salts in Health and Disease", Churchill Livingstone, Edinburgh, 1972.
(24) F. J. Millero, *Chem. Rev.*, **71**, 147 (1971).
(25) S. D. Hamann, "High Pressure Physics and Chemistry", Vol. 2, R. S. Bradley, Ed., Academic Press, New York, N.Y., 1963, p 144.
(26) D. Oakenfull and D. E. Fenwick, *Aust. J. Chem.*, **30**, 741 (1977).
(27) F. Garland and S. D. Christian, *J. Phys. Chem.*, **79**, 1247 (1975).
(28) G. A. D. Haslewood, *J. Lipid Res.*, **8**, 535 (1967).

Ionic Surfactants Applicable in the Presence of Multivalent Cations. Physicochemical Properties

Kōzō Shinoda* and Tsuyoshi Hirai

Department of Chemistry, Faculty of Engineering, Yokohama National University, Ooka-2, Minamiku, Yokohama, Japan 233 (Received March 21, 1977)

Ordinary ionic surfactants are salted out and cannot be used in water in the presence of multivalent cations, because they do not dissolve in hard water more than their saturation concentrations of multivalent salts of surfactants, i.e., neither micellization nor solubilization occurs. Calcium and magnesium salts of surface active anions, $C_{12}H_{25}OCH_2CH_2SO_4$ 0.5Ca (or Mg), which can dissolve well in water in the presence of bivalent cations at room temperature were prepared and the physicochemical properties of their aqueous solutions have been studied. The critical micelle concentration (cmc), the solubilizing power for cyclohexane, and the surface tension of aqueous solution above the cmc of $C_{12}H_{25}OCH_2CH_2SO_4$ 0.5Ca were respectively $^1/_9$th, 4.7 times larger, and 8 dyn/cm lower than those of sodium dodecyl sulfate. A liquid surfactant phase was observed above the Krafft point in the presence of a large amount of bivalent cations or a small amount of trivalent cations. This phenomenon manifests the continuous change from micelle (pseudophase) to liquid surfactant phase (true phase), i.e., from finite to infinite aggregation supporting the pseudophase separation model of micellar solution.

Introduction

Ordinary ionic surfactants are salted out and cannot be used in hard water, because they are not soluble in the presence of multivalent cations. The surface tension of the aqueous surfactant solution is not depressed well, because a hydrated solid (multivalent cation salt of) surfactant precipitates before the solution reaches the critical micelle concentration (cmc). Micelles are not formed, nor does solubilization of oily substances occur in the solution.

It is known that ionic surfactants dissolve well in water forming micelles above their Krafft points[1] and the Krafft point is the melting point of hydrated solid surfactant[2] regardless the number of valencies of gegenions.[3] The Krafft point of fatty acid soap is enhanced remarkably in the presence of very small amount of multivalent cations, such as calcium ions. In other words, the Krafft points of calcium alkane carboxylates are so high that they cannot dissolve in hard water. In the case of alkyl sulfate, however, the Krafft point is increased by replacing sodium by bivalent cations but as not much.[3-7] The Krafft point of calcium dodecyl sulfate is about 50 °C. If we could depress the Krafft point of a surfactant below room temperature by some devices, it can be used in the presence of calcium ions and will find many useful applications. The present investigation was undertaken to study the basic physicochemical properties of such compounds, $C_{12}H_{25}(OCH_2CH_2)_nSO_4$ 0.5Me, in water.

Experimental Section

Materials. Pure mono-, di-, tri-, and hexaoxyethylene dodecyl ethers were obtained from the Nikko Chemicals Co. The purity of these materials were more than 98% according to gas chromatographic analysis. Dodecyl polyoxyethylene sulfuric acids, $C_{12}H_{25}(OCH_2CH_2)_nSO_4H$, were synthesized by introducing SO_3 vapor into the respective polyoxyethylene dodecyl ethers at about 30–35 °C. Alkali salts were obtained by neutralizing these acids with the respective alkali hydroxide solution. Calcium salts were obtained by neutralizing these acids with suspended calcium oxide in a 2-propanol solution of the respective acids. Excess CaO was neutralized to $CaSO_4$ and separated

TABLE I: Krafft Points and Cmc Values of $C_{12}H_{25}(OCH_2CH_2)_nSO_4$ (1/z)Me Type Surfactants[a]

Ionic surfactants	Cmc, equiv/L at 25 °C	Krafft point, °C
$C_{12}H_{25}SO_4$ 0.5Ca	0.0024[b] (at 55 °C)	50[b]
$C_{12}H_{25}OCH_2CH_2SO_4$ 0.5Ca	0.00092[b]	15[b]
$C_{12}H_{25}(OCH_2CH_2)_2SO_4$ 0.5Ca	0.00071	<0
$C_{12}H_{25}SO_4$ 0.5Mg	0.0018[c]	25[c]
$C_{12}H_{25}OCH_2CH_2SO_4$ 0.5Mg	0.00096	<0
$C_{12}H_{25}(OCH_2CH_2)_2SO_4$ 0.5Mg		<0
$C_{12}H_{25}SO_4$ Na	0.0081	9
$C_{12}H_{25}OCH_2CH_2SO_4$ Na	0.0042[b]	5[b]
$C_{12}H_{25}(OCH_2CH_2)_2SO_4$ Na	0.0030	<0
$C_{12}H_{25}(OCH_2CH_2)_3SO_4$ Na	0.0028	<0
$C_{12}H_{25}(OCH_2CH_2)_6SO_4$ Na	0.0016	<0
$C_{12}H_{25}OCH_2CH_2SO_4$ K	0.0036	24
$C_{12}H_{25}OCH_2CH_2SO_4$ NH$_4$	0.0036	<0
$C_{12}H_{25}OCH_2CH_2SO_4$ Li	0.0045	<0
$C_{12}H_{25}OCH_2CH_2SO_4$ 0.5Mn		<0

[a] Data on $C_{12}H_{25}SO_4$ (1/z)Me are included for comparison. [b] Reference 20. [c] Reference 5.

by filtration. Unreacted ethers were extracted with petroleum ether.

Procedures. Solubility and Surface Tension Measurements. The procedures are described in the previous study.[8] The surface tension determined by the Wilhelmy plate method agreed with that obtained by drop weight method.

Krafft Point and Cmc Measurements. The procedures are described in the previous paper.[9] It was confirmed that the solubility at the Krafft point is equal to the cmc.

Solubilization Measurements. The procedures followed are found in previous papers.[10]

Results and Discussion

Krafft Points and Critical Micelle Concentration. The Krafft points and the cmc values of $C_{12}H_{25}(OCH_2CH_2)_nSO_4$ (1/z)Me type surfactants are summarized in Table I.

The Krafft points of all $C_{12}H_{25}(OCH_2CH_2)_nSO_4$ (1/z)Me type surfactants studied were lower than 15 °C as shown in Table I. This remarkable fact means calcium or

TABLE II: The Limiting Concentration of Cations Needed for the Infinite Aggregation of Surfactant Anions above the Krafft Point

Surfactants	Concn, wt %	Added salts	Ratio of equiv concn of cation vs. anion	Equiv concn of multivalent cation
$C_{12}H_{25}OCH_2CH_2SO_4$ 0.5Ca	0.7	$Al(NO_3)_3$	0.53_s	0.011
$C_{12}H_{25}OCH_2CH_2SO_4$ 0.5Ca	0.7	$LaCl_3$	0.53_s	0.011
$C_{12}H_{25}OCH_2CH_2SO_4$ 0.5Ca	1.0	$CaCl_2$	61	1.8
$C_{12}H_{25}(OCH_2CH_2)_2SO_4$ 0.5Ca	1.0	$CaCl_2$	21	0.56
$C_{12}H_{25}(OCH_2CH_2)_2SO_4Na$	1.0	NaCl	125	3.3
$C_{12}H_{25}(OCH_2CH_2)_2SO_4Na$	1.0	$CaCl_2$	80	2.1
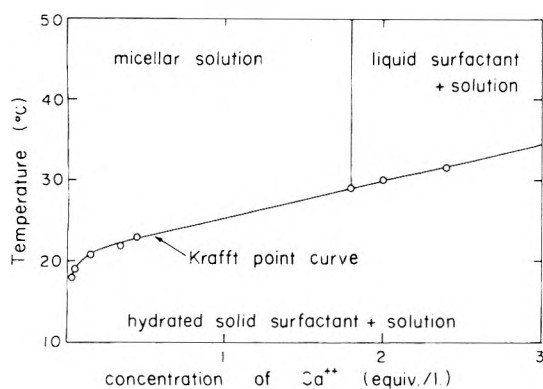
Figure 1. The effect of added $CaCl_2$ on the Krafft point of 1.0 wt % of $C_{12}H_{25}OCH_2CH_2SO_4$ 0.5Ca in water. The surfactant either disperses forming micelles or simply melts forming a two-phase solution above the Krafft point. Just as the melting point, the Krafft point changes with impurities and additives in the solvent.

magnesium salts of these anionic surface active ions are soluble and can be used in water at room temperature. The Krafft point of $C_{12}H_{25}OCH_2CH_2SO_4$ 0.5Ca is 15 °C and the solubility in water at that temperature is 0.030 wt %. The solubility of $C_{12}H_{25}OCH_2CH_2SO_4$ 0.5Ca increases with temperature and reaches 1.0 wt % at 18 °C. The effect of added $CaCl_2$ on the dissolution temperature of 1.0 wt % of $C_{12}H_{25}OCH_2CH_2SO_4$ 0.5Ca in water has been determined and is shown in Figure 1. The dissolution temperature was elevated from 18 to 25 °C in the presence of 0.8 equiv/L of calcium ions. A micellar solution is formed above these temperatures. This important fact implies that $C_{12}H_{25}OCH_2CH_2SO_4$ 0.5Ca or a similar compound listed in Table I is soluble in water at room temperature in the presence of a fairly large amount of calcium ions, i.e., in hard water or in brine. Sodium ether alcohol sulfates have been used for many years in commercial detergents and other technical products. Their tolerance for calcium is well known.[11] However, commercial $C_{12}H_{25}(OCH_2CH_2)_nSO_4Na$ contains an appreciable amount of $C_{12}H_{25}SO_4Na$, provided $\bar{n}$ is 3 or less, and $C_{12}H_{25}SO_4$ 0.5Ca is precipitated by added $CaCl_2$. However pure $C_{12}H_{25}OCH_2CH_2SO_4$ 0.5Ca is soluble in water under these conditions. Moreover, the properties of the calcium salt were proved to be better than those of the sodium salt.

The aggregation number of the micelle increases with added salts.[12-15] It becomes infinite in the presence of more than 1.8 equiv/L of Ca^{2+} in a solution of $C_{12}H_{25}OCH_2CH_2SO_4$ 0.5Ca as shown in Figure 1. The limiting concentration of gegenions necessary for the infinite aggregation of surfactants are summarized in Table II. The solution splits into two phases, i.e., an aqueous solution and a liquid surfactant phase, with the lesser amount of $CaCl_2$, if the oxyethylene chain is longer. Ordinary ionic surfactants dissolve in water forming micelles above the Krafft point so that the liquid surfactant phase was not observed. However, in the presence of a fairly large amount of multivalent gegenions a liquid surfactant phase
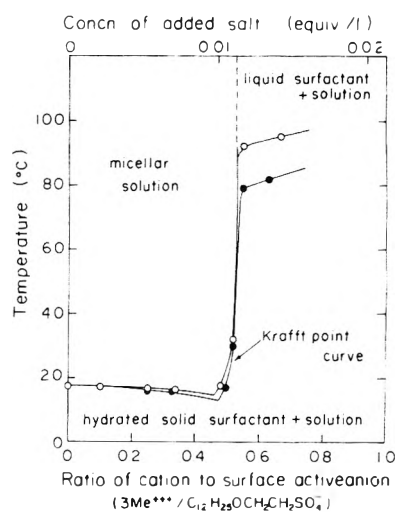

Figure 2. The effect of added $A(NO_3)_3$ and $LaCl_3$ on the solubility behavior of $C_{12}H_{25}OCH_2CH_2SO_4$ 0 5Ca.

TABLE III: Effect of Added Salts on the Krafft Points of $C_{12}H_{25}(OCH_2CH_2)_nSO_4Na$, i.e., Krafft Points of Multivalent Cation Salts of Surfactant Anions

Surfactants	Concn, wt %	Added salts	Krafft points	Ratio of equiv concn of cation vs. anion
$C_{12}H_{25}OCH_2CH_2SO_4Na$	1.0	$BaCl_2$	61	1.5
$C_{12}H_{25}(OCH_2CH_2)_2SO_4Na$	1.0	$BaCl_2$	36	1.5
$C_{12}H_{25}(OCH_2CH_2)_3SO_4Na$	1.0	$BaCl_2$	13	1.5
$C_{12}H_{25}OCH_2CH_2SO_4Na$	0.7	$Al(NO_3)_3$	82	0.63
$C_{12}H_{25}OCH_2CH_2SO_4Na$	0.7	$LaCl_3$	95	0.67

is observed above the Krafft point as shown in Figure 1. This is further evidence to support the conclusion that "the Krafft point is the melting point of hydrated solid surfactant".[2] Continuous change from micelles (finite aggregation) to liquid surfactant (infinite aggregation) with the concentration of added salts proves the pseudo-phase separation model of micellar solution, in which both the mass action model and the phase separation model are treated compatibly.[16] In studying the effect of added salts on the solubility behavior of $C_{12}H_{25}(OCH_2CH_2)_nSO_4Na$ (or 0.5Ca) it is useful to know the temperature above which this surfactant can be used in the presence of respective added salts. One example is shown in Figure 2. The minimum in the Krafft point curve as a function of the concentration of added salts may correspond to the eutectic mixture of Ca and La (or Al) salts of this surface
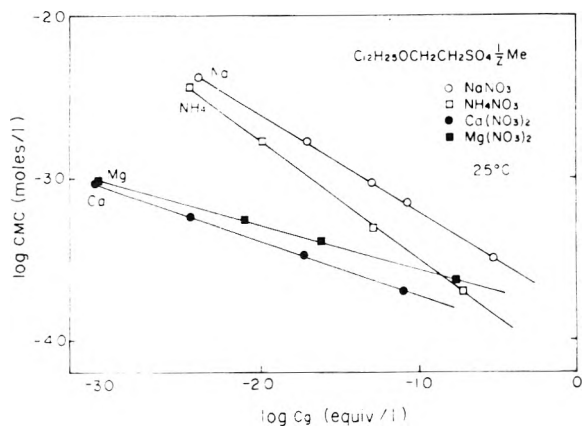
Figure 3. The effect of added salts (respective nitrates) on the cmc of $C_{12}H_{25}OCH_2CH_2SO_4$ $(1/z)$Me at 25 °C. The relation deviates from linearity at higher salt concentrations.

active ion. The dissolution temperatures of 0.7–1.0 wt % of $C_{12}H_{25}OCH_2CH_2SO_4$ $(1/z)$Me in the presence of various multivalent cations, i.e., the Krafft points in the presence of salts, are summarized in Table III. It is evident from Table III that two or three oxyethylene chains are necessary to depress the Krafft point below room temperature in aqueous solutions of $C_{12}H_{25}(OCH_2CH_2)_nSO_4$ $(1/z)$Me in the presence of Ba^{2+}, La^{3+}, or Al^{3+}.

The cmc values are depressed by (1) introducing ethyleneoxide groups between the hydrocarbon chain and ionic group[17-19] and (2) changing the gegenions from univalent to bivalent cations.[20] For example, the cmc of $C_{12}H_{25}OCH_2CH_2SO_4$ 0.5Ca was 0.00092 equiv/L. This value is about $^1/_9$th of the cmc of $C_{12}H_{25}SO_4Na$, i.e., the former is about 9 times more surface active than the latter. The cmc depression is explained as follows. Water will hydrate the oxyethylene group as well as the polar ionic group of the micelle-forming ions, and therefore gegenions will distribute not only outside of the ionic head groups of micelles, but in the hydrated oxyethylene core in the micelle, and this results in a decreased electrical potential at the micelle surface.

The cmc of ordinary ionic surfactants is given by the equation[21]

$$\ln \text{cmc} = -\frac{m\omega}{kT} + \frac{Kq}{Z_i}\left(\ln \frac{2000\pi\sigma^2}{DNkT} - \ln C_g\right) + \text{constant} \tag{1}$$

where m is the number of carbon atoms in the hydrocarbon chain, ω the cohesive energy change in transferring one methylene group from a hydrocarbon environment to an aqueous medium, Kg/Z_i the slope of the cmc as a function of the concentration of the gegenions, Z_i the number of charges of the gegenions, D the dielectric constant of the solution, σ the charge density on the micelle surface, and C_g the total concentration of gegenions in equivalents per liter.

Electrical energy per surfactant ion in micelle formation, the second term in eq 1

$$\frac{E_{el}}{kT} = \frac{K_g}{Z_i}\left(\ln \frac{2000\pi\sigma^2}{DNkT} - \ln C_g\right) \tag{2}$$

is reduced roughly to one-half, due to the change from univalent to bivalent gegenions. This factor explains the difference in the cmc values of sodium and calcium salts.

The effect of added salts on the cmc of $C_{12}H_{25}OCH_2CH_2SO_4$ $(1/z)$Me has been studied and is shown in Figure 3.
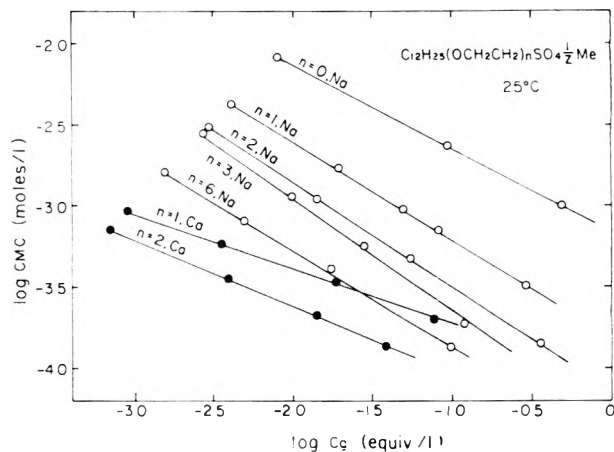

Figure 4. The effect of oxyethylene chain length on the cmc of $C_{12}H_{25}(OCH_2CH_2)_nSO_4Na$ and $C_{12}H_{25}(OCH_2CH_2)_nSO_4$ 0.5Ca as a function of $NaNO_3$ and $Ca(NO_3)_2$ concentrations, respectively, at 25 °C.

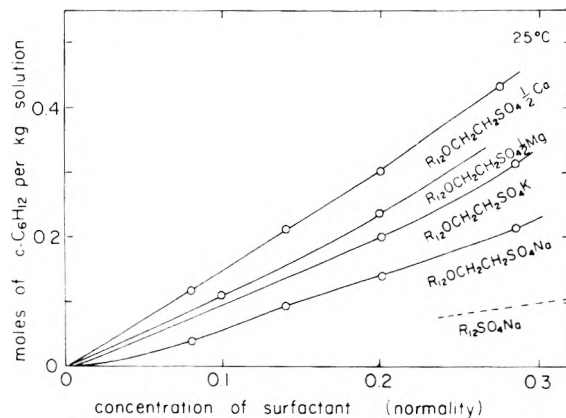**Figure 5.** The effect of the types of gegenions on the solubilizing power of $C_{12}H_{25}OCH_2CH_2SO_4$ $(1/z)$Me toward cyclohexane at 25 °C.

The logarithm of the cmc vs. the logarithm of the equivalent concentration of gegenions linearly changes as usual. The slope of $C_{12}H_{25}OCH_2CH_2SO_4Na$ was 0.59 and that of $C_{12}H_{25}OCH_2CH_2SO_4$ 0.5Ca was 0.35. The slope for the calcium salts is roughly one-half of that for the sodium salts. This fact is again explained by eq 2, because K_g values for Na and Ca, 0.59 and 0.70, do not change much, but $z = 1$ for Na^+ and $z = 2$ for Ca^{2+}.

The effect of oxyethylene chain length on the cmc of $C_{12}H_{25}(OCH_2CH_2)_nSO_4Na$ or 0.5Ca type of surfactant as functions of salt concentrations has been studied and plotted in Figure 4.

The cmc decreases with increasing oxyethylene chain length. Water will hydrate the oxyethylene chain of this type of ionic surfactants and gegenions will also distribute around the hydrophilic core of the micelle so that the electrical potential of the ionic heads seems significantly depressed with increasing oxyethylene chains.

Effect of the Types of Gegenions on the Solubilizing Power. The solubilization of cyclohexane in aqueous surfactant solution is determined and shown in Figure 5. Solubilizing powers of $C_{12}H_{25}OCH_2CH_2SO_4$ 0.5Ca, 0.5Mg, K, and Na were 4.7, 3.8, 3.3, and 2.3 times larger than that of $C_{12}H_{25}SO_4Na$. In the case of nonionic surfactants, the hydrophile–lypophile balance of nonionics gradually changes with their oxyethylene chain length. It has been considered in the case of ionic surfactants that the balance is fixed or changes but little with the type of gegenions. In the present study, however, it seems clear that the hyrophile–lypophile balance of this type of surfactants changes appreciably, along with the aggregation number

TABLE IV: Surface Tension above the Cmc in Aqueous Solutions of $C_{12}H_{25}OCH_2CH_2SO_4(1/2)Me$ at 25 °C

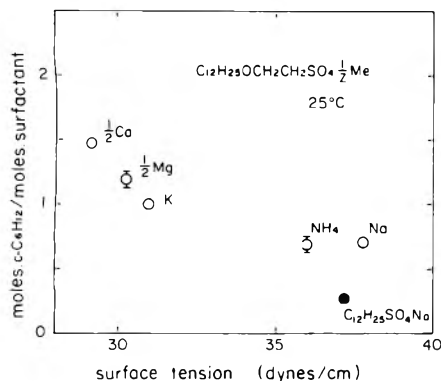| Surfactants	Surface tension, dyn/cm
$C_{12}H_{25}OCH_2CH_2SO_4Na$	37.8
$C_{12}H_{25}OCH_2CH_2SO_4NH_4$	36.0
$C_{12}H_{25}OCH_2CH_2SO_4K$	31.0
$C_{12}H_{25}OCH_2CH_2SO_40.5Mg$	30.3
$C_{12}H_{25}OCH_2CH_2SO_40.5Mn$	29.6
$C_{12}H_{25}OCH_2CH_2SO_40.5Ca$	29.2
$C_{12}H_{25}SO_4Na$	37.2

Figure 6. The correlation among the types of gegenions, the solubilizing power toward cyclohexane, and surface tension in aqueous solutions above the respective cmcs of $C_{12}H_{25}OCH_2CH_2SO_4$ (1/z)Me at 25 °C.

of the micelle and the solubilizing power depending on the types of gegenions present.

Surface tension. The surface tension above the cmc of the respective surfactants stay almost constant. These values change with the types of gegenions and are summarized in Table IV.

The relation between the solubilization of cyclohexane per mole of micellar surfactant and the lowest surface tension for a series of $C_{12}H_{25}OCH_2CH_2SO_4$ (1/z)Me are plotted in Figure 6. It is evident that the lower the surface tension, the larger the solubilizing power of this type of surfactant. The solubilization seems larger when the hydrophile and lyophile properties of the surfactants are well balanced.

References and Notes

(1) F. Krafft and H. Wiglow, *Berichte*, **28**, 2566 (1895).
(2) K. Shinoda in "Colloidal Surfactants", Academic Press, New York, N.Y., 1963, Chapter 1, pp 7–8.
(3) M. Hatō and K. Shinoda, *Bull. Chem. Soc. Jpn.*, **46**, 3889 (1973).
(4) H. Lange, *Kolloid-Z.*, **121**, 66 (1951).
(5) S. Miyamoto, *Bull. Chem. Soc. Jpn.*, **33**, 371 (1960).
(6) I. Satake, I. Iwamatsu, S. Hosokawa, and R. Matuura, *Bull. Chem. Soc. Jpn.*, **36**, 205 (1963).
(7) H. Lange and M. J. Schwuger, *Kolloid Z. Z. Polym.*, **233**, 145 (1968).
(8) K. Shinoda, M. Hato, and T. Hayashi, *J. Phys. Chem.*, **76**, 909 (1972).
(9) H. Kunieda and K. Shinoda, *J. Phys. Chem.*, **80**, 2468 (1976).
(10) R. S. Stearns, H. Oppenheimer, E. Simon, and W. D. Harkins, *J. Chem. Phys.*, **15**, 496 (1947).
(11) "Anionic Surfactants", W. M. Linfield, Ed., Marcel Dekker, New York, N.Y., 1976.
(12) K. Granath, *Acta Chem. Scand.*, **4**, 103 (1950).
(13) D. Stigter and K. J. Mysels, *J. Phys. Chem.*, **59**, 45 (1955).
(14) E. W. Anacker, *J. Phys. Chem.*, **62**, 41 (1958).
(15) K. J. Mysels and L. H. Princen, *J. Phys. Chem.*, **63**, 1696 (1959).
(16) Reference 2, pp 25–42.
(17) J. K. Weil, R. G. Bistline, and A. J. Stirton, *J. Phys. Chem.*, **62**, 1083 (1958).
(18) J. K. Weil, A. J. Stirton, R. G. Bistline, and E. W. Maurer, *J. Am. Oil Chem. Soc.*, **36**, 241 (1959).
(19) F. Tokiwa and K. Ohki, *J. Phys. Chem.*, **71**, 1343 (1967).
(20) M. Hatō and K. Shinoda, *J. Phys. Chem.*, **77**, 373 (1973).
(21) Reference 2, pp 41, 56.

Photocatalysis through Excitation of Adsorbates. 1. Highly Efficient *N*-Deethylation of Rhodamine B Adsorbed to CdS

Tadashi Watanabe,* Takuo Takizawa, and Kenichi Honda

Department of Synthetic Chemistry, Faculty of Engineering, The University of Tokyo, Hongo, Bunkyo-ku, Tokyo 113, Japan (Received January 5, 1977)

Although rhodamine B *(N,N,N',N'*-tetraethylrhodamine) aqueous solution is considerably stable to visible photoexcitation, the dye underwent a highly efficient photochemical *N*-deethylation accompanying acetaldehyde formation when powdered CdS was suspended in the aerated dye solution. This photochemical reaction took place mainly by the light absorption of adsorbed dye molecules and to a lesser extent by the excitation of CdS, but practically did not occur by the light absorption of dissolved dye molecules. A lowest estimate of the quantum efficiency for this *N*-deethylation gave the value of 0.46 by the excitation of the adsorbed dye. This value is incomparably much larger than the reported value of the quantum efficiency (ca. 10^{-7}) for the same photochemical reaction in pure aqueous solution. Taking into account the well-documented fact that most of the oxidative *N*-dealkylations are preceded by radical cation formation, and considering the low intersystem crossing probability (ca. 0.04) of the dye, the observed photochemical reaction is supposed to arise from the electron transfer from the adsorbed dye in its singlet excited state to the conduction band of CdS.

Introduction

Although a final distinction between electron and energy transfer mechanisms has not been made in the discussion of the spectral sensitization in photographic science,[1] most of the recent publications postulate the former mechanism on the basis of photographic[2] and electrochemical[3-5] measurements. However, the discussion is usually based

on rather indirect evidence such as the correlation between the redox potentials of dyes and the emulsion photographic density after development, the direction of sensitized photocurrent, or the effects of coexisting substances.

Studies on the behavior of sensitizing dyes after excitation on semiconductor surfaces are expected to provide more information on the sensitization process. These could

be carried out in two different approaches: photophysical and photochemical. The former includes the change in fluorescence lifetime and quantum yield, while the latter is concerned with the radical cation formation and/or subsequent chemical reaction of the dye molecule. Quite recently, these problems have drawn the attention of a number of workers. Muenter[6] verified the decrease in the fluorescence lifetime as well as the quantum yield of two cyanine dyes as they went from a gelatin environment to the surface of silver halides. Through the estimations of the sensitization rate constant (10^9–10^{10} s^{-1}) and the sensitization quantum yield (0.72–0.93), she concluded that spectral sensitization occurred by direct electron transfer from the singlet excited state of the dye to the silver halides. Ehrlich[7] observed the transient bleaching of a number of sensitizing dyes upon flash irradiation of the dyed emulsion layer. Based on the correlation between the conversion efficiency and the dyes' redox potentials, he also proposed an electron transfer scheme. Tani[8] detected ESR signals on irradiation of dyed emulsion systems and ascribed the signals to the dye radical cations generated by electron transfer to the substrate.

In the present investigation we directed our attention to the photochemical behavior of dyes adsorbed to semiconductor surfaces, with the hope that we could enrich our knowledge of the aspects concerning the sensitization process. If an electron transfer does take place from the excited adsorbed dye to the semiconductor substrate, the dye should, at least momentarily, be converted to a radical cation by this process. Unfortunately, little is known about such photooxidation reactions of dye molecules, compared with the photoreduction processes[9,10] on which many works have been carried out.

In this respect, we note that one of the typical reactions which can be initiated by the one-electron extraction from a molecule is the N-dealkylation of tertiary or secondary amines and nitrogen-containing heterocycles. Such N-dealkylations have been reported on sensitized photooxidation,[11–15] electrooxidation,[16,17] and chemical oxidation,[18,19] and in all cases a one-electron oxidation has been assumed as the initiation step.

Based on these considerations, we expected the occurrence of N-deethylation of rhodamine B, which is one of the typical dyes frequently employed in the spectral sensitization of a number of semiconductors, upon photoexcitation in the adsorbed state. An aqueous solution of rhodamine B is reported to be fairly stable to visible irradiation.[20,21] Cyanine dyes, which also possess N-alkylated heterocycles and are most extensively utilized in silver halide photography,[22] were not employed in the present study since their photooxidation is reported to result in a rather drastic decomposition of chromophores[23] and hence the reaction pathways seem difficult to follow. As the semiconductor substrate we used cadmium sulfide, as an extention of our investigations of electrochemical spectral sensitization on this material.[4] In order to obtain a high yield of the possible reaction product of the dye, dye solutions suspended with powdered CdS were illuminated with visible light. The experimental results are consistent with the electron transfer mechanism from the excited singlet state of adsorbed rhodamine B to the conduction band of CdS.

Experimental Section

Materials. Reagent grade rhodamine B (N,N,N',N'-tetraethylrhodamine) was supplied from Nakarai Chemicals Ltd., and was purified chromatographically. Rhodamine (completely N-deethylated) was synthesized by condensation of m-aminophenol with phthalic anhy-

dride in concentrated sulfuric acid at 190 °C and was subsequently purified according to the method reported by Ioffe and Otten.[24] N,N,N'-Triethylrhodamine (TER), N,N'-diethylrhodamine (DER), and N-ethylrhodamine (MER) were obtained from Kanto Chemical Ltd. and were purified chromatographically. Cadmium sulfide (95% pure) was supplied from Wako Pure Chemical Ltd. The powder, whose BET surface area was ca. 17.0 m^2/g, was used without any pretreatment. Distilled water was used as the solvent. The pH of the solvent was around 6.0, and was not controlled with any buffer solutions in order to avoid possible participation of buffering substances in the photochemical reaction process.

Illumination. A 500-W or a 1-kW xenon arc lamp (Ushio Electric) was used as the light source. The wavelength range of the illuminating light was selected by means of appropriate colored glass filters (Toshiba Kasei) and/or interference filters (Koshin Kogaku) with an average peak transmittance of 40% and a half-band width of 10 nm. Rhodamine B aqueous solution (usually 50 mL) with or without a known amount of CdS powder was put in a Pyrex cell having a flat window 23 mm in diameter, and assembled on a stirring machine. The cell was equipped with a gas inlet and outlet. The solution was, if necessary, deoxygenated by bubbling high purity nitrogen gas passed in advance through an activated copper column. Most of the experiments were carried out under aerated condition. After illumination, the CdS powder was separated off by centrifuging and the supernatant solution was analyzed. In some cases the composition of the adsorbed species was also analyzed after extraction with methanol.

Prior to monochromatic illumination experiments, the number of photons incident to the cell was determined for each interference filter, covering the wavelength range from 350 to 700 nm with intervals of 10 nm, by means of ferrioxalate actinometry at 390 nm[25] together with radiation energy measurements with a JASCO thermopile radiometer Model RMA-8.

Analyses. The synthesized and/or purified dyes as well as the photoproducts were analyzed by ultraviolet and visible spectroscopy (Shimadzu, Model MPS-5000), infrared spectroscopy (Shimadzu, Model IR-400), mass spectroscopy (Hitachi, Model RMU-7), and high performance liquid chromatography (JASCO, Model FLC-A700, with a spectrophotometer Model UVIDEC-1 as the detector, column HP-01-500 mm). Acetaldehyde was analyzed by the 2,4-dinitrophenylhydrazine method.[26] Hydrogen peroxide was detected by iodometry.

Results

Effect of CdS on the Photoreactivity of Rhodamine B. Rhodamine B aqueous solution is considerably stable to visible photoexcitation in the wavelength range covering its main absorption band (λ_{max} 555 nm). Curve b in Figure 1 shows the absorption spectrum of the homogeneous solution submitted to illumination with visible light from a xenon lamp for 10 h, and exhibits almost no difference from the original absorption (curve a). Curve c in Figure 1 shows the absorption spectrum recorded after 1 h of illumination of rhodamine B solution (2×10^{-5} M, 50 mL) containing 0.1 g of CdS powder suspended. Only the wavelength range longer than 550 nm was used in order to avoid the strong light absorption by CdS (λ <540 nm). By this illumination the absorption maximum of the solution shifted from 555 to 498 nm, and further illumination caused a much slower change (decrease in the absorbance at 498 nm), due presumably to some irreversible oxidation of the final product by the action of holes or positively
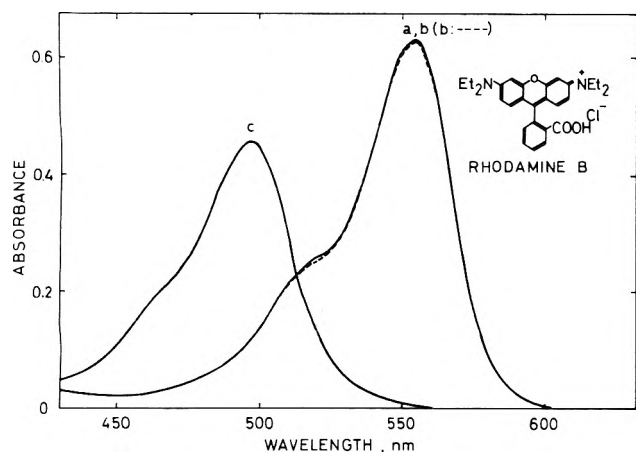
Figure 1. Change in the absorption spectrum on illumination of a rhodamine B aqueous solution. Initial solution (I) contained 50 mL of 2×10^{-5} M rhodamine B suspended with 0.1 g of CdS powder: (a) supernatant solution of I; (b) after illumination ($\lambda > 550$ nm) of (a) for 10 h; (c) after illumination ($\lambda > 550$ nm) of I for 1 h.
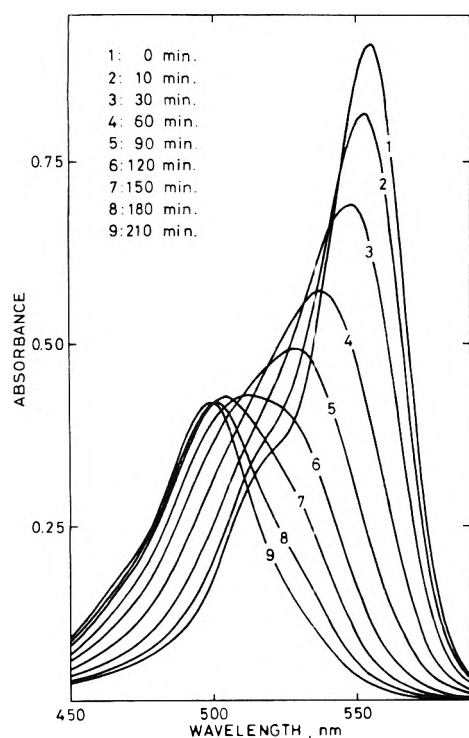

Figure 2. Change in the absorption spectrum of CdS-suspended rhodamine B aqueous solution with time of illumination: initial dye concentration, 2×10^{-4} M; CdS suspended, 0.1 g/50 mL; illumination, $\lambda > 540$ nm.

charged surface states generated by a minor light absorption by CdS. In general, the rate of disappearance of the 498-nm absorbing species was negligibly small compared with that of the spectral shift from 555 to 498 nm. In the course of illumination, the absorption maximum of the solution exhibited a gradual hypsochromic shift as shown in Figure 2. From Figure 2 the existence of a number of intermediates is suggested.

Products. The final photoproduct, which has an absorption maximum at 498 nm in aqueous solution, was presumed to be the completely *N*-deethylated compound (rhodamine), by an analogy to the spectral change among a series of thiazine dyes from methylene blue to thionine.[27] The final product was recrystallized and analyzed by the methods described above. The ultraviolet–visible (Figure 3) and infrared spectra nearly coincided with those of the authentic sample synthesized. The mass spectrum of the
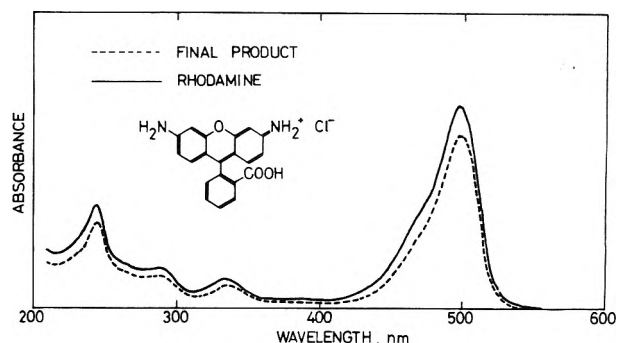

Figure 3. Ultraviolet-visible absorption spectra of the final photoproduct and of rhodamine.
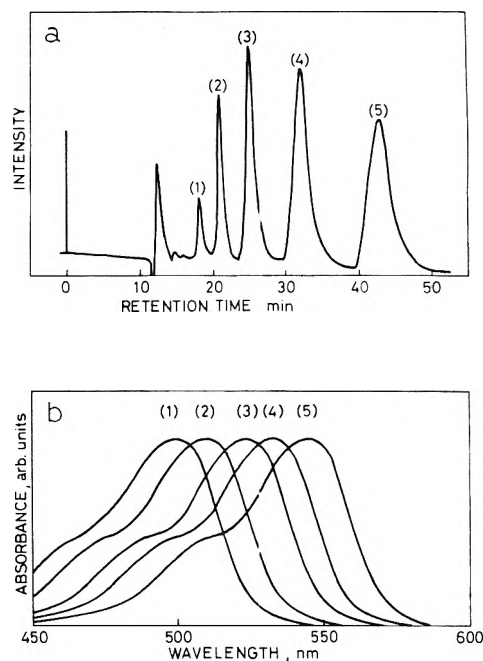

Figure 4. (a) Liquid chromatogram of an incompletely photoreacted rhodamine B aqueous solution: initial dye concentration, 2.6×10^{-3} M; CdS suspended, 1 g/40 mL; illumination, $\lambda > 540$ nm, 8 h; eluent, methanol, 0.5 mL/min; wavelength of detection, 510 nm. (b) Absorption spectra in methanol of the components appearing in the liquid chromatogram.

final product gave m/e 331 $[M]^+$, 315 $[M - NH_2]^+$, 286 $[M - COOH]^+$, 270 $[M - COOHNH_2]^+$, where rhodamine is expressed as M^+-Cl^-. Cochromatography on the liquid chromatograph also supported the coincidence of the final product with rhodamine. The yield of rhodamine from rhodamine B was estimated to be nearly 100%, by a calculation on the absorption spectra using the absorption coefficients of these two compounds.

An incompletely photoreacted solution was analyzed on the liquid chromatograph and the result is illustrated in Figure 4a. As is seen five components appeared altogether. The peaks (5), (4), (3), (2), and (1) were identified with rhodamine B, TER, DER, MER, and rhodamine, respectively, through cochromatography with the authentic samples. The absorption spectra (Figure 4b) of the corresponding peaks also coincided with those of the authentic samples. Spectroscopic properties of these five compounds are given in Table I.

Formal Quantum Efficiency. Figure 5 shows the liquid chromatograms of supernatant solutions in the early stage of photoreaction, in cases of monochromatic illumination at the wavelengths indicated on the curves. In most cases the compositions of the supernatant solution and of the adsorbed layer, checked through extraction with methanol, fairly coincided within experimental error. It is seen that

TABLE I: Spectroscopic Data for the Dyes

Dye	λ_{max}, nm		$\epsilon_{max}, \times 10^{-4}\, a$
	In MeOH	In water	L mol^{-1} cm^{-1}
Rhodamine B	547	555	11.5
N, N, N'-Triethyl-rhodamine (TER)	539	539	5.5
N, N'-Diethyl-rhodamine (DER)	525	522	7.2
N-Ethyl-rhodamine (MER)	516	510	6.1
Rhodamine	503	498	8.4

^{a} In dilute (10^{-6}–10^{-5} M) methanolic solution at 20 °C.
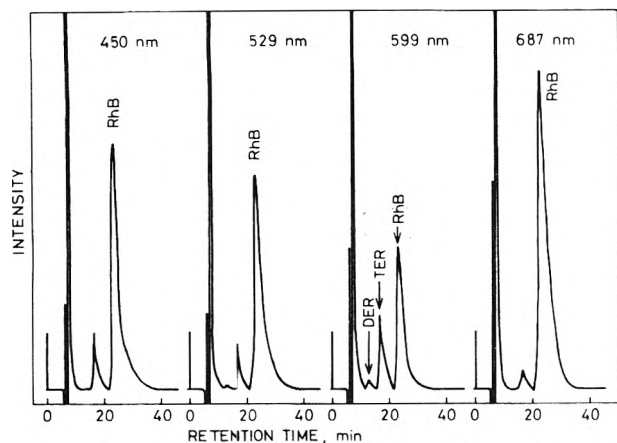
Figure 5. Liquid chromatograms of a rhodamine B solution submitted to monochromatic illumination at the wavelength indicated on each chromatogram. RhB, TER, and DER denote rhodamine B, triethyl-rhodamine, and diethylrhodamine, respectively: initial dye concentration, 10^{-4} M; CdS suspended, 1 g/50 mL; illumination, 10 min; eluent, methanol, 1 mL/min; wavelength of detection, 510 nm.
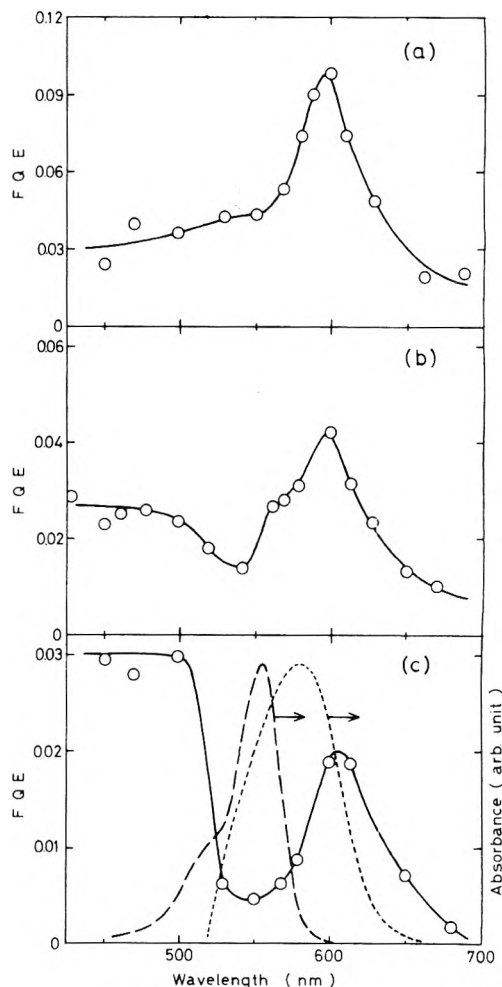

Figure 6. Spectra of the formal quantum efficiency (FQE) for the photochemical N-deethylation of rhodamine B (a–c) and absorption spectra of rhodamine B adsorbed on CdS (----) and in aqueous solution (- - -): (a) initial dye concentration, 10^{-4} M; CdS 1 g/50 mL; (b) initial dye concentration, 10^{-4} M; CdS 0.5 g/50 mL; (c) initial dye concentration: 10^{-3} M; CdS 1 g/50 mL.

the product is mainly TER, with a minor amount of DER. It was possible to obtain only TER as the detectable photoproduct by selecting the appropriate wavelength and period of illumination. This result might indicate that the present N-deethylation is a stepwise photochemical process necessitating the consecutive excitation of the initial and intermediate species. On the basis of the results shown in Figure 5, and by using the spectroscopic data of the compounds involved (Table I), it is possible to determine the efficiency of the N-deethylation as a function of the wavelength of the incident light with a known number of photons. Figure 6a–c shows the action spectra thus calculated under different experimental conditions. The ordinate denotes the formal quantum efficiency (FQE) defined as the number of eliminated ethyl groups per one incident photon. Naturally FQE constitutes the lowest estimate of the true quantum efficiency. The absorption spectrum of rhodamine B aqueous solution and that of the dye adsorbed to CdS, determined by reflection measurements on the dyed CdS powder, are also illustrated in the figure. The difference in the absorption maxima between these two states may be due to the different dielectric constants around the dye molecule.

The experimental conditions for the results shown in Figures 6a–c are different mainly in the molar dye/CdS ratio within the reaction cell. A change in dye/CdS ratio might lead to a difference in the following three factors: the amount of adsorbed dye on CdS, the filtering effect by the dissolved dye, and the light scattering by CdS powder.

It is seen in Figure 6 that the present photochemical N-deethylation of rhodamine B proceeds either by the

excitation of CdS (λ <540 nm) or by the light absorption of dye molecules adsorbed to CdS (λ ~600 nm). In the former wavelength region, the value of FQE remains nearly constant (0.03–0.04) irrespective of the different dye/CdS ratio. Since the filtering effect by the dissolved dye is not very prominent in this wavelength region, the FQE value obtained here can approximately be regarded as the true quantum efficiency.

The three factors mentioned above would highly affect the FQE value in the wavelength region around 600 nm. For example, the initial dye concentrations are the same (10^{-4} M) but the quantities of suspended CdS are different (1.0 and 0.5 g/50 mL) for Figures 6a and 6b. At this dye concentration, the filtering effect by the dissolved dye was negligible over the wavelength region longer than 610 nm. The quantity of rhodamine B molecules adsorbed to CdS in the cell amounted to 3.8 × 10^{-6} and 2.5 × 10^{-6} mol, respectively, for the Figures 6a and 6b. Thus an increase in the amount of adsorbed dye is accompanied by an increase in the FQE value. The remarkable decrease in the FQE value in Figure 6c compared with Figure 6a is supposed to arise mainly from the strong filtering effect of the homogeneous phase.

Light scattering by suspended CdS is considered to act in lowering the measured FQE values around 600 nm in every case, provided that the true quantum efficiency has a constant value in this wavelength region. We attempted to reduce the scattering effect (promote the reabsorption

TABLE II: Dependence of FQE on the Quantity of CdS in the Cell[a]

CdS quantity, g/50 mL	FQE[b]
2.00	0.13
4.00	0.13
6.00	0.24
8.00	0.27
10.00	0.46

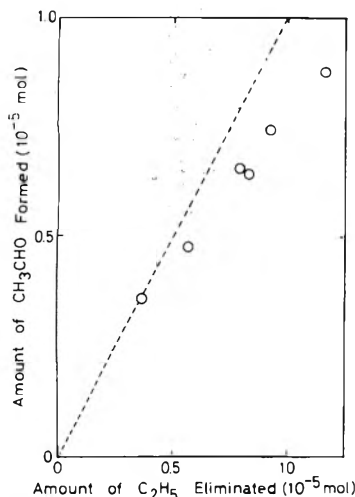[a] The initial concentration of rhodamine B was 4.4×10^{-4} M. Illumination at λ 600 nm for 20 min. [b] $\pm 10\%$.

Figure 7. Relationship between the amount of acetaldehyde produced and that of the ethyl groups eliminated in the course of the photoreaction: initial dye concentration, 5×10^{-4} M; CdS suspended, 2 g/50 mL; illumination, 620 nm, 20 min–3 h.

of the scattered light) by wrapping the reaction cell, except for the window, with aluminum foil. Table II shows the results of FQE measurements at 600 nm under such condition with different amounts of CdS powder added to the cell. With an increase in the amount of CdS from 2.00 to 10.00 g/50 mL, the fraction of the adsorbed dye over the total amount of the dye in the cell increased from 77 to 99%. The highest value of FQE thus obtained, 0.46, is still the lowest estimate of the true quantum efficiency. An attempt to determine the true quantum efficiency is now under way.

Based on the results shown in Figure 6 and Table II, one can conclude that the light absorption by adsorbed dye is much more effective than the excitation of CdS, for the present photochemical N-deethylation. This point will be discussed later.

Supplementary Results Concerning the Photoreaction. On addition of 2,4-dinitrophenylhydrazine into the CdS-suspended rhodamine B aqueous solution submitted to a prolonged illumination, a yellow-orange solid precipitated. This was identified as acetaldehyde 2,4-dinitrophenylhydrazone through cochromatography with an authentic sample. Figure 7 shows the relationship between the amount of acetaldehyde produced and that of the ethyl groups eliminated. It is seen that about one acetaldehyde molecule is formed per one N-deethylation. A slight deviation from the theoretical line at higher conversions, i.e., at longer illumination periods, might suggest the consumption of the acetaldehyde produced in some unknown process occurring on the illuminated CdS surface.

Hydrogen peroxide was detected by iodometry, and the quantum efficiency for H_2O_2 production was ca. 0.25 by the intrinsic excitation of CdS. However, details of the stoichiometry and quantum efficiency of H_2O_2 formation need further investigation, since both the production and decomposition of H_2O_2 seem to proceed on the illuminated

CdS surface.[28] The hydrogen peroxide thus produced is not responsible for radical cation formation (and subsequent N-deethylation) of the dye, as will be shown below.

When the CdS-suspended dye solution was completely deoxygenated, the photochemical reaction did not proceed at all. A CdS-suspended dye solution kept in darkness at 90 °C for more than 3 h did not undergo any spectral change. Visible illumination (λ >550 nm) to CdS-free homogeneous aqueous solutions dissolved with Cd^{2+} (1.0 M), S^{2-} (1.0 M), Fe^{2+} (1.0 M), $Fe(CN)_6^{3-}$ (1.0 M), I^- (1.0 M), hydrogen peroxide (1.0 M), or hydroquinone (0.01 M) did not bring about any noticeable change in rhodamine B, even in cases where the solution was saturated with oxygen at 1 atm (ca. 10^{-3} M).

In order to check the effect of nonsemiconducting solid materials on the photoreactivity of rhodamine B, a silica–alumina powder (Al_2O_3 13%) was employed. The powder, whose BET surface area was 540 m^2/g, had been prepared by heat treatment at 550 °C for 7 h in air. When 0.5 g of the powder was added to 25 mL of 10^{-3} M rhodamine B aqueous solution, about 98% (2.45×10^{-5} mol) of the dye was adsorbed to the powder. Subsequent illumination (2 h, λ >570 nm) of the suspension, however, did not cause any photoreaction of rhodamine B.

Discussion

The experimental results obtained in the present study can be summarized as follows.

(1) Rhodamine B undergoes an efficient photochemical N-deethylation accompanying acetaldehyde formation in the adsorbed state on CdS, while the homogeneous solution of the dye is practically nonphotoreactive.

(2) The quantum efficiency for this N-deethylation is higher than 0.46 by the excitation of the adsorbed dye, and is around 0.03–0.04 by the excitation of CdS.

(3) This reaction requires the presence of oxygen.

As regards to point (1), the stability of rhodamine B aqueous solution to visible photoexcitation has been reported by several authors. For example, the photoreduction of rhodamine B,[10] whose reaction pathways have been fairly understood, proceeds only through ultraviolet (λ <350 nm) irradiation. Evans[20,21,29] investigated the irreversible photofading of rhodamine B aqueous solution, though its mechanism remains unclarified even in his latest publication.[29] He obtained values of the order of 10^{-6} for the quantum efficiency of total photofading upon visible illumination. He also noticed the N-deethylation as a minor pathway in the course of photofading. According to his data,[20] the yield of N-deethylated products (TER and DER) was about 10% of the total photofaded products. It follows that the quantum efficiency for the photochemical N-deethylation of rhodamine B aqueous solution is of the order of 10^{-7}. This very small value explains the quasi-constancy of the absorption spectrum of the homogeneous solution during visible illumination (curve b in Figure 1). In view of the well-documented fact that most of the oxidative N-dealkylations are preceded by radical cation formation,[11-19] it is suggested that an electron exchange at the illuminated semiconductor–dye interface plays an important role in the present N-deethylation. Since the presence of silica–alumina powder (an efficient adsorbent) did not cause any photoreaction, adsorption (or rigidization) on a solid surface alone seems ineffective in the photoreactivity of rhodamine B.

According to the literature, the intersystem crossing probability of rhodamine B is very small (ca. 0.04 in water[30] and below 0.01 in ethanol[31]), though the data are for the homogeneous solution. Unless an unusual (more than tenfold) increase in the intersystem crossing probability

takes place upon adsorption to CdS, point (2) would indicate that the present N-deethylation by the excitation of adsorbed dye occurs via the singlet excited state of the dye.

The relatively low quantum efficiency mentioned in point (2) for the N-deethylation by the excitation of CdS is elucidated by the following considerations, assuming that the N-deethylation is initiated by extraction of an electron from the dye molecule. Excitation of CdS generates electron–hole pairs near the surface. It has been verified through electrochemical measurements[32] that photogenerated holes react effectively with CdS itself to cause dissolution according to

$$CdS + 2h_{val}^+ \rightarrow Cd^{2+} + S$$
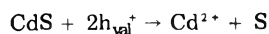
where h_{val}^+ denotes a hole in the valence band. In an electrochemical system, the photoelectron is withdrawn from the electrode–solution interface toward the external circuit. When a reducing agent is added to the electrolyte solution, a competitive oxidation between CdS and the reducing agent occurs by the action of holes. The fraction of the photoholes oxidizing the reducing agent is controlled mainly by the redox potential and the concentration of the latter.[32] We assume that a similar process is occurring on the illuminated surface of CdS powder suspended in the dye solution. Since in this case a local cell should be established at the CdS surface, the anodic process (oxidation of CdS and/or adsorbed dye by photoholes) must be compensated by the cathodic process (presumably the H_2O_2 formation through reduction of O_2 by photoelectrons). Since the quantum efficiency for H_2O_2 production was ca. 0.25, it follows that only a part of the photoholes can extract an electron from the adsorbed rhodamine B molecule.

Based on the above discussion, one can distinguish between energy and electron transfer mechanisms for the present N-deethylation by the excitation of adsorbed rhodamine B molecules. If one postulates an energy transfer from the adsorbed dye to CdS as the major cause for the radical cation formation (and the subsequent N-deethylation) of rhodamine B, the process must consist of the energy transfer

$$D_{ads}^* + CdS \rightarrow D_{ads} + A^+ + e_{cond}^-$$

and the subsequent one-electron abstraction from the adsorbed dye

$$D_{ads} + A^+ \rightarrow D_{ads}^+ + A$$

where D_{ads} denotes an adsorbed dye molecule, A a hypothetical energy acceptor state present within the forbidden gap of CdS, e_{cond}^- an electron in the conduction band, and the asterisk represents the excited state. Since the ionized acceptor, A^+, should naturally possess less oxidation ability than a hole in the valence band (the latter being situated at a more anodic potential than the former), the quantum efficiency for radical cation formation by the excitation of adsorbed dye should never exceed that by the excitation of CdS. Evidently this is not the case as is seen in Figure 6.

On the contrary, the electron transfer mechanism requires, in the first approximation, only a satisfactory energy level correlation between the conduction band edge of CdS and the electron-donating energy term of the excited dye. In fact, according to the calculation by Gerischer and Willig,[5] the latter energy term in polar solvents is situated 0.1–0.2 eV above the conduction band edge of CdS. Based on these considerations, we suppose that an electron transfer from the adsorbed dye in its
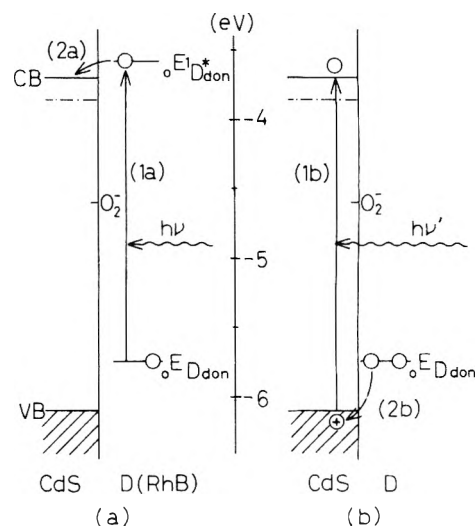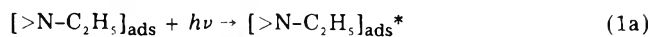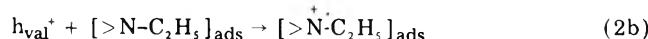
Figure 8. Schematic diagram of the initiation steps for the photochemical N-deethylation of rhodamine B on CdS by (a) excitation of adsorbed dye and by (b) excitation of CdS. $_0E_{1_{Ddon}}^*$ and $_0E_{D_{don}}$ denote the electron transfer energy terms of the excited singlet state and of the ground state, respectively, of rhodamine B in polar solvents, calculated by Gerischer and Willig.[5] The perpendicular scale is the electronic energy vs. vacuum.

singlet excited state to the conduction band of CdS is the principal pathway as the initiation step of the observed photochemical N-deethylation of rhodamine B. If we symbolize for simplicity an adsorbed rhodamine B molecule as $[>N-C_2H_5]_{ads}$, the above discussion leads to the following scheme for the initial stage of the present photoreaction. By the excitation of adsorbed rhodamine B

$$[>N-C_2H_5]_{ads} + h\nu \rightarrow [>N-C_2H_5]_{ads}^* \tag{1a}$$

$$[>N-C_2H_5]_{ads}^* \rightarrow [>\overset{++}{N}-C_2H_5]_{ads} + e_{cond}^- \tag{2a}$$

and by light absorption of CdS

$$CdS + h\nu' \rightarrow h_{val}^+ + e_{cond}^- \tag{1b}$$

$$h_{val}^+ + [>N-C_2H_5]_{ads} \rightarrow [>\overset{+\cdot}{N}-C_2H_5]_{ads} \tag{2b}$$

The sequence (1b)–(2b) is a process frequently encountered in photoelectrochemical[32] and photocatalytic[33] systems. On the other hand, any examples of photochemical reaction initiated by the process such as (1a)–(2a) have not been reported, and we call such a reaction photocatalysis through excitation of adsorbates. These processes are schematically illustrated in Figure 8. The absolute positions of energy levels in this figure are those calculated by Gerischer and Willig.[5] The conduction electron, e_{cond}^-, can be trapped by the surface oxygen to give a superoxide radical anion, according to

$$e_{cond}^- + O_{2ads} \rightarrow O_2^{-\cdot} \tag{3}$$

It has been reported that adsorption of oxygen to the CdS surface usually leads to the formation of a superoxide surface state, which has an energy level 0.91 eV below the conduction band edge, through trapping of conduction electrons.[34] At the present stage, the role of oxygen in the photochemical N-deethylation process remains ambiguous. One possibility is the direct participation of oxygen in the reaction pathway (N-deethylation resulting from the reaction between the dye radical cation and the superoxide radical anion). Another possibility is that oxygen acts simply for the establishment of band bending, which facilitates electron transfer, within the space charge region at the surface of CdS, by trapping conduction electrons.

Further investigations are now being undertaken for a better understanding of the overall reaction mechanism.

The rates of the processes (2a) and (2b) are expected to be highly influenced by the energy level correlations between the adsorbed dye and the semiconductor substrate. It follows that the efficiency of the heterogeneous N-dealkylation depends on the nature of dye–semiconductor combinations. Preliminary results are being obtained at present, and detailed discussion will be reported in future publications.

References and Notes

(1) W. West and B. H. Carroll in "The Theory of the Photographic Process", 3rd ed, C. E. K. Mees and T. H. James, ed., MacMillan, New York, N.Y., 1966, pp 233–277.
(2) T. Tani and S. Kikuchi, *Photogr. Sci. Eng.*, **12**, 80 (1968); R. W. Berriman and P. B. Gilman, Jr., *ibid.*, **17**, 235 (1973); I. H. Leubner, *ibid.*, **20**, 61 (1976); R. O. Loutfy and J. H. Sharp, *ibid.*, **20**, 165 (1976).
(3) H. Gerischer and H. Tributsch, *Ber. Bunsenges. Phys. Chem.*, **72**, 437 (1968); K. Hauffe, H. J. Danzmann, H. Pusch, J. Range, and H. Volz, *J. Electrochem. Soc.*, **117**, 993 (1970); R. Memming, *Photochem. Photobiol.*, **16**, 325 (1972).
(4) A. Fujishima, T. Watanabe, O. Tatsuoki, and K. Honda, *Chem. Lett.*, 13 (1975); T. Watanabe, A. Fujishima, and K. Honda, *Ber. Bunsenges. Phys. Chem.*, **79**, 1213 (1975); T. Watanabe, A. Fujishima, O. Tatsuoki, and K. Honda, *Bull. Chem. Soc. Jpn.*, **49**, 8 (1976).
(5) H. Gerischer and F. Willig, *Top. Curr. Chem.*, **61**, 31 (1976).
(6) A. A. Muenter, *J. Phys. Chem.*, **80**, 2178 (1976).
(7) S. H. Ehrlich, *Photogr. Sci. Eng.*, **20**, 5 (1976).
(8) T. Tani, *Photogr. Sci. Eng.*, **19**, 356 (1975).
(9) M. Nemoto, H. Kokubun, and M. Koizumi, *Bull. Chem. Soc. Jpn.*, **42**, 2464 (1969); R. Bonneau and J. Pereyre, *Photochem. Photobiol.*, **21**, 173 (1975).
(10) B. Stevens, R. R. Sharpe, and W. S. W. Bingham, *Photochem. Photobiol.*, **6**, 83 (1967); U. Krüger and R. Memming, *Ber. Bunsenges. Phys. Chem.*, **78**, 679, 685 (1974).
(11) R. F. Bartholomew and R. S. Davidson, *J. Chem. Soc. C*, 2342, 2347 (1971); R. F. Bartholomew, D. R. G. Brimage, and R. S. Davidson,

ibid., 3482 (1971); R. F. Bartholomew, R. S. Davidson, and M. J. Howell, *ibid.*, 2804 (1971).
(12) F. Khuong-Huu and D. Herlem, *Tetrahedron Lett.*, 3649 (1970).
(13) D. Herlem, Y. Hubert-Brierre, F. Khuong-Huu, and R. Goutarel, *Tetrahedron*, **29**, 2195 (1973); D. Herlem, Y. Hubert-Brierre, and F. Khuong-Huu, *Tetrahedron Lett.*, 4173 (1973); F. Khuong-Huu, D. Herlem, and Y. Hubert-Brierre, *ibid.*, 359 (1975); Y. Hubert-Brierre, D. Herlem, and F. Khuong-Huu, *Tetrahedron*, **31**, 3049 (1975).
(14) F. C. Shaefer and W. D. Zimmermann, *J. Org. Chem.*, **35**, 2165 (1970).
(15) J.-Y. Gal and T. Yvernault, *Bull. Soc. Chim. Fr.*, 839 (1972).
(16) J. R. Lindsay Smith and D. Masheder, *J. Chem. Soc., Perkin Trans. 2*, 47 (1976).
(17) B. L. Laube, M. R. Asirvatham, and C. K. Mann, *J. Org. Chem.*, **42**, 670 (1977).
(18) C. A. Audeh and J. R. Lindsay Smith, *J. Chem. Soc. B*, 1280 (1970); *ibid.*, 1741, 1745 (1971); J. R. Lindsay Smith and J. A. V. Mead, *J. Chem. Soc., Perkin Trans. 2*, 206 (1973); J. R. Lindsay Smith, R. O. C. Norman, and A. G. Rowley, *J. Chem. Soc., Perkin Trans. 1*, 566 (1973); J. R. Lindsay Smith and J. S. Sadd, *J. Chem. Soc., Perkin Trans. 2*, 741 (1976).
(19) G. Galliani, B. Rindone, and C. Scolastico, *Tetrahedron Lett.*, 1285 (1975).
(20) N. A. Evans, *J. Soc. Dyers Colour.*, **86**, 174 (1970); **89**, 332 (1973).
(21) N. A. Evans, *Text. Res. J.*, **43**, 697 (1973).
(22) L. G. S. Brooker in ref 1, pp 198–232.
(23) G. W. Byers, S. Gross, and P. M. Henrichs, *Photochem. Photobiol.*, **23**, 37 (1976).
(24) I. S. Ioffe and V. F. Otten, *Zh. Obshch. Khim.*, **31**, 1511 (1961).
(25) C. G. Hatchard and C. A. Parker, *Proc. R. Soc. London, Ser. A*, **235**, 518 (1956).
(26) G. R. Lappin and L. C. Clark, *Anal. Chem.*, **23**, 541 (1951).
(27) N. Wotherspoon and G. Oster, *J. Am. Chem. Soc.*, **79**, 3992 (1957).
(28) For example, illumination (λ >560 nm, 4 h) to a CdS-suspended (2 g/50 mL) aqueous solution of H_2O_2 (2 × 10^{-3} M) leads to the complete disappearance of H_2O_2 in the cell. Cf. R. E. Stevens, B. Ke, and D. Trivich, *J. Phys. Chem.*, **59**, 966 (1955).
(29) N. A. Evans, *Text. Res. J.*, **46**, 144 (1976).
(30) F. Willig and M. E. Michel-Beyerle, *Photochem. Photobiol.*, **16**, 371 (1972).
(31) A. K. Chibisov, H. A. Kezle, L. V. Levshin, and T. D. Slavnova, *J. Chem. Soc., Chem. Commun.*, 1292 (1972).
(32) T. Inoue, T. Watanabe, A. Fujishima, K. Honda, and K. Kohayakawa, *J. Electrochem. Soc.*, **124**, 719 (1977).
(33) J. C. Kuriacose and M. C. Markham, *J. Phys. Chem.*, **65**, 2232 (1961); R. B. Cundall, R. Rudham, and M. S. Salim, *J. Chem. Soc., Faraday Trans. 1*, **72**, 1642 (1976).
(34) P. Mark, *J. Phys. Chem. Solids*, **26**, 959, 1767 (1965).

Adsorption of Alkylamines on Iron. Energetics of Adsorption by the Contact Angle Method

R. Sangiorgi,* A. Passerone, and V. Lorenzelli

Centro Studi di Chimica e Chimica Fisica Applicata alle Caratteristiche di Impiego dei Materiali, C.N.R. Fiera del Mare, Pad. D-16129, Genova, Italy (Received August 26, 1976; Revised Manuscript Received April 20, 1977)

Adsorption of primary n-alkylamines, and consequent formation of a hydrophobic layer on an iron surface were studied using the contact angle method. It appears that this phenomenon is due to adsorption of the neutral species. There exists a functional relationship between the mole fraction of free amine in solution, and the quantity of amine present in the monolayer on the metal surface. This relationship contains the free energy of adsorption explicitly. From the best fit between the curves of the contact angle and the degree of coverage as a function of pH, the free energy of adsorption of single amines can be estimated as a function of the chain length.

Introduction

Adsorption of amines on metal surfaces from aqueous solutions has received much attention in the literature, but comprehension of the process still calls for further investigations.

The first research by Zisman et al. dates back to 1946;[1] it demonstrated[2] that adsorption takes place on the metal through diffusion of polar molecules in the solution and neither through deposition of a floating monolayer of insoluble polar molecules (as under the hypothesis of Langmuir-Bloddget), nor through exposure to high concentration of soluble organic material at the water–air interface. This same research also showed the formation of a hydrophobic film on a surface of platinum by alky-
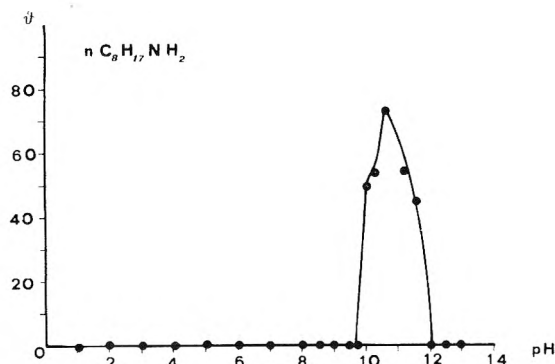
Figure 1. Contact angle vs. pH for n-octylamine (5×10^{-4} M).

Figure 2. Contact angle vs. pH for n-decylamine (5×10^{-4} M).

lamines, and this mechanism was attributed to competitive adsorption of RNH_2 and RNH_3^+ species present in the solution.[3]

Later, by measuring contact potential,[4] it was concluded that adsorption takes place in a monolayer with the positive pole toward the solution. Radiochemical methods were also used; it was demonstrated[5] that a monolayer may not be formed and that amine molecules are adsorbed either with the NH_2 group toward the metal or toward the solution. Nakagava[6] claimed that the amine is chemically adsorbed on the iron surface via the NH_2 group, pointed out a marked influence of the molecular area, and noted that the extent of chemical adsorption is independent of the length of the alkyl group; on the contrary Hackerman[7] claimed that the differences in molecular section area in a homologous series of amines are very small. Finally, by studying related problems, Murakava et al. claimed that, in the $Fe/HClO_4$ system, the RNH_3^+ ion can be adsorbed only at cathodic potentials; Aramaki and Fujii[9] concluded that adsorption is interrupted when the unshared pair of electrons on the nitrogen atom is blocked, for example, because they are involved in a hydrogen bond. Russian researchers,[10,13] who studied problems of inhibition, focused their attention on the effect of substituents in the chain, and demonstrated that the introduction of electron-donor groups, which increase the electron density on the nitrogen atom, decreases the minimum concentration necessary to protect the metal.

The purpose of the present work is to establish the conditions under which chemical adsorption takes place, and to evaluate free energies of adsorption of some n-alkylamines on iron.

Experimental Section

In view of the fact that the layer of adsorbed amine is strongly hydrophobic we have used the contact angle method to measure the compactness of the monolayer as a function of the pH of the solution.

According to this method, the iron sample is first dipped in the solution of the amine; after withdrawal a drop of solution is placed on the surface. The drop is then photographed and the value of the contact angle (advancing angle only) is read on the photographic film by means of a microscope with goniometric eyepiece, at a resolution of 20'.

It is well known[14] that to obtain reliable measurements of the contact angle it is necessary to work with surfaces that are as smooth and clean as possible to avoid ambiguities due to contact angle hysteresis. The Armco iron plates used were electropolished with a solution of the following composition: 70% $HClO_4$ = 18 vol %; 96% CH_3COOH = 82 vol %; current density = 10–15 A/dm². The cleaned plates, after having been repeatedly rinsed with distilled water, which completely wetted their surface,
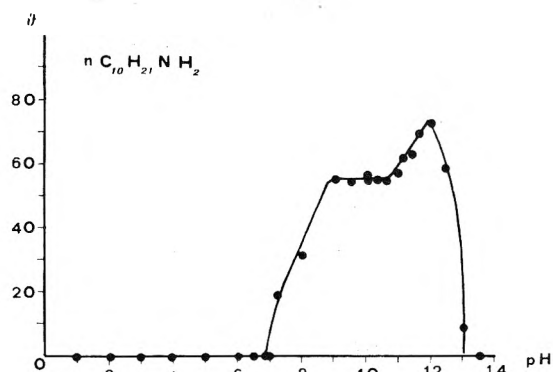

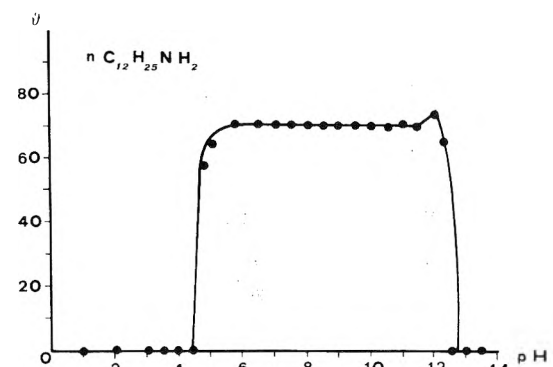**Figure 3.** Contact angle vs. pH for n-dodecylamine (5×10^{-4} M).
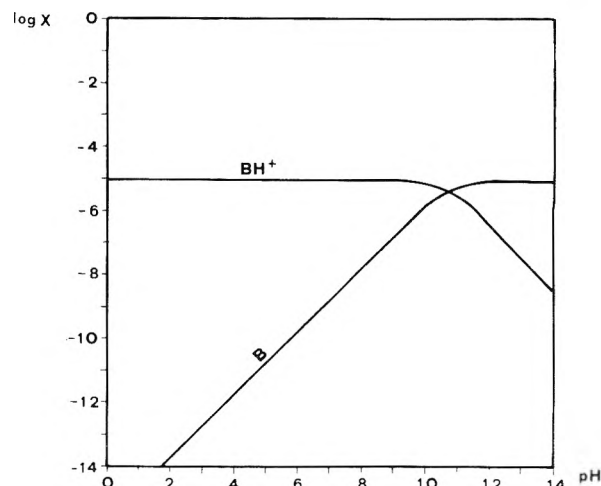

Figure 4. Relationship between the mole fraction of free amine (B) and amine ion (BH⁺) and solution pH for a total concentration $C = 5 \times 10^{-4}$ M and $pK_b = 3.366$.

were placed in contact with a solution containing an amine at 5×10^{-4} M. All glassware used for the tests was prerinsed with the solution to eliminate a decrease in concentration due to adsorption by glass. The pH of the solution was adjusted with NaOH or HCl.

Results and Discussion

(1) *Relationship between Contact Angle and pH*. By examining the experimental data (Figures 1–3) we note that the contact angle (ϑ) assumes values above zero only in the case of amines with eight or more carbon atoms. The range of pH over which finite contact angles are observed increases as the chain length increases.

If we compare Figures 1–3 with Figure 4, where we report the relation between log X (X represents the mole fraction of the amine) and pH, we note that the hydrophobic layer disappears when the mole fraction of free
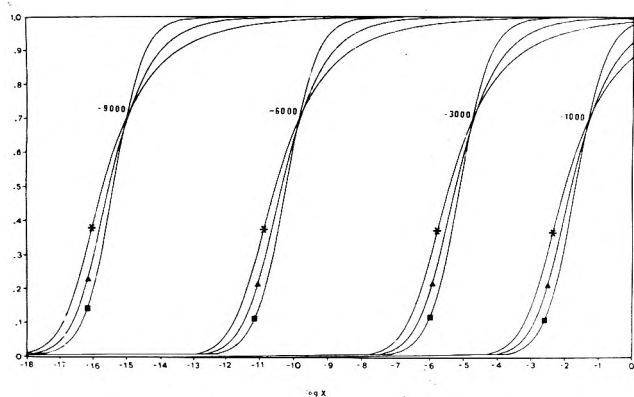
Figure 5. Surface coverage as a function of the logarithm of the mole fraction of an adsorbable species, for different values of $\Delta\mathcal{F}$: (■) n = 1; (▲) n = 2; (*) n = 4.

amine goes below a certain limit. Indeed the contact angle varies with pH (except at very high pH values) in a manner which is similar to that of the logarithm of the mole fraction of the free amine. At high pH values we note a steep decrease of the contact angle. As already suggested by Losev and Kabanov,[15] this is probably due to competitive adsorption of the OH⁻ ions on the metal surface. It may then be inferred that the adsorption can be attributed either to the protonated BH⁺ species or to the free amine. In the first case the drop in hydrophobicity at low pH values should be ascribed to the presence of positive charges on the surface of the iron. This may be due to the existence on the iron surface of an oxide layer which is still present, even after the polishing treatment used; at low pH the surface charge would be positive and BH⁺ would not adsorb. Experimentally, the pH at which a drop in adsorption is observed varies with the length of the alkyl radical of the amine. Following this model, a relationship between the length of the chain and the sign of the iron surface charge is to be invoked. For this reason we conclude that adsorption of BH⁺ is extremely unlikely.

A self-consistent, quantitative verification of the validity of the second hypothesis (namely, that the adsorbed species is the free amine) is presented in the next section.

(2) *Adsorption Isotherm.* The value of the contact angle formed by a drop of solution on the metal covered with a hydrophobic film is directly related not only to the hydrophobic power of the film, but also to its compactness. We shall therefore attempt to correlate the value of the contact angle with the degree of coverage of the surface. To this aim, we shall apply the adsorption isotherm method proposed by Agres[16] et al. for monolayer adsorption of organic substances; accordingly we use the relation

$$\frac{\varphi}{(1-\varphi)^n}\frac{[\varphi + n(1-\varphi)]^{n-1}}{n^n} = X\exp\frac{n\Delta F_w - \Delta F_o}{RT}$$

where φ is the fraction of area covered with organic molecules, and $(1 - \varphi)$ is the fraction of area covered with water molecules; n is the number of water molecules which are displaced from the surface after adsorption of a molecule of organic substance; X is the mole fraction of the organic substance in the solution.

ΔF_o is the change in Helmholtz free energy due to the transfer of an organic molecule from the solution phase to the adsorbed monolayer, and ΔF_w is the same for water.

In Figure 5 we plot the fraction of covered area (φ) as a function of the logarithm of the mole fraction of the adsorbable species in solution. The curve depends on the value of the free energy parameter. We note that, given
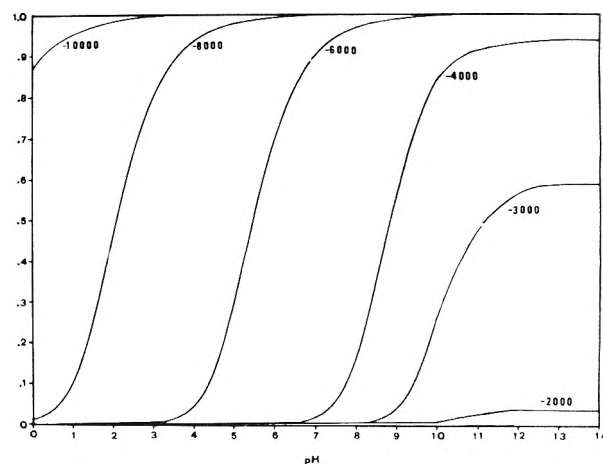

Figure 6. Surface coverage as a function of the solution pH for an amine at 5 × 10⁻⁴ M (pK_b = 3.366), for different values of $\Delta\mathcal{F}$ and n = 2.

TABLE I

Amine	$\Delta\mathcal{F}$, kcal/mol	Amine	$\Delta\mathcal{F}$, kcal/mol
n-C$_{12}$H$_{25}$NH$_2$	−6.5	n-C$_6$H$_{13}$NH$_2$	>−3.0
n-C$_{10}$H$_{21}$NH$_2$	−5.0	n-C$_4$H$_9$NH$_2$	>−3.0
n-C$_8$H$_{17}$NH$_2$	−3.5		

a certain concentration, it is possible to reach a degree of surface coverage very close to unity only when the total free energy of adsorption $\Delta\mathcal{F} = \Delta F_o - n\Delta F_w$ drops below a certain value. We also note the rapid fall of φ with log X; for a variation of two units in the logarithm of the mole fraction, the covered area is reduced by 70%. From Figure 5 it is also possible to investigate the influence of the cross sectional area of the organic molecule, which depends directly on number n; for low coverages and equal mole fractions in the solution, the greater the cross-sectional area of the molecule, the higher appears to be the degree of surface coverage. For high coverages the effect is reversed.

Since the mole fraction of free amine varies in a known way with the pH of the solution (through the pK_B which, for all the amines, is about 3.36), we can plot the degree of surface coverage directly as a function of pH using the above isotherm (Figure 6).

From existing data on molecular areas of octylyl-amine[2,17,18] and octadecylamine,[19] we assign an average cross-sectional area to our amines of 20 Å²; we use a value of 10.8 Å²[20] for water. It follows that an amine molecule, while adsorbing on an iron surface, displaces two molecules of water; for this reason we assume n = 2.

Comparing Figure 6 with the experimental curves, we see that the theoretical curves (which were drawn for different values of the free energy of adsorption) compare favorably with the experimental ones relevant to the various amines. In particular, if we compare the experimental graph of the contact angle vs. pH with the curves of Figure 6 we note that experimental and calculated curves can be superimposed by choosing a suitable value for the energy parameter. From this comparison we can evaluate the free energy of adsorption of the different amines (Table I). It is assumed that a surface begins to exhibit hydrophobicity after 55–60% of a monolayer has been formed.[21]

Different contributions cause the free energy of adsorption to become more negative as the chain length increases. According to the hydrophobic bond theory, interaction of nonpolar groups with water leads to an energy gain but also to a decrease in entropy;[22,23] it is

therefore reasonable to assume that the driving force giving rise to formation of the monolayer is the entropy gain associated with the removal of aliphatic side chains from water and with their transfer to the dense monolayer. Clearly, entropy gain per amine molecule must be proportional to the number of molecular nonpolar groups.

In the experimental graphs, we also note the existence of a maximum hydrophobicity peak. The existence of this peak can be explained by assuming that when maximum surface coverage is reached in the monolayer, amine molecules are rigidly compressed and, therefore, the contact angle is connected with the hydrophobicity of the chain terminal methyls. On the contrary when amine does not form a rigidly compressed monolayer, chains are mobile and hydrophobicity is rather given by the methylene groups of the chain. The critical surface tensions of the surface formed by these two groups[24] are for $=CH_2$, $\gamma_c = 31$ mN m^{-1}, and for $-CH_3$, $\gamma_c = 22$–24 mN m^{-1}.

This difference, together with the possibility that water molecules may remain caught up between the chains of adsorbed amine, can explain the variation in the contact angle.

Conclusion

The present study of adsorption of aliphatic amines on iron from an aqueous solution indicates that a relationship exists among the degree of coverage of the metal surface by amine, the pH of the solution, and the free energy of adsorption. Measurements of the contact angle as a function of pH suggest the following conclusion:

(1) Iron immersed in an amine solution adsorbs a hydrophobic layer over a pH range whose width increases with the length of alkyl group of the amine.

(2) An area of hydrophobicity is formed over a pH range which varies with the amine. Theoretically, we obtain a similar variation of the degree of coverage as a function of pH. The element which differentiates coverage curves is the free energy of adsorption. When it decreases, the pH range over which we find the maximum surface coverage (maximum hydrophobicity) is extended. Accordingly it is possible to estimate the variation of the free energy

of adsorption as a function of the length of the alkyl group.

(3) The contact angle is closely related to the compactness of the film and to its intrinsic hydrophobicity. A maximum hydrophobicity peak is observed in the graphs. This may be due to strong compression of the chains, which, as a result, point their terminal methyl groups toward the solution.

References and Notes

(1) W. C. Bigelow, D. L. Pickett, and W. A. Zisman, *J. Colloid Sci.*, **1**, 513 (1946).
(2) E. Shafrin and W. A. Zisman, *J. Colloid Sci.*, **4**, 571 (1949).
(3) R. L. Merker and W. A. Zisman, *J. Phys. Chem.*, **56**, 399 (1952).
(4) K. W. Bewig and W. A. Zisman, *J. Phys. Chem.*, **67**, 130 (1963).
(5) J. O'M. Bockris and D. A. J. Swinkels, *J. Electrochem. Soc.*, **111**, 736 (1964).
(6) S. Nakagava and G. Hashizume, *Denki Kagaku*, **36**, 570 (1968).
(7) K. Aramaki and N. Hackerman, *J. Electrochem. Soc*, **115**, 1007 (1968).
(8) T. Murakawa, T. Kato, and H. Sakai, *J. Metal Finish. Soc. Jpn.*, **19**, 8 (1968).
(9) K. Aramaki and S. Fujii, *Corros. Eng.*, **13**, 9 (1964).
(10) A. I. Altsybeeva, A. P. Dorokhov, T. M. Kuzinova, and S. Z. Levin, *Zashch. Met.*, **8**, 478 (1972).
(11) L. I. Antropov, V. M. Ledovskikh, and N. F. Kuleshova, *Zasch. Metal.*, **8**, 50 (1972).
(12) L. I. Antropov, V. M. Ledovskikh, and N. F. Kuleshova, *Zashch. Metal.*, **9**, 166 (1973).
(13) I. L. Rozenfel'd, V. P. Persiantseva, and T. A. Damaschina, *Zashch. Metal.*, **9**, 687 (1973).
(14) A. W. Neumann, *Adv. Colloid Interface Sci.*, **4**, 105 (1974).
(15) Cited by B. B. Damaschin, O. A. Petrii, and V. V. Batrakov, "Adsorption of Organic Compounds on Electrodes", Plenum Press, New York, N.Y., 1971, p 292.
(16) Z. M. Agres, A. M. Alcybeeva, S. Z. Levin, and V. S. Fedorov, *Zh. Fiz. Khim.*, **XLIX**, 986 (1975).
(17) N. K. Adam, "Physics and Chemistry of Surfaces", 3rd ed, Oxford University Press, London, 1941.
(18) E. L. Cook and N. Hackerman, *J. Phys. Chem.*, **55**, 549 (1951).
(19) R. J. Ruch and L. S. Bartell, *J. Phys. Chem.*, **64**, 513 (1960).
(20) T. Morimoto, M. Nagao, and F. Tokuda, *J. Phys. Chem.*, **73**, 243 (1969).
(21) H. A. Smith and H. M. Gill, *J. Phys. Chem.*, **61**, 1025 (1957).
(22) G. Némethy and H. A. Sheraga, *J. Chem. Phys.*, **36**, 3401 (1962).
(23) W. Kauzmann, "The Mechanism on Enzyme Action", W. Mac. Elroy and B. Glass, Ed., John Hopkins Press, Baltimore, Md., 1954.
(24) W. A. Zisman, *Ind. Eng. Chem.*, **55**, 19 (1963).

Absorbance of Aluminum Iodide Vapor in the Ultraviolet Region. The Dimer–Monomer Dissociation Equilibrium and the Vapor Pressure of Solid Aluminum Iodide

N. W. Gregory

Department of Chemistry, University of Washington, Seattle, Washington 98195 (Received March 7, 1977)

Aluminum iodide vapor, heated in the range 200–400 °C, develops with increasing temperature a new absorption maximum at 210 nm which appears to be associated with a charge-transfer transition in the monomer. Molar absorptivities at this wavelength have been assigned to monomer and dimer and the total absorbance behavior as a function of concentration and temperature correlated with the dimer–monomer dissociation equilibrium. Values for the enthalpy and entropy of sublimation of monomer (23.7 kcal, 37.6 cal deg^{-1} mol^{-1}) and dimer molecules (25.1 kcal, 43.0 cal deg^{-1} mol^{-1}) are also derived.

In the course of spectrophotometric study of vapor phase complexes formed between aluminum halide and transition metal halide molecules, vapors of pure aluminum bromide and of aluminum iodide, respectively, have been found to

show a steeply rising absorption shoulder as the usual cutoff limit (~190 nm) of the Cary 14H instrument is approached. At comparable concentrations the absorbance of the iodide extends further into the observable range

than that of bromide. When aluminum iodide vapor (in the concentration range 10^{-6} to 10^{-4} mol L^{-1}) is heated from ca. 200 to 400 °C an absorption peak at 210 nm emerges from the shoulder. This behavior does not seem to have been reported previously and it is found that the spectral change can be correlated with the monomer–dimer equilibrium (eq 1) in the vapor phase. Molar absorptivities

$$2AlI_3(g) = Al_2I_6(g) \tag{1}$$

at 210 nm have been assigned for each of the molecular forms, although with relatively large uncertainty as this wavelength lies on the shoulder of a strong absorbance band which appears to peak in the vacuum ultraviolet for the dimer molecule. However absorbance data from five independent samples give equilibrium constants for reaction 1 which correlate well with constants based on vapor density and vapor pressure data of Fischer, Rahlfs, and Benze[1] and with information (based on ref 1 and estimated entropies) published in the JANAF Thermochemical Tables.[2]

Experimental Section

Aluminum iodide was prepared by direct reaction of the elements (Baker's Analyzed Reagent Grade Al wire, ACS specification, and Allied Chemical BA Iodine, Resublimed, ACS Reagent Grade, 99.8%) in a Pyrex high vacuum system.

The reaction products were sublimed directly into quartz absorption cells; for three of the samples the quantity of aluminum iodide introduced was determined by atomic absorption analysis for aluminum after absorbance measurements were completed.[3] A visual estimate of the amount of solid sublimed onto the walls of the cell proved a satisfactory means of selecting quantities which could be completely vaporized with the absorbance remaining in the observable range. Samples were sublimed into the cells via Pyrex–quartz graded seals, with the Pyrex extensions finally sealed off with a flame. Cell volumes were determined by comparison of cell weight empty and weight filled with water. Cell path lengths b (cm), volumes (mL), and sample C_0 values (concentration (mol L^{-1}) equivalents of the total moles of Al in the cells) were as follows: (1) 1.00, 3.717, 1.319×10^{-4}; (2*) 10.0, 28.90, 1.187×10^{-5} (see following discussion); (3*) 10.0, ..., 2.537×10^{-6} (see following discussion); (4) 10.0, 29.3, 3.960×10^{-6}; (5) 1.00, 3.47, 1.190×10^{-4}.

Three calibrated thermocouples, placed at the cell center, at one of the windows and at the tip of the sidearm, respectively, were used to monitor temperatures. In the heating block the temperature of the center generally ran about 5 °C above that at the window and at the sidearm (the latter was independently controlled and kept the same as the window) when the samples were completely vaporized. When a condensed phase was present, the tip of the sidearm was kept slightly cooler than the window to prevent condensation on the latter. The temperature of the center of the cell was used as the basis for equilibrium constant calculations and for data plots in the figure displaying the homogeneous vapor behavior; for the saturation vapor pressures, absorbances were correlated with the temperature of the sidearm tip where crystals were observed to deposit.

Results and Discussion

Representative vapor phase spectra (from sample 2) are traced in Figure 1, showing the low temperature (virtually all Al_2I_6) and high temperature (virtually all AlI_3) limiting behaviors. The treatment described in following paragraphs indicates that the emergence of the peak at 210 nm
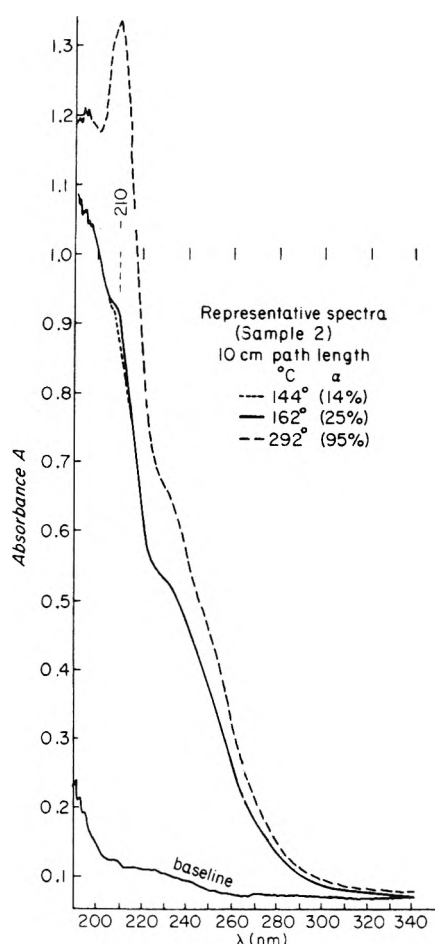
Figure 1. Traces of spectra recorded for aluminum iodide vapor at three temperatures (sample 2, Cary 14H spectrophotometer). α indicates the degree of dissociation calculated for reaction 1.

is associated with the increased degree of dissociation of the dimer as the temperature of the vapor is increased. The measured total absorbances A at 210 nm for all samples over the full temperature range studied are plotted in the form $\log AT/b$ vs. T^{-1} in Figure 2. The steeply rising portions of the curves at lower temperatures reflect the increase in vapor concentration with temperature when the vapor is in equilibrium with solid AlI_3. Absorbances for the various samples are seen to fall on the same line in this range, and the temperature at which each sample becomes completely vaporized is readily apparent.

At 700 K equilibrium constants K_1, for reaction 1,[1,2] predict degrees of dissociation for the various completely vaporized samples in the range 98.5–99.99%. At this temperature the average value of A/bC_0 for the three analyzed samples was 10700 ± 400 L mol^{-1} cm^{-1}. This is very close to the average value of ϵ_M (10600 ± 600) derived by treating the data from these three samples by the methods described in the following paragraph and was used together with the absorbances at 700 K to assign values of C_0 (marked above with an asterisk) for the two samples for which an aluminum analysis was not available.

The complete set of measured absorbances shown in Figure 2 was then correlated in various ways. Fifteen values (temperature range 140–310 °C) characterize mixtures with predicted (from JANAF K_1) C_D/C_M ratios larger than 0.1. A least-squares treatment of this data set in the form $A/bC_M = \epsilon_M + \epsilon_D C_D/C_M^2$ gave $\epsilon_M = 10200$ (std dev 5.6%) and $\epsilon_D = 10400$ (std dev 4.5%) L mol^{-1} cm^{-1}. For the other 16 all vapor mixtures (250–470 °C) C_D/C_M ratios were predicted to be less than 0.1 and $(A - \epsilon_D C_D)/C_M$ values for this set, using ϵ_D as derived above, were taken
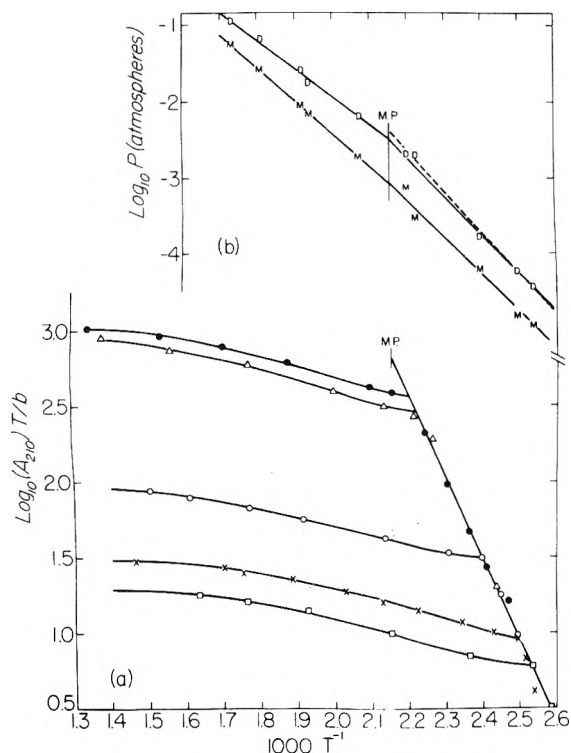
Figure 2. (a) log AT/b vs. T^{-1} for the various samples: (●) 1; (○) 2; (□) 3; (✕) 4; (△) 5. $A/b = \epsilon_M C_M + \epsilon_D C_D$. (b) Partial pressures, log P vs. T^{-1}, for monomer (M) and dimer (D). Values below melting point (equilibrium with solid AlI₃) based on equilibrium constants for (1) and total absorbance at point of intersection of curves for homogeneous vapor and vapor–solid equilibrium regions, Figure 2a. Values above melting point (equilibrium with liquid AlI₃) taken from data in ref 1.

TABLE I

	$\Delta H°$, cal mol^{-1}	std dev, %	$\Delta S°$, cal deg^{-1}	Std dev, %
2AlI₃(s) = Al₂I₆(g)				
(i)	25 200	3.2	43.4	4.4
(ii)	25 000	2.7	42.7	3.9
AlI₃(s) = AlI₃(g)				
(i)	24 100	7.5	38.4	11.2
(ii)	23 400	1.5	36.9	2.3

For the mean temperature 420 K, $\Delta H°$ and $\Delta S°$ data are shown in Table I.

Calculated partial pressures at the intersection points are shown in Figure 2b in relation to values representing equilibrium with the liquid phase (at higher temperatures) as reported by Fischer, Rahlfs, and Benze.[1] The solid line, drawn so as to connect the points at lower temperatures to a point of intersection with the FRB[1] data at the melting point, give somewhat smaller heats and entropy values (e.g., 23400 and 38.4, respectively, for the dimer) than derived in the treatment of the absorbance data. No other study of sublimation pressures of aluminum iodide appears to have been reported. $\Delta H°$(sublimation) for the dimer estimated in the JANAF Tables[2,4,5] is slightly larger (26.0 ± 1.8) kcal but within experimental error of the absorbance value. JANAF estimated $\Delta S°$(sublimation)[6–8] also appears too large (46.7 ± 4); however the lower limit of the rather large uncertainty includes the spectrophotometric value. JANAF estimated values for the monomer are 24300 cal and 39.7 cal mol^{-1} deg^{-1}, respectively, with the enthalpy in excellent agreement and the entropy slightly higher in comparison with the value derived here.

The large values of the molar absorptivities found for both monomer and dimer suggest that the absorbance bands are associated with charge-transfer transitions, perhaps similar in character in the two molecules but shifted to slightly longer wavelength for the monomer. The value of ϵ_D at the wavelength of the dimer peak (vacuum ultraviolet region) is of course expected to be substantially larger than the value at 210 nm. Charge-transfer transitions in iron halide compounds have been observed at slightly longer wavelengths (visible-UV region) and have been associated with transitions from orbitals with largely ligand π bonding or nonbonding character to orbitals with largely metal 3d character.[9] The steeply rising shoulder observed for aluminum bromide as the instrument cutoff limit (190 nm) is approached suggests that a behavior similar to AlI₃ may be observed for AlBr₃ in the vacuum ultraviolet region.

as ϵ_M, giving an average of 10990 (std dev 5.2%). A mean of 10600 L mol^{-1} cm^{-1} was finally selected as the best average for ϵ_M (130–400 °C).

To check the general correlation the derived molar absorptivities were then treated as temperature independent constants and used together with C_0 and A_{210}/b values, for completely vaporized samples with predicted C_D/C_M^2 ratios above 0.1, to derive values for K_1 (using the relationship $K_C = C_D/C_M^2 = K_p(RT) = (2\epsilon_M - \epsilon_D)(\epsilon_M C_0 - A/b)(2A/b - \epsilon_D C_0)^{-2}$). A least-squares treatment of log K_P vs. $1/T$ gave $\Delta H°(1) = -23500$ kcal mol^{-1} (std dev 7.7%) and $\Delta S°(1) = -34.3$ cal mol^{-1} deg^{-1} (std dev 11.2%). Within the rather large standard deviations, the results correspond to the JANAF values of -21800 and 31.4, respectively. The latter were, of course, used to obtain the initial estimate of ϵ_D (the initial estimate for ϵ_M required only that the amount of dimer be negligible at the highest temperatures); the correlation did not seem significantly improved when the value of ϵ_D was varied by ±1000.

Monomer and dimer partial pressures in equilibrium with solid AlI₃ were calculated (i) from the total absorbances for each of the five samples at the point of intersection of the homogeneous vapor phase curve and the saturation vapor pressure curve (Figure 2) together with C_0, ϵ_D, and ϵ_M; and (ii) using all the absorbance data at lower temperatures (16 values) together with JANAF values of K_1, ϵ_D, and ϵ_M. A least-squares treatment was used independently in each case and derived enthalpies and entropies are summarized below. The relatively large standard deviation for the monomer in treatment (i) reflects the small number of data points and its relatively low concentration in the equilibrium mixture.

References and Notes

(1) W. Fischer, O. Rahlfs, and B. Benze, Z. Anorg. Allgem. Chem., 205, 1 (1932).
(2) "JANAF Thermochemical Tables", Thermal Laboratory, Dow Chemical Co., Midland, Mich., June 1964.
(3) Appreciation is expressed to Dr. Eric Knudsen for performing the analyses.
(4) J. D. Corbett and N. W. Gregory, J. Am. Chem. Soc., 76, 1446 (1954).
(5) D. J. A. Dear and D. D. Eley, J. Chem. Soc., 4684 (1954).
(6) K. J. Palmer and N. Elliott, J. Am. Chem. Soc., 60, 1852 (1938).
(7) H. Gerding and E. Smit, Z. Phys. Chem., 50B, 171 (1941).
(8) K. K. Kelley, U.S. Bur. Mines Bull., 584 (1960).
(9) B. D. Bird and P. Day, J. Chem. Phys., 49, 392 (1968).

The Ultraviolet–Visible Absorption Spectrum of Vapors Generated in the Iron–Bromine System. Molecular Complexes and Vaporization Thermodynamics

N. W. Gregory

Department of Chemistry, University of Washington, Seattle, Washington 98195 (Received May 2, 1977)

Molar absorptivities have been assigned for the species $FeBr_2(g)$ and $Fe_2Br_4(g)$ at 250 and 280 nm and for $FeBr_3(g)$ and $Fe_2Br_6(g)$ at 300 nm, respectively, the wavelengths at which absorbance peak maxima are observed. Thermodynamic constants reported previously for these molecules, are found to predict concentrations which correlate satisfactorily absorbance data at various bromine pressures and temperatures. No evidence is found to suggest formation of substantial concentrations of mixed valence state intermediate molecules in the mixtures studied. Thermodynamic constants for the vaporization of $FeBr_2$ are derived from absorbance data.

The chemistry of the iron–bromine system at moderately high temperatures centers on $FeBr_2$. The decomposition pressure of bromine above $FeBr_3(s)$ reaches 1 atm around 139 °C with a relatively small partial pressure (0.015 Torr) of ferric bromide present.[1,2] At higher temperatures, still in the range below which $FeBr_2$ vapor molecules have a significant concentration, substantially higher concentrations of Fe_2Br_6 (and of $FeBr_3$) may be generated by reaction of $FeBr_2(s)$ with bromine. Thermodynamic data have been derived for $FeBr_3(g)$ and $Fe_2Br_6(g)$ from quantities of iron transported in Ar–Br_2 mixtures flowing over $FeBr_2(s)$ (200–400 °C) and from diaphragm gauge studies of the monomer–dimer equilibrium at higher temperatures. These molecules were assumed to be the only iron containing species present at significant concentrations.[2] Recently evidence for formation of numerous kinds of molecular complexes in metal halide vapor systems has been reported.[3-8] Particularly common are complexes of aluminum(III) and iron(III) halides with various transition metal dihalides. This raises a question concerning the importance of similar intermediates in the simple iron–bromine system, i.e., complexes of the form $Fe(II)Fe(III)Br_5$, $Fe(II)(Fe(III))_2Br_8$, etc. If the relative thermodynamic properties of such intermediates are similar to those observed in the chloride systems, their contribution to the iron transported in the transpiration experiments[2] is expected to be small. However, under the conditions used to study the iron(III) bromide monomer–dimer equilibrium, such estimates suggest appreciable amounts of Fe_3Br_8 may have been present. Direct information on the thermodynamic properties of mixed valence state bromide intermediates is not available. The dependence of the total concentration of iron in vapor molecules in equilibrium with $FeBr_2(s)$ on bromine pressure, as studied in the transpiration experiments, will not distinguish Fe_2Br_6 from Fe_3Br_8, or similarly, $FeBr_3$ from Fe_2Br_5.

Both iron(II) and iron(III) bromide vapors are found to have strong charge-transfer absorption bands in the UV–visible region of the spectrum;[9] mixed valence state intermediate molecules may also be expected to show absorbance in this wavelength range (200–800 nm).[18,19] In the present work absorbances of $FeBr_2$ vapor and of mixtures of bromine and $FeBr_2$ vapor have been studied over a substantial range of temperature and bromine pressures. Vapor mixtures with relatively high concentrations of iron and low concentrations of bromine would be expected to offer the best chance for detection of mixed

valence state complexes. The consistency of reported thermodynamic properties of $FeBr_3$ and of Fe_2Br_6 has been tested by use of predicted concentrations and observed absorbances to derive molar absorptivities for these molecules.

Iron(II) Bromide

Absorbances of vapors of four independently prepared samples of $FeBr_2$ were studied with a Cary 14H spectrophotometer in the temperature range 840–1100 K in the absence of excess bromine. In addition to their intrinsic interest values of the molar absorptivities of the monomer and dimer ($FeBr_2$ and Fe_2Br_4) were derived to provide a basis for predicting the contribution of these species to the total absorbance of the more complex Br_2–$FeBr_2$ mixtures. Samples were prepared in a high vacuum Pyrex System by direct reaction of dry bromine (Baker's Analyzed Reagent Grade, 99.3%) with Merck Reagent Grade iron wire (99.8%) and sublimed in vacuo into quartz absorption cells through a connecting quartz–Pyrex graded seal. A sample was isolated in its cell by sealing off the quartz sidearm with a flame.

For samples 1 and 2 (cell path lengths 2 and 5 cm, respectively) an excess of $FeBr_2(s)$ was present at all temperatures (835–916 K). Sample 3 (10 cm cell) was studied only with all the iron bromide in the vapor phase ($C_0 = 2.224 \times 10^{-5}$ mol L^{-1}, the concentration equivalent of the total number of moles of Fe in the cell) and sample 4 (1 cm cell) was studied both in the saturated vapor range and when completely vaporized ($C_0 = 4.345 \times 10^{-4}$, temperature range 901–1098 K). In the latter two cases the amounts of iron present were determined after the absorbance measurements by atomic absorption analysis.[10]

Cells were heated electrically in a stainless steel block and the controlled temperatures (±1°) measured with chromel–alumel thermocouples, calibrated at the melting points of tin and zinc. The temperature of the tip of the cell sidearm, T_3, generally 40 to 70 mm from the cell body, was controlled independently from that of the cell body, T_1. When absorbance measurements were made on vapors in equilibrium with $FeBr_2(s)$, condensed in the tip, T_3 was kept somewhat below T_1 to prevent condensation of solid on the cell windows. Under these circumstances vapor pressures established at T_3 and dimer–monomer equilibrium constants K_1 at T_1 were used to correlate the data. The effect of temperature on concentration was included by assuming uniform pressure throughout the cell. Cells were ca. 19 mm i.d.
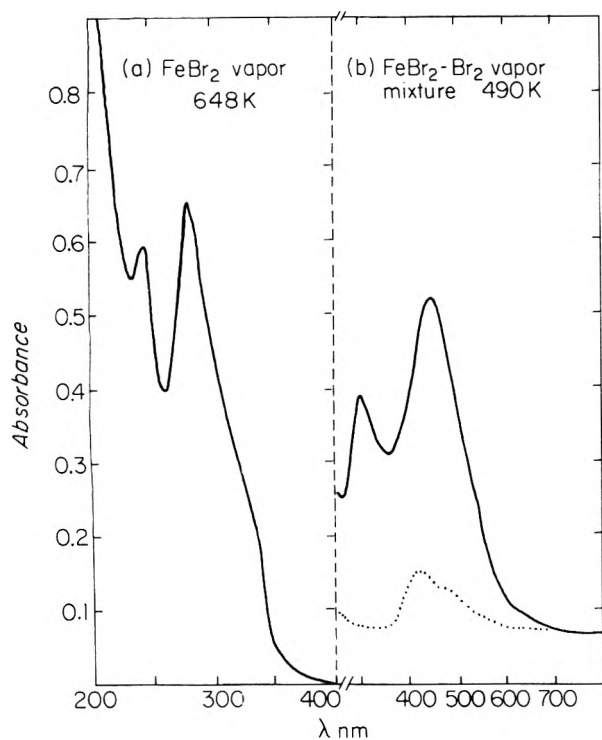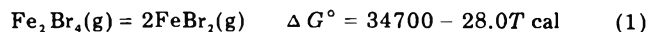
Figure 1. Tracing of representative adsorption spectrum: (a) FeBr$_2$ vapor (at 648 K) in equilibrium with solid FeBr$_2$ (at 633 K), quartz cell, 2 cm path length; (b) homogeneous vapor mixture with $C_{0(Fe)}$ = 2.07 × 10^{-5} and $C_{0(Br2)}$ = 8.41 × 10^{-5} mol L^{-1}. (-----, Br$_2$ absorbance at 25 °C). Temperature 490 K; calculated concentrations of various species: FeBr$_2$ (3.58 × 10^{-7}), FeBr$_3$ (1.30 × 10^{-5}), Fe$_2$Br$_4$ (5.30 × 10^{-8}), Fe$_2$Br$_6$ (3.61 × 10^{-6}), Br$_2$ (7.38 × 10^{-5}) mol L^{-1}. Quartz cell, 5 cm path length.

Results and Discussion. A representative spectrum is shown in Figure 1a. Two peaks, with maxima around 250 and 280 nm, respectively, are seen on the shoulder of an intense band extending into the vacuum ultraviolet.[11] No other bands were observed in the wavelength range out to 800 nm. Sakisaka, Ishii, and Sagawa have reported absorption spectra in the ultraviolet region for solid FeBr$_2$ and in the range of the present work observe peaks around 270 and 220 nm.[11] DeKock and Gruen have reported vapor phase and argon matrix spectra for FeCl$_2$ and observe peaks at 267, 241, and 210 nm.[12] These transitions are believed associated with charge transfer from molecular orbitals with largely the character of the outermost p orbitals on the halogen atoms to orbitals for which the metal 3d states are the major contributors. Bird and Day have described what appear to be similar transitions in FeCl$_4^-$.[13]

The total absorbances at the peak maxima are plotted in Figure 2 as ln AT_1/b (b is the cell path length) vs. $1/T_3$. The steeply rising portion of the plot corresponds to the increasing concentration of the saturated vapor in the presence of the solid phase. Regions in which samples 3 and 4 are fully vaporized are recognized by the relatively small change of absorbance with temperature. The temperature dependence of the absorbance was correlated with the concentrations of the vapor molecules in the following manner.

The concentrations of monomer and dimer, C_2 and C_4, respectively, in the saturated vapors were predicted from total torsion effusion pressures P_t reported by Sime[14] and equilibrium constants for the dimer–monomer reaction (1) based on a mass spectral study by Porter and Schoonmaker.[15] The equations $P_t = P_2 + P_4 = P_2 + K_1P_2^2$ then

$$\text{Fe}_2\text{Br}_4(g) = 2\text{FeBr}_2(g) \qquad \Delta G° = 34700 - 28.0T \text{ cal} \qquad (1)$$
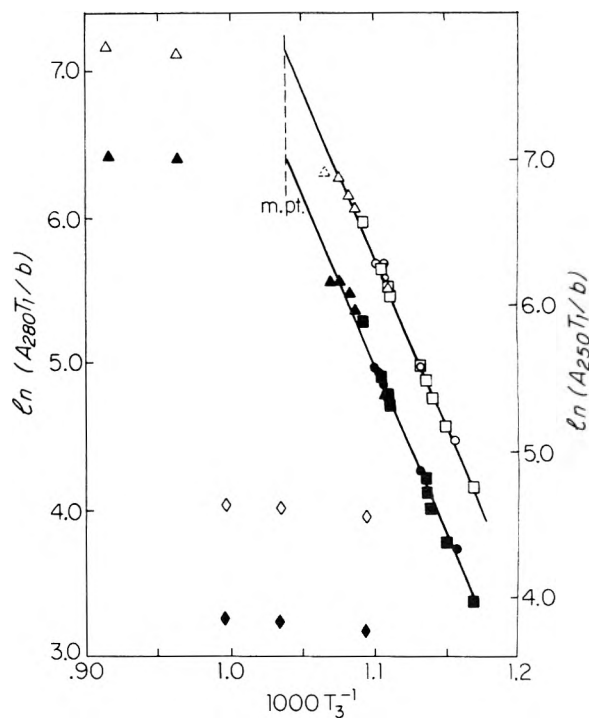

Figure 2. ln $A_{280}T_1/b$ (open symbols) and ln $A_{250}T_1/b$ (filled symbols, note change in scale for ordinate at right) vs. $1/T_3$ for vapor of iron(II) bromide: O, sample 1 (2 cm cell); □, sample 2 (5 cm cell); ◇, sample 3 (10 cm cell); △, sample 4 (1 cm cell). See Table I.[16]

lead to the concentrations of monomer and dimer. For completely vaporized samples, concentrations were derived from K_1, the total amount of iron, and the cell volume. The entire set of absorbances at each peak maximum, A_{250} and A_{280} (19 values at each wavelength for the saturated vapors and 5 for the superheated vapors; see Table I),[16] was then treated by least squares in the form $A/bC_2 = E_2 + E_4C_4/C_2$, neglecting the temperature dependence of the molar absorptivities. Mean values (and standard deviations) derived were as follows: at 280 nm for the monomer E_2 = 2560 (2.8%) and for the dimer E_4 = 6290 (3.1%); at 250 nm E_2 = 1990 (3.5%) and E_4 = 6250 (3.1%) L mol^{-1} cm^{-1}. Calculated C_4/C_2 ratios varied from 0.045 (sample 3, vapor at 1004 K) to 0.54 (sample 1, solid 906 K and vapor 921 K).[16] The relative absorptivities of the two species appear quite similar for the two peaks.

The monomer is the dominant species in the saturated vapor at the lower temperatures and values of E_2, E_4, and K_1 were used through the equation $A/b = E_2C_2 + E_4C_2^2RT_1/K_1$ to derive values for the standard enthalpy and standard entropy of sublimation of the monomer:

$$\text{FeBr}_2(s) = \text{FeBr}_2(g) \qquad (2)$$

	$\Delta H°$ (std. dev.), kcal mol^{-1}	$\Delta S°$ (std. dev.), cal mol^{-1} deg^{-1}
A_{280}	42.8 (0.52%)	36.1 (0.68%)
A_{250}	43.3 (0.71%)	36.7 (0.93%)

Using average values of 43.0 and 36.4, respectively, and the result given previously for (1), values of $\Delta H°$ = 51.3 kcal and $\Delta S°$ = 44.8 cal deg^{-1} mol^{-1} are obtained for 2FeBr$_2$(s) = Fe$_2$Br$_4$(g).

As a reverse test of the correlation values of E_2 and E_4 and absorbances for mixtures with predicted C_4/C_2 ratios larger than 0.2 were used to calculate K_1 values. For the all vapor mixtures, the relationship

$$K_C = K_P/RT = (E_4C_0 - 2A/b)^2/((E_4 - 2E_2) \times (A/b - E_2C_0))$$

was used; and for the saturated vapors

$$K_C = (A/b - P_t E_4/RT_1)^2/((E_4 - E_2)$$
$$\times (A/b - P_t E_2/RT_1))$$

A least-squares treatment of $\ln K_P = -\Delta H°/RT_1 + \Delta S°/R$ gave

	A_{280}	A_{250}	Ref 15
$\Delta H°(1)$, kcal (std. dev.)	38.6 (6.5%)	34.0 (7.2%)	34.7 ± 4
$\Delta S°(1)$, cal mol^{-1} deg^{-1} (std. dev.)	32.1 (8.4%)	27.2 (9.6%)	28.0 ± 5

While results are generally consistent uncertainties are large. The molar absorptivities of the two species are not sufficiently different for the measured absorbances to serve as a sensitive means of resolving the monomer–dimer equilibrium.

A direct vapor pressure correlation, in the form $\ln AT_1/b$ vs. $1/T_3$ gave only slightly larger standard deviations for an apparent enthalpy, 46.5 kcal (1.5%) and entropy, 46.2 cal deg^{-1} mol^{-1} (1.25%) of sublimation, and with a value of $E_2 = 3600$ (4.4%) at 280 nm and of 3100 (6.1%) at 250 nm, when correlated with Sime's effusion data assuming vaporization as only the monomer. However, on an all monomer basis the two samples which could be completely vaporized gave substantially lower and different E_2 values, 2732 for sample 3 and 2572 for sample 4 at 280 nm and 2404 and 2155 at 250 nm, respectively. Thus the overall correlation is substantially improved, with a standard deviation in the molar absorptivities from both sets of data combined of only 3%, when the concentration of dimer is assumed that predicted by Porter and Schoonmaker's equilibrium constants for reaction 1.
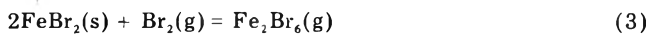
Iron(II) Bromide–Bromine Mixtures

When bromine is added to absorption cells containing FeBr$_2$, the absorbance of the vapor phase is considerably enhanced at lower temperatures, changes in character, and shows a marked dependence on the concentration of bromine.[9] Seven independently prepared samples, with bromine concentrations varying from 5.15×10^{-3} to 8.41×10^{-5} mol L^{-1}, were studied over the temperature range 588–810 K. Samples were prepared and handled as described in the previous section. In five cases absorbances of saturated vapors (equilibrium with FeBr$_2$(s)) were observed as well as the behavior of the superheated vapors (i.e., at temperatures such that all the iron bromide was in the vapor phase). Introduction of the desired amount of FeBr$_2$ could be estimated by observing the amount deposited as the sample was vacuum sublimed into the cell; similarly the desired concentration of free bromine could be approximated by observing the depth of its color in the cell prior to vacuum seal-off. The actual bromine concentrations were determined spectrophotometrically by measurement of the bromine absorbance at several temperatures in the range where FeBr$_3$(s) was unstable and iron(III) bromide vapor concentrations were still negligible.[17] As before the total amount of iron was finally determined by atomic absorption analysis.[10]

Results and Discussion. The general appearance of the spectrum of these mixtures was found similar to that observed earlier in a preliminary study using a Beckman DU spectrophotometer.[9] A trace of a representative absorption spectrum of a homogeneous vapor mixture is compared with that of FeBr$_2$ in Figure 1. Two maxima are observed; the one around 460 nm overlaps strongly with the major peak in the bromine spectrum and the other, around 300 nm, is at a slightly longer wavelength than the 280-nm peak observed for FeBr$_2$. However the concentrations of the iron(II) bromide species at the temperatures at which the FeBr$_2$–Br$_2$ mixtures were studied are very small (see Table II)[16] and the contribution of these molecules to the total absorbance around 300 nm is generally less than the experimental uncertainty of the measurement. The 300-nm band appears to lie on the shoulder of a stronger band which extends into the vacuum ultraviolet. Absorbances at the peak maximum at 300 nm were used to test the correlation with thermodynamic data; at this wavelength only the minor correction for the contribution of FeBr$_2$–Fe$_2$Br$_4$ was necessary, whereas for many of the mixtures bromine was the major contributor to the absorbance at the peak near 460 nm.
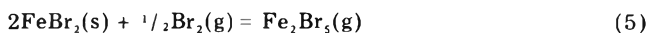
Data were treated first with the assumption that FeBr$_2$, Fe$_2$Br$_4$, FeBr$_3$, and Fe$_2$Br$_6$ and bromine were the only vapor molecules present, and second with the assumption that Fe$_2$Br$_5$ and Fe$_3$Br$_8$ were also present at concentrations predicted from estimated equilibrium constants. In addition to the results discussed for reactions 1 and 2 thermodynamic relationships 3–6 (and combinations thereof) were used to predict concentrations of the various species from which apparent molar absorptivities were then derived. The estimate for (5) corresponds to the assumption that $\Delta G°$ for the reaction Fe$_2$Br$_6$(g) = Fe$_2$Br$_5$(g)
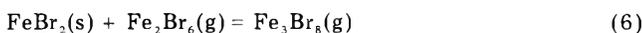
$$2FeBr_2(s) + Br_2(g) = Fe_2Br_6(g) \qquad (3)$$
$$\Delta G° = 16300 - 18.0T \text{ cal (ref 2)}$$

$$Fe_2Br_6(g) = 2FeBr_3(g) \qquad (4)$$
$$\Delta G° = 33250 - 32.0T \text{ (ref 2)}$$

$$2FeBr_2(s) + {}^1/_2 Br_2(g) = Fe_2Br_5(g) \qquad (5)$$
$$\Delta G° = 34500 - 29.4T \text{ (est)}$$

$$FeBr_2(s) + Fe_2Br_6(g) = Fe_3Br_8(g) \qquad (6)$$
$$\Delta G° = 10000 - 10.0T \text{ (est)}$$

$+ {}^1/_2 Br_2(g)$ is the same as that for FeBr$_3$(g) = FeBr$_2$(g) $+ {}^1/_2 Br_2(g)$. The estimate for (6) reflects a behavior noted by Dewing for a substantial number of chloride complexes of the form M(II)N(III)$_2$Cl$_8$.[3,8]

In the first series of calculations the concentrations (partial pressures) corresponding to the 14 measured absorbances (588–640 K) for vapors in equilibrium with FeBr$_2$(s) were evaluated in the following way. The partial pressure of free bromine at each temperature was calculated from the equation

$$P_{0(Br_2)}^2 - (2(1 + K_3)P_{0(Br_2)} + K_3 K_4/4)P_{Br_2}$$
$$+ (1 + K_3)^2 P_{Br_2}^2 = 0$$

where $P_{0(Br_2)}$ represents the pressure equivalent of the total amount of bromine (in excess over FeBr$_2$) in the cell and the equilibrium constant subscripts correspond to the reaction numbers given above. The concentrations of FeBr$_3$(g) and Fe$_2$Br$_6$(g) were in turn evaluated from the bromine pressure P_{Br_2} and K_3 and K_4. A correction for the difference between the cell body temperature T_1 at which the absorbances were measured and the cell sidearm T_3 (holding the condensed FeBr$_2$(s)) was made by assuming the total pressure of the two iron containing species was the same in the two regions.

For the superheated vapor samples (32 measured absorbances, 640–810 K) partial pressures of FeBr$_3$(g), P_3, and Fe$_2$Br$_6$(g), P_6, were derived from the equation

$$P_{app(Fe)} = 2(1/K_4 + K_2^2/K_1 K_3 K_4 P_{Br_2})P_3^2 +$$
$$(1 + K_2/(K_3 K_4 P_{Br_2})^{1/2})P_3$$

where $P_{\text{app(Fe)}}$ is the pressure equivalent of the total amount of Fe in the cell, $C_{0(\text{Fe})}RT_1$; the bromine pressure P_{Br_2} was taken as $P_{0(\text{Br}_2)} - P_{\text{app(Fe)}}/2$ which neglects only the amount of iron in the vapor phase as FeBr_2 and Fe_2Br_4, exceedingly small relative to P_{Br_2}. Values of P_3 and P_{Br_2} and the various equilibrium constants were then used to obtain P_2, P_4, and P_6.

The combined sets of data were then subjected to least-squares analysis in the form $A'RT_1/P_6 = E_3P_3/P_6 + E_6$ where $A' = A/b - E_2C_2 - E_4C_4$, E represents a molar absorptivity and the subscripts 2, 3, 4, and 6 indicate FeBr_2, FeBr_3, Fe_2Br_4, and Fe_2Br_6, respectively. Mean values (and standard deviations) for 590–810 K derived were $E_6 = 9600$ (3.9%) and $E_3 = 2570$ (6.5%) L mol^{-1} cm^{-1}. The calculated fraction of iron(III) bromide in the form of the monomer ranged in the various mixtures from 0.057 to 0.896. The data and relative partial pressures calculated are listed in Table II.[16]

In preliminary calculations assuming the presence of mixed valence state intermediates, predicted concentrations of Fe_2Br_5 based on (5) were found to be a factor of 10 or more less than those of Fe_3Br_8, based on (6) and in general negligible relative to the total concentration of the iron containing species in the vapor phase. Hence for the second series of calculations only Fe_3Br_8 was included. It was necessary to assume that thermodynamic values for (3), as derived by MacLaren[2] without inclusion of Fe_3Br_8, were valid. A trial calculation suggests that this is reasonable in that for 70% of the transpiration experiments the estimated concentration of Fe_3Br_8 was less than 2% of the total of Fe_2Br_6 and FeBr_3; only at the highest temperatures did the estimate rise as high as 6%. However, in the diaphragm gauge studies at higher temperatures, used to determine equilibrium constants for (4), the predicted amounts of Fe_3Br_8 ranged between 15 and 27%. Hence the results from these experiments were recalculated including the estimated concentrations of Fe_3Br_8 from (6) to derive a revised free energy expression for (4): $\Delta G^\circ = 35160 - 34.5T$. The resulting change in enthalpy is well within experimental error; however the apparent increase in entropy makes a significant change in values of K_4. With the inclusion of Fe_3Br_8, $P_{\text{app(Fe)}}$ was taken as $P_2 + P_3 + 2P_4 + 2P_6 + 3P_8$ and with $\text{FeBr}_2(\text{s})$ present $P_{\text{app(Fe)}} = K_2 + K_2^2/K_1 + P_3 + 2P_3^2/K_4 + 3K_6P_3^3/K_4$. $P_{\text{app(Fe)}}$ was calculated from the temperature dependence of the total amounts of iron in the equilibrium vapor phase observed by MacLaren[2] and P_3 (and P_6 and P_8) values then derived. For the superheated vapors $P_{\text{app(Fe)}} = C_{0(\text{Fe})}RT_1$ and $P_{\text{app(Fe)}} = (1 + K_2/(K_3K_4P_{\text{Br}_2})^{1/2})P_3 + (K_2^2/K_1K_3K_4P_{\text{Br}_2} + 1/K_4)P_3^2 + (K_6/(K_3K_4P_{\text{Br}_2})^{1/2})P_3^3$. Again no appreciable error results by taking P_{Br_2} as $P_{0(\text{Br}_2)} - P_{\text{app(Fe)}}/2$, which assumes $P_2 + 2P_4 + P_8$ is very small relative to P_{Br_2}. The partial pressures derived from these equations are listed in Table III.[16]

A least-squares treatment of the complete set of 46 measured absorbances at 300 nm in the form $A'RT_1 = E_3P_3 + E_6P_6 + E_8P_8$ gave $E_3 = 3100$, $E_6 = 8722$, and $E_8 = 20100$ L mol^{-1} cm^{-1}, with a standard deviation of $(A_{\text{obsd}} - A_{\text{calcd}})/A_{\text{obsd}}$ of 16.8%. The concentrations of Fe_3Br_8 derived for these mixtures were very small, in the range

1–7%, and its apparent contribution to the total absorbance appears small, in the experimental error range. The apparent molar absorptivity is larger than seems reasonable and is subject to very large uncertainty. From the large standard deviation one concludes that the data do not correlate as well when the estimate for Fe_3Br_8 is included as in the first treatment in which its concentration was assumed negligible.

No significant change in the appearance of the absorption spectrum was noted on comparison of samples with the largest and smallest predicted amounts of intermediate. The lowest bromine concentrations used represent a practical limit for the spectrophotometric determination of bromine. The standard deviations for the correlation neglecting the presence of intermediates are as small as can reasonably be expected when considered relative to the uncertainties in the absorbance measurements and the analytical determinations. Hence one concludes that under the conditions of this study mixed valence state intermediates are not present at concentrations sufficiently high to be detected spectrophotometrically around 300 nm. The absorbances observed in this region of the spectrum can be correlated satisfactorily using reported thermodynamic data for FeBr_3 and Fe_2Br_6 which appear to be the dominant species in the range of the study.

Supplementary Material Available: Tables I–III containing data and results of absorbance study of FeBr_2 and FeBr_2–Br_2 mixtures, and calculated partial pressures including estimates for Fe_3Br_8 with revised values of K_4 (5 pages). Ordering information is available on any current masthead page.

References and Notes

(1) N. W. Gregory and B. A. Thackrey, *J. Am. Chem. Soc.*, **72**, 3176 (1950).
(2) N. W. Gregory and R. O. MacLaren. *J. Phys. Chem.*, **59**, 110 (1955).
(3) E. W. Dewing, *Metall. Trans.*, **1**, 2169 (1970).
(4) H. Schafer, *Z. Anorg. Allg. Chem.*, **403**, 106 (1974).
(5) M. Binnewies and H. Schafer, *Z. Anorg. Allg. Chem.*, **407**, 327 (1974).
(6) G. N. Papatheodorou, *Z. Anorg. Allg. Chem.*, **411**, 153 (1975).
(7) G. N. Papatheodorou, *J. Phys. Chem.*, **77**, 472 (1973); *Inorg. Chem.*, **12**, 1899 (1973).
(8) H. Schafer, *Angew. Chem.*, **15**(12), 713 (1976).
(9) J. D. Christian and N. W. Gregory, *J. Phys. Chem.*, **71**, 1579 (1967).
(10) Analyses performed by Dr. Eric Knudsen and Mr. David Johnson.
(11) Y. Sakisaka, T. Ishii, and T. Sagawa, *J. Phys. Soc. Jpn.*, **36**(5), 1365 (1974).
(12) C. W. DeKock and D. M. Gruen, *J. Chem. Phys.*, **49**, 4521 (1968).
(13) B. D. Bird and P. Day, *J. Chem. Phys.*, **49**, 392 (1968).
(14) R. J. Sime and N. W. Gregory, *J. Phys. Chem.*, **64**, 86 (1960).
(15) R. F. Porter and R. C. Schoonmaker, *J. Phys. Chem.*, **63**, 626 (1959).
(16) Tables of experimental and calculated results are available as supplementary material. See paragraph at end of text regarding supplementary material.
(17) A. A. Passchier, J. D. Christian, and N. W. Gregory, *J. Phys. Chem.*, **71**, 937 (1967).
(18) H. McConnell and N. Davidson, *J. Am. Chem. Soc.*, **72**, 5557 (1950).
(19) M. B. Robin, *Inorg. Chem.*, **1**, 337 (1962).

Quenching of Singlet Oxygen by Aliphatic Amines[1]

Bruce M. Monroe

*Central Research and Development Department,[1] E. I. du Pont de Nemours and Company, Wilmington, Delaware 19898
(Received May 16, 1977)*

Publication costs assisted by E. I. du Pont de Nemours and Company

Rate constants for the quenching of singlet oxygen ($^1O_2$) for 22 aliphatic amines were measured by following inhibition of the self-sensitized photooxidation of rubrene in chloroform. In agreement with earlier studies, a correlation of quenching rate with amine ionization potential was found for amines with unbranched alkyl groups. However, substitution of the carbon α to the nitrogen reduces the quenching rate from that predicted by the ionization potential indicating that $^1O_2$ quenching is sensitive to steric effects. Typical rates are as follows: Et$_3$N, 6.5×10^7 L/mol s; Dabco, 5.2×10^7; Et$_2$NH, 1.5×10^7; and n-PrNH$_2$, 2.3×10^5. No measurable quenching ($k_q < 2 \times 10^5$) was observed for 2,2,6,6-tetramethyl-4-piperidinol (6) and N-(2-hydroxyethyl)-2,2,6,6-tetramethylpiperidine (9).

Amines are well known as quenchers of singlet oxygen ($^1O_2$). Since the initial discovery that 1,4-diazobicyclo-[2.2.2]octane (Dabco)[2] is a quencher of $^1O_2$, rate studies of $^1O_2$ quenching by aliphatic amines have been carried out in the gas phase[3] and in solutions of fluorocarbon-113[4] and methanol.[5] In general, a correlation between quenching rate ($k_q^{^1O_2}$) and ionization potential, with $k_q^{^1O_2}$ increasing as the ionization potential of the amine decreased, was observed. To investigate more fully the relationship between structure, ionization potential, and $k_q^{^1O_2}$, a technique has been developed which can rapidly and accurately measure $k_q^{^1O_2}$ and the quenching rates for a number of aliphatic amines determined.

Experimental Section

Materials. Rubrene (Aldrich) and chloroform (Fischer Certified Reagent) were used as received. Unless otherwise indicated, all the amines were commercial materials purified by distillation prior to use.

N-(2-Hydroxyethyl)-2,2,6,6-tetramethylpiperidine (9) was prepared by the reaction of equimolar amounts of 2,2,6,6-tetramethylpiperidine and ethylene oxide in a pressure vessel at 100 °C for 1 h, 120 °C for 1 h, and 150 °C for 8 h: mp 95 °C (lit. 96–98 °C).[6]

N-(2-Acetoxyethyl)-2,2,6,6-tetramethylpiperidine (10) was prepared from 9 by acetylation with acetic anhydride. A distillable oil was obtained. Anal. Calcd for C$_{13}$H$_{25}$NO$_2$: C, 68.68; H, 11.08; N, 6.16. Found: C, 68.70; H, 11.01; N, 6.32.

1-Methoxy-2-(N,N-diethylamino)ethane (3) was prepared from N,N-diethylaminoethanol by methylation with dimethyl sulfate: bp 136 °C (lit. 136 °C).[7]

Preparation of Solutions. Stock solutions of rubrene (8×10^{-4} M) (OD 546.1 nm ~ 4) were prepared by dissolving weighed amounts of rubrene in measured volumes of chloroform. To assure that the solutions with and without quencher had the same initial rubrene concentration, a weighed amount of quencher was dissolved in a measured volume of the stock solution. If necessary, the solution containing quencher was diluted with stock solution to the proper concentration of quencher. All rubrene solutions were shielded from light as much as practical during preparation. The volumetric flasks were wrapped in aluminum foil and much of the work was done in a laboratory with yellow lights. The solutions were not stored but were irradiated immediately after preparation.

A fresh stock solution was made up for each run.

Irradiation of Samples. To ensure that each sample received the same amount of light, the samples were irradiated on a "merry-go-round" apparatus[8] modified so that the turntable contained six 1-cm square holes. These permitted the samples to be irradiated directly in 1-cm UV cells. The 546.1-nm line of a Hanovia 679A36 450-W medium-pressure mercury vapor lamp was isolated by a combination of Corning C.S. no. 1-60, 3-68, and 4-72 filters.

Three-milliliter samples of rubrene in chloroform, with and without added quencher, were pipetted into 1-cm Pyrex ultraviolet absorption cells. These samples were irradiated simultaneously on the merry-go-round from 7 to 10 min, depending on the light intensity. Six samples, two with no quencher and two each of two different quencher concentrations, were irradiated at one time. The samples were open to the air during irradiation to allow oxygen to diffuse in to replace the oxygen consumed during the reaction.

At the concentration of rubrene used, a 1-cm pathlength absorbs 99.99% of the incident light. Irradiation was carried out until approximately half the rubrene had been consumed in the sample without quencher so that 99% of the incident light was still being absorbed. The quencher concentration was adjusted so that about one quarter of the rubrene was consumed in the sample with quencher. If the amount of reaction was less than 20% or more than 80% of the amount of reaction in the unquenched solution, the determination was repeated with a less or more concentrated quencher solution. To determine $k_q^{^1O_2}$ in oxygen-saturated chloroform, the samples were bubbled with oxygen for 2 min and tightly stoppered before irradiation.

Analysis and Calculation of Rate Constants. The optical density of samples at 440 nm (ϵ 2300) both before and after irradiation was measured on a Cary 14 spectrophotometer and the rubrene concentrations were calculated. Quenching constants were calculated by substitution of the quencher concentration and initial and final rubrene concentrations into eq 8.

Fluorescence Lifetimes. Fluorescence lifetimes were determined by phase shift using a modulated nitrogen lamp.[9]

Results and Discussions

In their study of $^1O_2$ quenching by transition metal chelates, Carlsson, Suprunchuk, and Wiles[10] developed a procedure for the determination of singlet oxygen
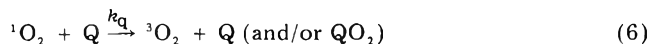
quenching constants based on inhibition of the oxidation of rubrene. A stream of $^1O_2$, generated by microwave discharge, is split into two equal streams and each stream passed over a stirred solution of rubrene in hexadecane, one containing quencher and one without. Quenching rate constants can be calculated from the difference in the amount of rubrene oxidized. Since microwave generation of $^1O_2$ requires low pressure (6 mmHg), this procedure cannot be used with volatile solvent or quenchers. Therefore, a procedure which employs a similar approach has been developed.

Our technique is based on inhibition of the self-sensitized photooxidation of rubrene. Rubrene (1) is an orange

1   2
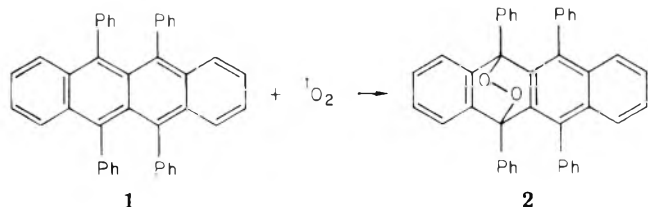
hydrocarbon which reacts cleanly with $^1O_2$ to form a colorless photoperoxide (2). When a solution of rubrene is irradiated in the presence of oxygen and a singlet oxygen quencher, the following reactions taken place:[11,12]

$$R + h\nu \rightarrow R^1 \tag{1}$$

$$R^1 + O_2 \xrightarrow{k_s} R^3 + {}^1O_2 \tag{2}$$

$$R^3 + {}^1O_2 \xrightarrow{k_t} R + {}^1O_2 \tag{3}$$

$${}^1O_2 \xrightarrow{k_d} {}^3O_2 \tag{4}$$

$${}^1O_2 + R \xrightarrow{k_{ox}} RO_2 \tag{5}$$

$${}^1O_2 + Q \xrightarrow{k_q} {}^3O_2 + Q \text{ (and/or } QO_2) \tag{6}$$

where R is rubrene, R^1 is the rubrene singlet, R^3 is the rubrene triplet, RO_2 is the rubrene photoperoxide, Q is the quencher, and QO_2 is the oxidation product of the quencher. Note that rubrene is both the sensitizer and $^1O_2$ acceptor.

If a quencher is present, $^1O_2$ disappears by three routes: nonradiative decay (reaction 4), reaction with rubrene (reaction 5), and quenching (reaction 6). In the absence of a quencher $^1O_2$ disappears by only two routes: nonradiative decay and reaction with rubrene.

Carlsson[10] has shown that, if two solutions of equal volume, one containing quencher and one without quencher and each having the same initial concentration of rubrene, are each exposed to the same amount of $^1O_2$, k_q can be calculated from the following equation:

$$k_q{}^1O_2 = \frac{k_{ox}([R]_F^Q - [R]_F^0) + k_d \ln ([R]_F^Q/[R]_F^0)}{[Q] \ln ([R]/[R]_F^Q)} \tag{7}$$

where [R] is the initial concentration of rubrene, $[R]_F^Q$ the final concentration of rubrene in the quenched solution, $[R]_R^0$ the final concentration of rubrene in the unquenched solution, and [Q] the quencher concentration.

It is seen that k_q can be calculated from four experimentally determinable quantities and two rate constants. Both the lifetime of $^1O_2$ ($1/k_d$)[13-15] and the rate of addition of $^1O_2$ to rubrene (k_{ox})[16] have been measured in a number of solvents. Rate determinations were carried out in chloroform because the relatively long lifetime of $^1O_2$ in this solvent allows measurements to be made at low amine

concentrations, thus minimizing potential complications which might arise from quenching of rubrene-excited states by the added quenchers.

Large errors will be introduced into the measured quenching constant if the rubrene excited states are quenched by the amine. In nondegassed chloroform a less than 1% change in rubrene fluorescence lifetime (13.8 ns) was observed in the presence of 0.2 M triethylamine or of 0.4 M n-propylamine. This indicates that the singlet quenching rates are less than 4×10^6 and 2×10^6 L/mol s, respectively. As a further check for excited state quenching, the rate constants for triethylamine and isobutylamine were redetermined using oxygen-saturated solutions.[5] Within experimental error the same values were obtained.

It is important to point out that this technique only measures the rate at which an additive removes $^1O_2$ from the system, not how it removes it. Without analysis of the products it is not possible to tell if the added compound quenches $^1O_2$ but is itself unchanged and/or reacts with $^1O_2$ to form an oxidation product (QO_2). The measured rate constant is actually the sum of the rate constants for quenching and for reaction with $^1O_2$. For compounds which are known to undergo oxidation with $^1O_2$, this technique can be used to measure oxidation rate constants.[17]

Determination of k_{ox}. The ratio of the decay rate of $^1O_2$ (k_d) to its rate of reaction with an acceptor (k_{ox}), a parameter called β, is a function of both the solvent and the acceptor.[18,19] Physically, β measures the concentration of acceptor at which half the $^1O_2$ will be trapped. It can be determined from an experiment in which solutions containing different concentrations of acceptor in the same solvent are exposed to the same amount of singlet oxygen. A plot of the reciprocal of the amount of singlet oxygen product formed vs. the reciprocal of acceptor concentration gives a straight line whose intercept is the amount of $^1O_2$ formed. β is given by the ratio of the slope to the intercept.

Five different determinations of β for rubrene in chloroform were made with rubrene varying from 4.13×10^{-4} to 8.63×10^{-4} M in four runs and from 4.8×10^{-4} to 1.6×10^{-3} M in the fifth. In each determination a set of samples with varying rubrene concentrations was irradiated at the same time on the merry-go-round. Rubrene disappearance was assumed to equal product appearance since rubrene does not undergo any other reaction with oxygen under these conditions. Since product formation is measured by the difference between two optical densities, it was necessary to run the reaction until about 20% of the rubrene had been consumed. For each sample the average of the initial and final concentrations was used.

From the five determinations a β of $(3.12 \pm 0.41) \times 10^{-4}$ M was found. From this value and the lifetime of $^1O_2$ in chloroform (60×10^{-6} s) measured by Merkel and Kearns,[14] a k_{ox} of $(5.3 \pm 0.7) \times 10^7$ L/mol s is calculated. This compares with a value of $(4.2 \pm 1.2) \times 10^7$ L/mol s for rubrene in chloroform measured by Stevens and Perez.[16] Substitution of these values into eq 7 gives

$$k_q{}^1O_2 = \frac{5.3 \times 10^7([R]_F^Q - [R]_F^0) + 1.7 \times 10^4 \ln ([R]_F^Q/[R]_F^0)}{[Q] \ln ([R]/[R]_F^Q)} \tag{8}$$

Since quenching constants are measured relative to the rate of reaction of $^1O_2$ with rubrene, the values of k_{ox} and, consequently, k_q ultimately depend on the value of k_d determined by Merkel and Kearns.

TABLE I: $k_q{}^1O_2$ for Aliphatic Amines

Amine	$k_q{}^1O_2$,[a] L/mol s	IP,[b] eV
Et$_3$N	6.5×10^7	8.08
n-Bu$_3$N	5.8×10^7	7.90
N-Methylpiperidine	5.3×10^7	8.29
Dabco	5.2×10^7	7.52[c]
$(n$-Pr$)_2$NH	1.8×10^7	8.54
Et$_2$NH	1.5×10^7	8.63
Piperidine	5.8×10^6	8.66
$(i$-Pr$)_2$NH	1.8×10^6	8.40
i-BuNH$_2$	4.1×10^5	9.30
n-BuNH$_2$	2.4×10^5	d
n-PrNH$_2$	2.3×10^5	9.40

[a] Values ±10%. [b] From ref 20. [c] Energy of first maximum in the photoelectron spectrum. [d] Ionization potential not reported in ref 20.
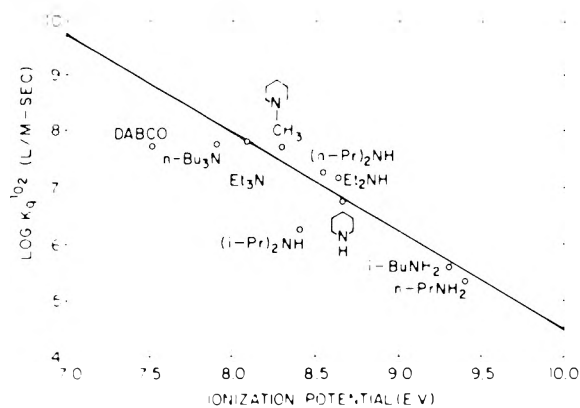

Figure 1. Plot of the log of the singlet oxygen quenching rate vs. amine ionization potential.

Effect of Ionization Potential. Singlet oxygen quenching rate constants were determined for a series of ten aliphatic amines (Table I) whose ionization potentials had been determined in a recent study by Aue, Webb, and Bowers.[20] A plot of log $k_q{}^1O_2$ vs. ionization potential is given in Figure 1. With the exception of Dabco and diisopropylamine a reasonable correlation between log $k_q{}^1O_2$ and ionization potential is observed.

It has been proposed that the quenching of $^1O_2$ by amines involves partial charge transfer from the amine to $^1O_2$. The correlation between log k_q and ionization potential observed in this work is consistent with the suggestion that quenching occurs by a charge transfer process and with the correlations between log $k_q{}^1O_2$ and ionization potential which have been previously found in other solvents.[3-5]

Evans[21] has demonstrated that for charge transfer quenching the quantity log $[k_q/(k_d - k_q)]$, where k_q is the quenching rate and k_d is the diffusion rate, rather than log k_q, should vary linearly with quencher ionization potential. However, since $k_d \gg k_q$ for all the compounds investigated here, such a plot would be identical with Figure 1, with the Y axis shifted by $-\log k_d$.

The effect of a β substituent on $K_q{}^1O_2$ was investigated for a series of variously substituted N,N-diethylamines. These values are tabulated in Table II along with the polar substituent constants for aliphatic systems. Although interpretation of these data is not straightforward since the magnitude of the effect of the substituent on the ionization potential of the amine cannot be precisely ascertained, electron-withdrawing substituents, which should increase the ionization potential of the amine, decrease the quenching rate. 7-(Diethylamino)-1-heptylamine, which possesses a slightly electron-donating

TABLE II: Effect of a β-Substituent on $K_q{}^1O_2$

Amine	$k_q{}^1O_2$, L/mol s	β-substituent	$\sigma_I{}^a$
Et$_3$N	6.5×10^7	$-$H	0
Et$_2$N(CH$_2$)$_7$NH$_2$	6.1×10^7	$-$(CH$_2$)$_5$NH$_2$	-0.05[b]
Et$_2$N(CH$_2$)$_2$OCH$_3$	3.8×10^7	$-$OCH$_3$	$+0.26$
Et$_2$N(CH$_2$)$_2$OH	3.0×10^7	$-$OH	$+0.25$
Et$_2$N(CH$_2$)$_2$CN	2.7×10^7	$-$CN	$+0.56$

[a] Polar substituent for aliphatic systems. From ref 22. [b] Constant for the ethyl group.

TABLE III: Steric Effect on $k_q{}^1O_2$

Amine	$k_q{}^1O_2$, L/mol s
CH$_3$N(CH$_2$CH$_2$OH)$_2$	2.1×10^7
(CH$_3$)$_3$CN(CH$_2$CH$_2$OH)$_2$	1.1×10^6

TABLE IV: $k_q{}^1O_2$ for Substituted Piperidines[a]

[a] In L/mol s. [b] No measurable quenching. [c] Rate of oxidation.[24]

long chain alkyl group, has a rate within experimental error of that for triethylamine. The substituent constant for this compound has been estimated by that for the ethyl group since the $-$NH$_2$ group, which is separated from the diethylamino group by seven carbon atoms, probably has little effect on the quenching rate. A strong correlation between quenching rate and substituent constant has been found for a series of para-substituted N,N-dimethylanilines in methanol.[23]

Steric Effect. From Figure 1 it can be seen that the measured $k_q{}^1O_2$ for diisopropylamine is a factor of 10 lower than what would have been predicted from its ionization potential. Since this might indicate that singlet oxygen quenching is susceptible to steric inhibition, this possibility was investigated more fully with hindered amines. Comparison of the rates for the methyl and *tert*-butyl substituted N,N-di-(2-hydroxyethyl)amines (Table III) indicates that replacement of an α-methyl group by an α-*tert*-butyl group reduces $k_q{}^1O_2$ by a factor of 20. This effect cannot be due to a change in ionization potential. Since the ionization potential of *tert*-butylamine is lower than that of methylamine by 0.4 eV,[20] the ionization potential of the *tert*-butyl compound should be lower than that of the methyl derivative.

To explore the steric effect more fully, quenching rates were determined for a series of piperidines and N-substituted piperidines (Table IV). The $k_q{}^1O_2$ for 2,6-dimethylpiperidine (**5**) is slightly lower than that for piperidine (**4**) indicating that introduction of a methyl group

TABLE V: Quenching Rates in Different
Solvents (× 10^7 L/mol s)

Amine	CH-Cl$_3$[a]	CH$_3$-OH[b]	CH$_3$-OH[c]	C$_6$H$_6$[c]	CS$_2$[c]	Fluoro-carbon-113[d]
Et$_3$N	6.5	1.5				0.21
Dabco	5.2	1.2	2.2	4.4	2.9	
Et$_2$NH	1.5	0.3				0.057
Piperidine	0.58	0.15				

[a] This work. [b] Calculated from β values in ref 5 and a lifetime of 7×10^{-6} s for $^1O_2$ in CH$_3$OH (from ref 14). [c] Calculated from β values in ref 28 and lifetimes given in ref 14. [d] Reference 4. (These values have been questioned, see ref 31.)

on each carbon α to the nitrogen atom inhibits quenching slightly. However, no quenching was observed with the 2,2,6,6-tetramethyl derivative 6. This suggests that the nitrogen atom and the $^1O_2$ molecule must come into close proximity, an observation consistent with a charge transfer quenching mechanism. A similar loss of quenching ability on α substitution was seen with the N-substituted derivatives 7, 9, and 10.

An unexpectedly high quenching rate, higher than that measured for triethylamine, was measured for the N-methyl derivative 8. It is known that this compound is efficiently oxidized by $^1O_2$ to an N-demethylated product.[24] The measured "quenching rate" is actually an oxidation rate since rates of these two processes cannot be distinguished by this method (vida supra).

Oxidation of amines by $^1O_2$ is well known.[24-27] Smith found that in pyridine solution triethylamine both quenches and is oxidized by $^1O_2$ with oxidation occurring about 10% of the time.[25] The mechanism of this oxidation has been discussed by Gollnick and Lindner.[26] For some reason the methyl group of 8 is readily attacked by $^1O_2$ while the N-2-hydroxyethyl and N-2-acetoxyethyl groups of 9 and 10 are not. While various mechanisms involving the nitrogen, $^1O_2$ molecule, and the methyl group could be written to rationalize this observation, in the absence of further data, they would be merely rationalizations since the factors which control partition between quenching and oxidation are not well understood.

Solvent Effects. Quenching constants for several of the amines in Table I have also been measured in other solvents. These values are summarized in Table V. Quenching rates in chloroform are higher than the corresponding rates in methanol by about a factor of 4. This suggests that, since the amine is hydrogen bonded to the solvent, it is a slightly less efficient quencher in methanol. The measured rates of di- and triethylamines are about a factor of 30 higher than the corresponding rates in fluorocarbon-113. Similar discrepancies have been discerned by other workers between rate constants measured in fluorocarbon-113 and those determined in other solvents.[28-31] Foote and Ching,[31] for example, found that the oxidation rate of bilirubin in chloroform was forty times

greater than that measured in fluorocarbon-113. It has been suggested that the reason for the discrepancy lies in a systematic error in the technique used to measure these rates rather than in a solvent effect.[31]

Conclusion

The rate of singlet oxygen quenching by aliphatic amines depends on two factors: (1) the ionization of potential of the amine, $k_a^{1O_2}$, increasing with decreasing ionization potential; and (2) the amount of substitution on the carbon atoms α to the nitrogen atom. Close approach of the nitrogen to the $^1O_2$ molecule must be necessary since highly hindered amines show no measurable quenching.

References and Notes

(1) Presented at the 172nd National Meeting of the American Chemical Society, San Francisco, Calif., Aug 29-Sept 3, 1976.
(2) C. Ouannès and T. Wilson, *J. Am. Chem. Soc.*, **90**, 6527 (1968).
(3) E. A. Ogryzlo and C. W. Tang, *J. Am. Chem. Soc.*, **92**, 5034 (1970); K. Fuwkawa and E. A. Ogryzlo, *Chem. Phys. Lett.*, **12**, 370 (1971).
(4) I. B. C. Matheson and J. Lee, *J. Am. Chem. Soc.*, **94**, 3310 (1972).
(5) R. H. Young, R. L. Martin, D. Feriozi, D. Brewer, and R. Kayser, *Photochem. Photobiol.*, **17**, 233 (1973).
(6) R. B. Moffett and B. D. Aspergren, *J. Am. Chem. Soc.*, **82**, 1604 (1960).
(7) F. F. Blicke and D. G. Sheets, *J. Am. Chem. Soc.*, **71**, 2856 (1949).
(8) F. G. Moses, R. S.-H. Liu, and B. M. Monroe, *Mol. Photochem.*, **1**, 245 (1969).
(9) B. M. Monroe, C.-G. Lee, and N. J. Turro, *Mol. Photochem.*, **6**, 271 (1974).
(10) D. J. Carlsson, T. Suprunchuck, and D. M. Wiles, *Can. J. Chem.*, **52**, 3728 (1974); D. J. Carlsson, G. D. Mendenhall, T. Suprunchuck, and D. M. Wiles, *J. Am. Chem. Soc.*, **94**, 8960 (1972).
(11) B. Stevens and J. A. Ors, *J. Phys. Chem.*, **80**, 2164 (1976).
(12) Unpublished work by A. Yee and G. S. Hammond has shown that rubrene singlet does not undergo any measurable amount of intersystem crossing to the triplet state. G. S. Hammond, private communication.
(13) D. R. Adams and F. Wilkinson, *J. Chem. Soc., Faraday Trans. 2*, **68**, 586 (1972).
(14) P. B. Merkel and D. R. Kearns, *J. Am. Chem. Soc.*, **94**, 7244 (1972).
(15) R. H. Young, D. Brewer, and R. A. Keller, *J. Am. Chem. Soc.*, **95**, 375 (1973).
(16) B. Stevens and S. R. Perez, *Mol. Photochem.*, **6**, 1 (1974).
(17) A similar procedure has been used to measure the quenching rate of singlet oxygen by α-tocopherol. S. R. Fahrenholtz, F. H. Doleiden, A. M. Trozzolo, and A. A. Lamola, *Photochem. Photobiol.*, **20**, 505 (1974).
(18) R. Higgins, C. S. Foote, and H. Cheng, *Adv. Chem. Ser.*, No. 77, 102 (1968).
(19) C. S. Foote and R. W. Denny, *J. Am. Chem. Soc.*, **93**, 5168 (1971).
(20) D. H. Aue, H. M. Webb, and M. T. Bowers, *J. Am. Chem. Soc.*, **98**, 311 (1976).
(21) T. R. Evans, *J. Am. Chem. Soc.*, **93**, 2081 (1971).
(22) S. L. Murov, "Handbook of Photochemistry", Marcel Dekker, New York, N.Y., 1973, p 203.
(23) R. H. Young, D. Brewer, R. Kayser, R. Martin, D. Feriozi, and R. A. Keller, *Can. J. Chem.*, **52**, 2889 (1974).
(24) D. Bellus, H. Lind, and J. F. Wyatt, *Chem. Commun.*, 1199 (1972).
(25) W. F. Smith, Jr., *J. Am. Chem. Soc.*, **94**, 186 (1972).
(26) K. Gollnick and J. H. E. Lindner, *Tetrahedron Lett.*, 1903 (1973).
(27) R. S. Davidson and K. R. Trethewey, *J. Chem. Soc., Chem. Commun.*, 674 (1975); *J. Chem. Soc., Perkin Trans. 2*, 169, 173, 178 (1977).
(28) C. S. Foote, E. R. Peterson, and K.-W. Lee, *J. Am. Chem. Soc.*, **94**, 1032 (1972).
(29) I. B. C. Matheson, J. Lee, B. S. Yamanaski, and M. L. Wolbarsht, *J. Am. Chem. Soc.*, **96**, 3343 (1974).
(30) P. B. Merkel and D. R. Kearns, *J. Am. Chem. Soc.*, **97**, 462 (1975).
(31) C. S. Foote and T.-Y. Ching, *J. Am. Chem. Soc.*, **97**, 6209 (1975).

Temperature Dependence of the Recombination Fluorescence of Photoionized Indole and N,N,N',N'-Tetramethyl-p-phenylenediamine in Organic Glasses. Consequences of Electron Tunneling and Diffusion

K. K. Ho and Larry Kevan*

Department of Chemistry, Wayne State University, Detroit, Michigan 48202 (Received March 4, 1977)

The recombination fluorescence seen when TMPD is photoionized in methylcyclohexane, 3-methylhexane, and 2-methyltetrahydrofuran glasses and when indole is photoionized in 2-propanol and ethanol glasses has been investigated. The initial intensity and decay rate of the recombination fluorescence decreases as the UV irradiation temperature is increased from temperatures below the glass transition temperature T_g of the matrix. This is interpreted in terms of electron tunneling to the cation in which the tunneling barrier height or electron trap depth increases slightly (0.05–0.2 eV) with increasing irradiation temperature. By considering how the matrix polarity affects the degree of electron trap deepening as well as the electron trap depth relative to the excited singlet level of the solute, we are able to understand the difference in magnitudes and their changes for the initial decay rate and the initial recombination fluorescence. At temperatures 10–30 K above T_g, depending on the matrix polarity, diffusive recombination dominates tunneling recombination and produces a peak in the recombination fluorescence unless the electron trap depth has dropped below the excited singlet of the solute. Thus, this type of experiment offers a simple diagnostic for distinguishing tunneling and diffusive recombination of electrons with cations in disordered matrices.

Introduction

The objective of this work is to explore the recombination mechanisms of electrons with cations in organic glassy matrices. In particular, we describe a new type of experiment that allows easy distinction between tunneling and diffusive recombination mechanisms. To study this problem we generate electrons and cations by ultraviolet (UV) photoionization of a heterocyclic amine in a glassy matrix. The ejected electrons are initially trapped and localized by potential minima in the disordered glassy matrix and these localized electrons can further deepen their potential well by inducing molecular orientation of the surrounding molecules.[1-4] Some of these localized electrons recombine with their parent ions to produce delayed luminescence which consists of both fluorescence and phosphorescence.[5-11] The fluorescence is usually less prominent in polar matrices where the electron trap depths are larger than in nonpolar matrices.

Directly excited UV phosphorescence of the solute molecule in organic glasses typically has a lifetime of several seconds. Thus the initial recombination process cannot be studied by measuring the total luminescence intensity or the recombination phosphorescence because the timescale is too long. However, the directly excited UV fluorescence of the solutes have typically short lifetimes of less than 10 ns; so by studying the much weaker recombination fluorescence intensity the initial recombination process can be probed.

In a previous study we investigated the temperature dependence of the recombination fluorescence of photoionized tryptophan in ethylene glycol/water and 9 M LiCl aqueous glasses and found that the initial recombination fluorescence decay rate decreased with increasing temperature at temperatures below the glass transition temperature of the matrix.[12] This behavior was interpreted in terms of a tunneling recombination between the electron and cation and stood in considerable contrast to the temperature dependence of the recombination phosphorescence observed previously in the same matrix.[13] The recombination phosphorescence in this same matrix oc-

curred on a longer timescale and could be interpreted in terms of diffusive recombination of the electrons with the cation. In the present work we have extended these studies to a variety of organic glasses comprising both polar glasses such as alcohols and nonpolar glasses such as alkanes in which the depth of the electron trap varies rather drastically. From the analysis of these experiments we have been able to distinguish tunneling and diffusive recombination mechanisms between electrons and cations and to delineate how these processes depend upon matrix polarity and upon the depth of the electron trap relative to the singlet level of the solute.

Experimental Section

Purification of the solvents and solutes has been described.[7,14,15] All the samples were prepared with a solute concentration of 1.5×10^{-3} M. The samples were sealed in 3-mm i.d. Spectrosil quartz tubes after repeated freeze–pump–thaw degassing cycles and a copper–constantin thermocouple was attached tightly to the outside wall of the sample tube. Samples were transferred from liquid nitrogen into a quartz dewar in which the temperature was regulated by the flow rate of cold helium gas. In this way temperatures below 77 K were conveniently attained. The photoionizing light source was an air-cooled Phillips SP 900 high-pressure mercury lamp with a filter system consisting of Corning filter No. 7-54 plus 2 mm of Pyrex glass; this gives light in the range 290–400 nm. This light could photoionize both solutes in the various matrices used. Irradiation of a pure solvent with this light gives only negligible background luminescence.

As described previously,[12] the luminescence was detected by a 1P 28 photomultiplier with its output fed to an oscilloscope after the irradiation light was interrupted by a magnetically controlled shutter. Great care was taken to eliminate solute phosphorescence when the recombination fluorescence was studied. For indole the following filter combination was found to transmit only fluorescence: Corning filters No. 7-54 and No. 7-60 plus 2-mm Pyrex glass plus 1.5-cm saturated $NiSO_4$ in water. For N,N,-
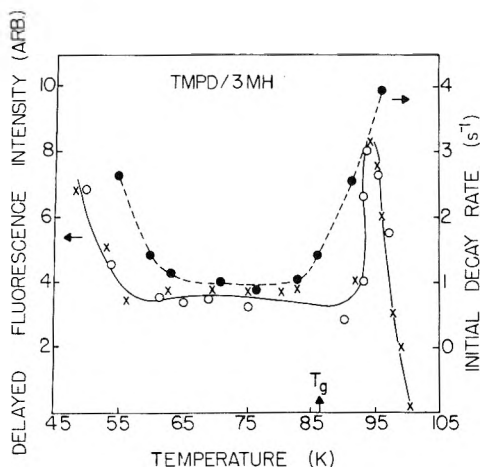
Figure 1. Initial intensity and initial decay rate of the UV induced recombination fluorescence of TMPD in 3-methylhexane vs. UV irradiation temperature. The open circles and X's are for two different runs and show the reproducibility.

N',N'-tetramethyl-p-phenylenediamine (TMPD) a filter combination of Corning filters No. 5-61 and No. 7-60 was used.

Directly excited fluorescence emission spectra were measured on an Aminco Model 1000 spectrophotofluorimeter.

Results

Figure 1 shows the temperature dependence of the initial recombination fluorescence intensity measured 100 ms after the UV photoionizing light was interrupted for TMPD in 3-methylhexane (3MH) glass from 45 to 100 K. From 45 to 55 K the initial recombination fluorescence intensity decreases by about a factor of 2. This intensity then plateaus at higher temperatures until the glass transition region is reached at which point the initial fluorescence intensity increases and goes through a maximum; beyond 100 K no recombination fluorescence is observable. Recall that each one of these points represents a new photoionization and a separate experiment. In addition to the initial fluorescence intensity, Figure 1 also shows the initial decay rate vs. temperature at which the photoionization is carried out. The decay curves are nonexponential as has been found previously for other matrices.[5-12] Therefore, an initial decay rate is defined as the tangent to the decay curves over the first one second of decay. As seen in Figure 1 the initial decay rate also decreases with temperature at low temperatures, plateaus in the middle temperature range, and then increases rather steeply above the glass transition temperature.

Essentially the same behavior is observed for the initial recombination fluorescence intensity and the initial decay rate for TMPD in methylcyclohexane (MCH) glass (Figure 2). Since both 3-methylpentane and methylcyclohexane are alkane glasses one would expect similar behavior. Figure 3 shows TMPD in 2-methyltetrahydrofuran (MTHF) glass which is a weakly polar glass. Here qualitatively the same kinds of effects are observed except that the decrease in the initial fluorescence intensity is considerably greater and amounts to nearly a factor of 10. Also the peak in the high temperature region in the initial fluorescence intensity is shifted to temperatures somewhat higher than the glass transition temperature. This is in contrast to the location of this peak in the alkane matrices where it occurred rather close to the glass transition temperature. Although the initial fluorescence intensity shows a more dramatic change with temperature in MTHF than in the alkane glasses the initial decay rate of the
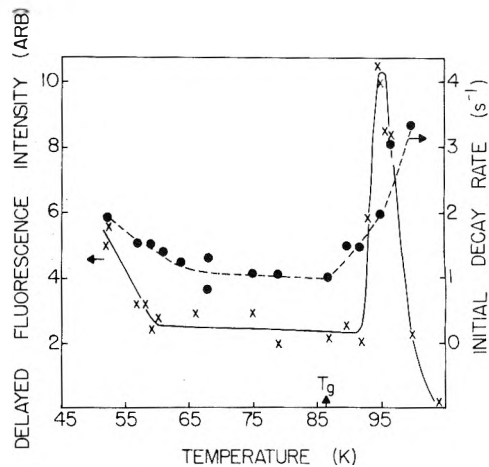

Figure 2. Initial intensity and initial decay rate of the UV induced recombination fluorescence of TMPD in methylcyclohexane vs. UV irradiation temperature.
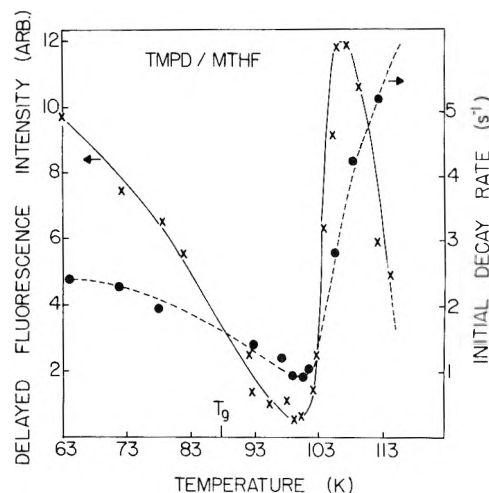

Figure 3. Initial intensity and initial decay rate of the UV induced recombination fluorescence of TMPD in 2-methyltetrahydrofuran vs. UV irradiation temperature.
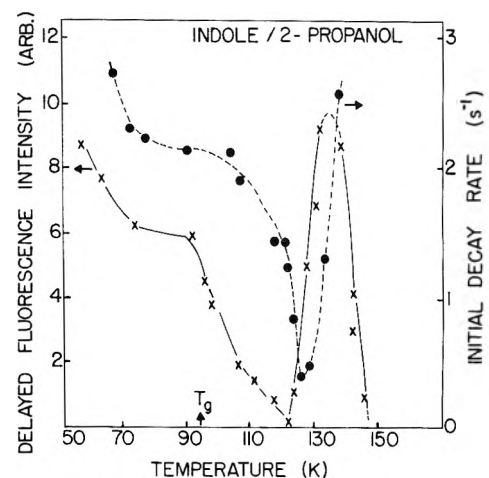

Figure 4. Initial intensity and initial decay rate of the UV induced recombination fluorescence of indole in 2-propanol vs. UV irradiation temperature.

recombination fluorescence decreases by a factor of 2 in MTHF which is similar to that found in the alkane glasses.

Figure 4 shows similar results for indole in 2-propanol glass. The same qualitative features are observed in this polar glass as seen in MTHF. The initial fluorescence intensity decreases by about a factor of 10 before going through the peak above the glass transition temperature. There also appears to be a small plateau in the initial
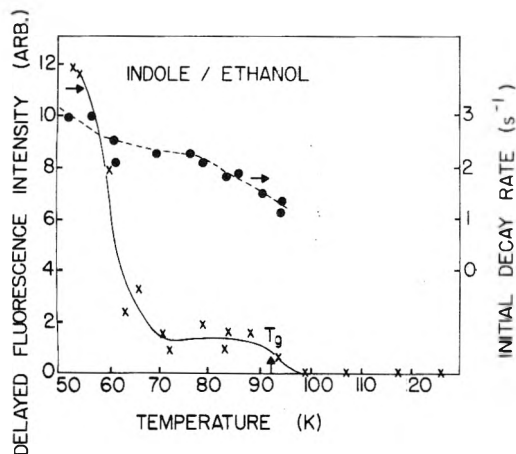
Figure 5. Initial intensity and initial decay rate of the UV induced recombination fluorescence of indole in ethanol vs. UV irradiation temperature.

Figure 6. Fluorescence intensity from direct UV excitation of indole in 2-propanol (O), tryptophan in ethanol (●), and TMPD in MTHF (▲) vs. temperature. The exciting wavelengths were 272, 270, and 310 nm, respectively.

fluorescence intensity decrease shortly before the glass transition temperature. The initial decay rate decreases by a considerably greater fraction in this glass, by about a factor of 5, before it begins to increase again at higher temperatures, coincident with the peak in the fluorescence intensity curve. The total integrated relative intensity of the recombination fluorescence in nonpolar matrices such as 3MP and MCH is about one-third the same integrated intensity from polar matrices such as MTHF and 2-propanol. This seems consistent with previously observed matrix polarity effects on the electron trapping efficiency.

Figure 5 shows results for indole in ethanol glass. Here the results are distinctly different than in the previous matrices. The initial fluorescence intensity shows a decrease by about a factor of 10 and then a slight plateau before the glass transition temperature. However, at higher temperatures the ethanol recombination fluorescence is not detectable and consequently there appears to be no peak in the initial fluorescence intensity curve at temperatures above the glass transition temperature. Similarly the initial decay rate decreases by about a factor of 2.5 over the temperature range for which the recombination fluorescence is observable. In general the behavior of indole in ethanol glass is very similar to that found previously for tryptophan in ethylene glycol/water (1:1 by volume) glass.[12] It is noteworthy that ethanol and ethylene glycol/water are the most polar of the organic glasses studied.

In order to be sure that the recombination fluorescence intensity decrease with increasing temperature in the low temperature region is not solely a temperature effect of the solute fluorescence, the temperature dependence of the directly excited fluorescence emission spectra of TMPD in MTHF, indole in 2-propanol. and tryptophan in ethanol were measured. Tryptophan was used in place of indole in ethanol for solubility reasons but tryptophan and indole are expected to behave similarly. The results of the temperature dependence of the fluorescence emission spectra are given in Figure 6. The temperature dependence is weak in all cases and the small temperature dependence observed is in the opposite direction from that of the recombination fluorescence. This shows that the temperature effect of the recombination fluorescence observed in the previous figures does not arise from a temperature effect on the solute emission. Because of the difficulty in making quantitative comparison between the experiments done in Figure 6 and those done in the previous figures we will neglect the small temperature effect of the directly excited fluorescence intensity in our
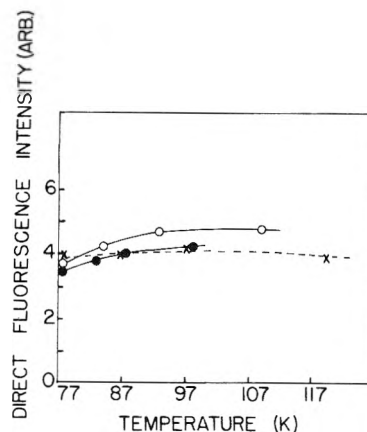
analysis. Our main objective in the analysis to follow will be to obtain trends between the different glassy matrices.

Discussion

Tunneling Recombination in the Temperature Region below T_g. We will find it convenient to discuss the results in Figures 1–5 in terms of two temperature regions. One temperature region is that below the glass transition temperature of the matrix, T_g, and the other region is that above T_g. In all matrices the initial decay rate of the recombination fluorescence decreases with increasing temperature in the region below T_g. Thus the decay process is clearly not temperature activated and hence is certainly not dominated by diffusive recombination of the electrons with the cations. Instead we suggest, in accordance with our earlier work on aqueous matrices,[12] that this decreasing decay rate is characteristic of a tunneling recombination process.

In general the tunneling rate depends on an electronic factor involving the shape of the potential barrier and on a nuclear factor involving the Franck–Condon principle and coupling to vibrational modes. For the present systems we have concluded that the tunneling barrier height is probably the dominant factor and we first discuss the results from this point of view. Then we will discuss the possible influence of other factors on the tunneling rate. We interpret the decreasing rate of initial tunneling decay as due to an increasing tunneling barrier height due to a deepening of the electron potential well during the timescale that we observe the recombination fluorescence. Previous optical absorption work at 77 K has clearly indicated that the electron trap depth increases with time in both polar and nonpolar matrices.[1,2,4,16,17] The evidence for this is that there is a transient spectral shift of the trapped electron absorption maxima to the blue with time after electron injection. The timescale for this shift depends upon the matrix polarity and is more rapid in more polar matrices. This appears to be due to electron induced molecular dipole rotation and orientation around the electron to deepen the potential well in which the electron finds itself. This process is clearly temperature dependent as shown by experiments in liquids[4,18,19] while in many matrices at 4 K the dipole orientation around the electron is complete at very long times.[3,20] Recent careful studies of the electron trap deepening indicated by its spectral shift have shown that even in polar alcohol matrices such as ethanol this spectral shift at 77 K is observable up to about 1 s.[17,21] Thus we expect that this trap deepening effect will in fact be occurring before and during the time

window that we see in our recombination fluorescence experiment.

The decrease in initial recombination fluorescence intensity with increasing temperature may be interpreted in the same way. As the temperature of the experiment increases, the electron trap deepens and less tunneling recombination occurs per unit time so the initial observed intensity decreases. Recall that the initial fluorescence intensity plotted in the figures is that observed 100 ms after the UV photoionizing light is interrupted.

Diffusive Recombination in the Temperature Region above T_g. Figures 1–4 show that the initial decay rate of the recombination fluorescence increases with increasing temperature at some region above T_g in the various matrices. The fact that this is not observed for ethanol in Figure 5 will be discussed later. This increasing initial decay rate with increasing temperature is characteristic of a temperature activated process and can be ascribed to diffusive recombination of the electron with a cation. Thus by monitoring the recombination fluorescence as a function of photoionization temperature one can easily pick out the temperature regions in which tunneling recombination dominates and in which diffusive recombination dominates. Coincident with the increasing initial rate at some temperature region above T_g, the initial recombination fluorescence intensity shows an increase which goes through a peak before going to zero. Remember that we monitor the initial recombination fluorescence intensity at a given time after UV photoionization. Therefore, as we reach the diffusive recombination region, this initial intensity should increase indicating a more rapid initial recombination rate of the electrons with a cation. However, at a sufficiently high temperature most of the recombination will have already taken place before our observation of the recombination fluorescence intensity begins. Thus, the initial intensity recorded at our particular observation time after UV photoionization will decrease to zero, giving rise to the peak in the recombination fluorescence intensity observed. We will find it convenient to refer to this peak as a diffusive peak characteristic of diffusive recombination of the electrons with cations.

Note that this diffusive peak occurs at about 10 K above the glass transition temperature in both of the alkane matrices, 3-methylhexane and methylcyclohexane. However, in methyltetrahydrofuran, which is a more polar matrix, the diffusive peak occurs at 20 K above the glass transition temperature and in the still more polar matrix, 2-propanol, the diffusive peak occurs at 29 K above the glass transition temperature. There is a clear correlation between matrix polarity and the temperature interval between the diffusive recombination peak associated with the fluorescence intensity and the glass transition of the matrix. This is just what we expect for a diffusive recombination process since the electron trap depth increases with increasing matrix polarity.[22] In more polar matrices more molecular motion is required, as indicated by a greater temperature above the glass transition temperature, for diffusive recombination of the electrons with the cations to be observed during our fixed time window after the UV photoionization process is interrupted.

Note that Figure 5 appears anomalous in that no diffusive peak occurs for the initial fluorescence intensity and the initial decay rate does not show an increase at temperatures above the glass transition temperature. In fact, the recombination fluorescence becomes too weak to observe above the glass transition temperature. This behavior is similar to that found previously for the pho-
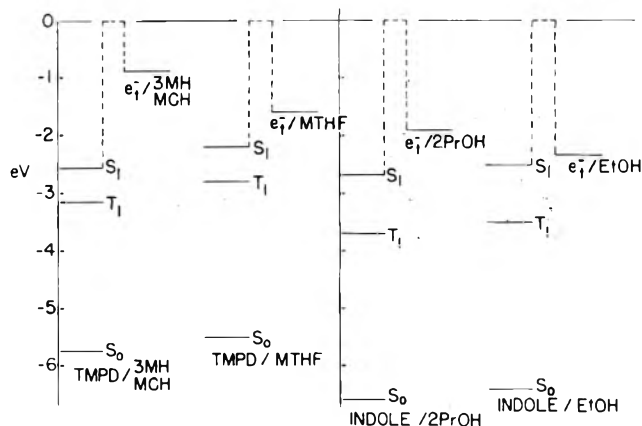
Figure 7. Energy level diagram for solutes and trapped electrons in various matrices at 77 K. The dashed lines represent schematic tunneling barrier heights.

toionization of tryptophan in ethylene glycol/water (EG/H$_2$O) matrices[12] in which a weak recombination fluorescence could be observed to temperatures about 60 K above the glass transition temperature, but which showed no diffusive fluorescence intensity peak in this region. An explanation for this behavior can be seen by referring to Figure 7. In this figure the electron trap depth at 77 K in ethanol is nearly the same as the excited singlet level of indole in ethanol. Thus, tunneling recombination may still produce the excited singlet state of indole and the consequent fluorescence. However, after the electron trap deepens diffusive recombination will not provide sufficient energy to populate the excited singlet state of indole. If we know the electron trap depth relative to the excited singlet level of the solute, we should be able to predict in a given matrix whether or not recombination fluorescence from a diffusive mechanism can be seen or not. This also may provide a method to evaluate electron trap depths in different matrices if a series of solutes with different excited levels is available.

Comparison of Tunneling Recombination in Different Matrices. Figure 7 summarizes the electron trap depths and the energy levels of the TMPD and indole solutes in the various matrices studied. The electron trap depths are determined from the photoionization thresholds at 77 K of the trapped electrons which have been recently evaluated;[22] the average trap depth for 3 MH and MCH is given for both in Figure 7. The electron trap depth in 2-propanol is estimated from its optical absorption maximum by analogy to ethanol. The photoionization thresholds for TMPD in alkane glasses (actually in 3 MP) and in MTHF have been measured.[23] These thresholds together with the fluorescence and phosphorescence maxima of TMPD in 3MP[24] and in MTHF[7] then determine the energy level structure shown. The photoionization threshold measured for tryptophan in ethanol of 6.4 eV[25] is assumed to apply to indole because of structural similarity. The photoionization threshold of indole in 2-propanol is estimated as 6.6 eV from the trends reported with matrix polarity.[23,25] The fluorescence and phosphorescence maxima of tryptophan in EG/H$_2$O at 77 K[26] are assumed to be similar to those of indole in both alcohol matrices. The photoionization thresholds for both the solutes and the trapped electrons are uncertain to about ±0.2 eV.

From Figure 7 we may compare the tunneling recombination process in matrices of various polarity. First note that the electron trap depths in the alkane matrices, methylcyclohexane and 3-methylhexane, are only 0.85 eV at 77 K and hence no reasonable amount of trap deepening

(we will see later that this is of the order of 0.1 eV) can drop the energy level of the electron below the excited singlet level of the TMPD solute. Thus in the alkane matrices Figures 1 and 2 show that the initial fluorescence intensity drops by about a factor of 2 in the tunneling recombination region which is consistent with the decrease in the initial fluorescence decay rate of about a factor of 2. Furthermore, from the plateaus in both the initial fluorescence intensity and the initial decay rate in the alkane matrices between about 65 and 80 K it appears that, within the time window of observation, the trap deepening effect is substantially complete at about 65 K at 0.1–1 s. The extent of trap deepening and the optical spectral shift seen in the process of electron localization which represents this trap deepening[22] are relatively small for nonpolar matrices such as alkanes. Thus, in these alkane matrices the easy distinction between the dominant tunneling and dominant diffusive recombination mechanisms is not so readily apparent in the intermediate temperature region about 20 K below the glass transition temperature. Figure 3 for TMPD in MTHF shows a significantly different picture. Again the initial decay rate decreases by about a factor of 2 in the tunneling recombination region which is consistent with the alkane glasses. This basically reflects about the same amount of trap deepening in MTHF glass, perhaps a little more, than in the alkane glasses. However, the initial fluorescence intensity decreases by about a factor of 10 in MTHF glass. This not only reflects the decrease in the initial decay rate but must also involve another factor. We believe that this other factor involves dropping some of the trapped electrons to energy levels below those which can excite the singlet level of the solute. In Figure 7 the electron trap depth in MTHF is not much above the S_1 level of TMPD and both are uncertain about ±0.2 eV. Thus, it appears that the electron energy level can drop near or below the solute singlet level. Although tunneling recombination to the singlet level may still be possible, it appears to become much less efficient than excitation of the excited triplet level of the solute.

In addition to electron trap deepening the solute singlet energy level may increase with temperature due to variation of the photoionization threshold of the solute. This threshold I_s may be written as $I_s = I_g + P^+ + V_0$ where I_g is the gas phase ionization potential of the solute, P^+ is the polarization energy of the positive ion, and V_0 is the conduction electron energy level.[27,28] V_0 and P^+ depend on density and hence are temperature dependent but V_0 dominates. In alkanes and alcohols V_0 decreases with increasing temperature so it will move all the solute energy levels up. Typically this may amount to 0.1–0.3 eV over the temperature range investigated. Thus, this factor will aid in dropping the electron energy level below the solute singlet level when the two levels are close together.

If we now move to considerable more polar matrices as represented by 2-propanol, we find that the initial decay rate decreases by about a factor of 5, instead of the factor of 2 for alkanes and MTHF, in the tunneling recombination temperature region. This is consistent with a greater absolute decrease in the trap deepening process in the 2-propanol matrix as compared to the less polar MTHF and alkane matrices. The initial fluorescence intensity decreases again by a factor of 10 or more which reflects not only the decrease in the initial decay rate but also the fact that the trapped electron energy level has dropped sufficiently close to the singlet level of the solute that excitation of the fluorescent state is inefficient. The relative positions of the electron and solute singlet levels appear quite similar in the MTHF and 2-propanol matrices

which correlates with their similar behavior. The ethanol matrix clearly continues the trend with matrix polarity of increasing closeness of the electron and solute singlet energy levels, and in the diffusive recombination region the relative energy levels have shifted so that the solute singlet is not excited.

By considering the polarity of the matrix, which will influence the degree of trap deepening with temperature over the time range that we are able to study, as well as the electron trap depth relative to the excited singlet level of the solute, we seem to be able to understand the trends with matrix polarity of both the initial decay rate and the initial recombination fluorescence intensity as a function of the photoionization temperature.

Application of a Simple Tunneling Model. To test whether the idea of trap deepening affecting the tunneling rate constant is physically reasonable we consider a simple one-dimensional tunneling model with a square barrier of height V_b and width d. The tunneling rate constant can be written as

$$k = \nu \exp[-2d(2m^*V_b)^{1/2}/\hbar] \tag{1}$$

where m^* is the electron effective mass, for which we use the electron rest mass m, $\hbar$ is Planck's constant divided by 2π, and ν is the preexponential factor. This equation has been used to treat electron tunneling with solutes in aqueous and organic glasses by assuming that ν is a temperature independent frequency factor of about 10^{15} s^{-1}.[29-31] However, in a molecular system in a matrix ν must involve the nuclear coordinate in a manner consistent with the Franck–Condon principle and coupling to the matrix and molecular vibrational modes. Consequently, ν may be temperature dependent, but in all treatments to date[32] the temperature dependence of ν results in a positive effective activation energy. Since our experimental results in the tunneling recombination region correspond to a negative effective activation energy it does not appear that the preexponential factor is dominant for the trends considered in this paper.

An increase of either the barrier height or width with increasing temperature can account for the trend we observe. To obtain an estimate of the magnitude of the increases required we have assumed $\nu = 10^{15}$ s^{-1} and have used the convenient form[29] of eq 1, $\log k = 15 - 0.44d V_b^{1/2}$, where d is in Å and V_b is in eV. For this assumed ν the scale of the calculated results may be off but the trends should be valid. The V_b values at 77 K have been taken as the electron trap depths based on photoionization thresholds. Then from the initial recombination fluorescence decay rate constants at 77 K we calculate tunneling distances of 22–37 Å as shown in Table I. Results for the ethylene glycol/water matrix are also included[12] for a more extensive comparison. Table I shows that there appears to be a distinct correlation of the tunneling distance with the polarity of the matrix. The longer distances apply to the nonpolar alkane matrices and the shorter ones to the polar alcohol matrices. A rough guide to the polarity of the bulk matrix is given by the room temperature static dielectric constant which is also given in Table I.

In Table I we present calculations on the barrier height changes assuming that the tunneling distance or barrier width calculated for 77 K is constant with temperature and on the barrier width changes assuming that the barrier height measured at 77 K is independent of temperature. In both cases the changes are relatively small and may be physically reasonable. We now try to assess whether we can make a decision about the dominance of either barrier height or width changes.

TABLE I: Summary of Initial Recombination Fluorescence Decay Constants in Different Matrices and Calculated Tunneling Barrier Heights and Widths from Eq 1[a]

Solute / Matrix	D_s^b	T_g,[b] K	ΔT,[c] K	Irrad temp, K	k, s⁻¹	Barrier height at constant width, eV	Barrier width at constant height, Å
TMPD / MCH	2	86	10	55	2.9	0.80	35.8
				65	1.1	0.85	36.9
				77	1.1	(0.85)	(36.9)
				93	1.0	0.85	37.0
TMPD / 3MH	2	86	10	55	2.8	0.80	35.9
				65	1.2	0.85	36.8
				77	1.2	(0.85)	(36.8)
				93	1.1	0.85	36.9
TMPD / MTHF	4.6	88	20	63	2.4	1.59	26.3
				77	2.1	(1.60)	(26.4)
				88	1.8	1.61	26.5
				99	0.9	1.68	27.0
Indole / 2PrOH	18	94	29	67	2.8	1.89	24.0
				77	2.5	(1.90)	(24.1)
				94	2.1	1.92	24.2
				126	0.4	2.11	25.4
Indole / Ethanol	24	93		48	3.3	2.24	21.7
				77	2.1	(2.30)	(22.0)
				93	1.3	2.37	22.3
Tryptophan / EG/H₂O	64	106		77	2.3	(2.30)	(21.9)
				106	1.8	2.33	22.1
				120	0.43	2.53	23.0

[a] The barrier heights are calculated at the constant width for 77 K rounded to two significant figures and the barrier widths are calculated at the constant height for 77 K. The selection of barrier heights at 77 K is discussed in the text. [b] Static dielectric constant at 293 K, D_s, and glass transition temperature, T_g, from ref 9. [c] Temperature interval between T_g and the fluorescence peak in the diffusion region; see text.

The origin of any barrier width change is presumably thermal expansion.[33] We will write a temperature dependent barrier width d_T as

$$d_T = d_0 + d_0 \alpha T \qquad (2)$$

where α is the coefficient of linear expansion and d_0 is the barrier width at 0 K. From the decay rate at two temperatures we may evaluate α. From the temperature extremes of the tunneling recombination region listed in Table I we find α ranges from 8 to 12 × 10⁻⁴ K⁻¹. To our knowledge values of α for the matrices studied have not been reported, but we may expect α to lie between the ranges of 0.2–0.6 × 10⁻⁴ K⁻¹ quoted for metals[34] and 2.3 × 10⁻⁴ K⁻¹ quoted for polyethylene at room temperature.[35] It appears that the α values for our matrices are about an order of magnitude less than the α values required to explain the temperature dependence of the recombination fluorescence decay. This suggests that barrier width changes are not the dominant factor controlling the electron tunneling rate, although some contribution from this source is not unlikely. In addition, the plateaus in decay rate observed in the alkane matrices are unexplained in terms of thermal expansion arguments since thermal expansion changes are expected to be continuous.

Increase in the tunneling barrier height with temperature can occur by electron trap deepening. We have already given independent evidence that the trap depth does appear to increase in the matrices we are studying. This is shown most dramatically for the more deeply trapped electrons in the polar alcohol glasses such as ethanol in which no diffusive recombination peak is seen at temperatures above the glass transition point. Also in the discussion of the decrease in the initial recombination fluorescence from TMPD in MTHF and from indole in 2-propanol it was found that there must be an additional factor besides that of the decrease in initial decay rate to explain the magnitude of the initial fluorescence intensity decrease observed. This is additional support for the existence of trap deepening in these matrices. The calculated trap deepening in Table I assuming a constant

barrier width amounts to about 0.05 eV in nonpolar matrices, about 0.1 eV in MTHF, and about 0.2 eV in alcohol matrices. We expect the deepening to be somewhat greater in more polar matrices because the optimum orientation of the polar molecular dipoles will cause a greater energy lowering than will the optimum orientation of the nonpolar alkane molecules. This difference is directly demonstrated by the magnitude of the optical spectral shifts associated with solvation of trapped electrons observed in pulse radiolysis[1,2,4,16–19,21] and 4 K radiolysis[3,20] experiments. These spectral shifts correspond to about 0.1 eV in alkane matrices and >1 eV in alcohol matrices. Thus our calculated barrier height changes seem quite reasonable. In the case of EG/H₂O we can make a more quantitative comparison because the optical absorption maxima shift with temperature for trapped electrons has been observed on a slow timescale over the same temperature range that we have studied.[36] The optical absorption shift is 0.2 eV from 77 to 120 K which is in excellent agreement with our calculated barrier height increase.

By using eq 1 we have implicitly assumed a one-dimensional tunneling model with an effective delta function distribution of electron–cation distances. We believe this may be approximately valid during our limited observation time. It has been shown for electron tunneling to a scavenger that the trapped electron distance distribution from a scavenger molecule maintains a quasi-step rise from zero at a given distance and then decreases at greater distances.[37,38] Within our particular observation time window the electrons at greater distances do not contribute to the observed fluorescence, so we effectively can consider a delta function distribution for the cation–electron separation. Furthermore, almost all the electrons produced by photoionization of a solute are correlated with their parent cations and recombine only with them.[24,39] Thus, we can ignore averaging due to a given electron being able to tunnel to more than one cation. A delta function distribution implies a first-order decay which is not observed experimentally over our entire observed time range.

However, we analyze the data only during a narrow time window which approximates first-order decay. Thus there is no real inconsistency.

If one considered the tunneling rate constant averaged over a homogeneous distribution of scavengers or cations and trapped electrons and assumes that the barrier height V_b is independent of time one finds[37,38] $k \propto V_b^{-3/2}$. Based on our measured rate constants this expression predicts quite large changes in the barrier height with temperature which seem physically unreasonable. For example in methylcyclohexane, $V_b = 0.85$ eV at 77 K implies 0.45 eV at 55 K; and in 2-propanol, $V_b = 1.90$ eV at 77 K implies 6.45 eV at 126 K. These values are much larger than the spectral shifts observed in these matrices. Therefore, the simple expression (1) appears to be approximately valid for our experimental conditions.

Another possible factor contributing to the decrease of the recombination fluorescence intensity with increasing temperature could be a temperature dependent change in the electron–cation distance distribution. One might expect that the number of electrons thermalized or trapped at a given distance from the cation should decrease with increasing temperature. Since the recombination fluorescence depends on the number of recombining electrons this effect could account for part of the qualitative behavior observed. Unfortunately, it is difficult to make a reliable estimate of this factor. Furthermore, this factor would not account for the quantitative difference between the temperature dependent decreases in the luminescence intensity and the initial decay rate in the more polar matrices.

In summary, we believe that our proposed interpretation of the initial recombination fluorescence intensity and decay rate vs. temperature gives a physically reasonable picture of the electron–cation recombination process in both polar and nonpolar matrices and offers a simple diagnostic for distinguishing tunneling and diffusive recombination of electrons with cations in disordered matrices.

References and Notes

(1) L. Kevan, *J. Chem. Phys.*, **56**, 838 (1972).
(2) J. T. Richards and J. K. Thomas, *J. Chem. Phys.*, **53**, 218 (1970).
(3) H. Yoshida and T. Higashimura, *Can. J. Chem.*, **48**, 504 (1970).
(4) W. J. Chase and J. W. Hunt, *J. Phys. Chem.*, **79**, 2835 (1975).
(5) C. Deniau, A. Deroulede, F. Kieffer, and J. Rigaut, *J. Lumin.*, **3**, 325 (1971).
(6) K. Yoshinaga, N. Yamamoto, and H. Tsubomura, *J. Lumin.*, **6**, 179 (1973).
(7) H. Moeckel, J. Yuen, and L. Kevan, *Int. J. Radiat. Phys. Chem.*, **7**, 251 (1975).
(8) A. C. Albrecht, *Acc. Chem. Res.*, **3**, 238 (1970).
(9) J. Moan and H. B. Steen, *J. Phys. Chem.*, **75**, 2887 (1971).
(10) D. Muller, M. Ewald, and G. Durocher, *Can. J. Chem.*, **52**, 407 (1974).
(11) M. Aubailly, M. Bazin, and R. Santus, *Chem. Phys.*, **2**, 203 (1973).
(12) J. Moan, K. K. Ho, and L. Kevan, *J. Chem. Phys.*, **63**, 1285 (1975).
(13) J. Moan, *J. Lumin.*, **6**, 256 (1973).
(14) H. Moeckel, J. Moan, and L. Kevan, *J. Phys. Chem.*, **77**, 3035 (1973).
(15) K. K. Ho, J. Moan, and L. Kevan, *Chem. Phys. Lett.*, **37**, 425 (1976).
(16) N. V. Klassen, H. A. Gillis, and G. G. Teather, *J. Phys. Chem.*, **76**, 3847 (1972).
(17) J. R. Miller, B. E. Cliff, J. J. Hines, R. F. Runowski, and K. W. Johnson, *J. Phys. Chem.*, **80**, 457 (1976).
(18) J. H. Baxendale and P. Wardman, *J. Chem. Soc., Faraday Trans. 1*, **69**, 584 (1973).
(19) J. H. Baxendale and P. H. G. Sharpe, *Int. J. Radiat. Phys. Chem.*, **8**, 621 (1976).
(20) T. Higashimura, M. Noda, T. Warashina, and H. Yoshida, *J. Chem. Phys.*, **53**, 1152 (1970); H. Hase, N. Noda, and T. Higashimura, *ibid.*, **54**, 2975 (1971).
(21) N. V. Klassen, H. A. Gillis, G. G. Teather, and L. Kevan, *J. Chem. Phys.*, **62**, 2474 (1975).
(22) L. Kevan, *Adv. Radiat. Chem.*, **4**, 181 (1974).
(23) A. Bernas, M. Gauthier, and D. Grand, *J. Phys. Chem.*, **76**, 2236 (1972).
(24) W. M. McClain and A. C. Albrecht, *J. Chem. Phys.*, **43**, 465 (1965).
(25) J. Moan, *Chem. Phys. Lett.*, **18**, 446 (1973).
(26) H. Steen, *Radiat. Res.*, **38**, 260 (1969).
(27) S. Noda, L. Kevan, and K. Fueki, *J. Phys. Chem.*, **79**, 2866 (1975).
(28) B. E. Springett, J. Jortner, and M. H. Cohen, *J. Chem. Phys.*, **48**, 2720 (1968).
(29) J. R. Miller, *Chem. Phys. Lett.*, **22**, 180 (1973); *J. Phys. Chem.*, **79**, 1070 (1975).
(30) J. Kroh and C. Strakowski, *Radiochem. Radioanal. Lett.*, **9**, 169 (1972); *Int. J. Radiat. Phys. Chem.*, **5**, 243 (1973); **7**, 23 (1975).
(31) K. I. Zamaraev, R. F. Khairutdinov, A. I. Mikhailov, and V. I. Goldansky, *Dokl. Akad. Nauk. SSSR*, **199**, 640 (1971); K. I. Zamaraev and R. F. Khairutdinov, *Chem. Phys.*, **4**, 181 (1974).
(32) J. Jortner, *J. Chem. Phys.*, **64**, 4860 (1976).
(33) B. J. Hales, *Biophys. J.*, **16**, 471 (1976).
(34) "Handbook of Chemistry and Physics", 55th ed, The Chemical Rubber Co., Cleveland, Ohio, 1974, p D 152.
(35) J. Brandrup and E. H. Immergut, Ed., "Polymer Handbook", Wiley-Interscience, New York, N.Y., 1966.
(36) J. Moan, *J. Chem. Phys.*, **60**, 3859 (1974).
(37) F. S. Dainton, M. J. Pilling, and S. A. Rice, *J. Chem. Soc., Faraday Trans. 2*, **71**, 1311 (1975).
(38) M. Tachiya and A. Mozumder, *Chem. Phys. Lett.*, **34**, 77 (1975).
(39) K. K. Ho and L. Kevan, *J. Phys. Chem.*, submitted for publication.

Effect of Dilution in Nonpolar and in Polar Liquids on the Dielectric Relaxation in Several Liquids

K. Baba and K. Kamiyoshi*

Research Institute for Scientific Measurements, Tohoku University, Sendai (980), Japan (Received December 17, 1976; Revised Manuscript Received May 5, 1977)

Dielectric relaxation in isoamyl bromide, n-octyl bromide, monochlorobenzene, and monobromobenzene has been observed at 16 °C in the pure state, in the diluted state in n-hexane, and in a mixture of the two of these polar liquids, and the following results have been obtained. Dielectric relaxation in isoamyl bromide and n-octyl bromide is of the Davidson–Cole type in the pure state but it changes into of the Debye type when sufficiently diluted in n-hexane. Dielectric relaxation in monochlorobenzene is of the Debye type both in the pure and diluted states. Two dielectric relaxations, both of the Debye type, are observed in a mixture of monochlorobenzene and monobromobenzene. One dielectric relaxation of the Davidson–Cole type is observed in the equimolar mixture of isoamyl bromide and n-octyl bromide. Two dielectric relaxations, one of the Debye type and the other of the Davidson–Cole type, are observed in a mixture of monochlorobenzene and isoamyl bromide, the Davidson–Cole type relaxation changing into the Debye type with the decrease of concentration of isoamyl bromide. From these experimental results it is presumed that the Davidson–Cole type dielectric relaxation is not due to intramolecular motions of an orientating molecule but to some cooperative motions between neighboring molecules.

Introduction

Since Davidson and Cole[1] first found that the Cole–Cole plot for the dielectric relaxation in glycerol and propylene glycol was represented by an asymmetric skewed arc (Davidson–Cole type) and not by a semicircle (Debye type), many researchers reported a similar relaxation in other liquids such as n-propyl nitrite[2] and 2-methylpentane-2,4-diol.[3] The origin of this Davidson–Cole type dielectric relaxation cannot be attributed to some properties of intermolecular hydrogen bonds, because this relaxation was found not only in liquids which have a hydrogen bond such as glycerol, but also in liquids which have no hydrogen bonds, such as isobutyl chloride.[4] Formerly, when the dielectric measuring apparatus in the microwave region could not be available, this dielectric relaxation was observed only in supercooled liquids. However its origin seems to have no connection with some characteristics accompanying the supercooled state, because it has also been observed in liquids at room temperature, for instance, n-octyl iodide at 20 °C.[5] It also appears that the Davidson–Cole type is not specifically a characteristic of associated liquids.

Several different models have been proposed for the interpretation of the mechanism by which the Davidson–Cole type relaxation occurs. In these proposed models, the origin is attributed either to some intramolecular motions of the orientating molecule itself,[6] or to some cooperative motions between neighboring molecules.[7-9] For instance, Matsumoto and Higasi[6] assume that long chain molecules can make different modes of dipole orientations not only by the rotation of the whole molecule but by the intramolecular flexing of various partial lengths of a long chain. This gives rise to a distribution of the relaxation time. According to their model, the Davidson–Cole type relaxation occurs if this distribution function satisfies some conditions. On the other hand, Glarum[7] proposes a different model, in which he assumes that a molecule can make dipole orientation instantaneously when a defect comes by diffusion to the neighboring position of this molecule. Though he does not make clear the character

of the defect, he certainly attributes the Davidson–Cole type relaxation to some cooperative motions of the molecules surrounding the orientating molecule.

In this paper we report some experimental results which are useful for the interpretation of the origin of the asymmetric dielectric relaxation in liquids. Dielectric measurements were made on isoamyl bromide, n-octyl bromide, monochlorobenzene, and monobromobenzene in the pure state, in the diluted state in nonpolar n-hexane, and also in a two-component mixture of these polar liquids. When the conditions surrounding the orientating molecule are altered by dilution in a nonpolar liquid or by mixture with another polar liquid, characteristics of the dielectric relaxation are expected to be little influenced if the origin of the Davidson–Cole type relaxation is in the orientating molecule itself, but they may be strongly influenced if the origin lies in the environmental conditions surrounding the orientating molecule.

Experimental Section

The dielectric constant ϵ' and dielectric loss ϵ'' at 1 MHz were measured by a capacitance bridge (General Radio Co., 716 CS-1), and at 2 GHz by a coaxial slotted line (General Radio Co., 874-LV). Measurements at 9, 24, and 50 GHz were performed by the usual waveguide method in which the change of the standing wave radio at a fixed position was observed when the sample length in the waveguide was varied continuously by a movable piston. All measurements were made at 16 °C. Dielectric measurements in the microwave region were made repeatedly three to five times on the same sample, and the mean error was less than 3% in ϵ' and ϵ''. The specimens used in the present measurement were of "extra pure" grade from Wakô Co., Japan.

Results

(a) *Pure State and Diluted State in Nonpolar n-Hexane.* Figure 1 shows the Cole–Cole plot for the dielectric relaxation observed in isoamyl bromide ($\epsilon_0 = 6.20$, $\epsilon_\infty = 2.07$) in the pure state and in the diluted state in
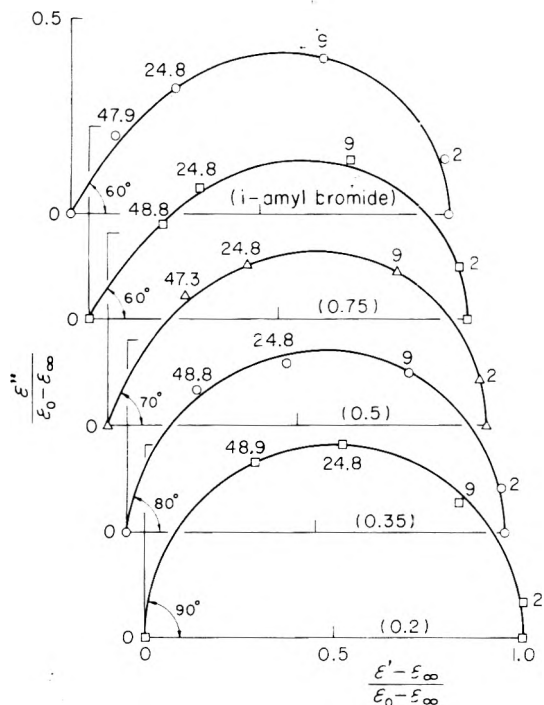
Figure 1. Cole–Cole plot for the dielectric relaxation observed in isoamyl bromide at 16 °C in the pure state and in the diluted state in n-hexane at 0.75, 0.5, 0.35, and 0.2 mole fraction. The frequency is given in GHz.

Figure 2. Variation of the relaxation time, τ, and the angle, α ($= \beta\pi/2$), with concentration at 16 °C when isoamyl bromide, n-octyl bromide, and monochlorobenzene are diluted in n-hexane.

n-hexane at concentrations of 0.75, 0.5, 0.35, and 0.2 in mole fraction. The low frequency end of this plot, ϵ_0, represents the value measured at 1 MHz, and the high frequency end, ϵ_∞, is the value n_D^2, the square of the optical refractive index. It is seen that in the pure state the Cole–Cole plot is represented by a skewed arc. The solid curve in this figure is calculated by the Davidson–Cole equation[1]

$$\frac{\epsilon' - \epsilon_\infty}{\epsilon_0 - \epsilon_\infty} = (\cos \varphi)^\beta \cos \beta\varphi$$

$$\frac{\epsilon''}{\epsilon_0 - \epsilon_\infty} = (\cos \varphi)^\beta \sin \beta\varphi \qquad (1)$$

where $\tan \varphi = \omega\tau$, τ being the relaxation time, and $\beta = \alpha/(\pi/2)$, α being the angle as indicated in Figure 1. The angle α was determined so that the calculated value was the best fit to the experimental values. For instance, in the case of pure isoamyl bromide, $\alpha = 60°$ was found to be the best fit. It is seen from these results that the angle α increases with the decrease of concentration tending to $\alpha = 90°$ in the sufficiently diluted state. That is, the type of dielectric relaxation in isoamyl bromide changes from the Davidson–Cole into the Debye type by dilution in n-hexane. The variations of the relaxation time and the angle of isoamyl bromide are shown in Figure 2 as a function of mole fraction. The relaxation time in this figure is the mean value of those calculated by each set of measured ϵ', ϵ'', and the measuring frequency.

Similar characteristics are found in the dielectric relaxation of n-octyl bromide ($\epsilon_0 = 5.14$, $\epsilon_\infty = 2.11$) in the pure and diluted states as shown in Figure 3 for the Cole–Cole plot and in Figure 2 for τ and α.

Figure 4 shows the Cole–Cole plot for the dielectric relaxation of monochlorobenzene ($\epsilon_0 = 5.80$, $\epsilon_\infty = 2.33$) in the pure state and in the diluted state in n-hexane at concentrations of 0.5 and 0.2 mole fraction. It is seen by these results that in all cases the experimental points lie close to a semicircle. Consequently, the dielectric re-
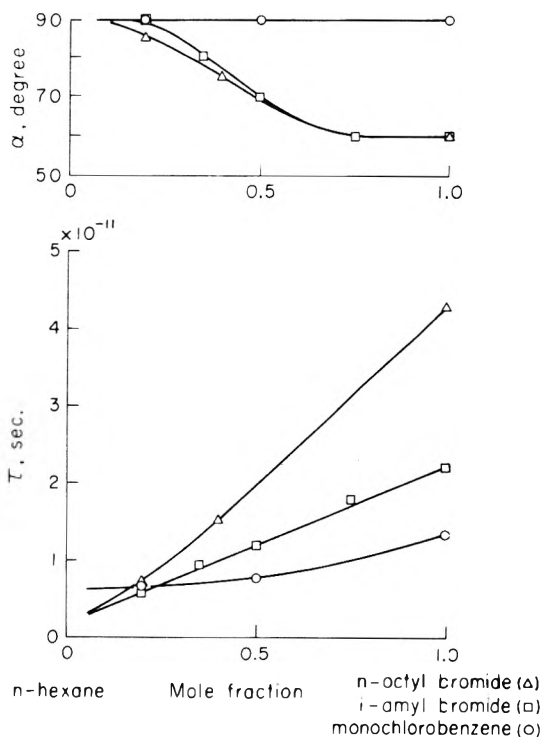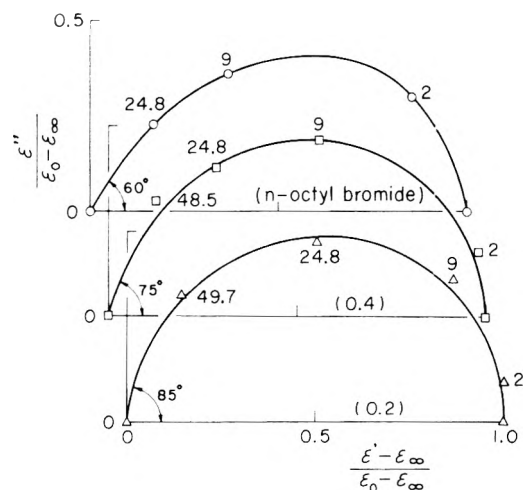

Figure 3. Cole–Cole plot for the dielectric relaxation observed in n-octyl bromide at 16 °C in the pure state and in the diluted state in n-hexane at 0.4 and 0.2 mole fraction. The frequency is given in GHz.
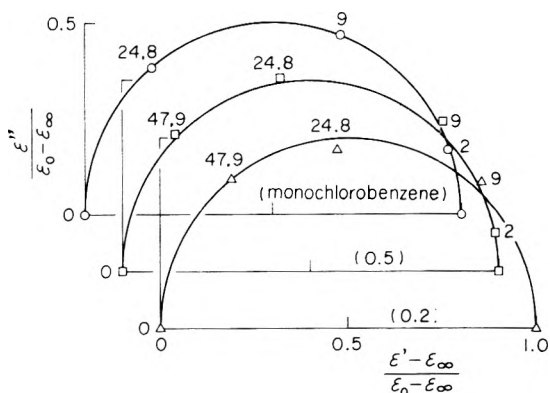

Figure 4. Cole–Cole plot for the dielectric relaxation observed in monochlorobenzene at 16 °C in the pure state and in the diluted state in n-hexane at 0.5 and 0.2 mole fraction. The frequency is given in GHz.
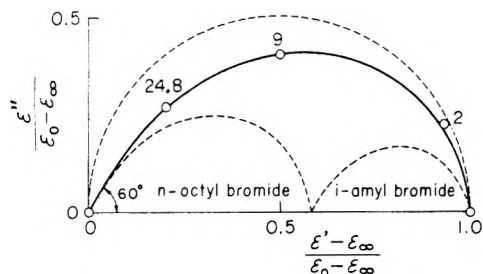
Figure 5. Cole–Cole plot for the dielectric relaxation at 16 °C in equimolar mixture of isoamyl bromide and *n*-octyl bromide. The frequency is given in GHz.
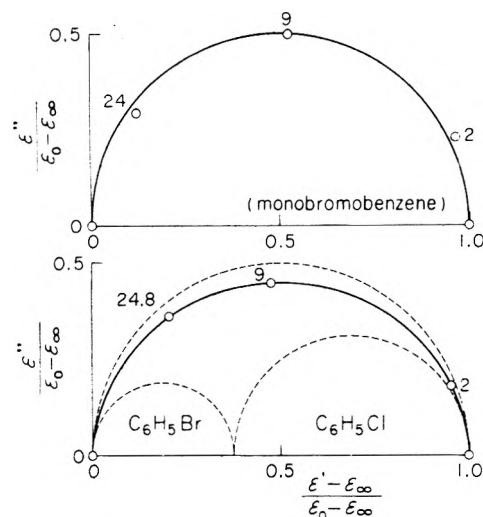

Figure 6. Cole–Cole plot for the dielectric relaxation at 16 °C in pure monobromobenzene, and in a mixture of monochlorobenzene and monobromobenzene at a concentration of 0.6:0.4 mole ratio. The frequency is given in GHz.

Figure 7. Cole–Cole plot for the dielectric relaxation at 16 °C in mixtures of monochlorobenzene and isoamyl bromide at concentrations of 0.75:0.25, 0.5:0.5, and 0.25:0.75 mole ratio. The frequency is given in GHz: dotted circle, monochlorobenzene component; dot-dash-curve, isoamyl bromide.

Figure 8. Variation of the relaxation time, τ, and the angle, α ($= \beta\pi/2$), with mole ratio at 16 °C in mixtures of isoamyl bromide + *n*-octyl bromide ($\triangle$), and isoamyl bromide ($\square$) + monochlorobenzene (O).

laxation in monochlorobenzene follows the Debye model both in the pure and diluted states.

(b) *Mixed State of Two Polar Liquids.* Figure 5 shows a Cole–Cole plot for the dielectric relaxation in an equimolar mixture of isoamyl bromide and *n*-octyl bromide. The plot is represented satisfactorily by one skewed arc with $\alpha = 60°$ and, consequently, by one common relaxation time.

Figure 6 shows a Cole–Cole plot for the dielectric relaxation in a mixture of monochlorobenzene and monobromobenzene ($\epsilon_0 = 5.55$, $\epsilon_\infty = 2.43$) at 0.6:0.4 mole ratio. The plot for pure monobromobenzene is also shown in this figure. The experimental points for this mixture cannot be represented by one semicircle. The solid curve in this figure represents the value calculated by eq 2 which will be explained later. Here it is assumed that the observed relaxation is the superposition of two Debye type relaxations as shown by dotted circles in the figure. Good agreement between experimental and calculated values is obtained.

Finally, Figure 7 shows a Cole–Cole plot for the dielectric relaxation in mixtures of monochlorobenzene and isoamyl bromide at three different concentrations of 0.75:0.25, 0.5:0.5, and 0.25:0.75 mole ratio. The solid curves in these plots represent the values calculated by eq 5 which will be explained later. These results indicate that in these mixtures the observed relaxation is the superposition of two different kinds of relaxations, the Debye type and the Davidson–Cole type, and that the type of relaxation of isoamyl bromide gradually changes from the Davidson–Cole into the Debye type with the decrease of concentration in the mixture. Figure 8 shows the relaxation time
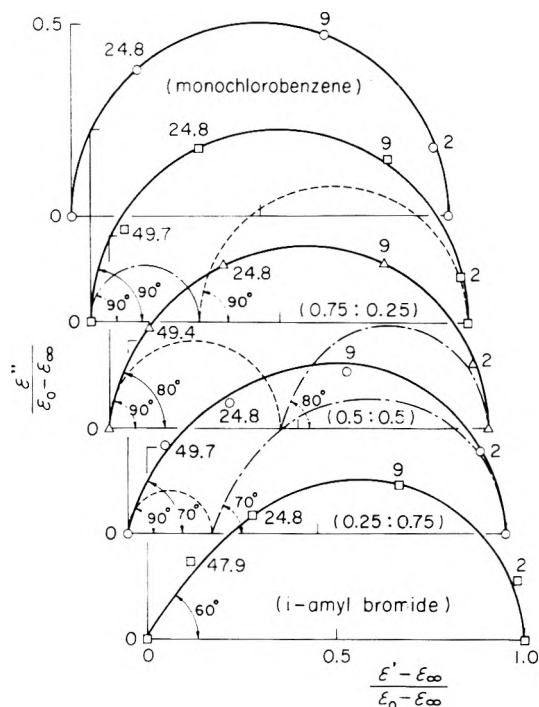
τ and the angle α of these two components as a function of mole fraction.

Discussion

Hassell and Walker[10] observed the dielectric relaxation at 15 and 60 °C of the solution of monochlorobenzene in *p*-xylene at a concentration of 5 wt % and found that the Cole–Cole plot is a semicircle at these two temperatures. This is in qualitatively accordance with the present experimental results. They also confirmed a similar con-

clusion on several other monosubstituted benzenes.

The dielectric relaxation of *n*-octyl bromide was measured by Vaughan, Lovell, and Smyth.[11] They found an asymmetric plot of dielectric constant against dielectric loss, and they gave the conclusion that the relaxation of alkyl halides commonly is a "left skewed arc" with the maximum of ϵ'' to the left of center of the complex plot. This left skewed-arc type relaxation has been predicted by Matsumoto and Higasi.[6] However later Mopsik and Cole[5] reported that this relaxation was ordinary a right skewed-arc type, which is in accordance with the present results.

Denney[4] measured the dielectric relaxation of isoamyl bromide in low temperature region and found that the Cole–Cole plot was represented by a skewed arc. He obtained the value $\beta = 0.57, 0.58, 0.59$, and 0.61 at 120.8, 126.6, 130.2, and 139.1 K, respectively. The present results show that $\beta = 0.67$ at 289 K. Berberian and Cole[12] have also shown that the value β of isoamyl bromide increases with an increase of temperature. A similar tendency is seen in other liquids such as dipropylene glycol,[13] or some α,ω-dibromoalkanes.[14]

Though the existence of high-frequency dielectric relaxation between ϵ_∞ and $n_D{}^2$ has been discussed,[15,16] we neglected it provisionally assuming that the difference, $\epsilon_\infty - n_D{}^2$, is not large even if it should exist.[17]

It may be presumed that relatively spherical and rigid molecules such as monochlorobenzene make the dipole orientation by the overall molecular rotation.[17] The present experimental results show that the relaxation time of isoamyl bromide which has a long chain as compared with the monochlorobenzene becomes smaller than that of monochlorobenzene in the diluted state, and also that the relaxation time in very diluted state is roughly equal in isoamyl bromide and *n*-octyl bromide. These facts suggest that the dipole orientation of isoamyl bromide and *n*-octyl bromide is performed by the intramolecular flexing of probably the end polar group only. The dielectric relaxation in isoamyl bromide is still observed in the supercooled state in low temperature region[4] where dipole orientation by rotation of the whole molecule seems to be very difficult.

For the representation of two superposed dielectric relaxations in the liquid mixture of monochlorobenzene and monobromobenzene, the following equations may be applied:[18,19]

$$\frac{\epsilon' - \epsilon_\infty}{\epsilon_0 - \epsilon_\infty} = \frac{C_1}{1 + x^2} + \frac{C_2}{1 + (kx)^2}$$

$$\frac{\epsilon''}{\epsilon_0 - \epsilon_\infty} = \frac{C_1 x}{1 + x^2} + \frac{C_2(kx)}{1 + (kx)^2} \tag{2}$$

where $x = \omega\tau_1$, $k = \tau_2/\tau_1$, τ_1 and τ_2 are relaxation times, and C_1 and C_2 are the normalized absorption intensities of the two dielectric relaxations in the mixture ($C_1 + C_2 = 1$). The value k must be determined so that the calculated values may be the best fit to the experimental values. No definitive relation for the calculation of C_1, C_2 has been found. Here we assume that the ratio C_1/C_2 is represented by the following relation:

$$C_1/C_2 = (\epsilon_{0(1)} - \epsilon_{\infty(1)})g_1/(\epsilon_{0(2)} - \epsilon_{\infty(2)})g_2 \tag{3}$$

where $\epsilon_{0(1)}$, $\epsilon_{0(2)}$, $\epsilon_{\infty(1)}$, and $\epsilon_{\infty(2)}$ are the limiting low and high frequency dielectric constants of two constituent liquids in the pure state, and g_1 and g_2 are the mole fractions of the mixture ($g_1 + g_2 = 1$).

In the case of the mixture of monochlorobenzene (subscript 1) and monobromobenzene (subscript 2), the following values were used for calculation: $\epsilon_{0(1)} - \epsilon_{\infty(1)} =$

3.47, $\epsilon_{0(2)} - \epsilon_{\infty(2)} = 3.12$, $g_1/g_2 = 0.6/0.4$, $k = (\tau_2/\tau_1) = (0.84 \times 10^{-11})/(2.28 \times 10^{-11}) = 0.37$. Consequently, we have $C_1/C_2 = 0.625/0.375$ by eq 3. The value k was chosen because it was the best fit to the experimental values. The calculated values are shown by a solid curve in Figure 6. Good agreement between experimental and calculated values is obtained. In pure state the relaxation time of monochlorobenzene ($\tau_1 = 1.34 \times 10^{-11}$ s) is smaller than that of monobromobenzene ($\tau_2 = 1.77 \times 10^{-11}$ s). However in the mixed state it is difficult to decide which is larger. We tried to calculate on two cases: $\tau_1 > \tau_2$ and $\tau_1 < \tau_2$. In Figure 6, the result in the case of $\tau_1 > \tau_2$ is shown. The viscosity of monochlorobenzene ($\eta_1 = 0.0090$ cP at 15 °C) is smaller than that of monobromobenzene ($\eta_2 = 0.0131$ cP at 15 °C) in the pure state. The viscosity of this mixture must be larger than η_1 but smaller than η_2. If the relaxation time varies in proportion to the viscosity, then τ_1 is expected to be larger in the mixed state than in the pure state and the reverse tendency is true for τ_2. If we assume that $\tau_1 < \tau_2$ in the mixed state, the value $k = (\tau_2/\tau_1) = (3.6 \times 10^{-11})/(0.89 \times 10^{-11}) = 4.0$ is found to be the best fit to the experimental values. Then, τ_1 is smaller in the mixed state than in the pure state, and τ_2 is larger in the mixed state than in the pure state. This seems to be inconsistent with the values of the viscosity. Therefore, only the result in the case of $\tau_1 > \tau_2$ is shown in Figure 6.

In the case of the mixture of isoamyl bromide (subscript 1) and *n*-octyl bromide (subscript 2) where two constituent liquids have a Davidson–Cole type relaxation, the following equations may be used for the analysis:

$$\frac{\epsilon' - \epsilon_\infty}{\epsilon_0 - \epsilon_\infty} = C_1(\cos\varphi_1)^{\beta_1} \cos\beta_1\varphi_1 +$$
$$+ C_2(\cos\varphi_2)^{\beta_2} \cos\beta_2\varphi_2$$

$$\frac{\epsilon''}{\epsilon_0 - \epsilon_\infty} = C_1(\cos\varphi_1)^{\beta_1} \sin\beta_1\varphi_1$$
$$+ C_2(\cos\varphi_2)^{\beta_2} \sin\beta_2\varphi_2 \tag{4}$$

where $\tan\varphi_1 = \omega\tau_1$, $\tan\varphi_2 = \omega\tau_2$, $\beta_1 = \alpha_1/(\pi/2)$, and $\beta_2 = \alpha_2/(\pi/2)$. Actual calculations showed that the best agreement with the experimental results was obtained by taking $k = \tau_2/\tau_1 = 1$ and $\alpha_1 = \alpha_2 = 60°$. Therefore, the Cole–Cole plot is expressed by one skewed arc with one common relaxation time, or simply is expressed by eq 1. In this case the calculated value is independent of the ratio C_1/C_2.

In the case of the mixture of monochlorobenzene (subscript 1) and isoamyl bromide (subscript 2) where one of the two constituent liquids has a Debye type relaxation and the other has a Davidson–Cole type relaxation, the following equations may be used for the analysis:

$$\frac{\epsilon' - \epsilon_\infty}{\epsilon_0 - \epsilon_\infty} = \frac{C_1}{1 + (\omega\tau_1)^2} + C_2(\cos\varphi_2)^{\beta_2} \cos\beta_2\varphi_2$$

$$\frac{\epsilon''}{\epsilon_0 - \epsilon_\infty} = \frac{C_1(\omega\tau_1)}{1 + (\omega\tau_1)^2} + C_2(\cos\varphi_2)^{\beta_2} \sin\beta_2\varphi_2 \tag{5}$$

where $\tan\varphi_2 = \omega\tau_2$ and $\beta_2 = \alpha_2(\pi/2)$. The ratio of the absorption intensities, C_1/C_2, of the two relaxations in the mixture was calculated by eq 3, and the values α_2 and $k = (\tau_2/\tau_1)$ were chosen so as to give the best agreement with the experimental results. It is assumed in this calculation that the dielectric relaxation of monochlorobenzene is always of the Debye type independently of the concentration in the mixture and the relaxation of isoamyl bromide of the Davidson–Cole type with different β values at different concentrations. The calculated values are shown by solid curves in Figure 7. The relaxation time τ

and the angle α of the two components determined by these analysis are shown in Figure 8 as a function of concentration. It is seen that the dielectric relaxation of isoamyl bromide gradually changes from the Davidson–Cole type into the Debye type by dilution in polar monochlorobenzene.

Though the observed results on the liquid mixture are found to be described fairly well by the superposition of two relaxations or by one skewed arc, possibilities of other combinations cannot be fully excluded because of the limited number of experimental points and of the experimental inaccuracy. Here we presume tentatively the following empirical rule from the present results. Those liquids whose dielectric relaxation is of the Debye type in pure state preserve this in the diluted states both in nonpolar liquids and in polar liquids. Those liquids whose dielectric relaxation is of the Davidson–Cole type in the pure state change the type of relaxation into the Debye type by sufficient dilution in nonpolar liquid and also in polar liquid whose relaxation is of the Debye type in the pure state. Those mixtures whose constituent liquids both have the Davidson–Cole type dielectric relaxation in the pure state show one common dielectric relaxation of the Davidson–Cole type. These results lead us further to presume that the origin of the Davidson–Cole type dielectric relaxation lies not in the intramolecular motions of the orientating molecule itself, but rather in some cooperative motions of the environment surrounding the orientating molecule.

According to the empirical rule proposed by Schallamach[20] on the dielectric relaxation in a two-component liquid mixture, one common relaxation is observed if the constituent liquids are both nonassociated or both associated. The present experimental results are not always consistent with this rule, because two dielectric relaxations are observed in the mixture of monochlorobenzene and monobromobenzene, the constituents being both nonassociated liquids. The mixture of nonassociated isoamyl bromide and n-octyl bromide follows Schallamach's rule.

References and Notes

(1) D. W. Davidson and R. H. Cole, *J. Chem. Phys.*, **19**, 1484 (1951).
(2) R. F. Grant, D. W. Davidson, and P. Gray, *J. Chem. Phys.*, **33**, 1713 (1960).
(3) G. E. McDuffie, Jr., and T. A. Litovitz, *J. Chem. Phys.*, **37**, 1699 (1962).
(4) D. J. Denney, *J. Chem. Phys.*, **27**, 259 (1957).
(5) F. I. Mopsik and R. H. Cole, *J. Chem. Phys.*, **44**, 1015 (1966).
(6) A. Matsumoto and K. Higasi, *J. Chem. Phys.*, **36**, 1776 (1962).
(7) S. H. Glarum, *J. Chem. Phys.*, **33**, 639 (1960).
(8) J. E. Anderson and R. Ullman, *J. Chem. Phys.*, **47**, 2178 (1967).
(9) D. D. Klug, D. E. Kranbuehl, and W. E. Vaughan, *J. Chem. Phys.*, **50**, 3904 (1969).
(10) W. F. Hassell and S. Walker, *Trans. Faraday Soc.*, **62**, 2695 (1966).
(11) W. E. Vaughan, W. S. Lovell, and C. P. Smyth, *J. Chem. Phys.*, **36**, 753 (1962).
(12) J. G. Berberian and R. H. Cole, *J. Am. Chem. Soc.*, **90**, 3100 (1968).
(13) E. Ikada, *J. Phys. Chem.*, **75**, 1240 (1971).
(14) S. Chandra and J. Prakash, *J. Chem. Phys.*, **54**, 5366 (1971).
(15) J. Ph. Poley, *J. Chem. Phys.*, **23**, 405 (1955).
(16) G. W. Chantry, "Submillimetre Spectroscopy", Academic Press, London, 1971, pp 177–187.
(17) S. K. Garg and C. P. Smyth, *J. Chem. Phys.*, **42**, 1397 (1965).
(18) K. Bergmann, D. M. Roberti, and C. P. Smyth, *J. Phys. Chem.*, **64**, 665 (1960).
(19) S. K. Garg and C. P. Smyth, *J. Chem. Phys.*, **43**, 2959 (1965).
(20) A. Schallamach, *Trans. Faraday Soc.*, **42A**, 180 (1946).

Azoxy Compounds and Oxadiaziridines. An ab Initio Study of the Ring Closure Reactions and of the Cis–Trans Isomerizations

Renzo Cimiraglia, Maurizio Persico, and Jacopo Tomasi*

Laboratorio di Chimica Quantistica ed Energetica Molecolare del C.N.R., Via Risorgimento 35,156 100 Pisa, Italy *(Received March 23, 1977)*

A description of different isomerization paths connecting *cis*- and *trans*-diimide *N*-oxide, and *cis*- and *trans*-oxadiaziridine is presented. The potential energy curves along the reaction path for the ground state and for the six lowest excited states have been determined by means of a CI treatment including the 20 most important configurations found in more extended CI calculations. The prediction of the interconversion mechanisms one can obtain from these calculations is in agreement with the experimentally known data and supports a hypothesis not yet confirmed on the O migration mechanism in asymmetric azoxy compounds.

Introduction

The number of experimental investigations on the azoxy compounds has grown in recent years especially because of the biological interest of such compounds.[1] A considerable portion of such investigations has been devoted to mechanistic studies of the photochemical rearrangement reactions which present some peculiar features not yet completely explained.

In fact, little is known so far about the isomerization mechanism of the azoxy compounds. We shall summarize here the most important conclusions of the research performed in this field. The azoxy group can exist both in cis and trans conformations, the former being less stable because of the steric repulsions between the substituents. It is possible to convert cis into trans azoxy compounds by heating; the activation energy for azoxybenzene is 24.8 kcal/mol in ethyl alcohol, 19.4 kcal/mol in n-heptane, and it is expected to be decidedly higher in aliphatic compounds.[2] Azoxy compounds can undergo, under irradiation, cis–trans isomerization or ring closure to oxadiaziridines. It has been shown, by quenching and sensitization experiments, that the former reaction in azoxybenzenes involves an excited singlet state.[3] The second reaction has been clearly observed only in alkyl deriva-
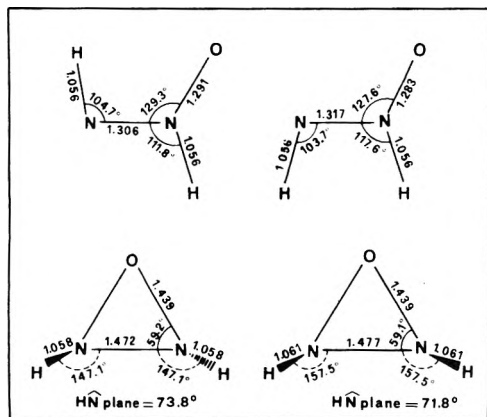
Figure 1. Geometries of the four stable species.

tives,[4] but the activation energy has not been determined.

The oxadiaziridines can also, in principle, have cis and trans conformations. The cis–trans interconversion implies an inversion at one of the pyramidal N atoms: the thermal barrier is expected to be decidedly high.[5,6] We have not found in the literature structure determinations which may prove the existence of cis and trans oxadiaziridines. This fact depends perhaps on the low stability of such compounds; alkyloxadiaziridines go back to the open chain precursors within a few hours at 20–30 °C.[4] The product of this reaction is generally a trans azoxyalkane, but in some cases also the cis form has been obtained, and it seems that the latter is favored in polar solvents.[7]

Some light on the relationship between the photochemical reactions of ring closure and of geometrical isomerization might be obtained from the experiments of Taylor and Riehl[8] if the interpretation given by the authors should be confirmed. If one admitted that the observed migration of the O atom in asymmetric arylalkylazoxy compounds passes through an unstable (and undetected) arylalkyloxadiaziridine, then it would be found that the formation of the ring requires rather energetic radiation, while the direct cis–trans isomerization of the azoxy compounds is easily obtained over a wider range of frequencies. In both cases the reaction involves only excited singlet states.

This short resume of only a selection of the experimental data concerning the photoisomerization of azoxy compounds shows that there are several hypotheses which require verification. The theoretical calculations we present in this paper may constitute a first step in this direction.

2. Physical Model and Computation Methods

We have selected for our investigation the simplest molecular system containing the azoxy group, the diimide N-oxide, and its isomers (see Figure 1). These compounds have never been synthesized nor detected, but they can be considered good models for the azoxyalkanes and the related oxadiaziridines and permit some extrapolations to the azoxyarenes.

We have computed the energy of the ground and of the first excited states at more than 150 points of the nine-dimension conformational space in order to obtain a representation of the most interesting features of the different hypersurfaces. The geometry optimization of the species which are found to be stable in the ground state has been performed by means of SCF calculations with the usual STO-3G basis set.[9] There is ample evidence to believe that such an approximation is sufficient to give a correct prediction of the bond lengths and angles. On the other hand, the STO-3G basis gives an incorrect prediction

TABLE I: Weights of the Configurations Used in Our CI Calculations in the Wavefunctions of _trans_-Diimide N-Oxide[a]

Configurations[b]	Electronic states				
	S_0	T_1	T_2	S_1	S_2
SCF ground state	0.9099				0.0089
(12,13)	0.0011	0.9330			0.7496
(11,13)			0.8827	0.8703	
(9,13)	0.0044	0.0082			0.0352
(12,22)	0.0001	0.0231			0.0008
(12,13)(12,13)	0.0566				0.0392
(11,13)(12,13)			0.0465	0.0563	
(10,13)(12,13)			0.0203	0.0237	
(9,13)(12,13)	0.0041	0.0022			0.0984

[a] Only the configurations having a weight $\geqslant 0.02$ in one electronic state at least have been reported. [b] Single and double excitations are indicated by one or two hole-particle couples.

of the relative stability between the unsaturated open chain isomers and the saturated three-membered rings at the SCF level as well as after extended CI (see Table I).

Our description of the energy hypersurfaces has been obtained by using a larger basis which in addition to the STO-3G functions has a further set of 2s and 2p diffuse Gaussians on the heavy atoms (STO-3G + sp basis set[10,11]). Calculations performed in our laboratory on other systems have shown that such a set is decidedly superior to the STO-3G set in describing excited states.

It may be remarked that the basis set we have selected does not contain d-type functions. It is well known that the addition of d functions to the heavy (nonhydrogen) atoms preferentially lowers the SCF ground state energy of three-membered rings with respect to that of the corresponding acyclic compounds.[12-14] Little is known about the differential influence of d functions on the ground state energies at intermediate geometries and on the excited state energies. The exclusion of d functions has been dictated only by economic considerations and there is the possibility that the picture of the energy hypersurfaces we have obtained might turn out to be slightly distorted.

The energies we shall use in the following discussion refer to CI wavefunctions obtained on a basis of 20 singly and doubly excited configurations (corresponding to 38 determinants). The selection of these configurations has been made by using more extended CI's performed with the CIPSI method[15,16] at three representative points of the conformation space: the points corresponding to trans N-oxide, to _trans_-oxadiaziridine, and to a geometry intermediate between the first two. All the determinants giving an appreciable contribution (more than 1–2%) to the wavefunction of at least one of the five electronic states S_0, S_1, S_2, T_1, T_2 at at least one of the three geometries have been selected and employed in the subsequent calculations. A novel CI program explicitly set up to take advantage of such limitation in the number of configurations has been employed. This strategy greatly reduces the computation times with respect to exhaustive CI procedures without loss of substantial information.[17] (If t is the time necessary to get a SCF calculation,[18] the extra time necessary to get the whole set of five wavefunctions is approximately $3t$–$8t$ when the CIPSI program is employed and $0.1t$–$0.3t$ when our CI program is utilized.)

The 20 configurations we have selected are specified in Table I which reports also the weights they have in the CIPSI calculations for the trans N-oxide. Such configurations are identified by means of a hole–particle operator acting on the SCF ground state wavefunction. The mo-

TABLE II: Energy of *trans*-Diimide N-Oxide (in au) and Relative Energies of the Other Species (in kcal/mol) According to Different Approximations

	STO-3G SCF	STO-3G SCF + CI[a]	STO-3G + sp SCF	STO-3G + sp SCF + CI[a]	STO-3G + sp SCF + CI (20 confg)	4-31G SCF
trans-Diimide N-oxide	-182.31656	-182.42279	-182.55522	-182.60660	-182.58692	-184.49002
cis-Diimide N-oxide	7.6		9.6		8.0	10.5
trans-Oxadiaziridine	-28.5	-2.0	22.5	49.6	42.4	47.6[b]
cis-Oxadiaziridine	-21.3		31.9		51.8	56.5[b]

[a] CI has been accomplished with the CIPSI method, with $\eta \simeq 0.04$ (for the meaning of η see ref 15).   [b] Reference 12.

lecular orbitals have been enumerated according to their (increasing) energies and MO correlation for different geometries has been performed according to the non-crossing rule.[19]

The photochemical implications we shall discuss in the following sections are derived from such a description of the energy hypersurfaces supplemented with qualitative considerations on the motion of a point representing the nuclear coordinates over such a set of surfaces.[20,21]

3. Results and Discussion

(a) *Geometries and Energies of the Ground State Species.* The ground state energy hypersurface presents several minima. In addition to the minima corresponding to the four species represented in Figure 1, we have found also minima corresponding to the following structural formulas: H_2NNO and HNONH. We shall not further consider in this paper the portion of the conformational space corresponding to these last species and shall confine our attention to the diimide N-oxides and to the oxadiaziridines.

The STO-3G optimized geometries of *cis*- and *trans*-oxadiaziridine have been already obtained by Pople and co-workers.[12] We have followed an iterative technique already tested[22] to obtain the best geometries for both the diimide N-oxides with the constraints of keeping the molecules planar and of maintaining the same length for the two NH bonds.[23] The bond lengths and bond angles have been determined with the precision of ±0.01 Å and ±1°, respectively. The resulting geometries are given in Figure 1.

Table II shows the energy of the *trans*-diimide N-oxide and the relative energies of the other molecules calculated with the methods described in the preceding section. As has been anticipated the STO-3G basis set favors closed structures, in contrast to both larger basis set calculations and experimental results.

The portion of the conformation space we have investigated corresponds with the interconversion paths schematically depicted in Figure 2. We shall report first on the ground state activation energies.

(b) *Thermal Isomerizations.* There are two possible paths for the cis-trans isomerization in the diimide N-oxide involving (I) an in-plane inversion of the N atom and (II) a rotation around the double bond. The transition state has been assumed to have a linear geometry in the H–N–N fragment in the first case and a rotation angle of 90° in the second. The R_{NN} distance which is rather sensitive to changes in the π bond has been optimized separately in both transition states, while for the other parameters intermediate values between those of the two isomers have been selected.[24]

The cis-trans isomerization of oxadiaziridine can occur only through the inversion of one of the two nitrogen atoms (path III of Figure 2); a second path involving the inversion of both N atoms has been attempted and discarded. The transition state has been assumed to have a planar nitrogen conformation. The bond lengths of the ring have been
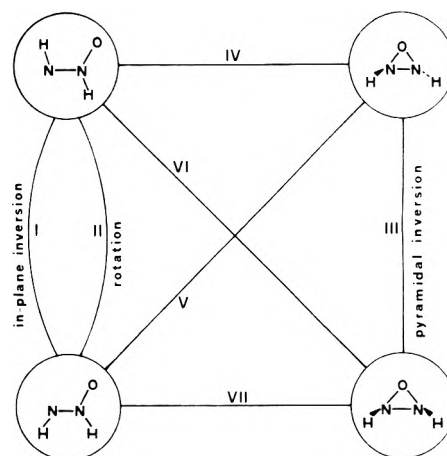

Figure 2. A sketch of the rearrangement paths investigated in this paper.

TABLE III: Ground State Activation Energies (in kcal/mol)

	Path	Energy
I	From *cis*-diimide N-oxide to trans by planar inversion	44.1
II	From *cis*-diimide N-oxide to trans by rotation	58.5
III	From *cis*-oxadiaziridine to trans	38.5
IV	From *trans*-oxadiaziridine to *trans*-diimide N-oxide	27.3
V	From *trans*-oxadiaziridine to *cis*-diimide N-oxide	14.6
VI	From *cis*-oxadiaziridine to *trans*-diimide N-oxide	5.8
VII	From *cis*-oxadiaziridine to *cis*-diimide N-oxide	23.6

optimized at the SCF level,[25] the other parameters have been kept at intermediate values between those reported in Figure 1.

The conversion between open and closed structures can follow four different paths (paths IV–VII in Figure 2). In all four cases we have adopted as leading parameter the ∠ NNO angle (α). The other coordinates are the bond lengths and the angles $P_1N_1N_2$ (β), $P_2N_2N_1$ (γ), $P_1N_1H_1$ (δ), $P_2N_2H_2$ (ϵ), where N_1 is the terminal nitrogen atom and H_1 the hydrogen bound to it, N_2 the nitrogen atom linked to the oxygen, and P_1, P_2 the projections of H_1 and H_2 on the plane of the heavy atoms.

To determine the position of the barrier we have varied α along the four paths with the other parameters varying linearly. At the top of the barrier found in this first approximation we have optimized the N–N and N–O bond lengths and the δ and ϵ angles.[26] A second cycle of calculations was then performed, using again α as leading parameter and making linear variations of the other internal coordinates in the intervals corresponding to the passage from the N-oxide to the intermediate and from the intermediate to oxadiaziridine.

The activation energies are reported in Table III. All values have been obtained, as discussed above, with CI

TABLE IV: Vertical Excitation Energies (in eV) for the Three First Excited Triplets and Singlets (CI Calculation)

trans-Diimide N-Oxide[a]		cis-Diimide N-Oxide[a]	
$^1A' \to {}^3A'$	2.34	$^1A' \to {}^3A'$	2.15
$^1A' \to {}^3A''$	4.21	$^1A' \to {}^3A''$	3.80
$^1A' \to {}^3A''$	5.77	$^1A' \to {}^3A''$	5.37
$^1A' \to {}^1A''$	4.44	$^1A' \to {}^1A''$	4.04
$^1A' \to {}^1A'$	6.00	$^1A' \to {}^1A''$	5.65
$^1A' \to {}^1A''$	6.24	$^1A' \to {}^1A'$	6.26
trans-Oxadiaziridine[b]		cis-Oxadiaziridine[a]	
$^1A \to {}^3B$	6.55	$^1A' \to {}^3A'$	6.49
$^1A \to {}^3A$	6.77	$^1A' \to {}^3A''$	6.68
$^1A \to {}^3B$	7.92	$^1A' \to {}^3A''$	8.22
$^1A \to {}^1B$	8.02	$^1A' \to {}^1A''$	7.81
$^1A \to {}^1A$	8.31	$^1A' \to {}^1A'$	8.42
$^1A \to {}^1B$	9.37	$^1A' \to {}^1A'$	9.20

[a] Symmetry point group C_s. [b] Symmetry point group C_2.

wavefunctions involving 20 configurations.

In the diimide N-oxide the in-plane isomerization (path I) is favored with respect to the rotational one (path II). It should be noticed that we have discarded a few configurations which contribute to depressing the rotational barrier. Actually, at the SCF level, path II is slightly favored (the two barriers differ by about 2 kcal/mol) and we cannot at present exclude that a larger CI calculation might confirm the SCF prediction. The barriers are of the same order of magnitude as those found in the analogous isomerization processes of the diimide molecule.[27] If one replaces hydrogens with bulky alkyl substituents in the azoxy compounds, the height of the barrier is expected to decrease because the cis-diimide N-oxide is further destabilized by steric repulsions. In similar compounds Merényi et al.[28] have found that even a CH_3 group is effective in lowering these barriers through hyperconjugative effects; thus the barrier for azoxyalkanes will be intermediate between the 44 kcal/mol found in the present computation and the 25–20 kcal/mol experimentally found for azoxybenzene.[2]

The value of 38.5 kcal/mol for the N inversion barrier in oxadiaziridine is in agreement with the generally accepted interpretation of the origin of this barrier.[5,6] In fact this barrier is some kilocalories per mole higher than the corresponding one in oxaziridine (CNDO, 33.9 kcal/mol;[29] ab initio SCF, 32.4;[30] experimental, 31–34[30,31]); in our molecule there is a more electronegative atom replacing the CH_2 group of oxaziridine and, as a consequence, the s character of the N lone pair increases. Such a lone pair becomes a pure p orbital in the transition state and consequently an increase of its s character produces a raising of the barrier.

The most overestimated barrier is probably the one corresponding to the conversion from trans-oxadiaziridine to trans-diimide N-oxide (IV). This barrier is considerably higher than that for the conversion to cis N-oxide (V). Experimentally, a cis/trans ratio of N-oxide equal to 30/70 has been found for the thermal ring opening reaction of diisopropyloxadiaziridine.[7] Such data indicate that process IV should have a barrier lower than process V. There is however the possibility that the inclusion of bulky substituents in our model systems might produce changes in the ratio of the two barriers going in the right direction.

The activation energy for process VI indicates that cis-oxadiaziridine undergoes fast ring opening, even at room temperature; the reaction cannot but be accelerated by alkyl substitution. Finally, a comparison of processes VI and VII indicates that thermal ring opening reactions of cis-oxadiaziridines should give a ratio of cis/trans N-oxides decidedly in favor of the trans isomer.
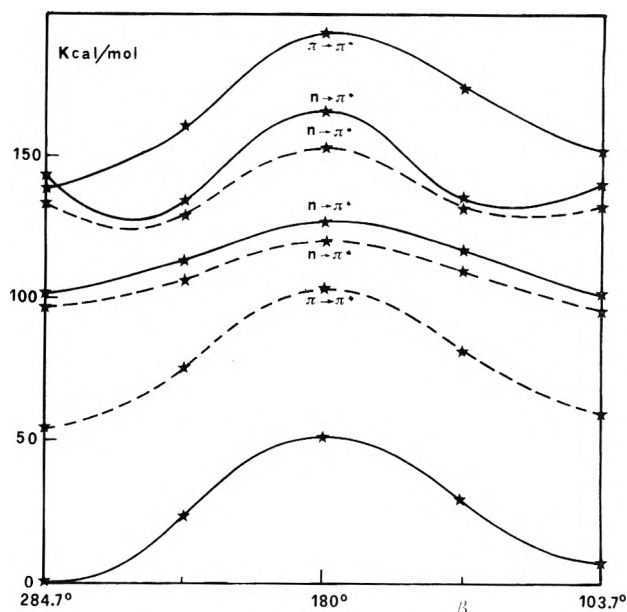

Figure 3. Cis–trans isomerization of the diimide N-oxide by in-plane inversion (path I). The full lines refer to singlet states and the dashed ones to triplet states. β is the $\angle H_1 N_1 N_2$ angle.

(c) *Excited States and Photochemical Isomerizations.* For the trans-diimide N-oxide we have found three low-lying singlet excited states (see Table IV). The first corresponds to a n → π* transition, and the calculated energy corresponds to a wavelength of 279.3 nm, in good agreement with the experimental data for azoxyalkanes[32,33] which exhibit a weak absorption near 280 nm. The second is a π → π* transition at 206.8 nm, corresponding to the strong absorption band found near 220 nm. The third transition, n → π* in character, at 198.8 nm has never been detected; the corresponding weak band is probably hidden under the one centered at 220 nm, which is spread. The nature of these excited states has been determined by inspection of the population analysis of the corresponding CI wavefunctions. Taking as reference the S_0 state, S_1 is characterized by a charge transfer from the O lone pair to the N_1 atom; S_2 shows a strong polarization of the π system toward the same N atom; S_3 mainly involves a transition from the N_1 lone pair to the π system. In the same interval of energies there are also three triplet states; the lowest (T_1) corresponds to a π → π* excitation with a moderate shift of electrons along the NO bond toward N_2; T_2 and T_3 show a charge distribution similar respectively to S_1 and S_3.

The same excited states are present also in the cis-diimide N-oxide. The agreement of our transition energies with the experimental ones is not so good as in the preceding case, probably because the selection of the 20 configurations chosen for the CI treatment has been performed on the trans isomer. The values of the transition wavelengths are 306.6 nm (n → π* transition, experimental value 280–290 nm[7,34]), 219.5 nm (n → π*, not detected experimentally), 198.0 nm (π → π*, experimental value 230 nm). The characterization of the states is the same as in the preceding molecule.

The oxadiaziridines show only short wavelength transitions (less than 160 nm) of scant photochemical interest.

The energy curves for the planar inversion and rotation mechanisms of the cis–trans isomerization processes are given in Figures 3 and 4. A further optimization of the N–N distance was performed at the midpoint of the transformation path.[35] The figures report the case corresponding to the optimization on the S_1 state but there
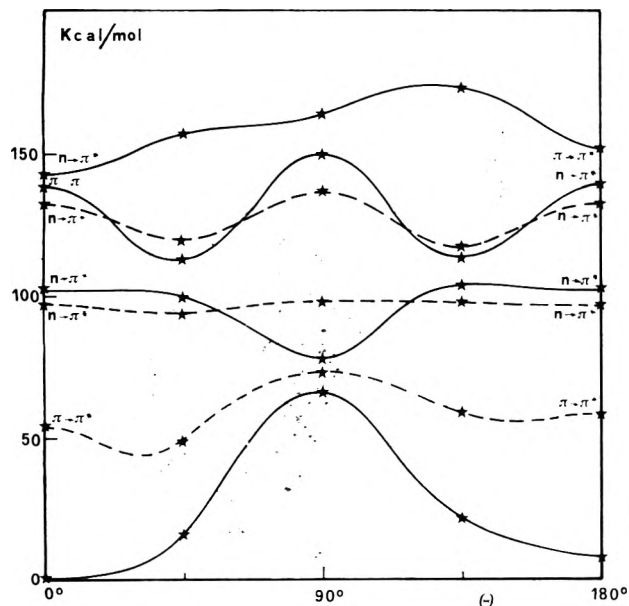
Figure 4. Cis–trans isomerization of the diimide N-oxide by rotation (path II). θ is the rotational angle.

is not a great difference in the other cases. In order to construct such curves, R_{NN} has been varied linearly from the value it has in the trans geometry to that found for the intermediate one and symmetrically from the intermediate to the cis conformer. The other internal parameters have been varied linearly over the entire range.

Rotation is clearly preferred to inversion. The former can occur in the S_1 $n \rightarrow \pi^*$ state which exhibits a symmetrical funnel to S_0: this feature of the S_1 surface is in agreement with the experiments leading to photoequilibrium mixtures which are composed of equal portions of cis and trans isomers.

The S_2 state too is reactive, having two nearly symmetrical funnels to the S_1 surface.

By examining Figure 4 one can see that the S_2 curve connects a $n \rightarrow \pi^*$ state in the trans conformation to a $\pi \rightarrow \pi^*$ state in the cis conformation, while in the in-plane inversion mechanism (Figure 3) such a change of electronic configuration does not occur. A clear pictorial explanation of this feature of the potential surface has been given by Gimarc[36] for the analogous case of the diimide molecule (HN=NH). Worthy of mention is another feature of this section of the potential surface which neatly distinguishes the diimide case from the diimide N-oxide. In the former molecule there is a crossing of the S_0 surface with T_1 in correspondence with the middle of the rotational path. In this region T_1 has a well marked minimum. In the N-oxide case there are no crossings, and at $\theta = 90°$ T_1 has a maximum. It can be remarked however that T_1 has in diimide a $n \rightarrow \pi^*$ character and that this transition in the N-oxide corresponds to the T_3 state which has again two small minima near $\theta = 45$ and $135°$.

The investigation of the photochemical ring closure reaction is more complicated. Excited and ground state energy curves for the paths IV–VII are reported in Figures 5–8. They have been obtained by using α as leading parameter and adopting a linear variation of the other coordinates.

Some features are common to the four graphs. (a) For all the triplet states there is a substantial increase of the energy in the portion of the reaction path preceding the S_0 barrier. Reaction mechanisms involving a triplet state can be thus discarded   (b) Also in the S_1 states there is a portion of the curve (again preceding the S_0 barrier)
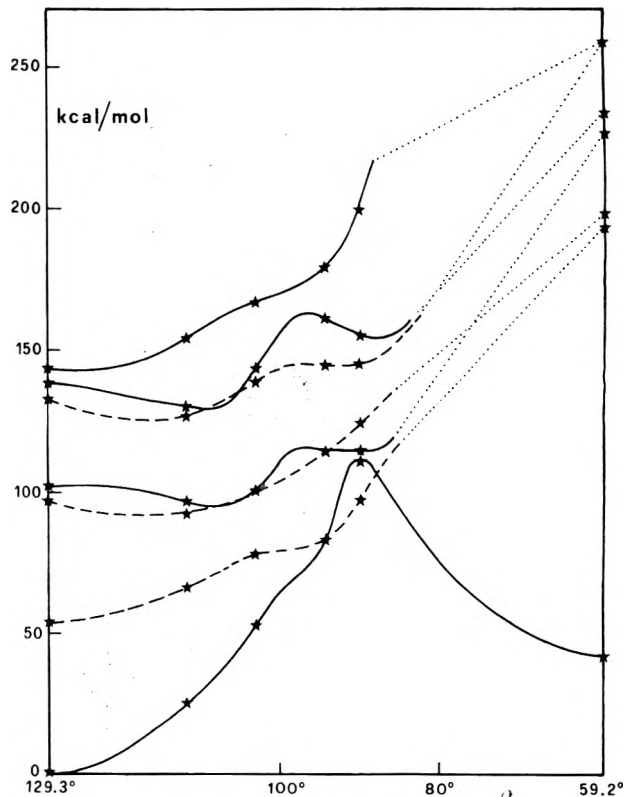

Figure 5. Potential energy curves along a schematic representation of the isomerization path connecting *trans*-diimide N-oxide to *trans*-oxadiaziridine (path IV). The dotted lines give the correlation of the energy curves with the vertical states of oxadiaziridine in an unexplored region. α is the $\angle$NNO angle.

Figure 6. Potential energy curves along a schematic representation of isomerization path connecting *cis*-diimide N-oxide to *trans*-oxadiaziridine (path V).

where the energy rises considerably but in paths IV, V, and VII there is also a favorable funnel to S_0. (c) The S_2 curves have a minimum at values of the reaction coordinate preceding the region where the energy of S_1 rises.

Figure 7. Potential energy curves along a schematic representation of the isomerization path connecting *trans*-diimide *N*-oxide to *cis*-oxadiaziridine (path VI).
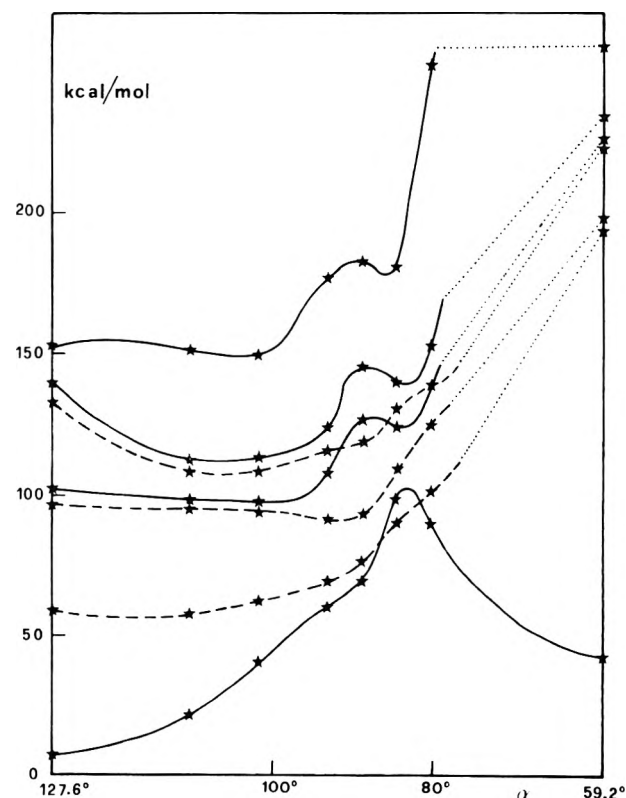

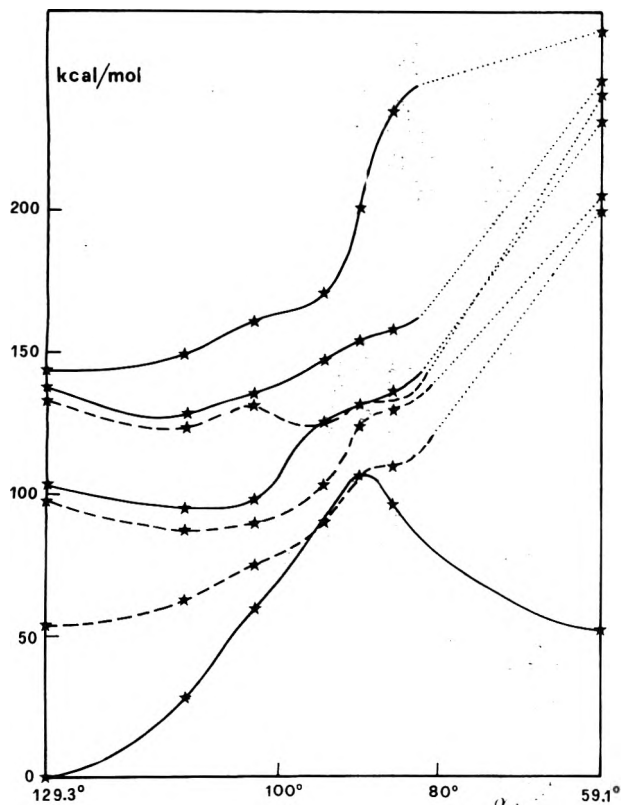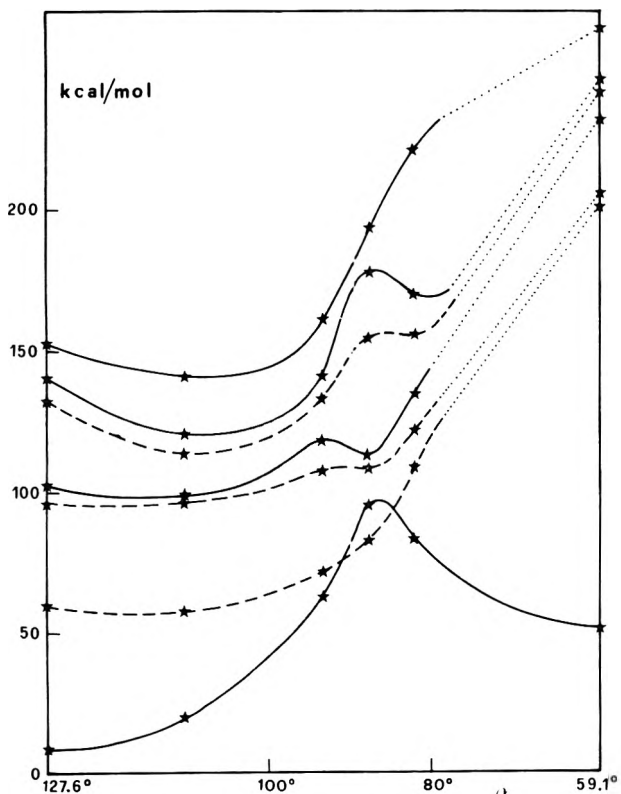**Figure 8.** Potential energy curves long a schematic representation of the isomerization path connecting *cis*-diimide *N*-oxide to *cis*-oxadiaziridine (path VII).

Ring closure mechanisms involving excitations to the S_1 state do not seem probable because there remains a noticeable barrier to pass. Alternative mechanisms involving excitations to S_2 (or S_3) followed by internal conversion to S_1 are more probable, although the relative positions
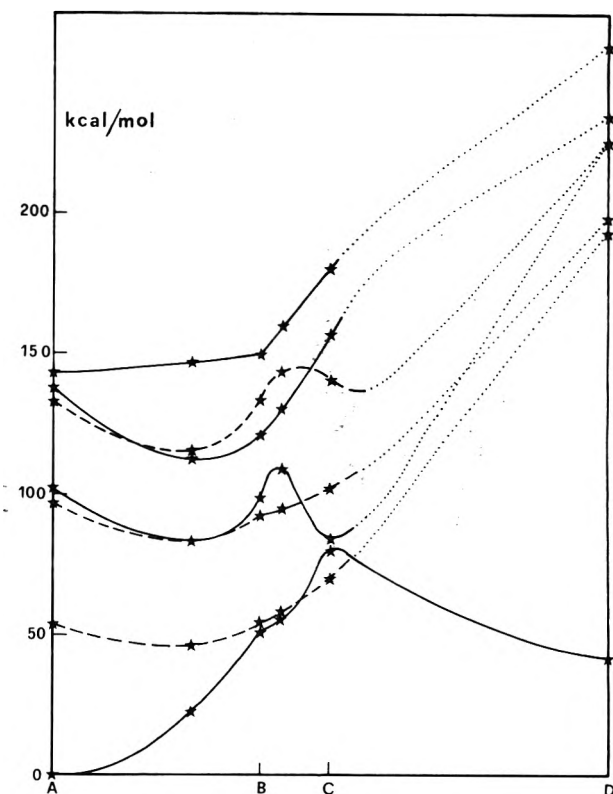

Figure 9. Potential energy curves along an improved representation of the isomerization path connecting *trans*-diimide *N*-oxide to *trans*-oxadiaziridine (compare with Figure 5). Points B and C indicate the α angles where an optimization of the S_2 and S_1 geometries has been performed.

of the maxima and the minima on such curves do not clearly indicate effective funnel mechanisms.

As there are no unambiguous answers, one is compelled to pass to a more detailed description of the reaction surface. After the initial excitation, the molecule will be pushed toward the minimum occurring in the S_2 surface. Such a minimum will correspond not only to a smaller value of the α angle but also to values of the other angles and lengths different from those corresponding to the vertical excitation. Such a displacement of the representative point on the conformation space can lead to more or less efficient funnels according to the shape of S_1 in this region.

An extensive investigation with the procedures we have adopted to obtain the energies is a rather hard task and we have limited ourselves to partially refining the description of path IV, which seems to be the best candidate (see Figure 5) for the photochemical ring closure reaction. First, with partial optimizations, we have localized with more precision the position in the conformational space where S_2 has a minimum. Then, we have selected an α value (103°) which does not correspond to the minimum of S_2 but rather to the region where the funnel to S_1 is more probable and we have optimized the S_2 geometry at this α value. As a further refinement of the description we have performed partial optimizations on the S_1 and S_0 surfaces in search of the best conditions for the $S_1 \rightarrow S_0$ funnelling, and then we have selected a second value for the α angle (94°) and performed a complete optimization of the S_1 state geometry.

Figure 9 partially depicts the improved description we have obtained. The points marked B and C[37] correspond to the α angles for which an optimization of respectively the S_2 and the S_1 state has been performed. In constructing the curves of Figure 9 the internal coordinates

have been varied linearly in the intervals trans-N-oxide–B, B–C, C–trans-oxadiaziridine. Such curves do not correspond to the best geometries we have found for some states at scattered values of the α angle, but Figure 9 gives a picture directly comparable to that of Figure 5 because in both cases all curves corresponding to a given α value correspond to the same geometry.

The mechanism for the ring closure reaction we have hesitatingly proposed before (excitation to S_2 followed by internal conversion to S_1 and then to S_0) appears more probable in this improved representation of the reaction path.

This example is sufficient to show that the representations of the reaction paths given in Figures 5–8 are too schematic and that better representations can lead to the discovery of more efficient reaction channels.

4. Conclusions

The ab initio calculations we have discussed in the present paper allow one to obtain an overall picture of the relative stabilities of the four isomers of the symmetric azoxyalkanes and of the possible interconversion paths. The linear structures are more stable than the cyclic compounds, the trans isomers more stable than the cis. This conclusion, which is in agreement with the experimentally known facts, is supplemented with quantitative predictions of the corresponding activation energies.

In addition one can predict that the photoisomerization process for the cis–trans isomerization of the azoxyalkanes prefers the mechanism which requires a rotation around the N–N bond; an absorption of light in the main absorption band of the azoxyalkanes is sufficient to permit this reaction. The thermal conversion process does not have such clear-cut requirements and the present prediction of a planar inversion necessitates further investigation.

The cis-oxadiaziridines are rather unstable compounds and probably they do not exist at room temperature as stable compounds; such isomers however have some interest as possible reaction intermediates.

The ring closure photoreaction has been shown to be possible, even if this prediction requires a confirmation from dynamical calculations. Among the four possible reaction paths the most favorable seems to be that corresponding to the trans-diimide N-oxide → trans-oxadiaziridine conversion (reaction path IV of Figure 2), but at least two other reactions appear to be possible (reaction paths V and VII). Such reactions do not involve triplet states and require rather energetic irradiations. The hypothesis of Taylor and Riehl[8] for explaining the O migration in alkylarylazoxy compounds finds thus a strong support.

Finally, the assignement of the UV absorption bands in the azoxyalkanes can be considered definitively confirmed.

References and Notes

(1) T. Miyadera in "The Chemistry of the Hydrazo, Azo, and Azoxy Groups", S. Patai, Ed., Interscience, New York, N.Y., 1975.
(2) S. B. Rhee and H. H. Jaffé, J. Am. Chem. Soc., 95, 5518 (1973).
(3) R. Tanikaga, Bull. Chem. Soc. Jpn., 41, 1664, 2151 (1968).
(4) F. D. Greene and S. S. Hecht, J. Org. Chem., 35, 2482 (1970).
(5) J. M. Lehn, Top. Curr. Chem., 15, 311 (1970).
(6) J. B. Lambert, Top. Stereochem., 6, 19 (1971).
(7) J. Swigert and K. G. Taylor, J. Am. Chem. Soc., 93, 7337 (1971).

(8) K. G. Taylor and T. Riehl, J. Am. Chem. Soc., 94, 250 (1972).
(9) W. J. Hehre, R. F. Stewart, and J. A. Pople, J. Chem. Phys., 51, 2657 (1969).
(10) K. Morokuma, S. Iwata, and W. A. Lathan in "The World of Quantum Chemistry. Proceedings of the First International Congress of Quantum Chemistry. Menton, France 1973", Reidel Publishing Co., Dordrecht, 1974, p 277.
(11) R. Cimiraglia and J. Tomasi, J. Am. Chem. Soc., 99, 1135 (1977).
(12) W. A. Lathan, L. Radom, P. C. Hariharan, W. J. Hehre, and J. A. Pople, Top. Curr. Chem., 40, 1 (1973).
(13) P. C. Hariharan and J. A. Pople, Chem. Phys. Lett., 16, 217 (1972).
(14) P. C. Hariharan, L. Radom, J. A. Pople, and P. v. R. Schleyer, J. Am. Chem. Soc., 96, 559 (1974).
(15) B. Huron, J. P. Malrieu, and P. Rancurel, J. Chem. Phys., 58, 5745 (1973).
(16) The number of determinants introduced in our CIPSI calculations is of the order of 80 000.
(17) It should be remarked that we have not enclosed in our set of configurations a few which have some weight only at the top of the barrier corresponding to the rotational cis–trans isomerization of the N-oxide. The exclusion of such configurations greatly reduces the computational burden at the cost of a slight overestimation of the ground state rotational barrier.
(18) The computer time necessary to get the starting SCF ground state wavefunction ranges between 240 and 660 s (on a IBM 370/158 machine) according to the number of cycles necessary to reach self-consistency.
(19) When limited CI calculations are performed, ensuring a correct MO correlation becomes a crucial point. We have checked the non-crossing rule with other criteria (see, for example, H. E. Zimmerman, Acc. Chem. Res., 5, 399 (1972)) and we think we have chosen the best correlations. The only exceptions to the noncrossing rule regard the in-plane cis–trans interconversion path for the diimide N-oxide. In this case there are the following correlations which produce a crossing: 17 cis ↔ 18 trans, 23 cis ↔ 22 trans (both of π type) and 18 cis ↔ 17 trans, 22 cis ↔ 23 trans (both of σ type).
(20) J. Michl, Top. Curr. Chem., 46, 1 (1974).
(21) J. Michl, Mol. Photochem., 4, 243 (1972).
(22) G. Alagona, E. Scrocco, and J. Tomasi, J. Am. Chem. Soc., 97, 6976 (1975).
(23) These assumptions can be justified by the presence of a π system and by some crystal structure determinations reported by R. Allmann in "The Chemistry of the Hydrazo, Azo and Azoxy Compounds", S. Patai, Ed., Interscience, New York, N.Y., 1975.
(24) The R_{NN} values are 1.300 Å (path I) and 1.381 Å (path II).
(25) Such optimization has been performed with the STO-3G basis set and then has been simply checked with the more extended basis set. The bond lengths are (in Å) $R_{N_1O} = 1.406$, $R_{N_2O} = 1.478$, $R_{NN} = 1.412$. N_1 is the inversion center.
(26) The geometries of the intermediates, after this cycle of optimizations, are the following (lengths in Å):

(IV) $R_{NN} = 1.526$, $R_{NO} = 1.374$, $R_{N_1H_1} = R_{N_2H_2} = 1.507$, $\alpha = 98°$, $\beta = 136.5°$, $\gamma = 128°$, $\delta = 71°$, $\epsilon = 64°$.

(V) $R_{NN} = 1.561$, $R_{NO} = 1.443$, $R_{N_1H_1} = R_{N_2H_2} = 1.507$, $\alpha = 88°$, $\beta = 129°$, $\gamma = 134°$, $\delta = 69°$, $\epsilon = 65°$.

(VI) $R_{NN} = 1.477$, $R_{NO} = 1.344$, $R_{N_1H_1} = R_{N_2H_2} = 1.508$, $\alpha = 102°$, $\beta = 143°$, $\gamma = 130°$, $\delta = 63°$, $\epsilon = 37°$.

(VII) $R_{NN} = 1.521$, $R_{NO} = 1.383$, $R_{N_1H_1} = R_{N_2H_2} = 1.509$, $\alpha = 94°$, $\beta = 130°$, $\gamma = 137°$, $\delta = 73°$, $\epsilon = 63°$.

(27) R. Cimiraglia, J. Riera, and J. Tomasi, to be published in Theor. Chim. Acta.
(28) G. Merényi, G. Wettermark, and B. Roos, Chem. Phys., 1, 340 (1973).
(29) A. Rauk, J. D. Andose, W. G. Frick, R. Tang, and K. Mislow, J. Am. Chem. Soc., 93, 6507 (1971).
(30) J. M. Lehn, B. Munsch, P. Millié, and A. Veillard, Theor. Chim. Acta, 13, 313 (1969).
(31) F. Montanari, I. Moretti, and G. Torre, Chem. Commun., 1086 (1969).
(32) B. W. Langley, B. Lythgoe, and L. S. Rayner, J. Chem. Soc., 4191 (1952).
(33) P. H. Gore and O. H. Wheeler, J. Am. Chem. Soc., 78, 2160 (1956).
(34) W. R. Dolbier, W. D. Lohele, and W. M. Williams, Chem. Commun., 867 (1972).
(35) The optimum bond lengths for the S_1 state are $R_{NN} = 1.412$ (path I), 1.366 (path II).
(36) B. M. Gimarc, J. Am. Chem. Soc., 92, 266 (1970).
(37) The B and C geometries have the following internal coordinates (lengths in Å):

B $R_{NN} = 1.457$, $R_{NO} = 1.354$, $R_{NH} = 1.057$, $\beta = 122°$, $\gamma = 125°$, $\delta = 58°$, $\epsilon = 73°$.

C $R_{NN} = 1.366$, $R_{NO} = 1.444$, $R_{NH} = 1.057$, $\beta = 140°$, $\gamma = 129°$, $\delta = 65°$, $\epsilon = 68°$.

Mechanism of Photogalvanic Effect in Thionine–Ferrous Salt Systems

Kiyotaka Shigehara and Eishun Tsuchida*

Department of Polymer Chemistry, Waseda University, Tokyo 160, Japan (Received May 20, 1977)

In the photoredox reaction between thionine and ferrous sulfate, the degree of photobleaching Δ, the overall photobleaching rate constant k, the photopotential ΔE, and the photocurrent I were measured under the fixed conditions by the use of a cross-illumination apparatus. From the relationship among Δ, k, ΔE, I, and the initial concentration of added ferric salt or the illumination light intensity, it was concluded that the electrode active species which generated the photoinduced electricity were the semiform of thionine and ferric ion produced by the photoredox reaction. Furthermore, the influence of added organic solvents, i.e., methanol and dimethylformamide on k and ΔE were discussed in relation to the state of electrode active species in solution.

Introduction

It is well known that thionine (Th) is photoreduced in

presence of ferrous salt yielding decolored semi-Th (S, one-electron reduced form) or leuco-Th (L, two-electron reduced form) and through a suitable electrode reaction, the energy stored in the charge-separated products (S or L and ferric ion) can be converted to the electric energy, which is the so-called photogalvanic effect.[1-5] The mechanism of the photoredox reaction was considered to be as shown in eq 1, in which the main reactions are

$$\text{Th} \xrightarrow[\substack{\text{dark, Fe}^{3+}, -\text{H}^+ \\ \text{disproportionation}}]{h\nu, \text{Fe}^{2+}, \text{H}^+} \text{S} \xrightarrow[\text{dark, Fe}^{3+}]{} \text{L} \tag{1}$$

described in eq 2–5, whereby S and L have a protonated

$$\text{Th} + \text{Fe}^{2+} + \text{H}^+ \xrightarrow{h\nu} \text{S} + \text{Fe}^{3+} \tag{2}$$

$$\text{S} + \text{S} \xrightarrow[\text{disproportionation}]{} \text{L} + \text{Th} + \text{H}^+ \tag{3}$$

$$\text{L} + \text{Fe}^{3+} \xrightarrow[\text{dark}]{} \text{S} + \text{Fe}^{2+} \tag{4}$$

$$\text{S} + \text{Fe}^{3+} \xrightarrow[\text{dark}]{} \text{Th} + \text{Fe}^{2+} + \text{H}^+ \tag{5}$$

structure at pH 1–4.[6] Most of the investigators regarded S and Fe^{3+} as the electrode active species (anode and cathode, respectively), and the mechanism of electron recycling was considered as in eq 6, although it still remained unclear.

$$\text{anode} \leftarrow (\text{e}) \leftarrow \underset{\substack{\uparrow \\ h\nu}}{\left(\overset{\text{Th}}{\underset{\text{S}}{\bigcirc}} \right)} \underset{}{\left(\overset{\text{Fe}^{2+}}{\underset{\text{Fe}^{3+}}{\bigcirc}} \right)} \leftarrow (\text{e}) \leftarrow \text{cathode} \tag{6}$$

Rabinowitch found the effect of added ferric salt on the photopotential ΔE,[1] although the purity of ferrous salt used was not described and was neglected. Furthermore, few investigators have reported about the photocurrent I by using a double-Pt electrode cell, and also the effective ΔE measured by the double-Pt electrode cell was scarcely

reported. They measured only the difference between the light potential and dark potential with Pt–caromel or Pt–Ag(AgCl),[1] from which the factors that influence the effective ΔE could not be recognized.

The efficiency of photoenergy conversion is believed to be about $10^{-3}\%$ (electric power output × 100/incident solar energy, and 0.1% when divided by incident monochromic light of about 600 nm which is the absorption maximum of Th). The reasons for this small value are as follows: (1) a short circuit in the solution due to the encounter of the electrode active species (eq 4 or 5), and (2) a short circuit on the surface of the electrodes (mainly on anode) due to the formation of local cells. In order to increase the efficiency of photoenergy conversion or in order to prohibit the two kinds of short circuits, the electrode active species must be confirmed.

In this paper, the effects of the illumination light intensity, the initial concentration of added ferric ion, and the solvent composition on ΔE and I were examined by using a rapid-scanning cross-illumination apparatus and a double Pt-electrode cell. The active species and the mechanism of electron recycling were also studied.

Experimental Section

Materials. Th (Tokyo Kasei, Co. Ltd., reagent grade, Cl salt) was recrystallized twice from 50% aqueous ethanol solution before use and its purity was confirmed by thin-layer chromatography eluted with 5% 2-propanol-chloroform. Analytical grade ferrous sulfate (Tokyo Kasei, Co. Ltd.), which contains 0.005% Fe^{3+}, was used without further purification. The content of Fe^{3+} was checked by the electronic spectra by using standard Fe^{3+} solution (Tokyo Kasei, Co. Ltd.). Water and methanol were distilled twice and dimethylformamide (DMF) was distilled five times before use.

Apparatus. The overall photobleaching rate constant k and the degree of photobleaching $\Delta\%$ were measured by a stopped-flow rapid-scanning spectrophotometer (Union Giken, Co. Ltd., RA-1300) modified for cross-illumination systems, which has a 100-W tungsten illumination light source and a 50-W measuring light source. The intensity of the latter was weakened to 0.03% of that of the former by using neutral filters, and it was confirmed that the illumination of the latter had no influence on the photoredox reaction (Figure 1). The photopotential ΔE and photocurrent I of the Th–Fe^{2+} system were measured by using the attachment illustrated in Figure 1b or the photocell illustrated in Figure 2.

Measurements. Solvents were bubbled for 1 h with pure N_2 which was completely deoxygenated by oxygen ab-
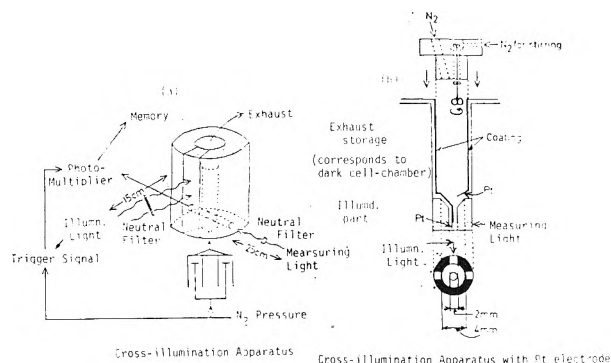
Figure 1. A cross-illumination apparatus (a) and one with a Pt electrode (b). The exhaust of (a) connects to the Pt-electrode part as shown in (b). The distance between Pt electrodes is 2.4 mm, and the surface area of each electrode is 0.13 cm². In (b), the exhaust storage was kept in the dark, which corresponds to the dark cell chamber, and the illuminated 2-mm flow cell corresponds to the lighted cell chamber.
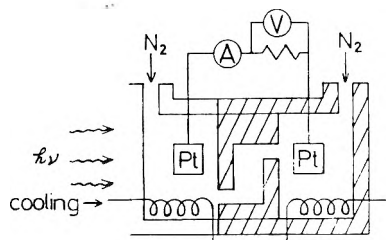
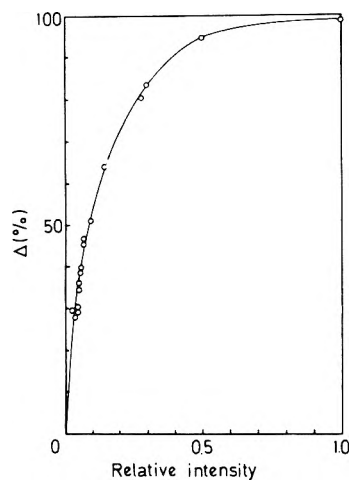

Figure 2. Photocell with a double-Pt electrode. The surface area is 2.0 cm².

Figure 3. Relationship between the relative intensity of illumination light and Δ: $[Th]_0 = 4.3 \times 10^{-5}$ M, $[FeSO_4]_0 = 4.3 \times 10^{-3}$ M, $[Fe^{3+}]_0 = 2.15 \times 10^{-7}$ M, pH 2.0, aqueous H_2SO_4 under N_2, 25 °C. The relative intensity was 1.0 = 10 mW/cm².

Figure 4. Relationship between relative intensity of illumination light and log k. Conditions are same as in Figure 3.

Figure 5. Relationship between Δ and ΔE. Conditions are same as in Figure 3. ΔE was measured using the apparatus of Figure 1.

periment except for the experiments of Figures 3–5 and 7.

Results and Discussion

The overall photobleaching rate constant k, the degree of photobleaching $\Delta\%$ $(([S] + [L]) \times 100/[Th]_0)$, the photopotential ΔE, and the photocurrent I of the Th–FeSO₄ aqueous system were measured using the apparatus illustrated in Figure 1. The intensity of illumination light was controlled by neutral filters to obtain the relationship with Δ (Figure 3). The Δ value increased with the relative light intensity and reached 100% if the intensity was strong enough. Next, the relationship between the relative light intensity and k is shown in Figure 4. The k value increased proportionately to the relative light intensity (in Figure 4, the axis is represented by log k), in contrast to the hyperbolic curvature of Figure 3. This difference is attributed to the influence of back reaction, i.e., (1) the k values were determined from the initial section of the time-decay curvature supposing a pseudo-first-order process in eq 2 and 3, so that the back reactions of eq 4 and 5 can be neglected; and (2) if the Δ value is large enough and the solution becomes transparent, it will be difficult to proceed with further photobleaching, because the possibility of back reactions increase.

According to the Nernst equation, the theoretical value of photopotential E_{calcd} can be represented as follows: (A) assume S is the anode active species

sorption towers, i.e., alkaline pyrogallol aqueous, sodium dithionite aqueous, and chromous perchlorate aqueous–zinc amalgam. Then, Th and ferrous sulfate were dissolved individually and two solutions were introduced into the syringes of the cross-illumination apparatus under N_2 and were rapidly mixed in the 2-mm flow cell illustrated in Figure 1a. The rapid spectral changes due to the photobleaching of Th were measured with time and k was determined from the initial section of time-decay curvatures according to the pseudo-first-order plots and $\Delta\%$ was also obtained from the final absorption intensity at the certain photoequilibrium state. The values ΔE and I were measured under the same conditions by using the attachment or the photocell described above and their stationary values were recorded. The intensity of illumination light was adjusted to 10 mW/cm² in every ex-

$$E^{S,Th/Fe^{3+},Fe^{2+}} = 0.47 + 0.0592 \times$$
$$\log ([S]/[Th][H^+])_L([Fe^{3+}]/[Fe^{2+}])_D \qquad (7)$$

$$E^{S,Th/Th,S} = 0.00 + 0.0592 \times$$
$$\log ([S]/[Th][H^+])_L([Th][H^+]/[S])_D \qquad (8)$$

$$E^{S,Th/S,L} = 0.17 + 0.0592 \times$$
$$\log ([S]/[Th][H^+])_L([S]/[L])_D \qquad (9)$$

$$E^{S,Th/H^+,H_2} = -0.18 + 0.0592 \times$$
$$\log ([S]/[Th][H^+])_L([H^+]/[H_2])_D \qquad (10)$$

(B) assume L is the anode active species

$$E^{L,S/Fe^{3+},Fe^{2+}} = 0.30 + 0.0592 \times$$
$$\log ([L]/[S])_L([Fe^{3+}]/[Fe^{2+}])_D \qquad (11)$$

$$E^{L,S/Th,S} = -0.17 + 0.0592 \times$$
$$\log ([L]/[S])_L([Th][H^+]/[S])_D \qquad (12)$$

$$E^{L,S/S,L} = 0.00 + 0.0592 \times$$
$$\log ([L]/[S])_L([S]/[L])_D \qquad (13)$$

$$E^{L,S/H^+,H_2} = -0.35 + 0.0592 \times$$
$$\log ([L]/[S])_L([H^+]/[H_2])_D \qquad (14)$$

where, E_0 for $Fe^{3+}|Fe^{2+}$ is 0.77 V,[7] E_0 for $Th|S$ is 0.30 V,[4] and the suffixes L and D represent the electrode reactions in a lighted chamber (on the anode) and in a dark chamber (on the cathode), respectively. In Figure 5, the relationship between Δ and ΔE_{obsd} or E_{calcd} according to eq 7 is illustrated, assuming that the disproportionation constant of eq 3, $k_d = [S]^2/[L][Th] = 0.01$ (k_d is believed to be 0.01–0.05[1,6]). First, eq 9 and 13 are less probable, because the solution in the dark chamber was not photobleached and it is quite difficult to consider that S was transported from the lighted chamber to the dark chamber, the distance of which is almost infinite on the molecular scale. Second, eq 10, 12, and 14 are also negligible, because the values calculated according to the equations are much smaller than the ΔE value observed. Thus there remains the possibility of eq 7, 8, and 11. However, we must note that E_0 is changed by chemical environments, for example, E_0 for $Fe^{3+}|Fe^{2+}$ in 1 M aqueous NaCl decreases to 0.69 V as determined from a polarography study. Namely, the actual E_0 is always smaller than that presented in the above equations, which further decrease the ΔE value.

In Figure 6, the effect of added ferric ion on ΔE was shown. The ΔE value increased with an increase in the initial concentration of added ferric ion, which may indicate that the ferric ion participates in the electrode reaction. From the consideration of this result and the report of Rabinowitch,[1] it is quite reasonable to regard the ferric ion as the cathode active species. The ΔE value decreased at higher concentrations of added ferric ion, because the increase in the backward reaction of eq 5 or 4 decreased the anode active species. Thus we can neglect the possibility of eq 8.

For the condition that $[S] < [Fe^{3+}]$ or $[L] < [Fe^{3+}]$, the photocurrent I might be proportional to $[S]$ or $[L]$. In Figure 7, the dependence of I on the Δ value is represented. The relationship between Δ and I showed bell-shaped curvature and it is very similar to that between Δ and $[S]_{calcd}$, in which K_d is supposed to be 0.01 (the shape of Δ–$[S]_{calcd}$ curvature does not change with the value of K_d). From this result, it may be concluded that the anode active species is S in the photoredox system composed of Th and ferrous salt. Hence eq 7 can be recognized as the most possible mechanism for the photogalvanic effect.

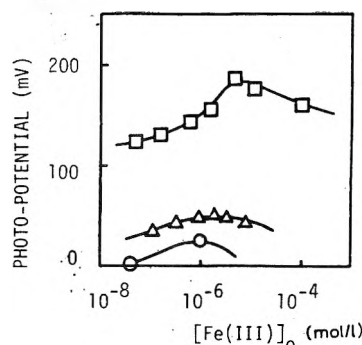The inconsistency between ΔE observed and that cal-

Figure 6. Relationship between $[Fe^{3+}]_0$ and ΔE: (O) $[Th]_0 = 1.0 \times 10^{-6}$ M, ($\triangle$) $[Th]_0 = 1.0 \times 10^{-5}$ M, ($\square$) $[Th]_0 = 4.3 \times 10^{-5}$ M, $[Fe^{2+}]_0/[Th]_0 = 100$. ΔE was measured using the apparatus of Figure 1. Other conditions are same as in Figure 3.
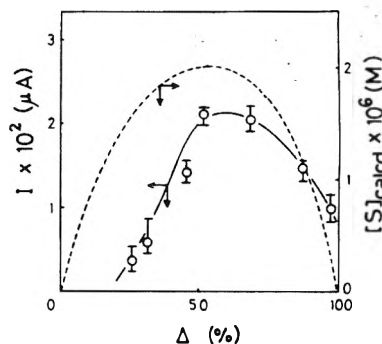

Figure 7. Correlation between Δ, I, and $[S]_{calcd}$. $[Fe^{3+}]_0 = 5.0 \times 10^{-5}$ M. I was measured using the apparatus of Figure 1. Other conditions are same as in Figure 3.
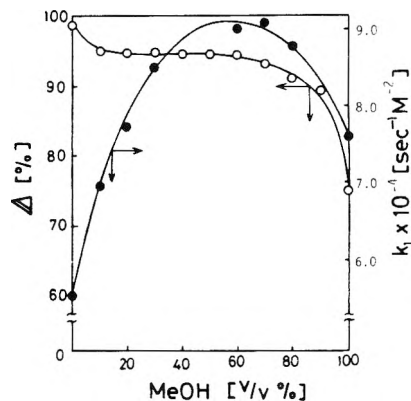

Figure 8. Relationship between methanol content and Δ and k. Conditions are same as in Figure 3.

culated (Figure 5) is caused not only by the decrease of E_0 described above, but also by the formation of local cells on the anode surface. Unfortunately, the influence of local cells cannot be taken account in eq 7–14, so that the Nernst equation does not exactly represent the photopotential obtained in these photogalvanic cells. In other words, [S] indicated in eq 7 is not a simple concentration term, but is the effective concentration of S on the surface of the anode, i.e., [overall concentration of S on the anode surface] – [the concentration of S cancelled by the formation of local cells]. However, as far as the formation of local cells is concerned, the conclusion obtained from the results represented in Figures 6 and 7 is not changed.

It is well known that the polarity of the solvent largely influences the reactions between ionic species. Figures 8 and 9 illustrate the effect of added methanol or DMF on the Δ and k values of the Th–FeSO$_4$ system. The Δ value gradually decreased with the amount of added organic solvents and then more steeply decreased when the amount
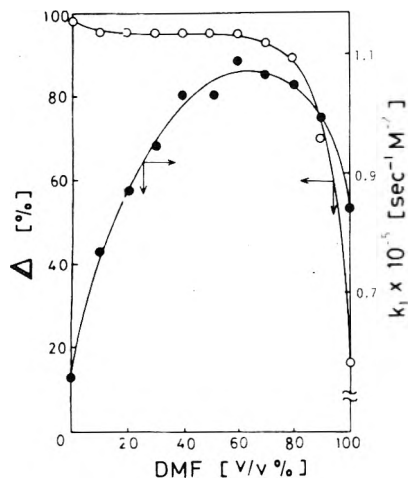
Figure 9. Relationship between DMF content and Δ and k. Conditions are same as in Figure 3.
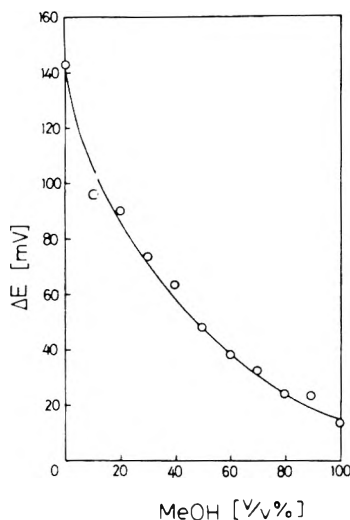

Figure 10. Relationship between methanol content and ΔE. ΔE was measured in the photocell of Figure 2. Conditions are same as in Figure 3.
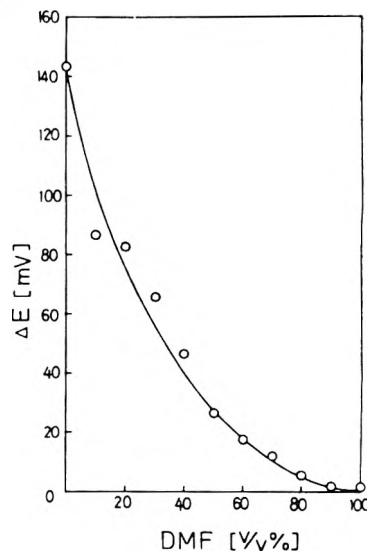

Figure 11. Relationship between DMF content and ΔE. ΔE was measured in the photocell of Figure 2. Conditions are same as in Figure 3.

exceeded 80%. Furthermore, the k value steeply increased with the content and showed a maxima at about 60%. In the intercationic reactions, the decrease of solvent polarity generally yields ion pairs between the cations and the corresponding counteranions, which decreases the activation energy of the reaction between the cations due to the decrease in solvation and due to the enhancement in frequency factor. In the present system, since the reactants are all cationic species as described in eq 2-5, the increase of methanol or DMF content (or the decrease of polarity) may result in the formation of ion pairs with anions, which further decrease the activation energy for desolvation and the electrorepulsive force between the reactants (cations). Therefore reactions 2-5 more easily occur with an increased amount of organic solvents, and the magnitude of

this influence is in the order, (5) $\simeq$ (4) > (3) > (2), from consideration of the apparent charges and structures of the reactants. In applying this concept to the results of Figures 8 and 9, (a) k is determined from the initial section of time-decay curve, so that k is almost dependent on eq 2 and increases with the content of organic solvents, and (b) while Δ depends on both eq 2 and to 5, Δ decreases with the content with the predominant influence being eq 4 and 5. Especially when the content is over 60%, the participation of eq 4 and 5 is not negligible even in the calculation of k (the supposition of a pseudo-first-order process became incorrect) and the k value apparently decreased. Hence ΔE, which was measured using the photocell illustrated in Figure 2, decreased with the content due to an increase in the possibility of back reactions or an increase in the short circuit in solution (Figures 10 and 11).

From these results, in order to obtain a larger amount of photoinduced electricity using photogalvanic cells the following must be done: (i) prohibition of back reaction between S and Fe^{3+}; (ii) prohibition of local cells; (iii) prohibition of disproportionation between S, which decreases the electrode active S species; and (iv) prohibition of ion pair formation. One possibility to satisfy (i), (iii), and (iv) is the incorporation and immobilization of dye nuclei into some cationic polymer supporters.

References and Notes

(1) E. Rabinowitch, *J. Chem. Phys.*, **8**, 551, 560 (1940).
(2) E. Rabinowitch and L. F. Epstein, *J. Am. Chem. Soc.*, **63**, 69 (1941).
(3) S. Ainsworth, *J. Phys. Chem.*, **64**, 715 (1960).
(4) R. Hardwick, *J. Am. Chem. Soc.*, **80**, 5667 (1958).
(5) J. Schlag, *Z. Phys. Chem. (Frankfurt am Main)*, **20**, 53 (1959).
(6) G. Granik, L. Michaelis, and M. P. Schubert, *Science*, **90**, 422 (1939); *J. Am. Chem. Soc.*, **62**, 204 (1940).
(7) W. C. Schumb, M. S. Sherrill, and S. B. Sweetser, *J. Am. Chem. Soc.*, **59**, 2360 (1937).

COMMUNICATIONS TO THE EDITOR

Cyclobutane Thermal Decomposition Rates at 1300–1500 K

Sir: Recent publications from other laboratories[1-4] have indicated that rate constants for a number of unimolecular reactions, previously thought to be well characterized, actually become anomalously low at temperatures above ~1100 K.[5] At least two quite different theoretical explanations have been put forward to account, partially or entirely, for the observed anomaly.[2,3,6] To date, all of the anomalously low rate data have come from absolute-rate single-pulse shock tube experiments where reactions were carried to high extents of conversion.[7] Comparative-rate single-pulse shock tube studies on a number of these suspect systems, for example, the structural isomerization of cyclopropane to propene,[8,9] have not indicated any deviation from strict Arrhenius behavior. This lack of agreement has hampered efforts to determine whether the reported anomaly is a characteristic behavior of these reactions, in need of theoretical justification, or merely an experimental artifact associated with high conversion in some absolute-rate studies. We wish to report here our initial results from a rate study of another system previously suggested as anomalous, cyclobutane → 2 ethene, using an experimental technique not heretofore used for the study of these reactions. Our data support a continuation of the low temperature Arrhenius parameters for this reaction up to at least 1500 K.

Reaction mixtures containing 5.0% cyclobutane in argon were heated by incident shock waves in a shock tube of rectangular cross section, previously described elsewhere;[10] and cyclobutane dissociation rates were deduced by monitoring density gradients in the reacting gas behind the incident shock waves, via the laser schlieren method described by Kiefer et al.[11] Fifteen experiments were run over the range 1308–1498 K, and all of these gave density profiles that showed evidence of approximately exponentially decaying endothermicity. One expects a constant density gradient behind a shock wave in a system which undergoes chemical reaction at a constant rate. However, for cyclobutane at these temperatures there will be significant percentages of decomposition within the time scale of our experiments, resulting in significantly lower reaction rates, decreasing rates of enthalpy change, and thus decreased laser beam deflection, as we observed. Extrapolation of the low temperature rate constant implies cyclobutane half-lives at 1300, 1400, and 1500 K of 5.5, 1, and 0.2 μs, respectively. Below 1300 K there was no detectable endothermicity, presumably because the reaction was proceeding too slowly, and above 1500 K the initial exponential decay collapsed into the "spike" or dead time caused by passage of the shock front through the laser beam, and could not be resolved. Shocks in pure argon gave flat density profiles except for the shock front spike. Temperatures behind incident shocks were calculated from measured incident shock velocities, using an ideal, one-dimensional shock model which assumed complete equipartition of energy and no chemical reaction. Enthalpy polynomials for cyclobutane were calculated from vibrational assignments given by Shimanouchi.[12]

From each recorded density profile, laser beam deflection due to cyclobutane dissociation at "time zero" was estimated by extrapolating the exponential portion of the trace back to the middle of the spike, assumed to represent the time at which the shock front had reached the center of the laser beam cross section. From this datum, values for initial density gradient and reaction rate constant were calculated as described by Miller.[10] Rate constants (k) thus obtained are shown in Figure 1. Also shown are the rate constants corrected to infinite pressure (k_∞). Ratios of k/k_∞ were interpolated from Forst method calculations by Frey, as reported by Barnard et al.[2] For each experiment, three points are shown, connected by a vertical line. These points correspond to assumed inert diluent gas (argon) collision efficiencies (β_p, pressure/pressure basis) of 0.01, 0.07, and 0.15, and reflect current lack of knowledge of the parameter under conditions of the present study. However, because of heavy reactant loading (5%) the fall-off corrections are not very sensitive to the value chosen. The collision efficiency for cyclobutane was assumed to be 1.0.[13] Figure 1 also shows Arrhenius lines deduced from static studies at lower temperatures,[14] and from fully corrected high pressure rate constants obtained above ~1100 K by Barnard et al.[2] in their absolute rate single-pulse study. Clearly the present rate constants, even before correction for fall-off, are about an order of magnitude larger than the single-pulse shock tube results, while corrected rate constants from the present study lie close to, but slightly above, an extrapolation from earlier work at ~700 K. There is no evidence of anomalous behavior below the upper limit of this study, 1500 K.

The densitometric techniques used for our experiments avoid many potential sources of systematic error that may affect the absolute rate single-pulse method, such as nonideal shock reflection, turbulence behind reflected shocks, substantial boundary layer growth, and sampling of products of uncertain thermal history. However, the present method is more abstract in that the nature of processes occurring in the heated gas is assumed, and cannot be confirmed by conventional chemical analysis. A full description of the observed laser beam deflection hinges on the assumption that the apparently exponential deflection decay after passage of the shock front was directly related to cyclobutane dissociation. This assumption is supported by (a) the absence of beam deflection, except for the spike, from shocks run in pure argon; (b) measurements by Skinner et al.[15] which indicated that further reaction of product ethene should be immeasurably slow under the present conditions; and (c) *rates of decay* of laser beam deflection which correlate well with decay rates predicted from the rate constants calculated from initial *magnitudes* of beam deflection.

Our rate constants calculated from laser beam deflection are, of course, subject to various sources of error such as uncertainty in post-shock gas density ($\lesssim 10\%$), index of refraction of cyclobutane ($\lesssim 10\%$), and estimated beam deflection at time zero ($\lesssim$ a factor of 2). Contributing to the latter uncertainty are factors which lead to deviation from true exponential decay: unimolecular fall-off, small changes in bulk index of refraction as the reaction proceeds, and temperature drop due to reaction endothermicity. An additional problem is that equipartition of
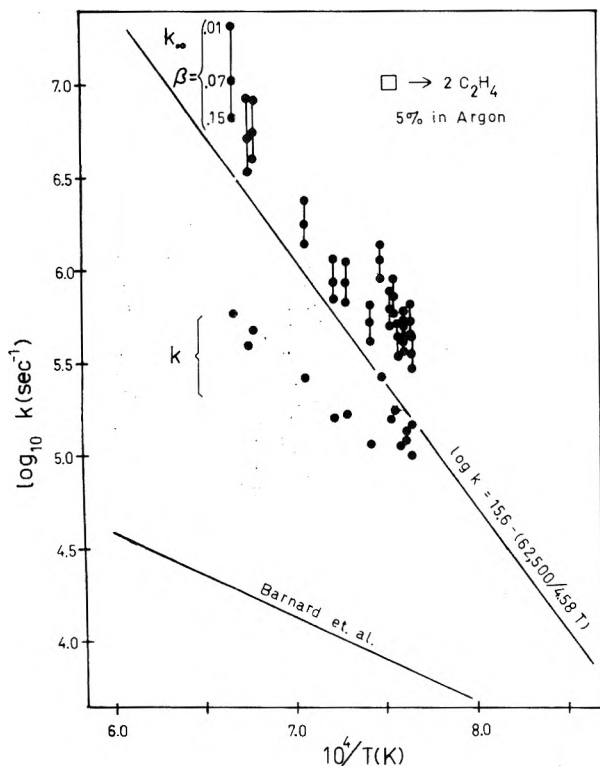
Figure 1.

energy is not instantaneous upon passage of the shock front through the gas, so the reaction is not turned on instantaneously. Thus, there is some arbitrariness about the choice of time zero. Considering these factors and the ≤ 25 K possible systematic error in our temperature calculations,[13] we feel the present data are in acceptable agreement with the low temperature rate constants.[14]

Further study of this and other similar reactions previously reported to appear "anomalous" is in progress.

Supplementary Material Available: Details of the experimental procedure and experimental data and data reduction procedures (7 pages). Ordering information is available on any current masthead page.

References and Notes

(1) J. N. Bradley and M. A. Frend, *Trans. Faraday Soc.*, **67**, 72 (1971).
(2) J. A. Barnard, A. T. Cocks, and R. Y-K. Lee, *J. Chem. Soc., Faraday Trans. 1*, **70**, 1782 (1974).
(3) J. A. Barnard, A. T. Cocks, and T. K. Parrott, *J. Chem. Soc., Faraday Trans. 1*, **72**, 1456 (1976).
(4) J. A. Barnard and T. K. Parrott, *J. Chem. Soc., Faraday Trans. 1*, **72**, 2404 (1976).
(5) Actually, the onset of the anomaly correlates better with log k (s^{-1}) ≈ 3.0 than with temperature.
(6) (a) H. Eyring and A-L. Lev, *Proc. Natl. Acad. Sci., U.S.A.*, **72**, 1717 (1975); (b) *Chem. Eng. News*, **53** (15), 27 (1975).
(7) In the "absolute-rate" method, gas reaction temperatures are calculated from measurements of incident and/or reflected shock wave velocities; in the "comparative-rate" method, gas reaction temperatures are calculated from extent of reaction of an internal standard molecule, for which Arrhenius parameters are well known.
(8) P. Jeffers, D. Lewis, and M. Sarr, *J. Phys. Chem.*, **77**, 3037 (1973).
(9) P. Jeffers, C. Dasch, and S. H. Bauer, *Int. J. Chem. Kinet.*, **5**, 545 (1973).
(10) J. Miller, Ph.D. Thesis, Cornell University, Ithaca, N.Y., 1974.
(11) (a) J. H. Kiefer and R. W. Lutz, *J. Chem. Phys.*, **44**, 658 (1966); (b) W. D. Breshears, P. F. Bird, and J. H. Kiefer, *ibid.*, **55**, 4017 (1971).
(12) T. Shimanouchi, *Natl. Stand. Ref. Data Ser., Natl. Bur. Stand.*, **No. 11** (1967).
(13) Actual experimental data, intermediate and final calculated results, and a description of data reduction procedures are available as supplementary material. See paragraph at end of text regarding supplementary material.
(14) S. W. Benson and H. E. O'Neal, *Natl. Stand. Ref. Data Ser., Natl. Bur. Stand.*, **No. 21** (1970).
(15) (a) G. B. Skinner, R. C. Sweet, and S. K. Davis, *J. Phys. Chem.*, **75**, 1 (1971). (b) If we were to assume that all of the product ethene *did* further decompose to C_2H_2 + H_2 cyclobutane dissociation rates calculated from measured density gradients would be lowered by about a factor of 8, which would still leave k_∞ values about an order of magnitude larger than those reported by Barnard et al.[2]

Department of Chemistry   **D. K. Lewis***
Colgate University   **S. A. Feinstein**
Hamilton, New York 13346

Department of Chemistry   **P. M. Jeffers**
State University College
Cortland, New York 13045

Special Centennial Tapes

4 Historic Symposia!   24 Speakers!   Custom Packaging!   Special Prices!

☐ Milestones in Physical Chemistry

8 Speakers — 315 Figures
Length: 5 Cassettes — 8 Hours
PRICE: $45 (postpaid)

The Speakers:

G. T. Seaborg — 40 Years of Transuranium
Elements

D. Hodgkin — Structure of Molecules in
Crystals

G. Porter — Chemistry in Microtime

P. J. Flory — Thermodynamics of Polymer
Solutions

W. O. Baker — Chemistry of the Solid State

L. C. Pauling — Perspectives in Chemical
Bonding & Structure

H. Eyring — Reaction Rate Theory

J. H. Van Vleck — Evolution of Theoretical
Chemistry in America

☐ Structure and Quantum Chemistry
+
Evolution of Magnetic Resonance

8 Speakers — 210 Figures
Length: 4 Cassettes — 6 Hours
PRICE: $35 (postpaid)

The Speakers:

J. A. Pople — Orbital Studies of Molecular
Structure & Stability

H. G. Drickamer — Pressure & Electronic
Structure

F. H. Stillinger — Quantum Chemistry &
Eccentric Behavior of Liquid Water

R. Zwanzig — Molecular Hydrodynamics

H. S. Gutowsky — 30 Years of Relaxation

J. S. Waugh — Alchemy of Nuclear Spins

H. M. McConnell — Spin Labels

F. A. Bovey — NMR of Macromolecules

☐ Evolution of Kinetics

8 Speakers — 140 Figures
Length: 4 Cassettes — 6 Hours
PRICE: $35 (postpaid)

The Speakers:

B. S. Rabinovitch — Perspectives on
Vibration Energy Relaxation in
Unimolecular Reactions

W. A. Noyes, Jr. — Photochemical Kinetics

R. A. Marcus — Trends in Theoretical
Chemical Kinetics

K. F. Freed — Radiationless Processes in
Polyatomic Molecules

G. B. Kistiakowski — Early Years of Gas
Phase Chemical Kinetics

J. C. Polanyi — Recent Studies of Infrared
Chemiluminescence & Fluorescence

S. Claesson — Diffusion Rates & Chemical
Reaction Kinetics

J. Jortner — Intramolecular Dynamics in
Excited Molecular States

— SPECIAL PRICE —

☐ BUY ALL THREE SETS — ONLY $85 (postpaid)
SAVE $30!

ORDER FROM:
American Chemical Society
1155 Sixteenth St., N.W.
Washington, D.C. 20036
ATTN: DEPT. AP

Name

Address

City   State   Zip

(allow 4 to 6 weeks for delivery)